A Multiple Angle Detection System For Coherently Scattered X-ray Signatures

Catharine Helen Malden

University College London

Submitted for

The Degree of Doctor of Philosophy

The University of London

February 1998

ABSTRACT

Coherent scatter measurements have previously shown promise as a method for detection and identification of materials. However, the time required for measurements is rather long and the computer power required to analyse the data can be quite considerable. A multiple angle coherent scatter system has been designed and built to assess the feasibility of using this technique as an alternative to a single angle coherent scatter system. An application of detecting the presence of explosives within baggage to go on board aircraft was used to test the multiple angle system.

A cadmium zinc telluride detector was found to be suitable to be used with the multiple angle system. A model of the system was used to determine the number of angles required and to determine the characteristics of the collimator that would be suitable with this detector. The objective of this work was to develop a simple method of analysing the data yielded from multiple angle coherent scatter system. This has been achieved by plotting the scatter signatures in the form of energy-angle diagrams and using these plots to determine the optimum energy windows to be used with each scatter angle.

Samples of 4 mm of Semtex and 6 mm of SX2 were detected with 0% false alarm rate at 100% detection rate with a single energy window centred at a planar spacing of 3.3 Å. A detector array with collimation has been built to fit within the dimensions of an existing baggage scanner. This caused an increase in the scatter volume and hence the explosive sample constituted a smaller part of it. The results were that the false alarm rate was higher than for the initial system, at 37.5%

It is concluded that the multiple angle detection of coherent scatter signatures is a promising method for the detection of explosives and that it could be used for several other applications in the future.

CONTENTS

FIGURES

TABLES

CORRIGENDA

p 19 line 17 'there is further information' should read 'further information'

p 20 line 30 'raman' should read 'Raman'

p 22 line 16 'energies greater than 511 keV' should read 'energies greater than 1.02 MeV'

p 43 line 6 'transmitted photons' should read 'directly transmitted photons'

p 47 eqn 2.2 should read $$R(FWHM) = \frac{2.35}{\sqrt{N}} x100\%$$

p 48 line 8 'determined by the sum' should read 'determined by the quadrature sum'

p 54 line 6 and p 173 line 1 'Narthrop' should read 'Northrop'

p 84 figure 3.6 should have a scaling factor of 0.94 applied to the x axis

p 97 line 4 'increased energy resolution' should read 'poorer energy resolution'

p 127 eqn 4.1 should read $$\sigma(N_1, N_2, N_3...) = \sqrt{N_1 + N_2 + N_3...}$$

p 135 eqn 4.2 should read $$V(N_1, N_2, N_3...) = \sqrt{1/N_1 + 1/N_2 + 1/N_3...}$$

p 162 line 2 'alarm rate is lower' should read 'alarm rate is higher'

p 165 line 27 'due change' should read 'due to a change'

ACKNOWLEDGEMENTS

I would like to acknowledge the receipt of an EPSRC studentship under the Postgraduate Training Partnership of University College London and Sira Ltd. I was also a member of a collaborative group between the Medical Physics Department at UCL, the Clinical Physics Department at St Bartholomew's Hospital and the Police Scientific Development Branch, who funded much of this work.

I would like to thank my supervisors, Dr Robert Speller (UCL) and Dr Tony Allnutt (Sira Ltd). There were also many other people who have been invaluable over the last three years. These include Dr Russell Luggar, Dr Dick Lacey and the rest of the Radiation Physics group at UCL. I am also grateful to Dr Julie Horrocks for allowing me use of the lab at St Bartholomew's Hospital.

I would like to express particular appreciation to Neil Cohen of the Physics Department, UCL for running diffraction measurements for me, and allowing me unlimited access to the JCPDS database.

The workshops at UCL, PSDB, Sira Ltd and St Bartholomew's have also all been vital in building much of the equipment used in this work.

CHAPTER 1

INTRODUCTION AND THEORY

The objective of this study is to investigate an alternative method of using coherently scattered energy dispersive X-ray signatures for material identification, by making measurements at several scatter angles simultaneously. In doing this, information could be collected from the same volume of interest for each angle. It was proposed that a system would be built for a specific application. An analysis procedure would be developed which would be simple and that was to be designed with the application in mind. The final aim of this project was to design and build a full multiple detector array and collimation system for coherent scatter measurements and to investigate the design implications required for the specific application.

In order to investigate the possibilities of using a multiple angle system, an application was required with which to evaluate it. This application was the detection of explosives in baggage. This has been carried out in collaboration with the Police Scientific Development Branch (PSDB), through whom both technical and financial support were available. The requirements for this research from the PSDB *(Lacey 1995)* were to develop methods of coherent scatter which could identify the presence of sheets of explosives hidden within passenger baggage. The first section of this chapter therefore covers a review of security screening for detection of explosives in baggage to be taken on board aircraft.

The remainder of this chapter includes a review of the theory of X-ray scatter and diffraction and how coherent scatter came to be considered as a useful method of material analysis. More recent developments in the applications of coherent scatter are

described, with a discussion of the various methods used. A description of the objectives of this work, including the hypothesis which accompanies it is also given.

1.1 Review of explosives detection

1.1.1 History

On 11 August 1982 a bomb exploded under a seat of a Pan America flight from Tokyo to Honolulu. This was the first known incidence of the use of a plastic explosive to bomb an aeroplane. Later in the same month another bomb was found on a Pan America flight to Rio de Janeiro. In February 1986 a suitcase was opened, in Israel, and Semtex was discovered moulded into the lining. At a similar time a gym bag was found at London Heathrow airport with Semtex pressed into sheets and hidden in a false base. These were all discovered by routine opening of baggage.

The 21st of December, 1988, is the date of what is perhaps the most well known bombing of an aeroplane. Pan America flight 103 exploded in the sky above Lockerbie in Scotland and 230 people were killed. It has been reported by the Federal Bureau of Investigation (USA) that the bomb, thought to have caused the explosion, was made of Semtex hidden in a music cassette player *(Polski 1994)*. This event was to prove to be a catalyst for an increase in aviation security in several countries. By March 1989 experts from 14 countries met in the USA to "identify and propose measures to prevent and detect placement of explosive substances on board aircraft". They agreed that "examinations be undertaken for promoting international co-operation for making explosives more detectable" *(Cartwright 1994)*.

The need for special aviation security measures have been formally recognised since 1969 when the first major hijackings started to take place, however this was primarily for the detection of weapons *(Polski 1994)*. The Aviation Security Improvement Act in October 1990 directed the Federal Aviation Administration (FAA) to develop a testing program in consultation with outside experts before giving its approval to any detection system. Many technologies are currently being looked at including 18

methods of bulk detection and 22 trace detection methods *(Fultz 1994)*. It is hoped that these technologies should become more automatic wherever possible, however it is generally accepted that no one technology will provide an infallible system and that human involvement will remain. It is also suggested that multiple technologies combined with psychological and social observations will be the key to future security *(Stix 1992)*.

It is not officially known yet what caused the Trans. World Airlines Flight 800 to crash off Long Island, New York, on 22 August 1996. However, there has been much speculation in the world's press that this might have also been a bomb attack *(Eddy 1997)*.

1.1.2 Plastic explosives

Plastic explosives were developed during World War II as weather resistant alternatives to trinitrotoluene (TNT) *(Urbanski 1984)*. These are usually made of some type of explosive in powder form with a plasticine like base (such as latex) into which the explosive is mixed. This provides a substance which can be easily moulded into whatever shape is required, and which can be easily detonated by forming the plastic explosive around the detonator. The main attraction of these explosives to terrorists is that they are odourless and malleable.

RDX (cyclotrimethylenetrinitramine) is a white crystalline powder which consists of a carbon and nitrogen ring with hydrogen and oxygen attached ($C_3N_6H_6O_6$) *(McCrone 1950)*. This is the chemical used by Royal Ordnance to make a plastic explosive called SX2 *(Royal Ordnance, Bridgwater 1997)*. The other explosive used for this work is the more commonly known Semtex. Semtex is generally 50% RDX and 50% PETN (pentaerithritol tetranitrate) but the exact composition can vary *(Lacey 1996)*. PETN is also a white crystalline powder, the full chemical composition of which is $C_5H_8N_4O_{12}$ *(Booth and Llewellyn 1947)*. These two explosives together have been described as "the most serious threats in aircraft sabotage, because they can be easily moulded for concealment, are very stable in the absence of a detonator and are able, in small

amounts, to destroy a large aeroplane in flight. They are in fact the explosives most commonly used for this purpose." *(Fainberg 1992)*. A sample of each of SX2 and Semtex were made available for X-ray scatter measurements by the PSDB.

1.1.3 The requirements of a baggage scanning system

There are many requirements of a baggage scanning system whether it be for hand-held luggage or hold baggage. These can be summarised as follows:

- The system must be able to detect a bomb before the bag reaches the aeroplane.
- It must be rapid, automatic and non-destructive.
- The probability of success must be high with very few false alarms.
- There should be no radiation hazard and it should be a robust system that can be run by nominally trained staff.
- The cost must also be acceptable to the passengers *(Grodzins 1991)*.

However, there is further information is required that is not available. For successful detection, other factors need to be considered such as the type of materials that are carried in baggage and their relative frequency. These also vary according to the destination of the flight. The weight, shape and kind of explosive are often unknown as well, especially as the explosives can be home made. Therefore any tests carried out on an explosive detection system must be specific about which types of explosives are being identified. Also attempts must be made to investigate a good cross-section of case contents, including materials which may be used in an attempt to mask the presence of an explosive.

The analysis procedure for any baggage scanning system also has certain requirements. There is maximum detection rate with minimum false alarms and ideally the system would also be automated so that variations in response between individual operators do not effect the systems ability to detect the explosive.

1.1.4 Methods for explosive detection

There are three groups into which the methods of explosive detection, which are currently being developed, can be placed. These are nuclear, X-ray and trace. Each of these is reviewed in the following sections.

1.1.4.1 Nuclear methods

Nuclear methods rely on interactions with the atomic nucleus. Neutrons or high energy photons are used and the characteristics of the photons or neutrons which are emitted by the nucleus can be interpreted to identify the material in question. Explosives are characterised by their high concentrations of nitrogen and oxygen. The closest confounder to this is polyurethane which has an 8% probability of being confused with an explosive group *(Gozani 1992)*. In 1989, thermal neutron activation (TNA, where a thermal neutron is captured by the nucleus and a characteristic γ-ray is emitted) was thought to be the best method of detecting explosive *(Stix 1992)*, but was found to have problems detecting small amounts of explosives, as were used in the bombing over Lockerbie. Since then there have been many developments in nuclear methods *(Gozani 1996)*. However, the equipment required for nuclear methods is very bulky and expensive and hence not particularly suitable for deployment in an airport environment.

1.1.4.2 Trace methods

There are several methods which involve traces of explosive being tested. These include biochemical reactions *(Leginus 1993)* which are sensitive, specific, easy to use, portable and non-destructive. However, a human is required to carry out the test and therefore is only useful for small numbers of cases. Other trace methods include ionisation sources, frequency modulated infra red detectors, ion trap mass spectrometers and raman spectroscopy *(Polski 1994)*.

1.1.4.3 X-ray methods

Improvements in spatial resolution, dynamic range and energy resolution of X-ray detectors, as well as an increase in computer power, have helped to improve the detection of explosives in baggage using X-ray methods. There are two main approaches, based on either transmission imaging or scattering techniques.

Transmission technologies include computed tomography and effective atomic number methods. Computed tomography has the advantage that it can reconstruct any part of a bag in three dimensions *(Heiskanen and Roder 1996)*, however this is an expensive system due to the number of detectors required and the computer image reconstruction.

Dual energy systems use two incident X-ray beams of different energies. The effective atomic number of the material can be calculated from the difference in attenuation suffered by the two beams. Improvements in transmission systems have included the use of cadmium telluride detectors for improved spatial and energy resolution *(Eisen 1996)*. A further development is a stereoscopic system that has been developed by i2i vision, Nottingham. Two fan beams are set at 30° and the images from them are reconstructed in a binocular-like view *(Grodzins 1993)*.

Scatter techniques utilise either elastic or inelastic scatter of X-rays. Inelastic methods include back scatter imaging *(Hall and Jacoby 1993)*. At energies of 100 keV to 10 MeV the Compton effect dominates any scatter. This can be used to scatter through 180° to image beneath the surface of an object. The advantage with back scatter is that it allows for a one sided inspection geometry, which is useful when the far side of an object is not accessible. However the disadvantages are that the counting statistics are low and that multiple scatter can blur the image. Also, the penetration is only a few centimetres depending on the energy of the incident beam. Back scatter imaging has also been used in conjunction with transmission imaging for scanning of trucks. However the energies needed for penetration of the truck are very high and therefore a large accelerator is needed *(Hussein et al. 1996)*.

Elastic or coherent scatter has also been used for detection of explosives in baggage. The scatter patterns produced by the crystalline nature of the explosives are unique to individual materials. High purity germanium detectors have been used to detect scatter patterns from explosives within baggage *(Speller et al. 1993, Strecker et al. 1993, Harding 1995, Luggar et al. 1997, Hnatnicky 1996).*

1.2 X-ray scatter theory

As this work employs an X-ray coherent scatter method to investigate the possibility of detecting explosives in baggage, the following section gives a review of the theory of X-ray scatter.

When an X-ray photon passes through a material there are four main interactions that can occur. These are coherent scattering, the Compton effect, the photoelectric effect or pair production. Pair production only occurs at energies greater than 511 keV and hence is not considered further in this thesis. The following sections describe the remaining three mechanisms in more detail.

1.2.1 Coherent scatter

Rayleigh scattering, elastic scattering and coherent scattering are all terms used to describe a photon scattered from a bound electron with no loss of energy. Coherent scattering means that that the wavelength and phase of the scattered photon are the same as for the incident photon. For coherent scatter to occur the electron must be bound to the atom so that the atom can take up the recoil due to the interaction. The probability of coherent scatter occurring is greater at higher Z (see figure 1.1) and the probability is reduced as the energy increases i.e. the wavelength decreases (see figure 1.2).

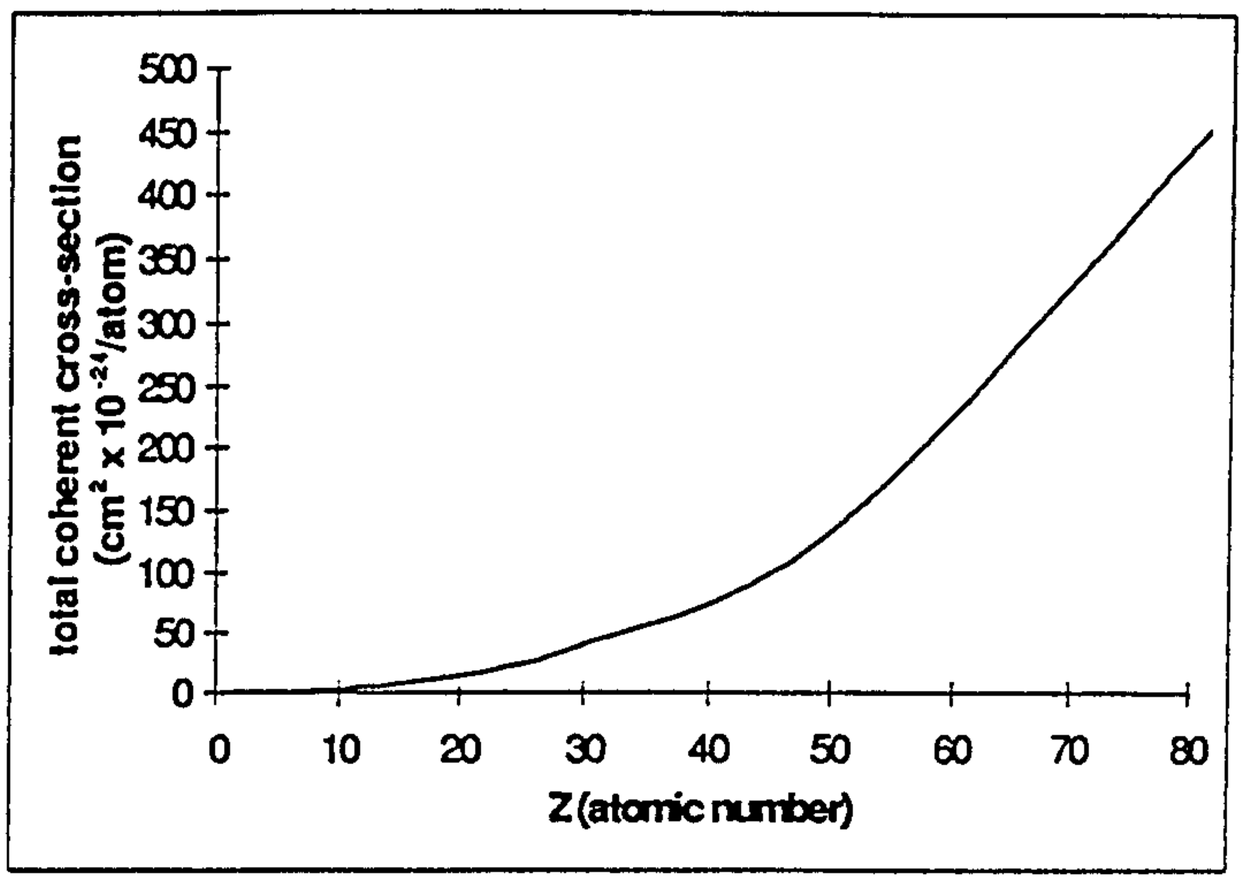

Figure 1.1 The variation of total coherent scatter cross-section as a function of atomic number for an energy of 30 keV (data from Johns and Cunningham 1983)

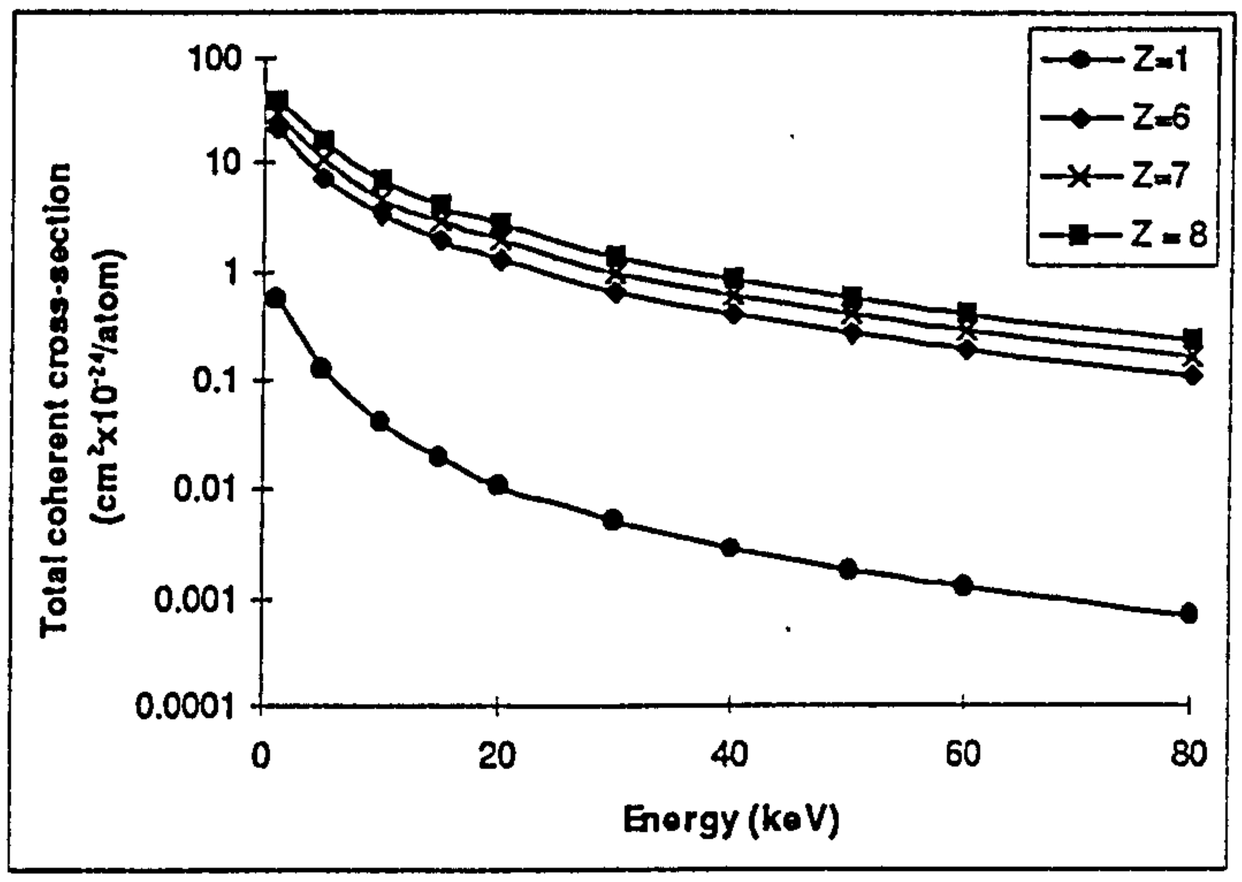

Figure 1.2 The variation of total coherent scatter cross-section as a function of energy for atomic numbers of 1, 6, 7 and 8 (data from Johns and Cunningham 1983)

1.2.1.1 Scattering by an electron

When an interaction occurs between a free electron and an X-ray photon, the electron is set into oscillatory motion. An accelerating or decelerating electron emits an electromagnetic wave, and in this sense the electron is said to scatter the X-ray photon. The Thomson formula is an approximation that describes the interaction of an unpolarised X-ray beam with a free electron and assumes that the electron is free and at rest. It is given by:

$$\left(\frac{d\sigma_{Th}(\theta)}{d\Omega}\right) = \frac{1}{2} r_0^2 \left(1+\cos^2\theta\right) \qquad [1.1]$$

where $d\sigma_{Th}(\theta)/d\Omega$ is the differential scattering cross-section per unit solid angle per electron, r_0 is the classical electron radius (2.82×10^{-15}m) and θ is the angle between the incident and scattered beams. A derivation is given in Cowley (1981).

The solid angle $d\Omega$, between the angles of θ and $d\theta$, is given by $d\Omega = 2\pi \sin\theta d\theta$, thus equation 1.1 can be written as

$$\frac{d\sigma}{d\theta} = \pi r_0^2 \left(1+\cos^2\theta\right)\sin\theta \qquad [1.2]$$

The total cross-section is obtained by integrating equation 1.2 over values of θ from 0° to 180°. This cross-section, σ_0, is called the Thomson classical scattering coefficient for a free electron and is given by:

$$\sigma_0 = \frac{8\pi}{3} r_0^2 \qquad [1.3]$$

1.2.1.2 Scattering by an atom

The process described above is for a free electron, however if the electron is bound to an atom then the conditions are slightly different. Scattering in an atom is mainly due to the electrons, as the nucleus is too massive to oscillate at such high frequencies, as are induced by the X-rays. If the scattered waves are in phase then the amplitude of the scattered beam is Z times the amplitude from a single electron. However, a difference in phase results in destructive interference, which causes reduced amplitude. This loss of amplitude in a coherent scattered event is described by the atomic form factor.

1.2.1.3 Form factors

A quantity $F_{coh}(x,Z)$, the atomic scattering factor, is used to describe the efficiency of scattering for a given atomic number (Z) and for a given momentum transfer (x). The momentum transfer is the momentum transferred to a photon when it is deflected through an angle θ and is defined as:

$$x = \frac{1}{\lambda}\sin\left(\frac{\theta}{2}\right) \qquad [1.4]$$

where λ is the wavelength of the incident photon and θ is the angle between the incident and scattered photon

The form factor accounts for the fact that an atom is not simply a point charge, but has a finite spatial distribution and therefore exhibits interference between wavefronts scattered from individual electrons within the atom. The square of the form factor is the probability that the Z electrons in the atom take up the recoil momentum without absorbing any of the photon energy. As it accounts for wave interference between scattering from the different electrons, these values are unique for each material. The probability of scatter for a particular material is given by :

$$\left(\frac{d\sigma}{d\Omega}\right) = F^2(x,Z)\left(\frac{d\sigma}{d\Omega}\right)_{Th} \qquad [1.5]$$

where F is the form factor and $(d\sigma/d\Omega)_{Th}$ is the Thomson cross-section.

1.2.1.4 Scattering from molecules

For scatter from molecules the situation is more complicated still, as interference can be caused by both intramolecular and intermolecular effects. The form factors can be either measured experimentally or estimated from a model, several of which have been suggested. A summary of these can be found in Morin and Berroir (1983), but in simple terms they are:

i) to assume no inter-atomic forces, ii) to assume a free molecule *(Blum 1971)* [developed a model which assumes a nearly spherical molecule for water], iii) use of empirical results *(Narten and Levy 1971)*

Since then many authors have improved the methods for calculating form factors by Monte Carlo techniques *(Williamson and Morin 1983, Neitzel et al. 1985, Persliden and Carlsson 1986)*, and also by relativistic calculations *(Roy et al. 1993)*.

The atomic or molecular form factor accounts for the interference of scatter from different electrons within the atom or molecule, but not for interference caused by any regular periodicity of those atoms or molecules within the material. This is accounted for by a geometrical structure factor and is the basis of diffraction which will be discussed in section 1.3.

1.2.2 Compton scatter

If the interacting X-ray has sufficient energy compared with the binding energy of the electron, then the electron will appear unbound to the photon. The X-ray will be deflected through an angle θ and a proportion of its energy will be taken up by the

electron. The amount taken up is related to the scatter angle, θ. As total energy and momentum are conserved, the energy of the scattered X-ray photon can be written as:

$$h\nu' = \frac{h\nu}{1 + \frac{h\nu}{m_0 c^2}(1 - \cos\theta)} \qquad [1.6]$$

where $h\nu$ is the incident photon energy, $h\nu'$ is the scattered photon energy and m_0c^2 is the rest mass energy of an electron (511 keV). The derivation of equation 1.6 is shown in Evans (1982). The energy of the scattered photon increases with decreasing θ, hence at very small angles the difference between the incident and scattered photons is virtually negligible, see figure 1.3.

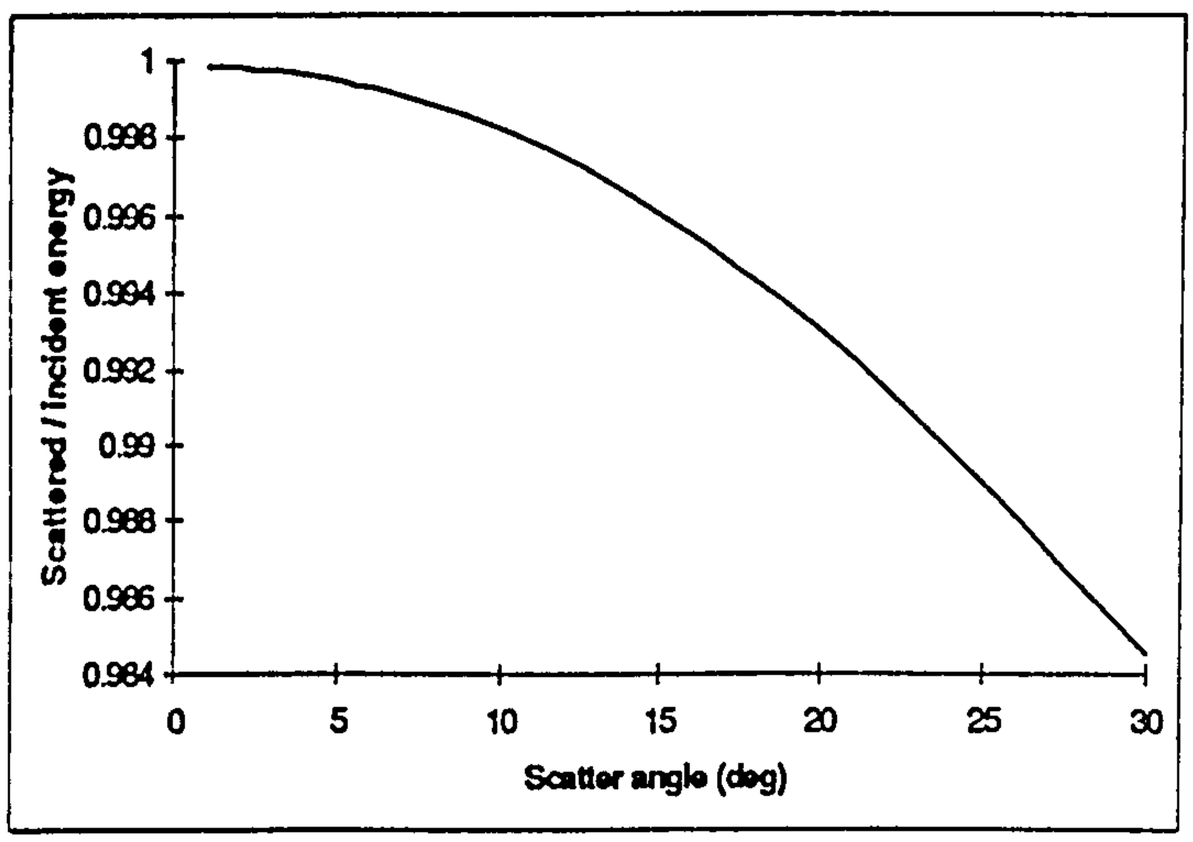

Figure 1.3 The ratio of scattered to incident energy for the Compton interaction as a function of angle, at 60 keV

The total number of electrons available for a scattering event is fixed and therefore coherent and Compton scatter events can be considered as competitive.

1.2.3. Absorption and attenuation of photons

The other effect that can occur to the X-ray is absorption. This can be caused by the photoelectric effect or the Compton effect or both. In the photoelectric effect the energy of the incident photon is entirely taken up by an electron of an atom. This

excess energy can either cause the electron to escape entirely from the electron shells of the atom, or to be promoted to a higher energy level. If the electron escapes then it could be stopped elsewhere in the material and hence the energy is totally absorbed in the material. If the electron is promoted then a 'hole' is left in the inner shell. This is an unstable state and so an outer electron will fill this hole. A characteristic photon or an Auger electron is simultaneously emitted with an energy equal to the difference between the energies of the two shells.

Attenuation is the effect on an X-ray beam of all three of these processes (coherent scatter, Compton scatter and absorption). The probability of attenuation is governed by the total cross-sections. These can be calculated by integrating the differential cross-sections for the individual processes over all angles. These can then be used to generate tables of attenuation coefficients for a range of incident photon energies.

1.3 X-ray diffraction

Crystalline materials display strong coherent interference effects for certain scatter angles. It is this phenomenon that has been exploited in the identification of crystals by their diffraction patterns. A crystal is defined as a sample of solid substance with a regular shape, having its surface bounded by plane facets of characteristic shape with characteristic angles between them *(Cambridge Thesaurus of Physics 1984)*. A crystal lattice expresses three dimensional periodicity and the structure of the crystal is considered as the matter that constitutes one unit cell. This can be one or several atoms, ions or molecules. Diffraction is defined as elastic scattering by a crystal whereby intense scattering occurs in discrete directions. The *geometrical structure factor* is defined by the periodicity of the crystalline material and causes the diffracted wave to have a specific amplitude and phase angle. These angles and intensitities of scatter are used for the unique indentification of materials. Diffraction effects can be observed with wavelengths which are smaller than, but comparable with, the unit cell lengths.

1.3.1 The Bragg equation

The Bragg equation gives the conditions under which the discrete directions for intense scatter are given. Consider a set of lattice planes, of equidistant planar spacing d(hkl), as in figure 1.4(a), where h, k and l are the three orthogonal directions. The incident plane wave has a vector of $\mathbf{k}_o$ and an incidence angle of θ with respect to the lattice plane. This angle is known as the Bragg angle as it is the complementary angle to the conventional incident angle in optics.

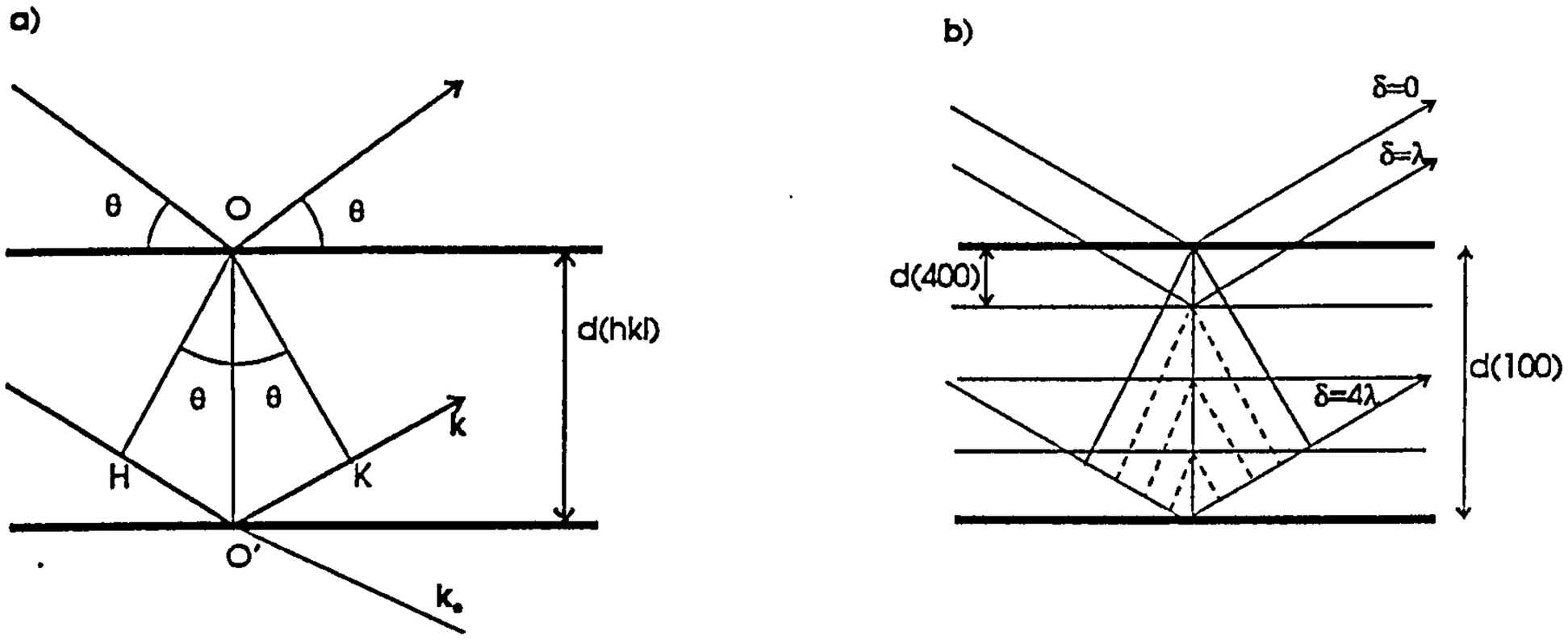

Figure 1.4 The vectors for the Bragg condition

Any points on one lattice plane scatter waves which are in phase if the incidence angle is the Bragg angle. If this condition is met then the path difference (δ) between the waves scattered by two adjacent planes is the same wherever the points are on the plane.

$$\therefore \delta = HO + OK$$

$$= 2d(hkl)\sin\theta \qquad [1.7]$$

The in-phase condition, called the Bragg condition (or Bragg law) becomes:

$$2d(hkl)\sin\theta = n\lambda \qquad [1.8]$$

where d is the atomic planar spacing, θ is the angle between the incident beam and the plane, n is the order of diffraction and λ is the wavelength of the incoming photon. The general condition for this is shown in figure 1.4 (b). The planar spacings which give rise to intense scattering can be plotted against those intensities to give a unique diffraction pattern for a given material.

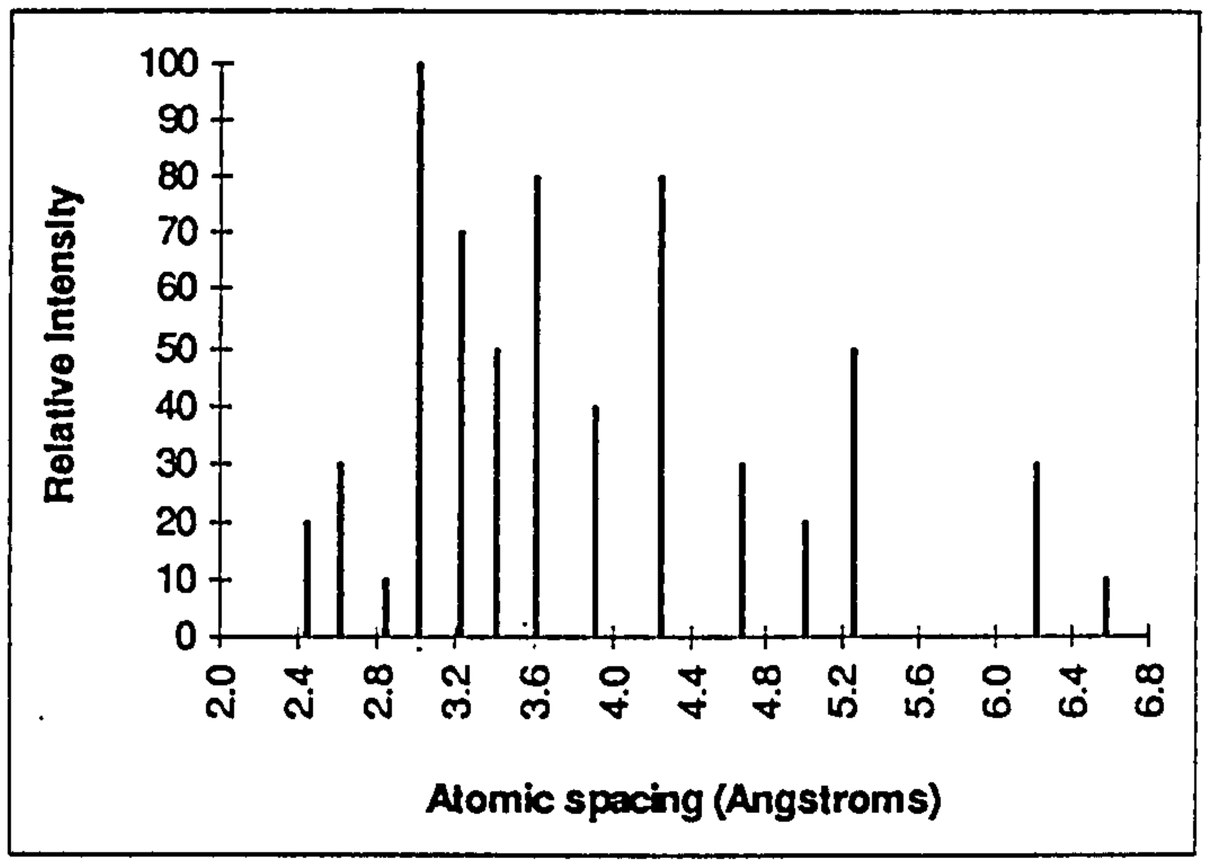

Figure 1.5 An example of diffraction lines

Figure 1.5 shows an example of typical diffraction lines. The atomic planar spacings (d values from the Bragg equation) are given in units of Angstroms (Å) and the intensities have been normalised to the highest peak.

1.4 Two methods of diffraction measurement

As shown by equation 1.8, the Bragg condition is $2d(hkl)\sin\theta = n\lambda$. Therefore in order to probe a range of values of d, either λ must be kept constant and θ varied (as with Debye-Scherrer measurements) or a constant θ can be used with an incident spectrum containing a range of wavelengths *(Giessen and Gordon 1968)*. Thus coherent scatter measurements can be carried out in two ways. To optimise the momentum transfer resolution so that the form factors can be identified, the measuring resolution for both the fixed and the varying parameter must be good. Angular

dispersive measurements use a monoenergetic primary source and require a detector with high position sensitivity, to minimise the error on the measurement of θ. Energy dispersive measurements employ a polyenergetic input beam at a single θ and the detector must have good energy resolution to reduce ΔE (i.e. the error on λ).

The advantage of energy dispersive over angular dispersive methods is that the flux from a polyenergetic source is considerably higher (e.g. an X-ray tube can produce ~$10^{11\text{-}12}$ photons s^{-1} sr^{-1} mm^{-2}) than that from a monoenergetic source (e.g. a radioisotope of Am^{241} can produce 6.6 x 10^6 photons s^{-1} sr^{-1} mm^{-2}; *Armstrong et al. 1993*). However, developments in quasi-monoenergetic X-ray tubes, where the emitted beam is filtered by a sample of the target material, have gone a long way to reduce this *(McDaid et al. 1995, Harding et al. 1995, Webster et al. 1996)*. A quasi-monoenergetic tube can produce 5 x 10^8 photons $s^{-1}sr^{-1}mm^{-2}$ at 150 kV_p, whereas a polyenergetic beam is of the order of 5 x 10^{11} $s^{-1}sr^{-1}mm^{-2}$ that is three orders of magnitude more *(Harding et al. 1995)*.

The disadvantage of the energy dispersive method is that θ is required to be well defined. The result of this is that the scatter beam must be heavily collimated, and therefore much of the scattered flux is not detected. A further disadvantage is the variable spectral intensity, as different regions of momentum transfer are interrogated with different intensities, whereas angular dispersive diffraction uses a fixed intensity.

Hence both methods suffer a severe loss of flux either before the scatter occurs (angular dispersive) or after the scatter (energy dispersive).

1.5 Use of coherent scatter

Radiographic techniques have been used for many years as methods of non-invasive testing of internal materials, both in medical and industrial applications. For transmission imaging it is imperative that only photons transmitted directly through the object be detected. It is for this reason that much effort has been placed in the development of collimation systems to ensure the removal of unwanted scattered photons. However, whilst attempting to optimise mammographic scatter grids, Muntz et al. (1983) found that the coherent component of the scatter was highly forward peaked. Not at 0°, as was previously assumed *(Kerr et al. 1980)*, but in fact at a small angle from the beam path. Johns and Yaffe (1983) reported similar findings and investigations began into the cause of this small angle maximum, as theoretical calculations had suggested that the maximum should be at 0° *(Morin and Berroir 1983)*.

Further measurements revealed that Lucite, polyethylene and water have their maximum coherent scatter cross-sections at different angles *(Muntz et al. 1983)*. They also found a large variation in the scatter spectra from different angles for polyethylene and concluded that interference was the only possibility for causing this type of behaviour. This lead to more experimental measurements on coherent scatter in lead and tin *(Bradley and Ghose 1987)* and water, nylon and Lucite *(Bradley et al. 1989)* to be studied. Good agreement with theoretical values was found at large scatter angles, but at smaller angles the differences were greater.

The discrepancy which arises between the theoretical and experimental results is caused by intermolecular and intramolecular interference effects of scatter from within a material. These effects can be corrected for by using the relevant form factor with the Thomson cross-section for coherent scatter. These form factors are unique to individual molecules and this has led to the use of coherent scatter for the characterisation of materials. The first method was to use the ratio of coherent to Compton scatter *(Leichter et al. 1984, Bradley and Ghose 1984, Hardie-Brown et al. 1987)*. The two scatter types are collected in the same measurement at a scatter angle

where the coherent and Compton peaks can be differentiated. This has the useful effect that errors due to both attenuation and geometry are reduced since these effects for both types of scatter are identical *(McDaid et al. 1995)*. However coherent scatter is proportional to the product of the atomic number and the density, but Compton scatter is only proportional to the density. Therefore taking the ratio of these two functions cancels out the fact that the coherent scatter is sensitive to the density as well as the atomic number of the material being tested. It has been shown that coherent scatter alone can be used to characterise a material *(Harding and Kosanetsky 1985, Mossop et al. 1987, Harding and Kosanetzky 1987)*.

Since then there have been many applications using coherent scatter. In medicine these have included measurement of bone density *(Harding et al. 1990, Ndlovu et al. 1991, Royle and Speller 1991, Speller and Royle 1992, Newton et al. 1992)* and characterisation of breast tissue *(Evans et al. 1991)*, gall stones *(Speller and Royle 1992)* and urinary stones *(Dawson et al. 1996)*.

Coherent scatter has also been found to be useful in industrial applications. Contaminants in food are often difficult to detect with transmission techniques, as the attenuation values of such materials as chocolate and plastic can be very similar. However, a carefully chosen scatter angle can increase the image contrast between these two materials *(Luggar et al. 1993, Martens et al. 1993, Luggar and Gilboy 1994)*.

A further application that is more relevant to this work is the identification of plastic explosives within baggage *(Speller et al. 1993, Strecker et al. 1993)*. This work has been developed with particular attention to optimisation of the measurement system *(Luggar et al. 1995, Harding 1995)* and improvement of analysis methods *(Wilder et al. 1995, Blaffert 1995, Speller et al. 1996, Luggar et al. 1996a)*.

1.6 Energy dispersive coherent scatter measurements

Energy dispersive diffraction can be used to penetrate large samples *(Royle and Speller 1991)* by using high energy X-rays (typically up to 70 keV). However the effect of using higher energies is that the scatter angles become smaller. It has been shown that by using this method characteristic scatter patterns from different materials can be measured *(Harding et al. 1987 and Kosanetzky et al. 1987)*. Furthermore, quantitative information about a combination of materials may be obtained. This was originally demonstrated on bone phantoms consisting of bone and bone marrow simulants *(Royle and Speller 1991)* but has also been used on excised bones *(Speller and Royle 1992, Farquharson 1996)*. The relative heights of the diffraction peaks from the bone and marrow can be used to determine their absolute quantities *(Royle 1992)*.

1.6.1 An experimental set-up for energy dispersive coherent scatter measurements

As described in section 1.4 an energy dispersive coherent scatter system uses a polyenergetic source and measures the scatter signatures at well defined scatter angles. Figure 1.6 shows a schematic diagram of a laboratory experimental set-up for the energy dispersive coherent scatter system. This system shown includes an industrial X-ray tube with a tungsten target. This type of X-ray tube has been used because the water cooling system allows long continuous running times without causing overheating problems. Aluminium filtration is used on the X-ray tube to reduce the low energy X-rays as they would be scattered to angles where the coherent cross-section is low. Also, the low energies would be severely attenuated in the sample and hence the intensity on reaching the detector would be extremely low and of little use. The tube also has a lead collimator on the exit window to restrict the divergence of the incident beam. The whole tube is encased inside a lead housing to reduce X-rays being emitted from the tube in directions other than the in the incident beam.

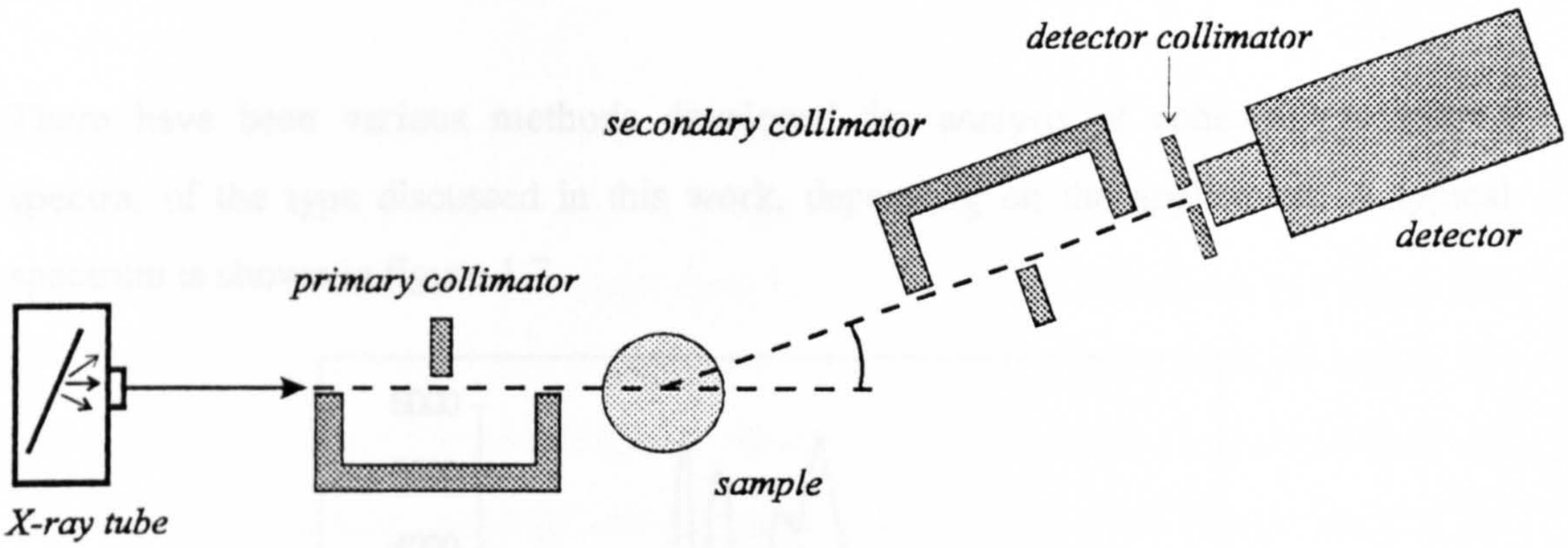

Figure 1.6 A schematic diagram of a laboratory energy dispersive coherent scatter system

The primary collimator has the function of defining the beam width. This collimator can be rotated and translated to assist alignment with the X-ray beam. The secondary collimator is designed in the same way and can be moved to define an angle with the primary beam, thus also defining the scatter volume. The sample is positioned between the primary and secondary collimators within the scatter volume. The collimators are both made of a high atomic number material and can be adjusted to provide any collimation width.

A detector is positioned close to the secondary collimator and is encased in a lead housing to prevent photons reaching it other than through the collimator. The lead housing has a collimator over the detector window to allow the scattered photons to reach the detector.

The signal from the preamplifier of the detector is fed into a pulse shaping amplifier. The amplified pulses are then converted to digital signals using an analogue to digital converter. This acts as a multi-channel analyser and sorts the signals into the appropriate energy channels. Finally the information is displayed on a personal computer. The spectrum can be displayed in various formats and some analysis such as the integrated counts in a certain region of interest can be calculated directly on the screen.

1.6.2 Analysis procedures for energy dispersive coherent scatter measurements

There have been various methods developed for analysis of coherently scattered spectra, of the type discussed in this work, depending on the application. A typical spectrum is shown in figure 1.7.

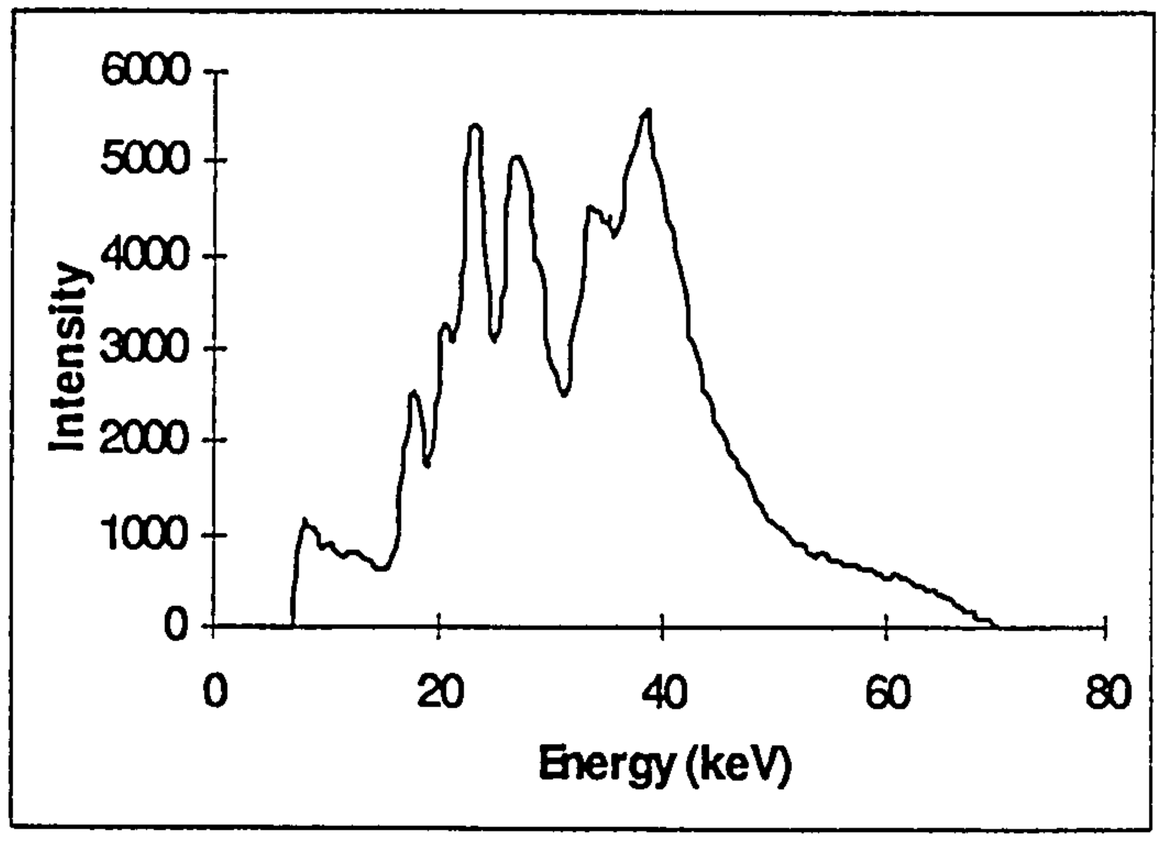

Figure 1.7 A typical coherently scattered spectrum

For assessment of osteoporosis in bone there are two peaks of interest, within the spectra, from the bone and the bone marrow. A ratio method *(Royle and Speller 1995)* has been used to provide quantitative information about the two components. However, for identification of one material within several others, for instance the identification of an explosive within a piece of luggage, a more rigorous approach is required. Principal component analysis (PCA) has been used *(Luggar at al. 1997)* to provide a statistical certainty that the characteristic pattern from an explosive is present within a pattern containing many other materials. Other methods, such as comparison with a library of spectra from known materials *(Strecker 1995)* and neural net based analysis *(Wilder et al. 1995)*, have also been applied. However all of the methods so far investigated for the identification of a material within several others require extensive computational analysis. It is therefore with this in mind that the subject of this thesis is introduced, a multiple angle coherent scatter system.

1.7 Multiple angle coherent scatter measurements

A variation of the coherent scatter system is proposed which measures the energy dispersive scatter signatures over a range of scatter angles simultaneously. The hypothesis is to use a multiple angle system, such that both variations of energy and angle are measured (see figure 1.8). It is suggested that by using multiple angles the optimum scatter angle for more than one material will be satisfied. A further advantage is that different planar spacings can be interrogated by the most intense part of the incident spectrum, by using a range of scatter angles. Also more information, per unit time, could be collected from a single scatter volume by using multiple scatter angles.

It is suggested that the addition of angular resolution and energy resolution may allow a system which does not require stringent definition of either energy or angle (i.e. a compromise between energy and angular dispersive diffraction). The advantage in relaxing the requirements of the energy resolution is that more detectors could be considered, a number of which do not require cooling.

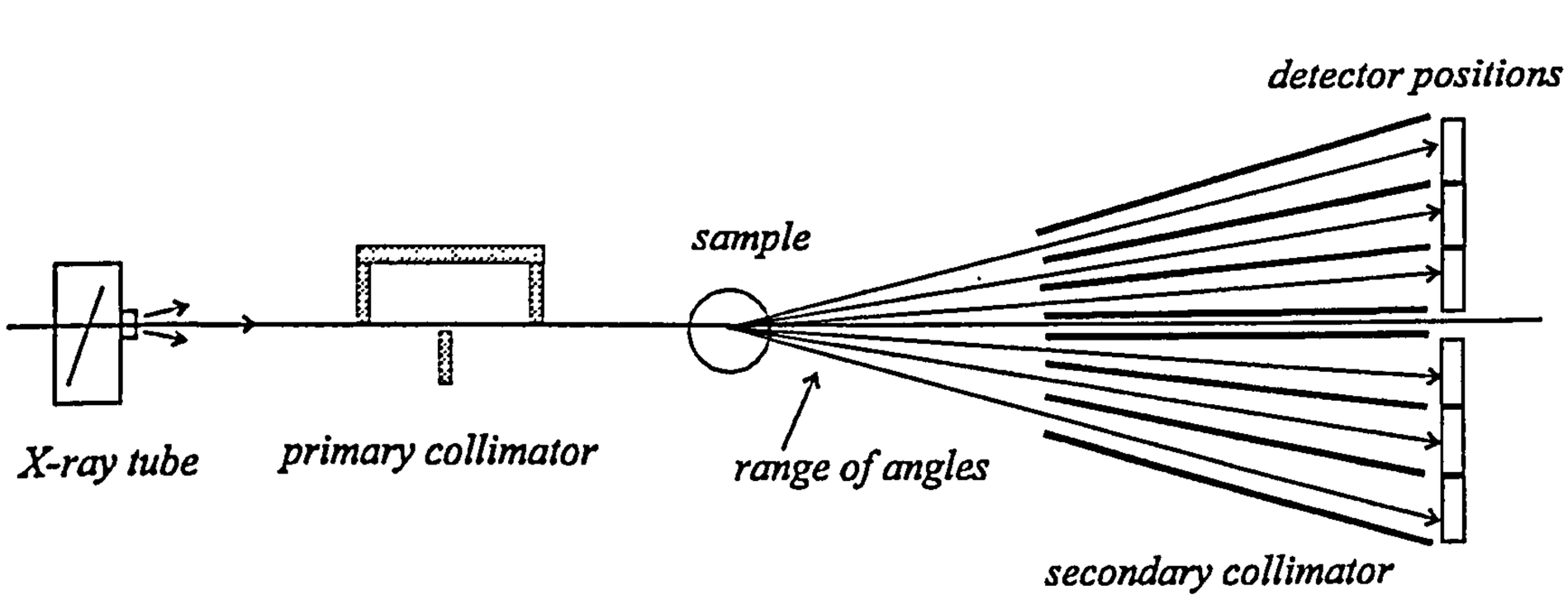

Figure 1.8 A schematic diagram of a multiple angle detector system for coherent scatter measurements

1.7.1 Proposal of an analysis procedure for a multiple angle system

Previously, the energy dispersive coherent scatter method has relied entirely on the high energy resolution in order to identify the diffraction pattern of a substance. Using both energy and angular information, certain 'areas' within the energy-angle space, which correspond to particular planar spacings, could be used to provide a simple identification method for the presence of a single material (such as an explosive) amongst other materials. The analysis procedure proposed is that energy windows, matching specific planar spacings, be set for each angle (i.e. detector) and intensity thresholds set for an alarm signal. Windows have previously been used as a method of maximising the difference between two types of materials *(Strecker et al. 1993, Luggar and Gilboy 1995)*. Various windows could be set for each angle and a combination of the signals used. In other words the differences between the counts obtained from a case with an explosive and a case without an explosive would be analysed.

1.8 Conclusions

This chapter has introduced the multiple angle energy dispersive coherent scatter system including a suggestion for how the scatter signatures could be analysed. The theory of coherent scatter and diffraction has been presented including a review of previous uses of coherent scatter. The application which has been chosen to test the multiple angle system is baggage scanning. This is a useful application with which to test the limits of the system since there are constraints of time and false alarm as well as being a complicated problem to address due to the large range and variations of baggage and contents which are required to be interrogated.

1.9 Work undertaken

The work undertaken and results achieved are described in the following chapters. In Chapter Two ionising radiation detectors are reviewed and a suitable detector is selected. Also a model of a coherent scatter system is used to decide what geometry would be suitable for the system, with the new detector, and how many detectors might be required.

Chapter Three investigates the characteristics of the chosen detector and covers the design considerations and construction of a multiple angle system which uses a single detector. The preliminary results of scatter signatures using this detector are also presented.

Chapter Four looks at the measurements taken from this multiple angle system and explains how an analysis procedure has been developed. The results of this analysis procedure are then discussed

Chapter Five describes the design of a multiple detector system with an array of detectors which has been set up to fit within the dimensions of a baggage scanner. Comparisons are made with the single detector multiple angle system and suggestions for how a coherent scatter system for baggage scanning may be optimised are given.

Finally Chapter Six concludes this work and suggests some developments and improvements for the future.

CHAPTER 2

PRELIMINARY CONSIDERATIONS FOR A MULTIPLE ANGLE SYSTEM

This chapter will discuss the parameters which must be considered when choosing a detector which would be suitable for use with the multiple angle coherent scatter system. A method of analysis for identification of the explosives is suggested. A suitable detector is chosen and a mathematical model of an energy dispersive coherent scatter system has been used to gain some insight into the effects of varying the geometrical set-up of the system, and investigate the number of detectors which might be required.

2.1 The diffraction data

In order to identify a material accurately, the diffraction data are needed for the material. This is a set of spacings and relative intensities, unique for each individual material. A database of JCPDS diffraction data *(Joint Committee of Powder Diffraction Studies 1961)* has been built up since 1961 and contains approximately 77,000 materials. All these data have been measured using standard diffraction techniques of angular dispersive diffraction either from single crystals (Laue diffraction) or from powder samples (Debye-Scherrer method).

To produce an effective baggage scanning system it is important to obtain the effect of the case contents on the scattered spectra, and thus to evaluate the ability to detect the explosives. Information, such as frequency of certain contents and materials which may be used to mask the explosive, is required. To address this problem a variety of

materials must be examined. The range of materials which can be carried in baggage is extremely large and therefore it would be impossible to measure all the combinations and variations. A further problem is that it would also be impractical and expensive to have all, or even a large sample of, fillings measured on a diffractometer. This means that simulating suitcase fillings would be reliant on the materials already in the JCPDS database. There are also difficulties with this, as all the data are normalised to the most intense peak before it is published. Therefore it is not possible to directly compare or combine two materials.

However, baggage scanning for security is only looking for a small range of illicit materials, and in this work it is RDX based sheet explosives. It does not matter what the harmless case contents are, so long as the explosives can be identified. As explained in section 1.1.2, SX2 and Semtex are manufactured explosives. Although diffraction data is available for pure samples of RDX and PETN, it was not known exactly what the diffraction data for SX2 and Semtex should be. Semtex and SX2 are both made with a plasticine-like material to bind together the explosive powders. Therefore the diffraction data were measured using a Philips X'pert θ-2θ Cu K_α anode diffractometer *(Cohen 1997)*. Figure 2.1 shows the planar spacings and relative intensities, for SX2 and Semtex, as measured by this diffractometer.

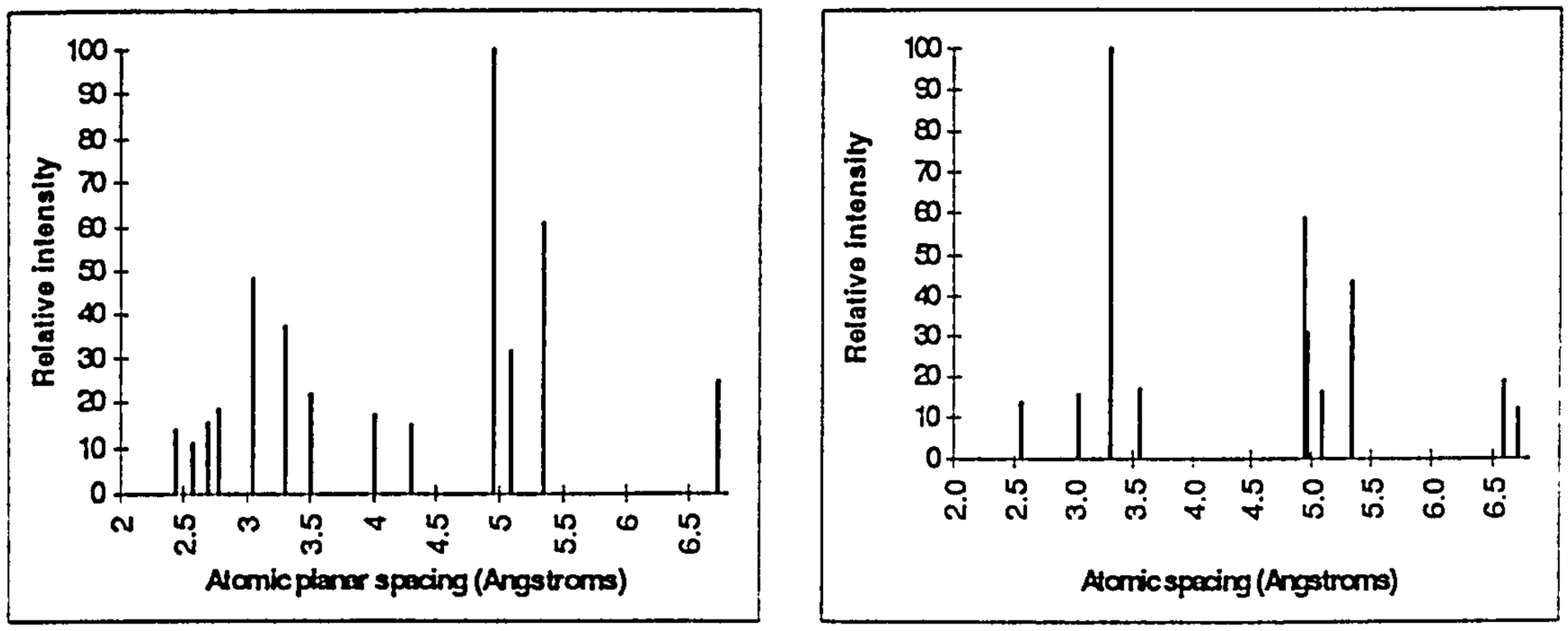

Figure 2.1 The measured diffraction data for SX2(left) and Semtex (right)

2.1.1 Identification of the explosive from the diffracted information

The most intense peaks in both these sets of diffraction data occur in three different regions. 3-3.5 Å, 4.9-5.3 Å and 6.6-6.7 Å. It was therefore suggested that the identification of the intensities in these three regions could be utilised for an analysis procedure.

2.1.2 The range of angles to be considered in a multiple angle system

There are several factors to be taken into account when deciding the optimum range of angles that should be included in the multiple angle coherent scatter system for measurements of SX2 and Semtex. These are as follows :

- The momentum transfer range of the prominent diffraction peaks for SX2 is 0.075-0.21 $Å^{-1}$ and for Semtex is 0.075-0.20 $Å^{-1}$.
- The scatter volume is defined as the volume of intersection between the primary and scattered beams. The smaller the scatter angle the longer the length of the scatter volume, which becomes effectively infinite at 0°. Figure 2.2 shows the length of the scatter volume as a function of the scatter angle. Assuming the scatter volume is filled by the suitcase to be measured, a longer scatter volume reduces the fraction of that volume taken up by the piece of explosive, hence relatively reducing the signal from the explosive. Therefore scatter volumes are required not to be excessively long, compared to the typical thickness of the explosive likely to be encountered.
- The theoretical differential cross-section for coherently scattered photons decreases with increasing angle (see figure 2.3). At above 7.5° the intensity becomes less than 20% of the maximum intensity and therefore was considered too low to make use of as measurement times must be minimised. It should be noted that calculated cross-sections do not take into account form factors. In fact the maximum is not at

zero but at a finite small angle. However above 5° the calculation is generally accurate.

- The opening angle of the collimation on the front of the X-ray tube was 1.43°. Therefore scatter should not be measured below this angle, so as to avoid including transmitted photons.

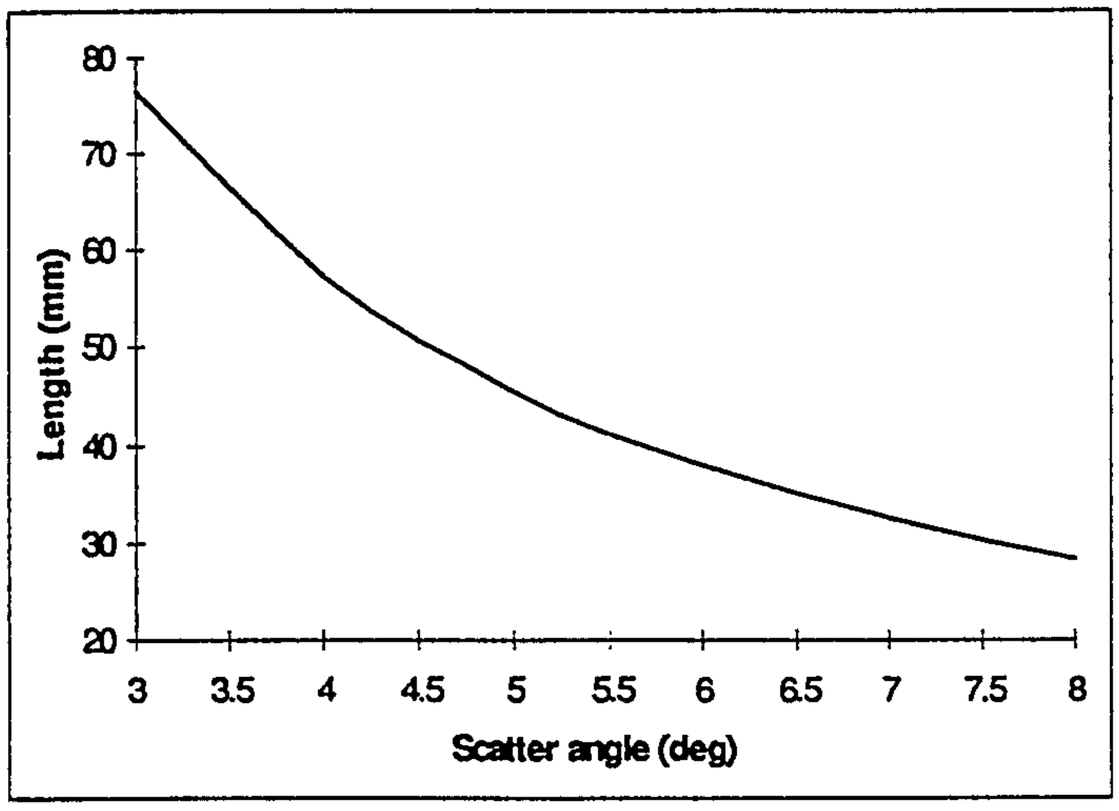

Figure 2.2 Scatter volume length as a function of scatter angle

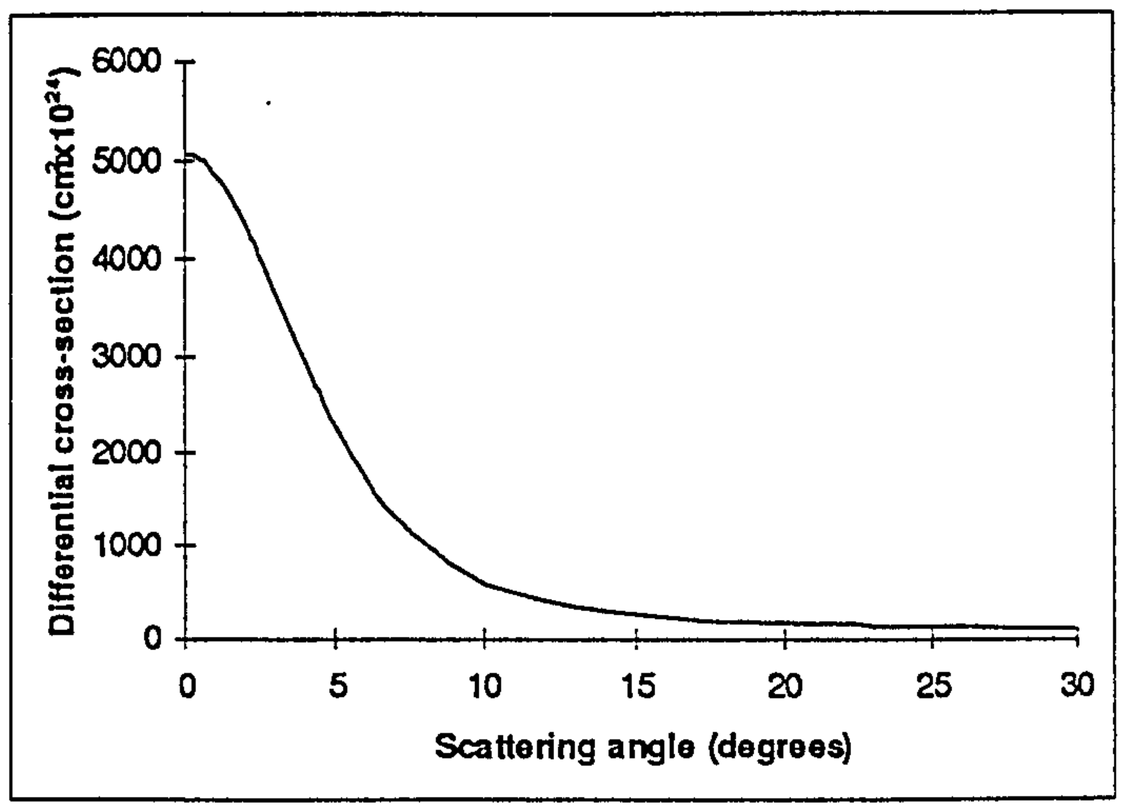

Figure 2.3 Variation of theoretical differential coherent scatter cross-section with angle for a free oxygen atom at 60 keV (data from Hubbell et al. 1975)

Taking these factors into account, the range of scatter angles which has been chosen to be measured in the multiple angle coherent scatter system is 3° to 7.5 °. This range has high differential cross-section and reasonable size scatter volumes. This range also does not include transmitted photons and covers the range of momentum transfer values required by SX2 and Semtex. This momentum transfer range fits within a 70 kV_p incident spectrum and therefore this is the incident energy spectrum which has been selected for this application.

2.2 The detector for a multiple angle system

This section describes the requirements of the detector needed for a multiple angle scatter system. It was proposed that germanium detectors may not be suitable for a multiple detector system because they are expensive and bulky, therefore smaller and cheaper detectors would be preferred. As has been discussed in section 1.7, it is suggested that by using multiple angles the requirements of the energy resolution could be relaxed. A review of radiation detectors and the types that might be suitable are surveyed and a detector with the optimum characteristics (as described in section 2.2.1) is chosen.

2.2.1 Requirements of the detector

Two effects broaden the width of the diffraction peaks are energy resolution and angular blurring. Both these functions effect the momentum transfer resolution as:

$$\Delta x/x = [(\Delta\theta/\theta)^2+(\Delta E/E)^2]^{1/2} \qquad [2.1]$$

where $\Delta x/x$ is the momentum transfer resolution, $\Delta\theta/\theta$ is the angular blurring and $\Delta E/E$ is the energy resolution. The momentum transfer resolution is important as the form factors are a function of momentum and hence this resolution affects how well a material can be identified, by its peaks.

The angular blurring ($\Delta\theta/\theta$) is governed by the acceptance angle of the collimators, that is the opening angle defined by the width, height and length of the collimator. This acceptance angle has the effect of allowing a range of scatter angles through the collimator. See figure 2.4.

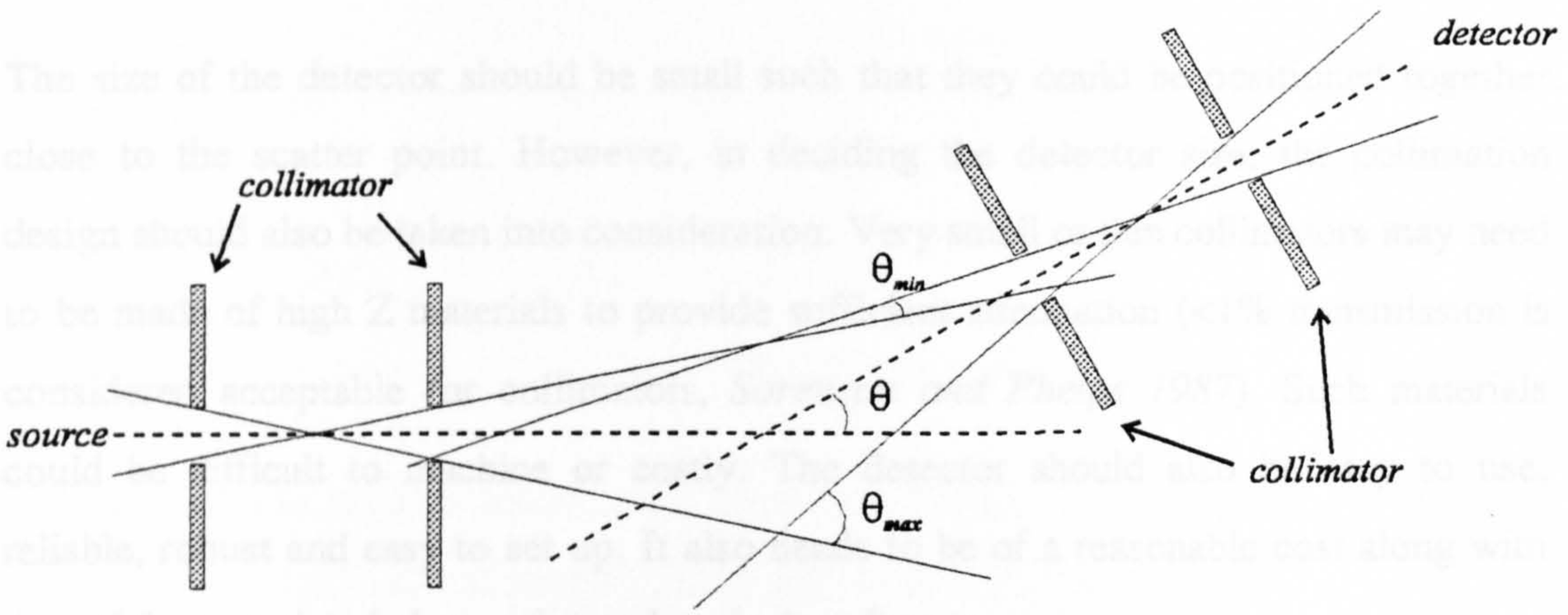

Figure 2.4 The range of scatter angles 'allowed' by the acceptance angle of the collimator

The Bragg relationship states that $n\lambda = 2d\sin\theta$ (equation 1.8), therefore a change in scatter angle, θ, will change the wavelength, λ, which satisfies a particular planar spacing, d. Hence, the effect of allowing a range of scatter angles through the collimators is that the diffraction peak is satisfied by a range of λ, and therefore the diffraction line is blurred as a function of energy. Luggar et al. *(1996b)* showed that the distribution of this blurring function was not strictly Gaussian in shape, but that a Gaussian distribution would give a reasonable approximation.

An increase in the acceptance angle of the collimators has two effects. The first is that the angular blurring increases and hence the peaks broaden. However wider collimation also allows a greater flux and hence the signal to noise ratio (SNR) is improved, for a given measurement time. In considering energy resolution and angular blurring, the energy resolution should always be the best available so as to allow a higher SNR whilst maintaining an overall momentum resolution.

Other requirements are that the intrinsic efficiency should be close to 100%, for energies of up to 70 keV. This efficiency will be governed by both the thickness of the detector and the material from which the detector is made. The higher the atomic number of the detector material, then generally, the greater the efficiency.

The size of the detector should be small such that they could be positioned together close to the scatter point. However, in deciding the detector size, the collimation design should also be taken into consideration. Very small or thin collimators may need to be made of high Z materials to provide sufficient attenuation (<1% transmission is considered acceptable for collimators, *Sorenson and Phelps 1987*). Such materials could be difficult to machine or costly. The detector should also be easy to use, reliable, robust and easy to set up. It also needs to be of a reasonable cost along with that of the associated electronics and analysis software.

2.2.2 Radiation detectors

For a material to be suitable for measurement of the energy of incident gamma rays i.e. spectroscopic applications, all the energy of each photon must be totally absorbed in the material. The energy of the photon must also be converted, by some means, into electrons that can then be collected as an electrical signal. The photoelectric effect is the main interaction where all the energy associated with the interaction is deposited in a single interaction. Therefore for a material to be useful as a gamma detector it must have a high probability of the photoelectric interaction occurring at the energy required. Figure 2.5 shows a schematic diagram of the probabilities of the three possible interactions (which deposit energy) of photoelectric effect, Compton scattering and pair production as functions of atomic number and energy. For a greater probability of the photoelectric effect at a given energy, the atomic number must be as high as possible. For the energies of 10-70 keV, used in this work, the photoelectric effect is dominant at atomic numbers of approximately 25 upwards.

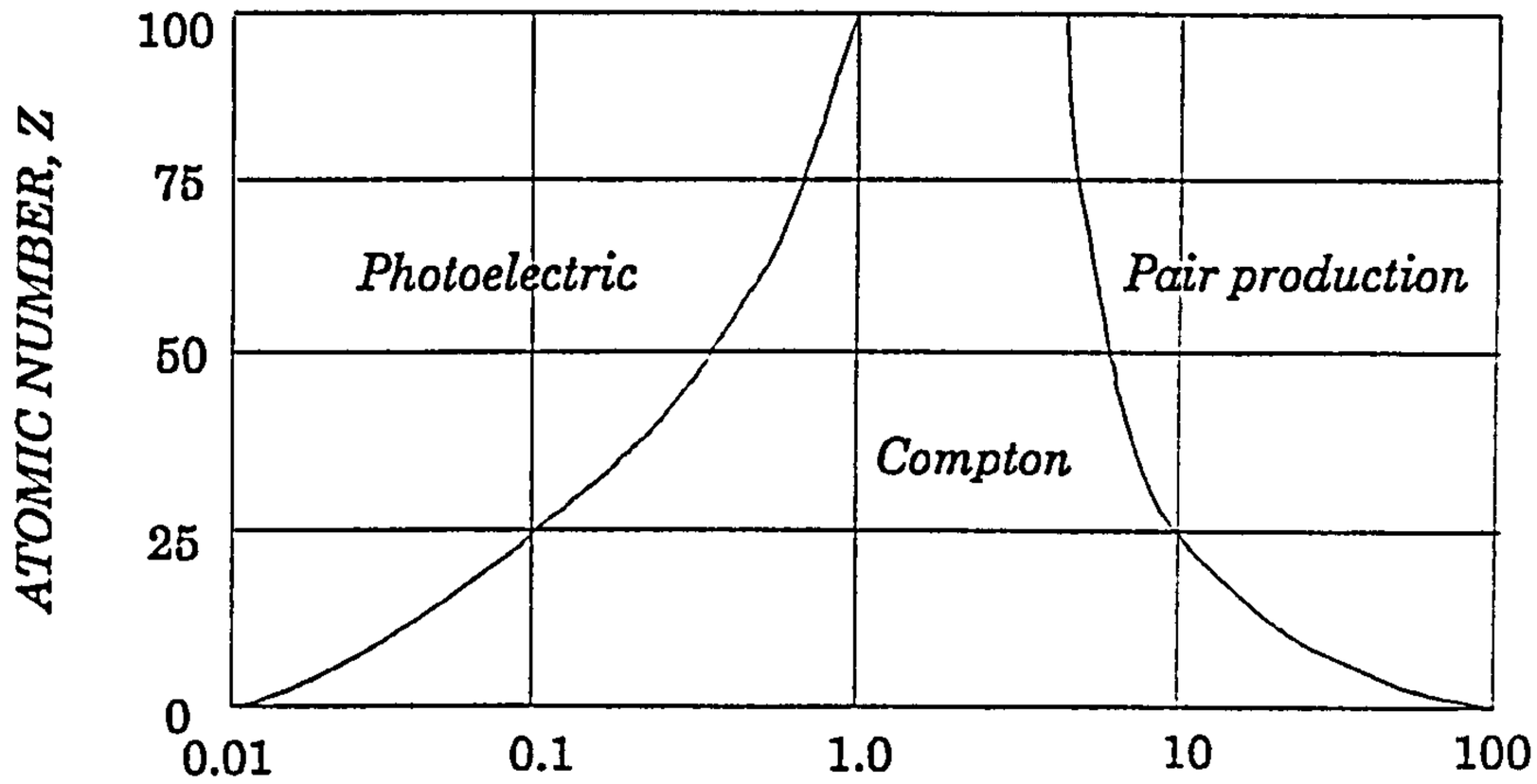

Figure 2.5 The predominating (most probable) interaction as a function of energy and atomic number (from Sorenson and Phelps 1987)

For spectroscopic work it is necessary to run the detector such that each quantum of radiation is recorded individually. For this purpose, the two most important parameters are energy resolution and efficiency, when choosing a detector.

2.2.2.1 Energy resolution

Energy resolution is determined by the fluctuations in the response of the detector to the incident radiation. These fluctuations are caused by drifts in operating characteristics of the detector, sources of random noise and statistical noise. The statistical contribution is the most important as it cannot be changed, however perfect the other two may be. It is caused by the variation in the number of ion pairs produced per incident photon. The associated statistics are Poissonian and therefore the shape of the associated photo peak is Gaussian. The limiting resolution is R where :

$$R = \frac{2.35}{\sqrt{N}} \qquad [2.2]$$

where N, the number of counts, has to be greater than 55,000 in order to achieve energy resolution better than 1%.

In reality R can be 3 to 4 times lower than calculated. This is because the events are not actually independent of each other and therefore are not governed exactly by Poissonian statistics. The difference between the calculated and measured statistics are defined by the Fano factor, F, where :

$$F = \frac{\text{observed variance}}{\text{poissonpredicted variance}} \qquad [2.3]$$

Therefore the real statistical limit is :

$$R_{min} = 2.35\sqrt{F/N} \qquad [2.4]$$

The overall energy resolution of the peak is determined by the sum of the statistical and electronic noise in the detector system :

$$(\Delta E)^2_{overall} = (\Delta E)^2_{statistical} + (\Delta E)^2_{electronic} \qquad [2.5]$$

where ΔE is the full width at half maximum (FWHM) of a peak at energy, E.

2.2.2.2 Efficiency

Efficiency can be defined in several different ways. The absolute efficiency is the ratio of number of quanta emitted by the source, to the number of pulses recorded. This is not just a characteristic of the detector, but is effected by the geometry of the whole system. The intrinsic efficiency is the efficiency of the detector itself and is defined as the number of pulses recorded over the number of quanta incident on the detector face. The intrinsic peak efficiency is the number of interactions depositing their full energy in the detector divided by the number of quanta incident on the detector. It is this intrinsic peak efficiency that is the most important when choosing a detector for this application since it measures the number of incident photons that are recorded in the multi-channel analyser within each peak.

There are three general types of radiation detector. These are gas filled, scintillation and solid state. Gas detectors are generally not efficient for high energy measurements as the density is not high and therefore the photons are not easily stopped. Scintillation detectors have better efficiency, but the energy resolution tends to be poor due to the statistical fluctuations that are associated with the conversions of gamma ray to light and light to electron. Solid state detectors are more efficient due to being denser and have lower statistical noise as there are many electron hole pairs produced per quanta of radiation. It is for these reasons that it was decided that a solid state detector would be the most suitable for this application. The following sections describe in more detail the principles of solid state detectors and reviews the major types available.

2.2.3 Semiconductor detectors

Semiconductor radiation detectors have been used since the early 1960's. Their advantages other than energy resolution are that they are compact in size, have fast timing characteristics and the effective thickness of the detector can be matched to the application. The band gap in a semiconducting material is generally ~1 eV, whereas in an insulator it is ~ 5 eV. This is shown schematically in figure 2.6. Electrons in the valence band are bound to specific sites in the crystal whereas those in the conduction band are free to migrate throughout the material. In a semiconducting material if an electron is elevated to the conduction band, by some mechanism, then it can freely flow. This can occur through absorption of thermal energy, but also an excitation process can elevate an electron to the conduction band and leave a hole in the valence band. Both the hole and the electron will move under the influence of an electric field.

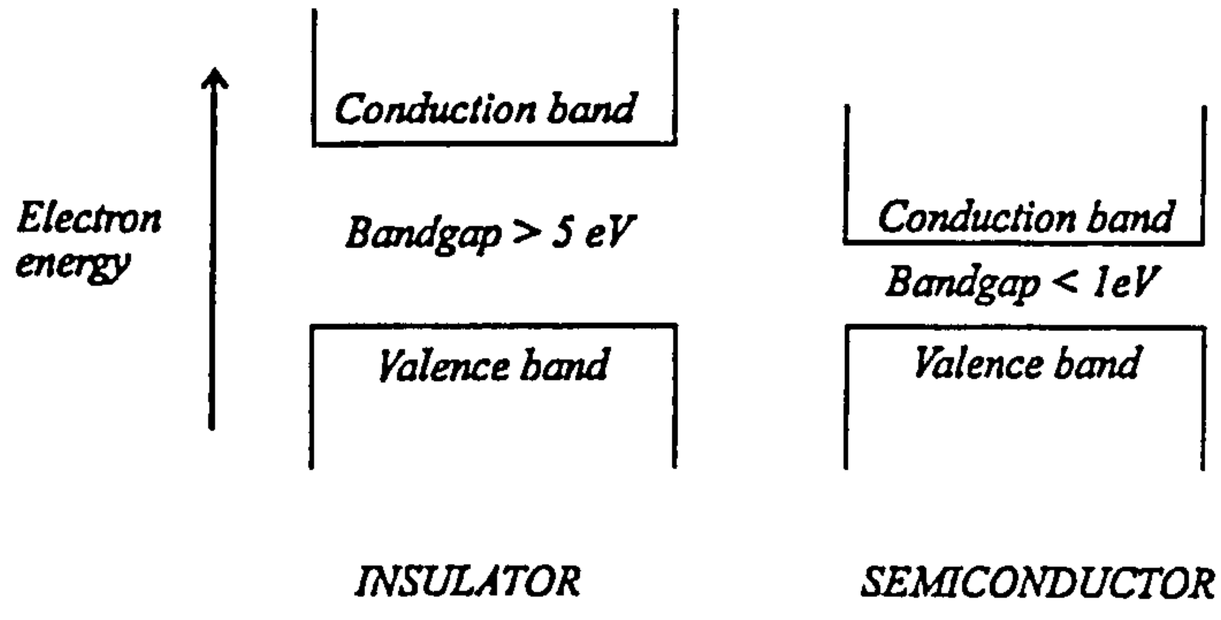

Figure 2.6 A schematic diagram of the conduction and valence bands in a semiconductor

The size of the band gap in a semiconductor determines the probability with which an electron can be elevated to the conduction band, thus a small gap will facilitate elevation. The probability per unit time that an electron-hole pair is thermally generated is :

$$p(T) = CT^{3/2} \exp\left(\frac{-E_g}{2kT}\right) \qquad [2.6]$$

where T = absolute temperature, E_g = band gap energy, k = Boltzmann's constant and C = constant for the material.

For semiconductors where the band gap at 300K is small, such as germanium (0.67 eV) and silicon (1.12 eV), cooling to 77K (liquid nitrogen temperature) reduces the probability of thermal excitation. This is why both these detectors are operated with a cryostatic cooling system. However, the advantage of these detectors is that the energy required per electron-hole pair is small, 2.96 eV for germanium and 3.76 eV for silicon. This means that because of the large number of electron-hole pairs produced, this provides low statistical noise in the measured signal.

However, the requirement of cryostatic cooling is both cumbersome and expensive and therefore there has been much interest in developing semiconducting materials with larger band gap energies that can therefore be used at room temperature. This is

because the larger bandgap means that there is less chance of thermal excitation and hence cooling is not required.

2.2.4 Room temperature semiconductor detectors

For a semiconductor to be used at room temperature for spectroscopy it must have a band gap that is large enough to minimise thermal noise yet small enough to permit good energy resolution (i.e. many electron-hole pairs are produced per interaction). The optimum value is 1.4-1.5 eV *(Armantrout et al. 1977)*. The material also needs a high atomic number to maximise the probability of photoelectric interaction. High charge carrier mobilities and long charge carrier lifetimes will also ensure good charge collection efficiency at the electrodes. The method of crystal growth should ensure high purity and homogeneity, with no defects and sufficient size for good intrinsic efficiency. The electrodes should introduce no defects, impurities or barriers to charge collection.

Over the last decade there has been much interest in improving the performance of room temperature semiconductor detectors. Most of the materials are binary compounds both with and without doping materials added and improvements have arisen because of the developments in crystal growth methods. Several materials have been investigated with varying levels of success. The materials that have not been so successful include CdSe, ZnTe, TlBr, AlSb, BiI_3 PbO, CdS and ZnSe *(Schieber et al. 1996b)*. The reason for these materials not being useful, even though in theory they should be, is due to crystal growth problems, stability over time and charge carrier trapping problems.

Trapping is caused by deep impurities or structural defects that introduce energy levels near the middle of the forbidden gap. These act as 'traps' for charge carriers, and are usually held for longer than the time period in which that carrier could contribute to the correct pulse. Other deep impurities can act as 'recombination centres', where an electron (or hole) is trapped and then another carrier recombines with it and that part of the signal is not collected. Recombination through trapping centres is more common

than direct recombination and both trapping and recombination contribute to the loss of charge carriers.

The trapping length is the average distance travelled before trapping occurs (see equation 2.7).

$$\tau = tv \qquad [2.7]$$

where τ is trapping length, t is mean life time and v is average drift velocity. Ideally the trapping length should be longer than the detector dimensions to minimise the effect.

The main detectors that have been proven to be usable at room temperature are GaAs, HgI_2, CdTe, $Cd_{1-x}Zn_xTe$ and PbI_2. These detectors are reviewed including a brief history. The characteristics, advantages and disadvantages, as applied to this application, are discussed. Table 2.1 shows the characteristic parameters for each of these detectors. (It should be noted that there is some variation in the published values due to differences in experimental set-up.) Those quoted in this table are intended to be representative of average values. Only the cost of the detector itself is quoted, as the electronics (amplifiers, ADC and software) would be much the same for each detector type.

	GaAs	HgI_2	CdTe	CdZnTe	PbI_2
Band gap (eV) [Ponpon and Siffert 1996]	1.42	2.1	1.47	1.68-2.1	2.3
Electron mobility ($cm^2V^{-1}s^{-1}$) @ 300K [Ponpon and Siffert 1996]	8500	100	1000	1000	8
Hole mobility ($cm^2V^{-1}s^{-1}$) @ 300K [Ponpon and Siffert 1996]	420	4	80	100	2
Electron lifetime (s) [Ponpon and Siffert 1996]	10^{-7}	10^{-7}	10^{-6}	10^{-6}	10^{-6}
Hole lifetime (s) [Ponpon and Siffert 1996]	10^{-7}	10^{-8}	10^{-6}	10^{-6}	10^{-6}
Electron mobility-lifetime product (cm^2V^{-1}) [calculated]	8.5×10^{-4}	1×10^{-5}	1×10^{-3}	1×10^{-3}	8×10^{-6}
Hole mobility-lifetime product (cm^2V^{-1}) [calculated]	4.2×10^{-5}	4×10^{-8}	8×10^{-5}	1×10^{-4}	2×10^{-6}
Density (gcm^{-3}) [Schlesinger et and James 1995]	5.35	6.4	6.2	6.0	6.2
Effective atomic number [Schieber et al. 1996b]	32	62	50	48	63
Resistivity (Ω cm) [Schieber et al. 1996b]	10^{8}	10^{13}	10^{9}	10^{11}	10^{12}
w value (eV)) [Ponpon and Siffert 1996]	4.3	4.15	4.4	5.0	4.9
Fano factor [Ponpon and Siffert 1996, Bertuccio et al. 1997b]	0.12	0.04-1	0.04-1	0.04-1	0.19-0.34
Energy resolution @ 59.5 keV(%) [Schlesinger and James 1995, Patt et al. 1996, Khusainov 1992, Parnham 1996b, Shah 1996],	20%	3%	5%	4%	9%
Energy resolution @ 122 keV(%) [Eberhardt et al. 1970, Iwanczyk et al. 1995, Richter and Siffert 1992, Hamilton et al. 1994]	2-3 %	1.64%	3.3%	1.64%	N/A
Maximum thickness available [EEV 1996, Eurorad 1996, eV Products 1996, Schlesinger and James 1995]	<200µm	1mm	10mm	10mm	500µm
Efficiency @ 70 keV [calculated] (Monte Carlo calculation) [Scannavini 1996]	14.5% (11%)	100%	100% (94%)	100% (94%)	26.5%
Cost of off-the-shelf detector ($) [EEV 1996, Eurorad 1996, eV Products 1996]	1000	2000	600	600	N/A

Table 2.1 A summary of the characteristics of promising room temperature semiconductor detectors

2.2.4.1 Gallium arsenide (GaAs)

Gallium arsenide is a semiconductor which has been considered as a radiation detector since the early 1960's *(Harding et al. 1960, Mayer 1962)*. It was the first detector to be considered as the best compromise for room temperature operation *(Dearnaley and Narthrop 1964)* and also to demonstrate good energy resolution *(Eberhardt et al. 1970)*. The average density and atomic number are similar to germanium (which is presently the most used semiconductor detector for spectroscopic studies).

The mobilities of the electrons and holes in gallium arsenide are very high (8000 $cm^2V^{-1}s^{-1}$; and 420 $cm^2V^{-1}s^{-1}$ respectively). This is somewhat off-set by the electron and hole lifetimes which are average (both 10^{-7}s). The observed lifetimes tend to be shorter than the theoretical ones (quoted above) because other mechanisms other than direct recombination assist in the recombination process. This is most likely to be due to a high density of trapping and recombination centres. It has been suggested that there is more trap assisted recombination than direct recombination *(McGregor and Kammerand 1995)*. It is still not known what causes these traps, but deep donor defects are thought to be the cause *(McGregor and Kammerand 1995)*.

The resisitivity of gallium arsenide ranges from 10^7 to 10^8 Ωcm. This limits the bias voltage that can be used, as a high bias voltage will cause the leakage current to increase. However a high bias is desirable as the velocity with which the electrons and holes reach their respective electrodes is dependent upon it.

One of the problems with gallium arsenide detectors is the growth methods. The epitaxy methods (grown in thin layers) are unable to grow crystals thicker than 200 μm and therefore are very inefficient. The bulk methods are able to grow larger crystals, but at present are very much inferior in quality. For good energy resolution the impurity concentrations would need to be reduced.

Currently there are very few applications of gallium arsenide detectors as there is much competition from other room temperature detectors. Most of the work is concentrated

on improvement of growth methods and reduction of impurities. It is hoped that gallium arsenide could be a replacement for silicon *(Bertuccio et al. 1997a)*. Work has also been carried out to improve the electrode contacts and this has led to the use of higher bias voltages and therefore better charge collection efficiency *(Nava et al. 1997)*.

2.2.4.2 Mercuric iodide (HgI_2)

Mercuric iodide was first used as a nuclear spectrometer in 1971 *(Willig 1971)*. It has a very high resistivity and therefore can be used at room temperature with a very low leakage current. The band gap is wide (2.3 eV) which means that the thermally generated noise is also low. These characteristics imply that mercuric iodide would be an excellent choice for a room temperature detector. However the electron and hole mobilities are low (100 $cm^2V^{-1}s^{-1}$; and 4 $cm^2V^{-1}s^{-1}$ respectively) and the lifetimes are short (10^{-7}s for an electron and 10^{-8}s for a hole). This means that the lifetime hole product is small and therefore the charge collection efficiency is reduced. This can be improved by using a high bias, which is allowed by the higher resistivity *(Bao et al. 1995)*.

The density (6.4 gcm^{-3}) and effective atomic numbers (62) are both high which means the probability of a photoelectric interaction is high and therefore these detectors have good intrinsic efficiency.

An ideal material for crystal growth should have high thermal conductivity, so that it melts and recrystallises quickly, with no solid phase transitions, so that the crystals formed have few defects. Unfortunately neither is true of mercuric iodide. It undergoes a destructive, solid state, phase transformation at 127° C and this prevents growing through solidification from its melting point at 250 °C *(Whited and Schieber 1979)*. The most commonly used growth methods are vapour phase growth and seeded growth *(Burger et al. 1995)*. However the crystals that are grown are very fragile and can be easily damaged during detector fabrication. This, and the fact that the growth yield is low means that mercuric iodide is an expensive detector.

Applications of mercuric iodide detectors have included fluorescence analysis, detectors for use in space and synchrotron radiation detection *(Ponpon and Siffert 1996)*. They have also been used for several medical imaging applications such as arrays for breast imaging *(Tornai et al. 1997)* and gamma cameras *(Patt et al. 1997)*.

These detectors have also been used for energy dispersive X-ray diffraction measurements of sugar and salt *(Iwanczyk et al. 1995)*. Detectors of 5 x 5 mm and of less than 500µm thickness were used. The detectors were cooled by a peltier cooler and thus achieved an energy resolution of 1.1% at 59.5 keV. The coherent scatter results were taken for both mercuric iodide and germanium detectors and the results from the two detectors were similar.

2.2.4.3 Cadmium telluride (CdTe)

Cadmium telluride was suggested as a possible semiconductor detector by De Nobel and Kroeger *(1962)* and it was first developed as a room temperature detector in 1967 *(Akutagawa et al. 1967)*. The electron and hole mobilities are average (1000 $cm^2V^{-1}s^{-1}$; and 80 $cm^2V^{-1}s^{-1}$respectively), but the lifetimes are relatively long (10^{-6}s for both electrons and holes). This gives cadmium telluride a very good mobility-lifetime product for both electrons and holes (0.01 cm^2V^{-1} for electrons and 8 x 10^{-5} cm^2V^{-1} for holes). Density is high (6.2 gcm^{-3}) and effective atomic number is good (50) which gives a high probability for photoelectric interactions.

Growing crystals with low levels of impurities is again a difficulty, but the crystals are stable and rugged and are more readily available than mercuric iodide. However there are problems due to polarisation after long periods of irradiation. This is caused by long term trapping at deep levels (i.e. mid gap) and is probably due to doubly charged cadmium vacancies *(Hage-Ali and Siffert 1992)*.

There has been much work carried out to improve the energy resolution of cadmium telluride. This has included hemispherical detector shapes for single carrier collection *(Richter and Siffert 1992)* and cooling with thermoelectric coolers. However there is

disagreement as to whether cooling below 0° C is beneficial *(Khusainov 1992)* or not *(Dusi et al. 1995, Chirco et al. 1996)*. There has also been research into pulse shape discrimination and pulse shape compensation *(Jones and Woollam 1975, Niemela 1996a and b)*. Significant improvements have also been made by alloying with zinc telluride. This is discussed in detail in section 2.2.4.4.

Applications of cadmium telluride detectors have been many-fold. In the medical field there has been use in nuclear medicine such as gamma cameras and cameras for positron emission tomography *(Scheiber and Chambron 1992, Eisen et al. 1996)*, surgical probes *(Entine et al. 1989, Squillante and Entine 1992, Hage-Ali et al. 1996)* and bone densiometry equipment *(Entine et al. 1989, Scheiber and Chambron 1992)*. In industrial applications there has been nuclear materials characterisation *(Entine et al. 1989, Arlt et al. 1992)*, back scatter measurements and X-ray fluoroscopy *(Squillante and Entine 1992)*.

2.2.4.4 Cadmium zinc telluride ($Cd_{1-x}Zn_xTe$)

The first cadmium zinc telluride spectrometers were produced in the early 1990's *(Doty et al. 1992, Butler et al. 1992)*. Since then much of the effort previously put into cadmium telluride has been transferred to cadmium zinc telluride. Adding zinc telluride to cadmium telluride forms an alloy of cadmium zinc telluride. This has the effect of lowering the levels of lattice defects, increasing the band gap (1.68-2.1 eV, depending on the amount of zinc) and increasing the resistivity (~10^{11} Ωcm). The reduction in lattice defects means that the hole mobility is improved (100 $cm^2V^{-1}s^{-1}$) and consequently the hole mobility-lifetime product is also improved (10^{-4} cm^2V^{-1}). The increased band gap reduces the thermally created noise and the increased resistivity reduces the leakage current. The increased resistivity means that higher bias voltages can be used and therefore the charge collection efficiency is improved.

Crystals of cadmium zinc telluride can be grown larger and at a reduced cost than that of cadmium telluride *(James et al. 1995)* and methods used for crystal growth include the high pressure Bridgman method. Cadmium zinc telluride does not appear to show

any short term polarisation effects *(Butler et al. 1992)* although the recent development of these detectors means that long term effects have not yet been assessed.

Cooling has also been carried out and the results appear to show a consistently improved energy resolution performance *(Niemela et al. 1996a, Parnham 1996b)*. Pulse shape discrimination using $Cd_{1-x}Zn_xTe$ improves the tailing effect by rejecting incomplete charge pulses *(Hess et al. 1994, Lund et al. 1996a)*.

Applications of cadmium zinc telluride are increasing and in some cases taking over from cadmium telluride. Medical applications include arrays for gamma cameras *(Barber 1996, Scheiber and Chambron 1996)*, detectors for high energy tomography *(Rossi et al. 1996)* and probes for radioactive tracers *(Lorenz et al. 1994)*. Industrial applications include ^{235}U enrichment measurements *(Ruhter and Gunnick 1994, Lavietes et al. 1996)*, atomic number discriminating baggage scanning *(Eisen 1996)* and submillimetre resolution spectrometers *(Mayer et al. 1997)*.

2.2.4.5 Lead iodide (PbI_2)

Lead iodide has been under investigation since the 1970's as a semiconductor detector *(Roth and Willig 1971, Manfredotti et al. 1977)*. There are several characteristics that make it attractive for use as a room temperature detector. The band gap is 2.3 eV and the resistivity is very high at 10^{13} Ω cm, the electron and hole lifetimes are also good (both 10^{-6}s). However there are also characteristics which cause some severe problems, such as the mobilities of the electrons and holes which are very slow (8 $cm^2V^{-1}s^{-1}$; and 2 $cm^2V^{-1}s^{-1}$ respectively).

There are also problems with crystal growth. The crystal is made of layers of Pb-I-Pb. The van der Waals bonds between these layers are very weak and therefore the crystals are very delicate. The thicknesses of the crystals are therefore limited to 0.5 mm *(Lund et al. 1995)* and although the material is of high density with high atomic number, this lack of thickness results in poor efficiency.

Lead iodide is very similar to mercuric iodide, but it does have some advantages including higher thermal and chemical stability, a wider band gap and no destructive phase transition when cooling *(Deich and Roth 1996)*.

The applications are limited due to the difficulties in building the detectors and the poor energy resolution. However lead iodide has been suggested as a detector for applications where energy resolution is not required such as high energy imaging requirements *(Lund et al. 1995)*. There has also been an investigation into the use of detectors at high temperatures and lead iodide had been found to function well up to 100 °C *(Shah et al. 1997)*.

2.2.4.6 Which room temperature detector would be suitable?

The requirements stated for the choice of detector were that the energy resolution should be the best that could be achieved, with 100% intrinsic efficiency at 70 keV, and should be easy to use, rugged and small in size. It was decided that the most suitable detector for the application of a multiple angle coherent scatter system for the identification of explosives in baggage was cadmium zinc telluride. This is because it has the best quoted energy resolution (~4% at 60 keV, although in reality it is likely to be larger than this value, see section 3.2.3) for a robust and stable detector, a size of up to 10 mm^3, an intrinsic efficiency of almost 100% at 70 keV, a cost of ~$600 per detector and is easily available. Mercuric iodide has been used for energy dispersive X-ray diffraction measurements *(Iwanczyk et al. 1995)*, but it is more expensive than cadmium zinc telluride ($2000 compared with $600), has a maximum thickness of 1 mm and the crystal is quite delicate. Therefore cadmium zinc telluride was determined to be the best choice.

It was calculated that to obtain 100% efficiency for energies up to 70 keV a cadmium zinc telluride detector of 2 mm thickness would be required. The thickness should not be any greater than required as charge trapping effects are worse in a thicker detector. The efficiency was calculated by using XCOM *(Berger and Hubbell 1987)* to provide

the linear attenuation properties of cadmium zinc telluride. If the incident intensity is assumed to be unity then the transmitted intensity can be calculated (see equation 2.8).

$$I = I_0 e^{-\mu x} \qquad [2.8]$$

where I is the transmitted intensity, I_0 is the incident intensity, μ is the linear attenuation coefficient and x is the thickness of the detector crystal. The efficiency has been calculated as:

$$\text{Efficiency} = \left(1 - \frac{I}{I_0}\right) x100\% \qquad [2.9]$$

where I_0 is given the nominal value of 1. The transmitted intensity is 0.2% of the incident intensity at 70 keV, see figure 2.7.

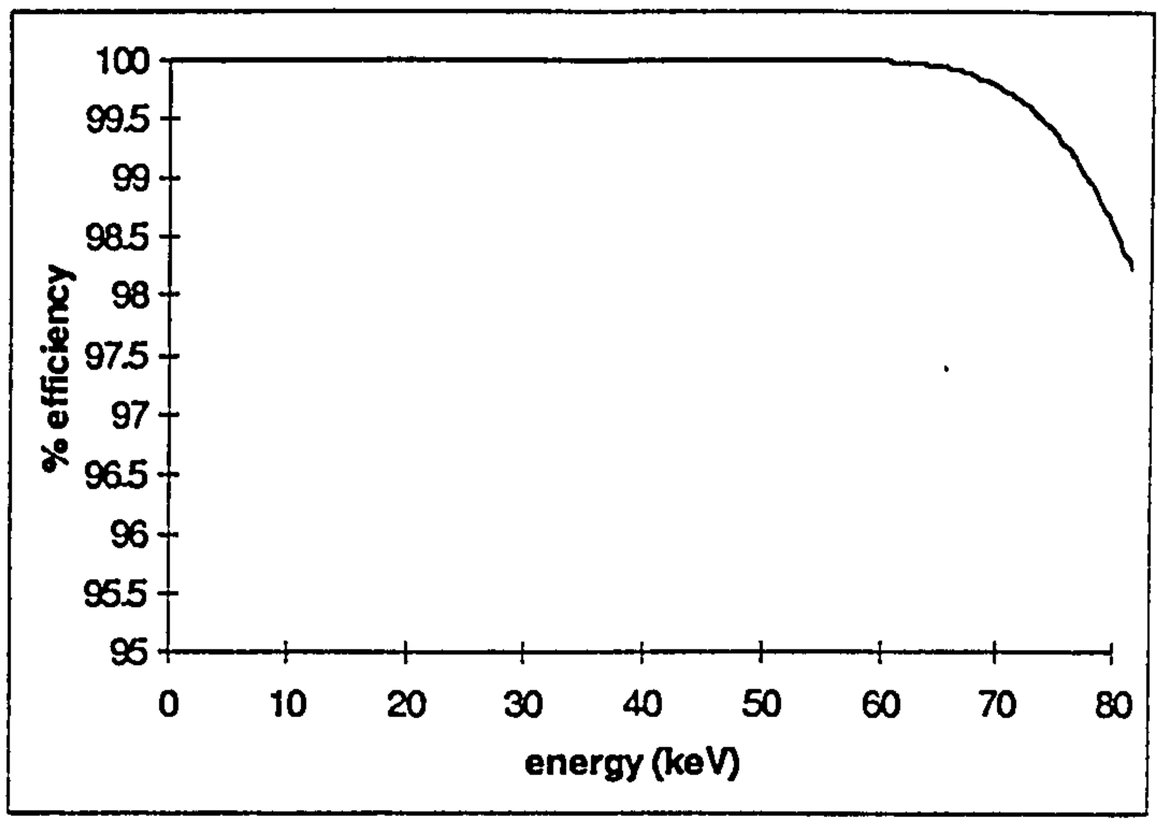

Figure 2.7 The intrinsic efficiency of a 2 mm cadmium zinc telluride crystal in the energy range 0 to 80 keV (calculations made from data from XCOM (Berger and Hubbell 1987)).

2.3 A model of a coherent scatter system

There are several reasons why a model or computer simulation can be useful. Various parameters that affect a result can be changed in a model without having to design and carry out many different experiments. A model can often produce results much more quickly than an experiment and also can simulate equipment that is not available or which would be very expensive to make available. A model can also be used to investigate the effect of individual parameters which may not be possible in an experiment. However a model usually has limitations as well. For any system other than the most basic there are often simplifications and therefore a model is rarely perfect. The performance of the model will need to be confirmed by experimental measurements.

The primary purpose in using this model was to investigate the characteristics needed for a multiple angle coherent scatter system suitable for use with cadmium zinc telluride detectors before they were available. This choice of detector affects the geometry of the scatter system and thus the geometrical variations of the collimators have been considered. The model also allowed the number of detectors required for a multiple angle system to be determined, by simulating energy dispersive scatter signatures from a range of angles and considering them together as in various numbers (e.g. 5 or 10 scatter signatures together).

The model also aided an investigation into the effects of the orientation of the crystals within the sample of SX2 on energy dispersive and angular dispersive measurements.

2.3.1 Description of the model

An existing model of a coherent scatter system (*Farquharson 1996)* was used to simulate a multiple angle system. The model was used to predict the diffraction profile for SX2 for a range of angles and collimation geometries. The model is divided into six parts, each of which take into account either a physical or systematic effect. These are:

- Polyenergetic incident spectrum
- Blurring effects of the collimators due to their acceptance angle
- Coherent cross-section probabilities
- Photon attenuation of the sample material
- Energy resolution of the detector
- Inclusion of Compton scatter

The program used the measured diffraction data (from section 2.1) which was then corrected for the different effects, listed above. Use of this model allowed variations of geometries to be considered whilst taking into account the effects of the rest of the system and the material being investigated.

2.3.2 Validation of the model

Before using the model, the model must be validated against experimental results. The model can then be used to determine the limits of the required parameters within a multiple angle system.

The material used to evaluate the model was SX2. Scatter signatures were measured from the SX2 with a coherent scatter system (which is described in section 1.6.1), with a germanium detector used for the high and symmetrical energy resolution. This energy resolution was used so as to ensure that the modelling of the effect of the geometry of the system was correct. The collimation consisted of slits with widths of 1 mm and length of 150 mm (0.38° acceptance angle in the horizontal plane). This collimation was chosen to ensure that the angular blurring was the dominant blurring function so that it could be assessed in the model. Scatter signatures were taken over a range of angles from 3° to 7° in intervals of 1°. The incident spectrum was 70 kV_p with tube current of 20 mA. The measurement time was 100s. Figure 2.8 shows scatter signatures from a range of scatter angles for SX2. This explosive was in a sheet form of 3 mm thickness and was positioned perpendicularly to the incident beam, i.e. measured through the smallest dimension.

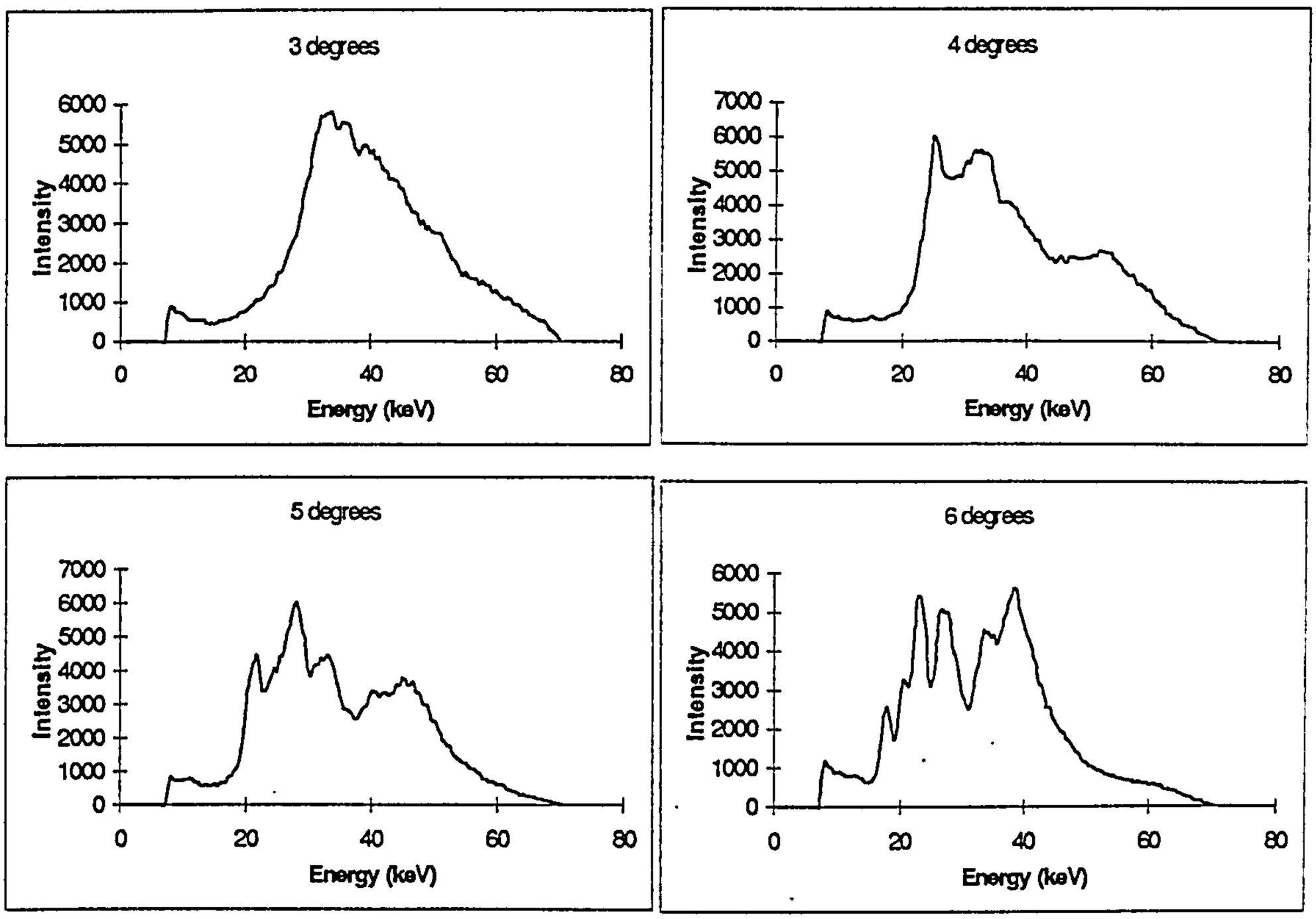

Figure 2.8 Scatter signatures for a range of angles for a 3 mm sample of SX2 with the 0.38° collimation, measured with a germanium detector on an energy dispersive system.

From these experimental results of SX2 it can be seen that the diffraction peaks occur at a lower energy for the higher scatter angles, as expected from the Bragg equation. A higher angle will satisfy a higher wavelength and hence a lower energy, for a given planar spacing. The angular blurring function is a fixed proportion of the energy of a given peak *(Luggar et al. 1996b)* and hence is less at lower energies. Thus, the effect of angular blurring is less at higher angles. It can be seen in figure 2.8 that the scatter

signatures for 6° and 7° have better resolved peaks than for the lower angles. The general shape of the polyenergetic incident spectrum can also be seen.

2.3.2.1 The effect of orientation of the sample

The angle at which the sheet of explosive was placed to the incident beam had a strong effect on the scatter signature. This effect was measured at 90°, 67.5°, 45°, 22.5° and 0° to the incident beam, as shown in figure 2.9. The sample used was a 3 mm thick piece of SX2 at 5° scatter angle. The collimation had an acceptance angle of 0.38°. Figure 2.10 shows the scatter signature results from this investigation.

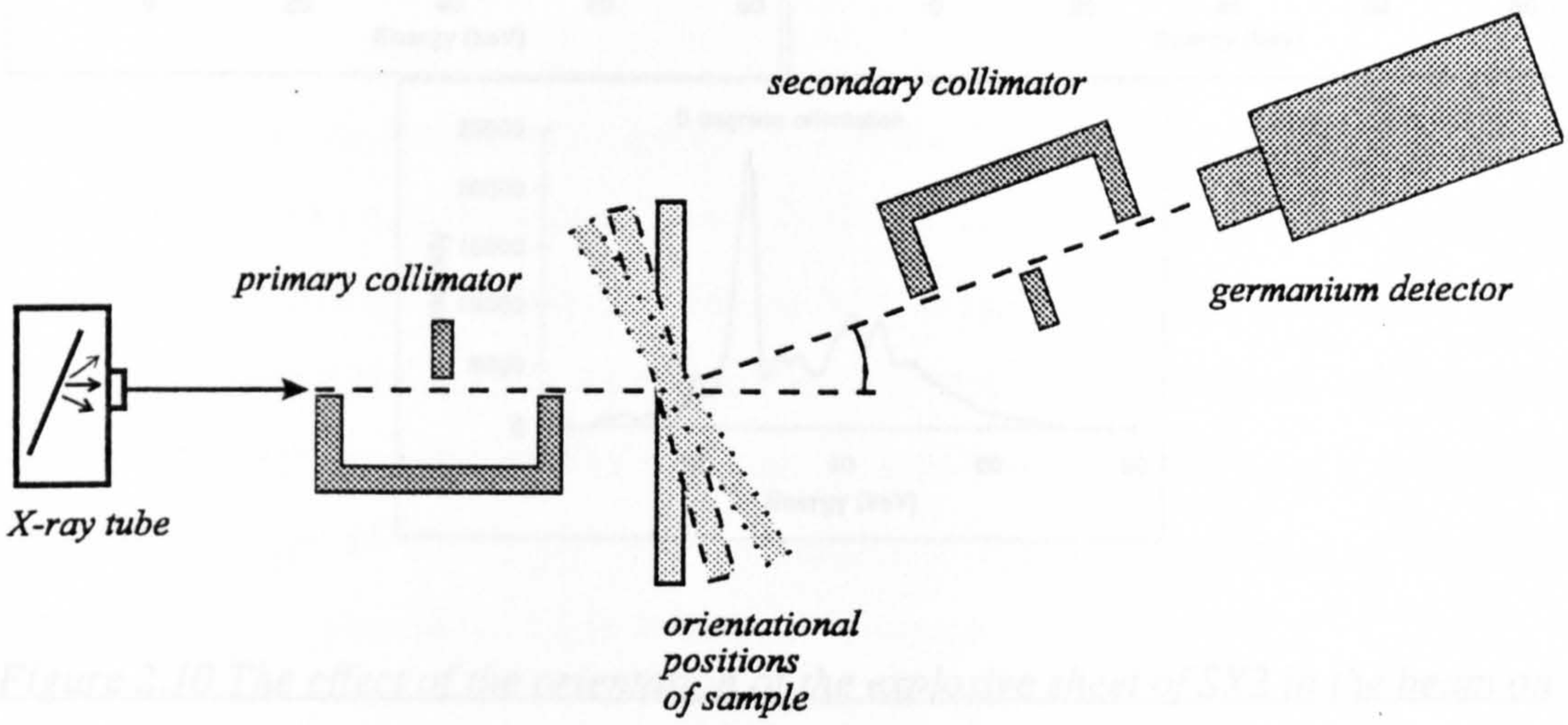

Figure 2.9 Diagram of the different orientational positions of the sheet of explosive within the beam

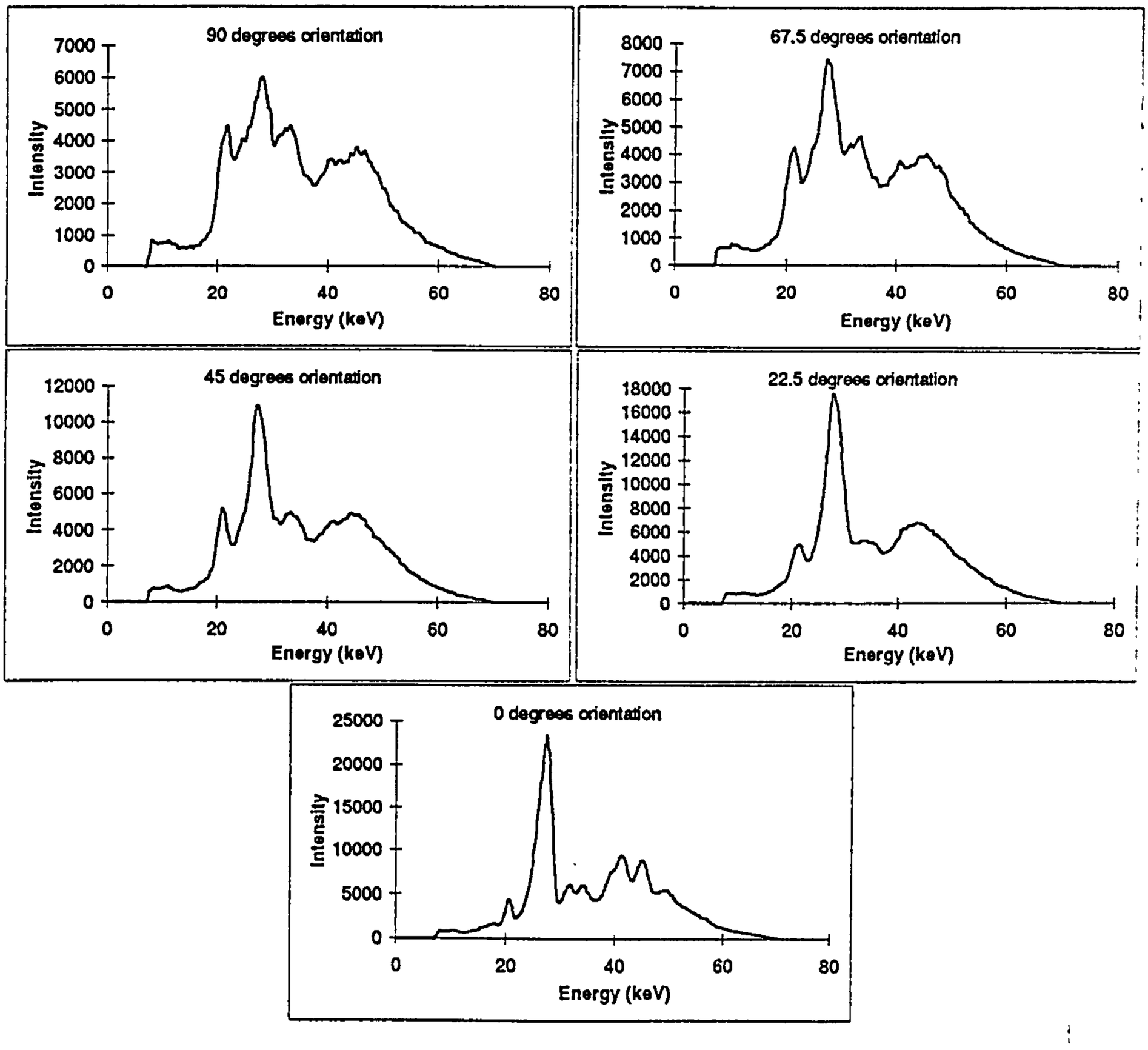

Figure 2.10 The effect of the orientation of the explosive sheet of SX2 in the beam on the scatter signature

The effect of changing the angle at which the sheet explosive is placed to the incident beam, is that the intensities of the peaks vary. The reasons for these variations in intensity within the signatures are as follows. Energy dispersive X-ray diffraction relies on the random orientation of the planar spacings within the sample such that all planar spacings are investigated *(Giessen and Gordon 1968)*. The method of manufacture of the crystals for this explosive forms the crystals into plate shapes. The rolling out process, to form sheets of the explosive, causes these crystals to align rather like in slate *(Royal Ordnance, ICI 1997)*. This alignment means that the crystals are no longer randomly orientated in the sample and hence there are some preferential orientations. Consequently, certain planes are preferentially orientated such that they give rise to

stronger intensities than they otherwise would. Likewise, other planes produce weaker intensities than in a random orientation. It can be seen in figure 2.10 that the peaks do not move in position (i.e. along the energy axis) but that the intensities vary considerably as the explosive sheet is rotated within the beam. This alignment of the crystals has been noted by Royal Ordnance in their speed of detonation experiments *(Brett et al. 1986)*. A second, less important, reason for the change in intensity is that in rotating the sample, the thickness through which the beam must pass increases and thus the effect of attenuation increases. Therefore the peaks at lower energies suffer a reduction in intensity.

2.3.3 Comparison of the modelled and experimental results

The model was run for the same parameters as for the experimental results in figure 2.10. It was found that the closest match between the model and the experiment was when the sheet of explosive has been turned to an angle of 22.5° to the incident beam. Figure 2.11 shows the modelled and experimental results for a range of scatter angles from 3° to 7° for a sample of SX2 using an incident beam of 70 kV_p and a collimation acceptance angle of 0.38°, for 22.5° orientation. The experimental and modelled results have been plotted on the same axis for each angle.

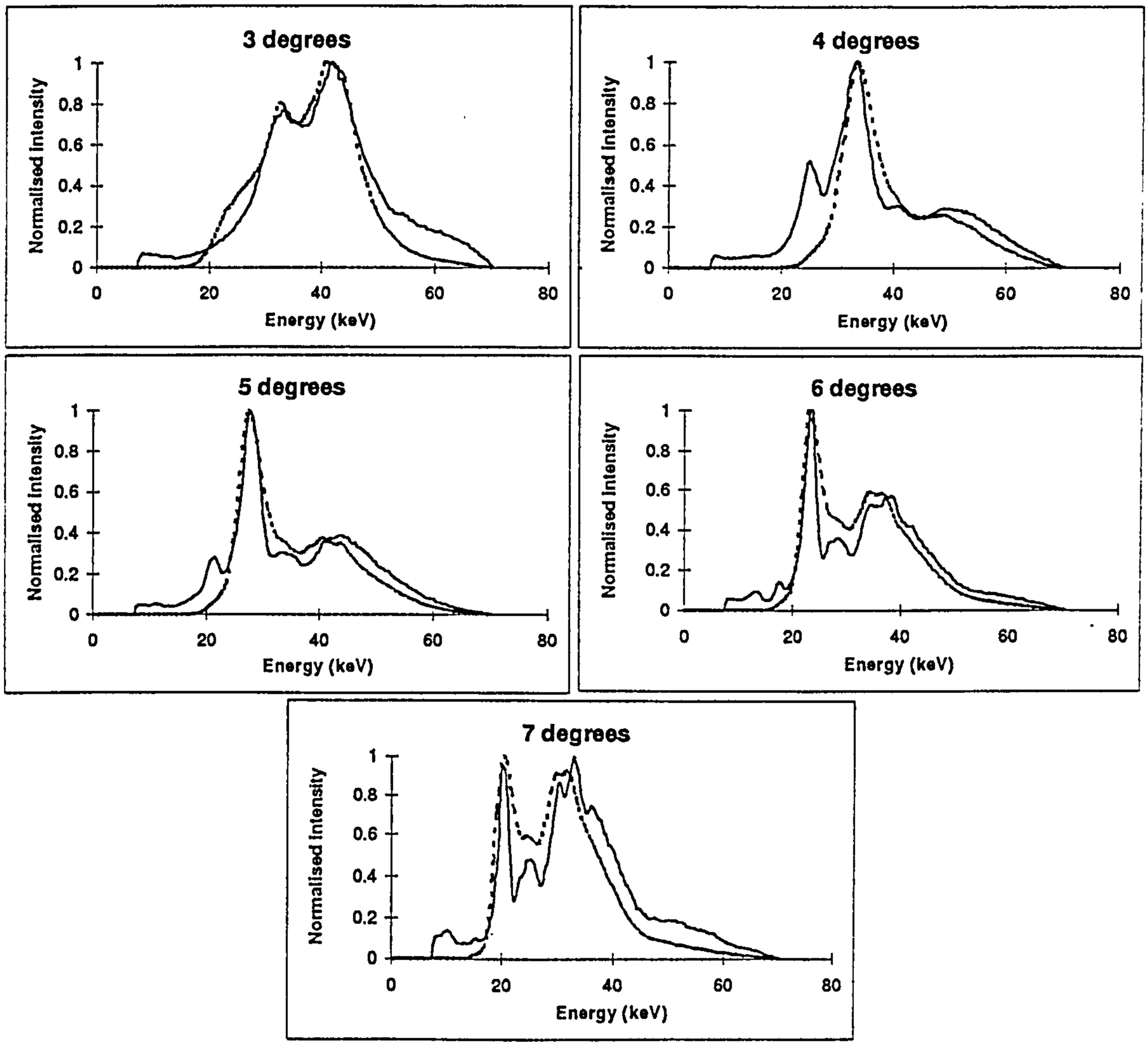

Figure 2.11 Comparison of model and experiment (at 22.5° orientation to the incident beam) for SX2 with 0.38° collimation (model is dotted line, experiment is solid line)

It is suggested that at this angle the sheet is most similar in position, in relation to the X-ray beam, to the standard diffraction measurements (see figure 2.12). That is, as the sample does not have random orientation (as is required both by energy dispersive and standard diffraction measurements), the preferential orientations appear to be the same in both types of measurement. The diffractometer measurement were made at angles of 6° to 36°, with the median being 21°. This matches best with the energy dispersive scatter measurements taken at 22.5°.

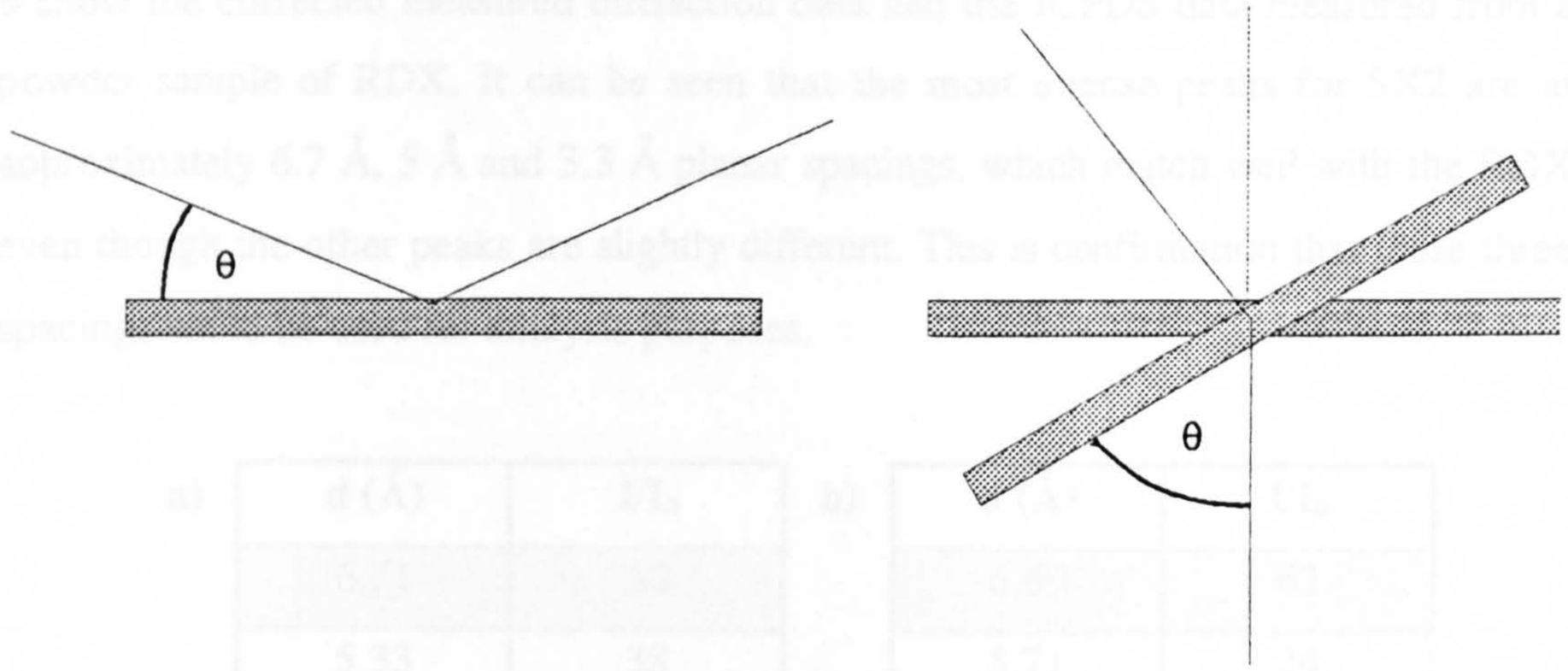

Standard diffractometer *Energy dispersive*

Figure 2.12 The orientational angles in the standard diffractometer (Philips X'pert) and the energy dispersive measurements

It is not known what the orientation of an explosive within a case might be, however parallel to the side of the case (i.e. 90° orientation) is most probable *(Lacey 1996)*, and is the orientation used in this work. Therefore the model was required to simulate this orientation. However the measurement of the diffraction data with the diffractometer meant that the intensities match the orientation of 22.5° the best.

To model the spectra more realistically an empirical method was used to correct the intensities of the measured standard diffraction data such that they predicted those of the 90° orientation in the energy dispersive system. This was achieved by calculating the ratio of each of the peaks, from the experimental data at 22.5° and 90°, and applying it to the diffraction data used to run the model. Although the peaks in the experimental spectra are blurred and the intensities already affected by attenuation and coherent scatter probability, this correction method gives a good approximation.

The effect of correcting the intensities for the orientational effect is that they became more like the powdered RDX data published by JCPDS. Hence the energy dispersive measurement taken at 90° orientation produced diffraction intensities closer to those from a random sample than the standard diffractometer measurements. Table 2.2 a and

b show the corrected measured diffraction data and the JCPDS data measured from a powder sample of RDX. It can be seen that the most intense peaks for SX2 are at approximately 6.7 Å, 5 Å and 3.3 Å planar spacings, which match well with the RDX even though the other peaks are slightly different. This is confirmation that these three spacings could be used for analysis purposes.

a)

d (Å)	I/I_0
6.71	58
5.33	38
5.08	15
4.94	77
4.34	35
4.02	13
3.50	42
3.30	100
3.03	46
2.76	15
2.68	12
2.42	11

b)

d (Å)	I/I_0
6.69	62
5.71	24
5.37	13
5.01	68
4.35	40
4.16	13
4.02	29
3.77	13
3.51	42
3.30	50
3.03	100
2.93	26
2.87	16
2.76	54
2.69	20
2.55	36
2.43	20
2.36	17

Table 2.2 a the measured and corrected SX2 data and b the JCPDS data for RDX

Figure 2.13 shows the modelled and experimental results for the same range of scatter angles as for figure 2.12, but with 90° orientation. The modelled results were run with the corrected diffraction data.

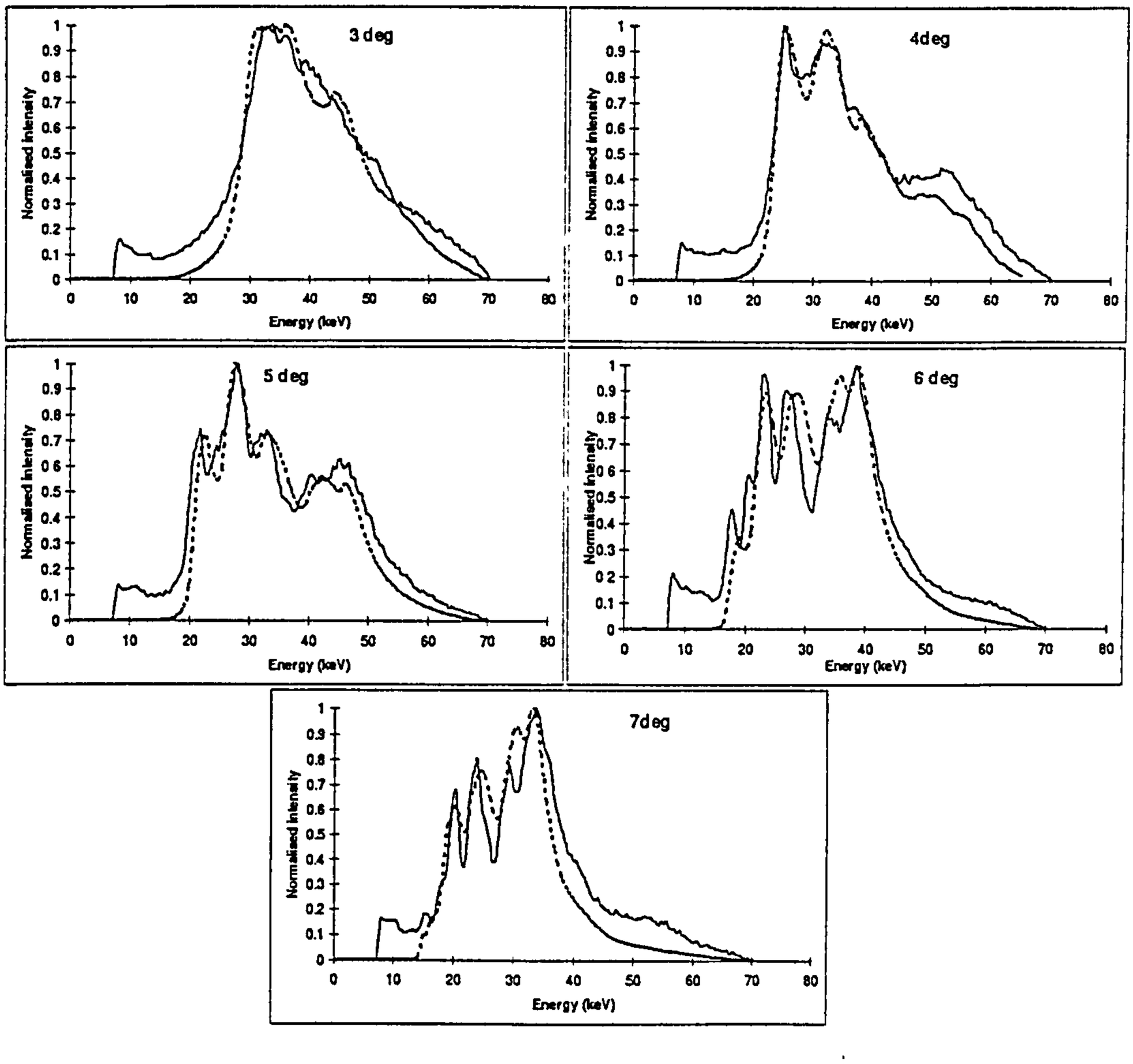

Figure 2.13 Comparison of model and experiment (corrected for 90° orientation to the incident beam) for SX2 with 0.38° collimation (model is dotted line, experiment is solid line)

A comparison was carried out between the model and the experiment based on peak positions, widths and intensities. The positions of the peaks are due to the diffraction data used and the scatter angle. The intensities are affected by the diffraction data, the coherent scatter cross-section, the amount of attenuation and the shape of the incident spectrum. The widths are governed by the angular blurring and energy resolution. Table 2.3 gives a summary of the comparison for each scatter angle and for each aspect. The 'main peak' is defined as the peak with the greatest intensity which has been normalised to 1 in figure 2.13. Thus the 'second peak' is the second most intense peak. The peaks are, in general, too close to calculate the full width at half maximum and therefore the width is given as full width at three-quarter maximum (FWTQM).

Angle (°)	Position (energy axis)	Width (energy axis)	Intensity (normalised)
3	Main peak 0.7 keV apart	Main peaks match well, but too wide to calculate FWTQM	Ratio of intensities of main to second peak 0.99 for model and 0.95 for experiment
4	Main peak 0.3 keV apart, second peak 0.5 keV apart	Main peaks match well, but too wide to calculate FWTQM	Ratio of main to second peak 0.98 for model and 0.94 for experiment
5	Main peak 0.4 keV apart second peak 2.5 keV apart	Main peak 12.9% model, 14.3% experiment, second peak 13.7% and 12.3%	Ratio of main to second peak 0.72 for model and 0.73 for experiment
6	Main peak 0.5 keV apart, second 0.4 keV, others up to 4 keV	Main peak too wide, second peak 12.4% experiment, 17.2% model	Ratio of main to second peak 0.90 for model and 0.95 for experiment
7	Main peaks 0.4 keV apart, second 3 keV, others within 3 keV	Main peak too wide, second peak 9.3% experiment, 17.8% model	Ratio of main to second peak 0.76 for model and 0.81 for experiment

Table 2.3 A summary of the comparison between the experimental and modelled results for 90° orientation.

In comparing the model and experiment the widths of the peaks are the most important since it is the energy resolution and angular blurring which dominate the ability to distinguish the peaks and hence identify the materials. To summarise table 2.3, in comparing the experiment and model, the main peak positions are within 0.7 keV and others within 4 keV of each other, the measurable widths are all within 8.5% and the ratio of main to second peak is within 5%.

The requirement of this model is that it provides information on collimation and number of scatter angles. The peaks which have been determined to be useful for analysis are for planar spacings of 3.3 Å, 5 Å and 6.7 Å. Although the widths are not identical in all the spectra, the model is neither consistently narrower or wider than the experiment. All of the peaks of interest can be distinguished in both the model and the experiment for scatter angles of 4° to 7° and therefore the model has been used further to investigate geometry and number of scatter angles.

2.4 Determining the tolerance of geometry and number of detectors

The aim of this model was to aid in the design of a multiple angle coherent scatter system with cadmium zinc telluride detectors. The model was used to determine the limit of the geometry of the collimation system to match the detectors. It was used in two ways, to vary the acceptance angles of the collimators and to vary the number of angles to be collected simultaneously. Worsening the energy resolution (from a germanium detector to a cadmium zinc telluride detector) has the effect of increasing the blurring of the peaks in the scatter signatures. A large acceptance angle of a collimator also blurs the peaks. However, the advantage of increasing the acceptance angle is that the number of photons passing through the collimators per unit time is increased. Thus a compromise must be sought between the energy resolution of 4% for the cadmium zinc telluride detectors and collimator acceptance angle, such that the blurring is tolerable with the best achievable photon rate.

2.4.1 The effect of increased acceptance angle

The model was used with an energy resolution of 4% to simulate the cadmium zinc telluride detector and was run for a range of collimation acceptance angles from 0.19° to 1.52°. Figure 2.14 shows these for a scatter angle of 5° for SX2.

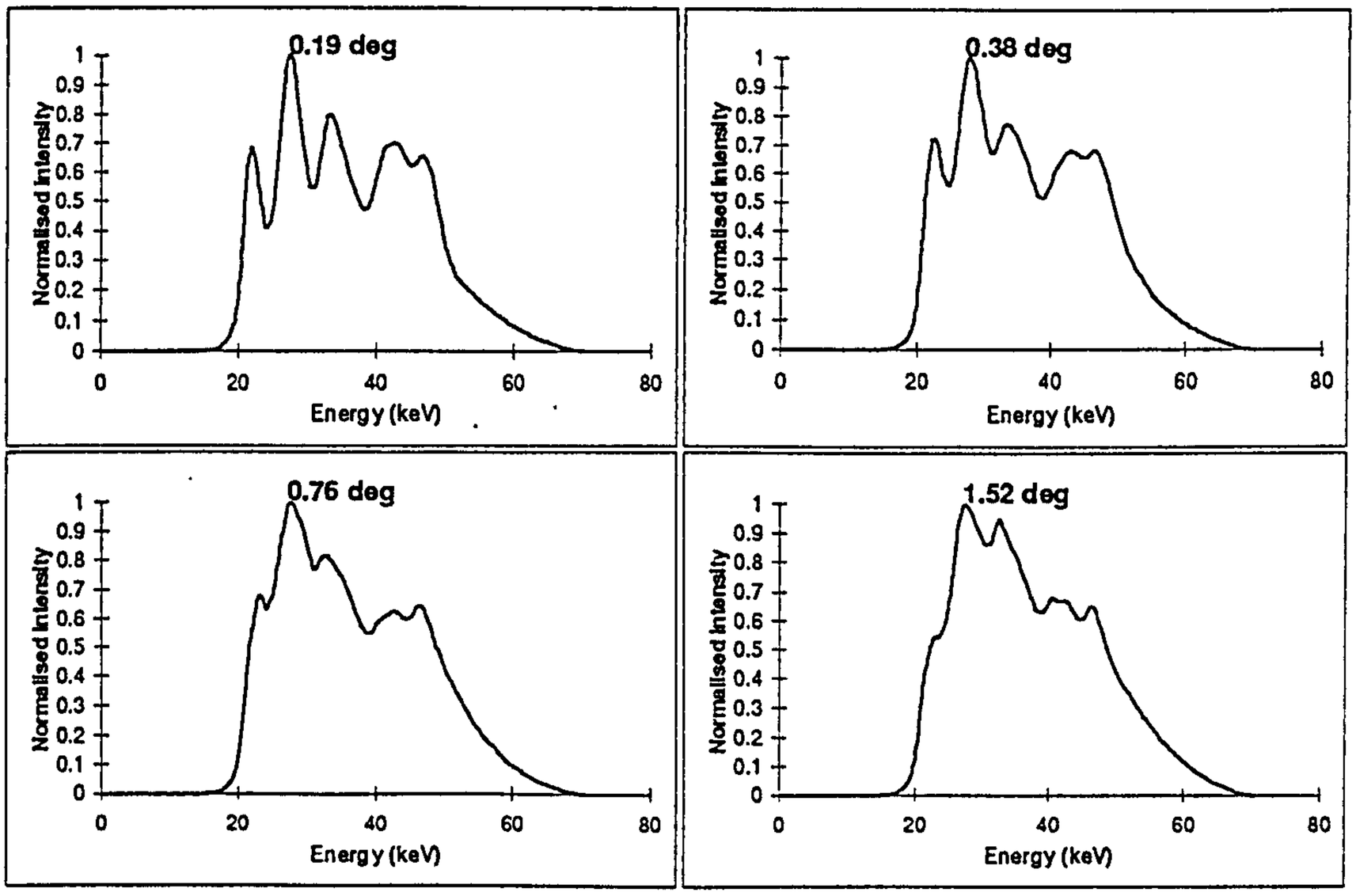

Figure 2.14 The effect of various acceptance angles for 4% energy resolution for SX2 measured at 5° scatter angle

The three peaks (3.3 Å, 5 Å and 6.7 Å at 21 keV, 28 keV and 43 keV respectively) can be seen for 0.19° and 0.38° and at 0.76° there is still a 5% difference between each peak and adjacent trough. However, at greater acceptance angles (1.52°) the peaks are no longer identifiable. Therefore it is concluded that the range of collimation used with a cadmium zinc telluride detector should have an acceptance angle of no greater than 0.76°.

2.4.2 An ideal energy-angle diagram

The scatter signatures from the multiple angle coherent scatter system have been displayed in the form of an energy-angle diagram. This is a three dimensional plot where two axes represent energy, scatter angle and intensity is shown by a grey scale. It is essentially a set of scatter signatures, such as have been shown in previous diagrams, placed together in order of scatter angle. The advantage of such a plot is that information from all the angles used can be considered together. This plot is viewed from above the energy and scatter angle plane and the intensity axis is represented as a grey scale.

Figure 2.15 shows an energy-angle plot for SX2 that has been modelled for a system with perfect energy resolution and collimation i.e. it is an ideal system. It can be seen from this plot that the lines corresponding to individual planar spacings are satisfied by a range of angles.

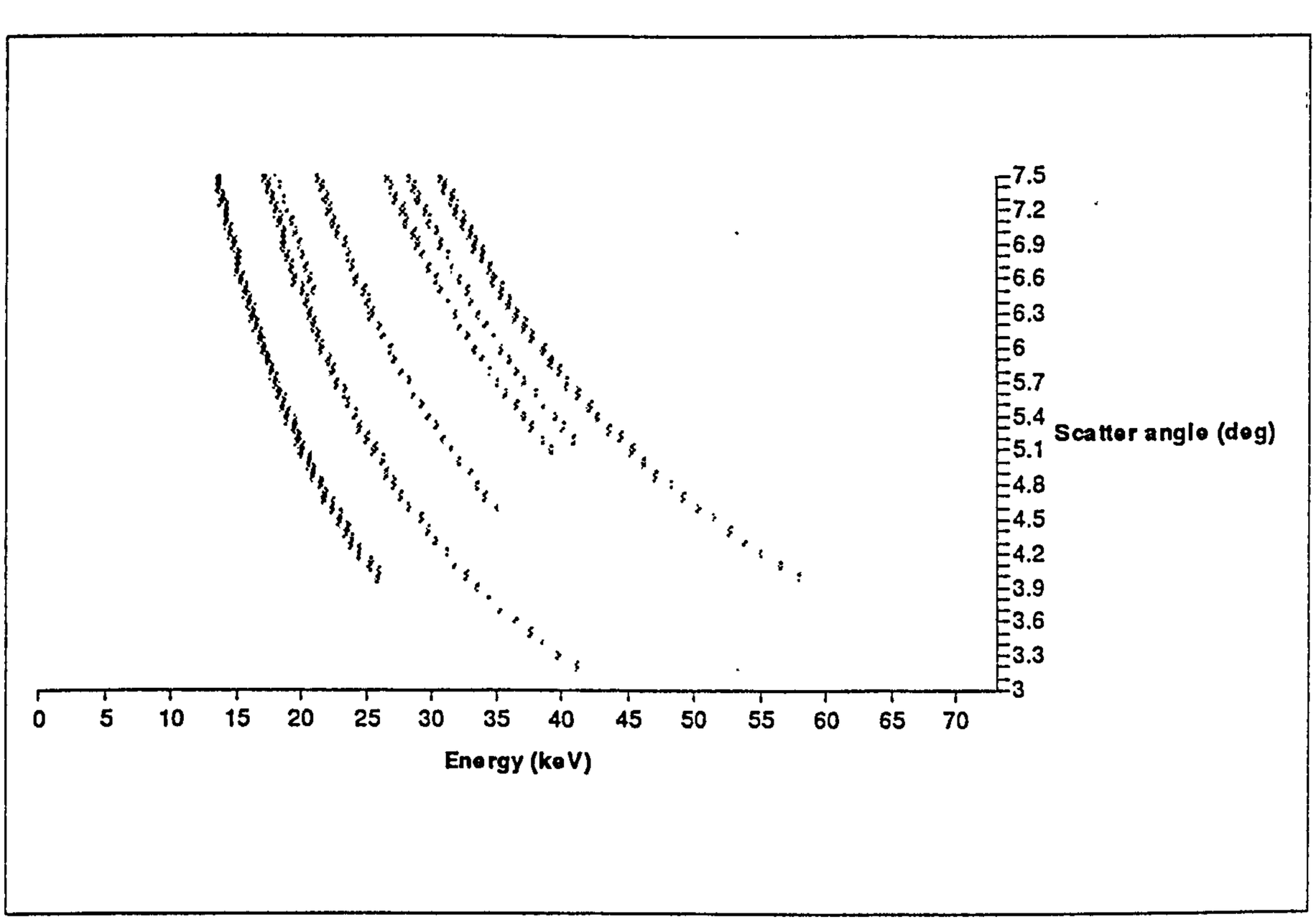

Figure 2.15 An ideal energy-angle diagram for SX2

The scatter signatures have been plotted as energy-angle diagrams because each material and therefore each explosive has a unique set of energy angle diffraction curves. It is these curves that will be used for identification purposes. As these curves are made up of a particular diffraction line, measured at several angles, it follows that analysis of the whole curve, rather than an individual line, will provide a more intense signal. In an experimental system this means that the SNR for the diffraction curve will be greater than for an individual peak.

2.4.3 Analysis of the energy-angle diagrams

It has been suggested that the decision as to whether an explosive is present can be based on the relative ability to distinguish the main diffraction lines in the explosive (these can be seen as diffraction curves in the ideal energy angle plot in figure 2.15). This is difficult to quantify and therefore the criterion has been arbitrarily set that if the three main diffraction lines of SX2 (at 3.3 Å, 5 Å and 6.7 Å) can be distinguished by eye then the number of detectors used is sufficient.

2.4.4 The effect of the number of scatter angles

The number of scatter angles defines the number of scatter signatures that can be put together to make an energy-angle diagram. The more scatter signatures there are the easier it is to identify a diffraction curve because there is more information provided to form each curve.

Figure 2.16 shows the effect of different numbers of scatter angles. All the plots show angles ranging from 3° to 7.5° with 4% energy resolution and 0.38° collimation angle of acceptance (this value was chosen as an average). The range of intervals is 0.1° (46 scatter angles), 0.25° (19 scatter angles), 0.5° (10 scatter angles) and 1.0° (5 scatter angles).

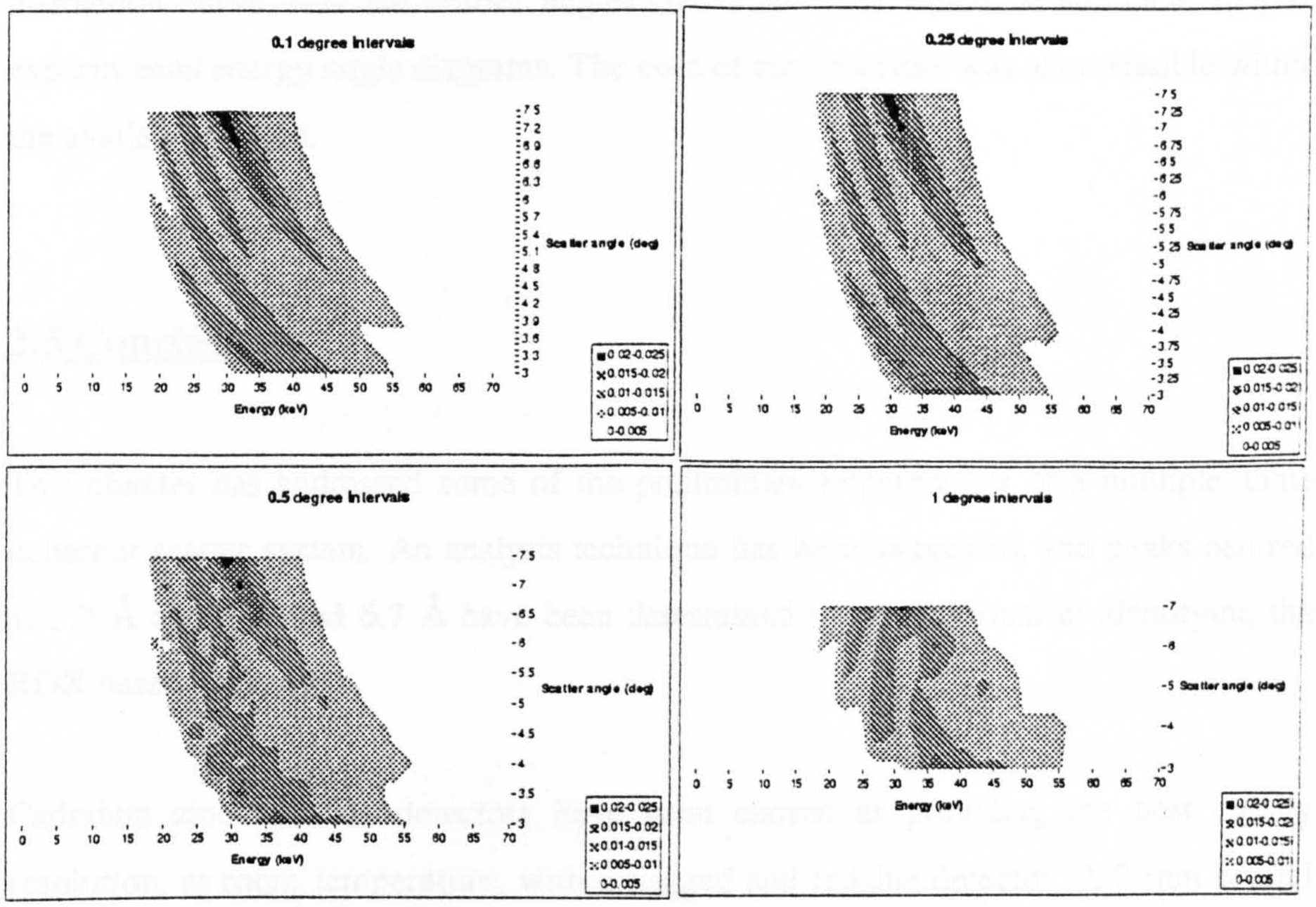

Figure 2.16 The effect of 0.1°, 0.25°, 0.5° and 1.0° intervals of scatter angles in the energy-angle diagram

It can be seen from these energy angle diagrams that the information for each peak over a range of angles can be seen simultaneously and that each diffraction line is satisfied by the maximum intensity of the incident spectrum at a different angle (3.3 Å at 7.1°, 5 Å at 4.7° and 6.7 Å at 3.5°). This is an advantage of a multiple angle system, as suggested in section 1.7.

In all but the 1.0° intervals the diffraction lines are clear to pick out. It is difficult to identify the diffraction lines in the 1.0° plot because the displacement along the energy axis by a change in 1.0° for each diffraction line is approximately 4 keV. This is equivalent to the spacing between adjacent diffraction lines. Therefore scatter patterns from adjacent angles appear to join between the wrong diffraction lines. The effect is worsened because the program used to display the data *(Excel)* worsens the effect as it includes a smoothing algorithm. It was decided that, although ideally as many detectors would be used as possible in order to maximise the information in a

diffraction curve, that ten scatter angles (0.5° intervals) would be sufficient to plot experimental energy angle diagrams. The cost of ten detectors was also possible within the available budget.

2.5 Conclusions

This chapter has addressed some of the preliminary requirements of a multiple angle coherent scatter system. An analysis technique has been suggested, and peaks centred at 3.3 Å and 5 Å and 6.7 Å have been determined to be important in identifying the RDX based explosives.

Cadmium zinc telluride detectors have been chosen as providing the best energy resolution, at room temperature, with a rugged and reliable detector. A 2 mm crystal of cadmium zinc telluride has been calculated to be sufficiently thick to be 98.8% efficient at 70 keV (see section 2.2.4.6).

A computer simulation of the coherent scatter system has been shown to be in good agreement with experimental results. This model has been used at an energy resolution of 4% to predict the effect of using a cadmium zinc telluride detector. It has also been used to determine that the acceptance angle of the collimation, used with a cadmium zinc telluride detector, should be no greater than 0.76° and that 10 scatter angles would be a suitable number to be measured.

CHAPTER 3

DESIGN AND CONSTRUCTION OF A COHERENT SCATTER SYSTEM

The aim of this thesis is to investigate the optimum design of a multiple angle coherent scatter system. The optimisation has been carried out in three stages. The first consists of a single detector and a single angle collimator used for consideration of the design of a multiple angle collimator and an investigation into the suggested planar spacings for the analysis. The second system consists of a multiple angle collimator with a single cadmium zinc telluride detector. This is used to optimise the analysis procedure (discussed in chapter 4). The final system consists of an array of detectors and a multiple angle collimator and is used to suggest how a realistic system could be designed for use as a baggage scanner. This chapter presents the design, construction and testing of the first two systems. Measurements taken with the single detector single angle system are shown as well as preliminary measurements from the single detector multiple angle system.

3.1 Description of the detector

Having chosen a cadmium zinc telluride detector as a suitable detector to use, an eV-180 detector *(eV Products, Pennsylvania, USA)* was bought. The crystal was $Cd_{(1-x)}Zn_{(x)}Te$ (where x=0.1) and the detector configuration was metal-semiconductor-metal. The contacts were of gold of 0.1 μm thickness. The crystal size was 5 x 5 x 2 mm and was irradiated from the cathode side through the 2 mm crystal thickness. The detector crystal was encased within a tube shaped brass housing of 10 mm diameter.

This had a 250 μm beryllium window located in front of the 5 x 5 mm face of the crystal. The crystal was mounted directly onto the back of a BNC connector. This was attached to the preamplifier, eV-550 *(eV Products, Pennsylvania, USA)*, as shown in figure 3.1.

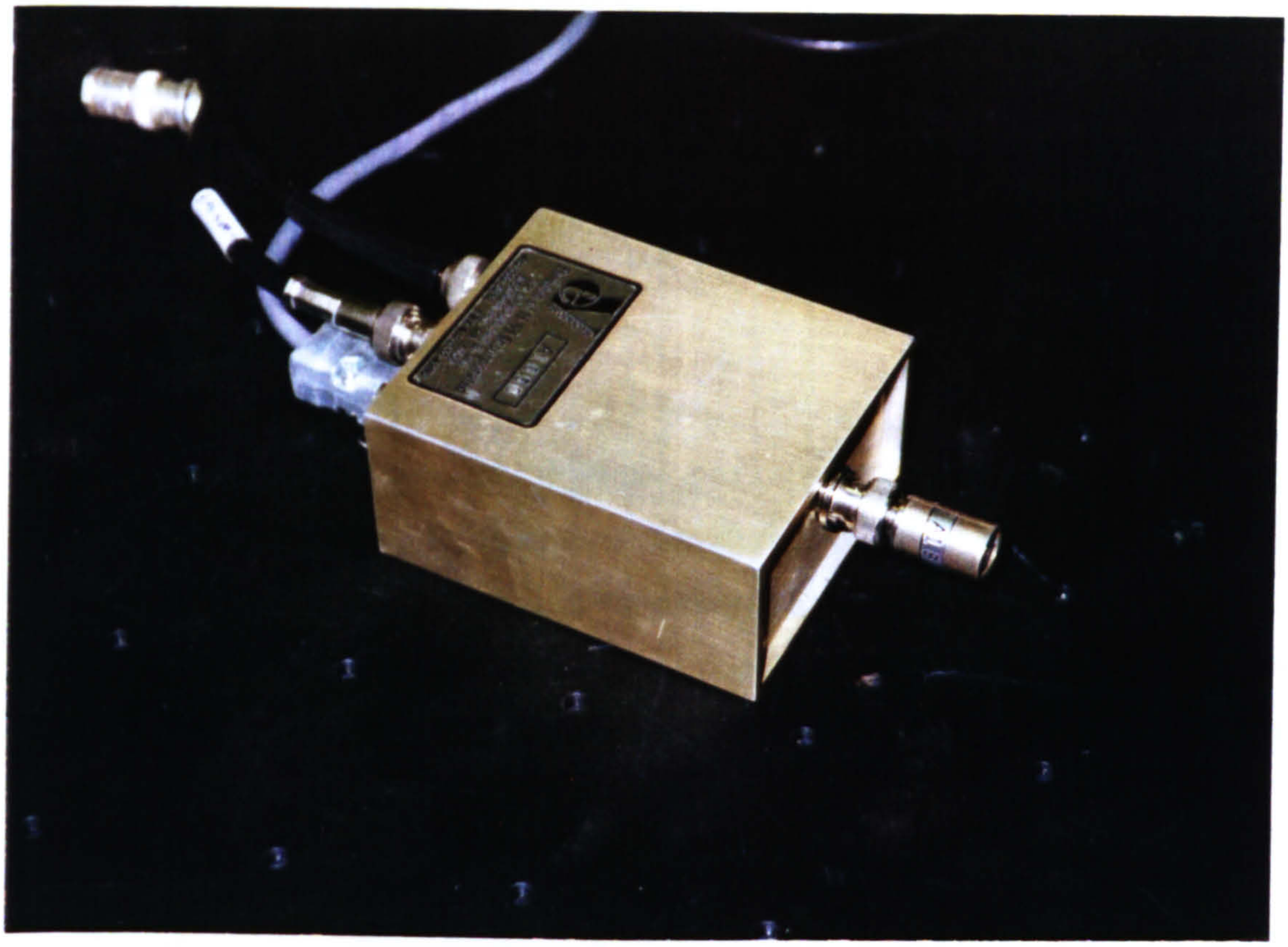

Figure 3.1 A photograph of the eV 180 cadmium zinc telluride detector with the preamplifier box attached.

The other electronic components, used with this detector and preamplifier, were a spectroscopy amplifier (EG&G Ortec 855 dual spectroscopy amplifier) and an analogue to digital converter and multiple channel analyser (EG&G Ortec 92X Spectrum Master). The associated software was 'Maestro' (EG&G Ortec), used to analyse and display the spectral data on a personal computer.

3.2 Evaluating the detector

Before the detector was used to measure scatter signatures, it was tested with radio-isotope sources to ensure that it fell within the criteria of the manufacturer's specifications. This also involved varying the bias voltage and amplifier shaping times to optimise the energy resolution. Prior to these measurements a pole-zero correction was carried out to correct for the signal pulse tail under-shooting or over-shooting the base line.

3.2.1 The optimum operating bias

A high bias voltage is required to maximise the charge collection efficiency. However, a high bias will also increase the leakage current and therefore it is essential to use a compromise bias voltage *(Niemela et al. 1996a)*. A range of bias voltages from 100-500 V was tested and the energy resolution of the 59.5 keV line from an americium 241 spectrum was calculated for each bias value. Figure 3.2 shows the spectra collected from this range of bias voltages.

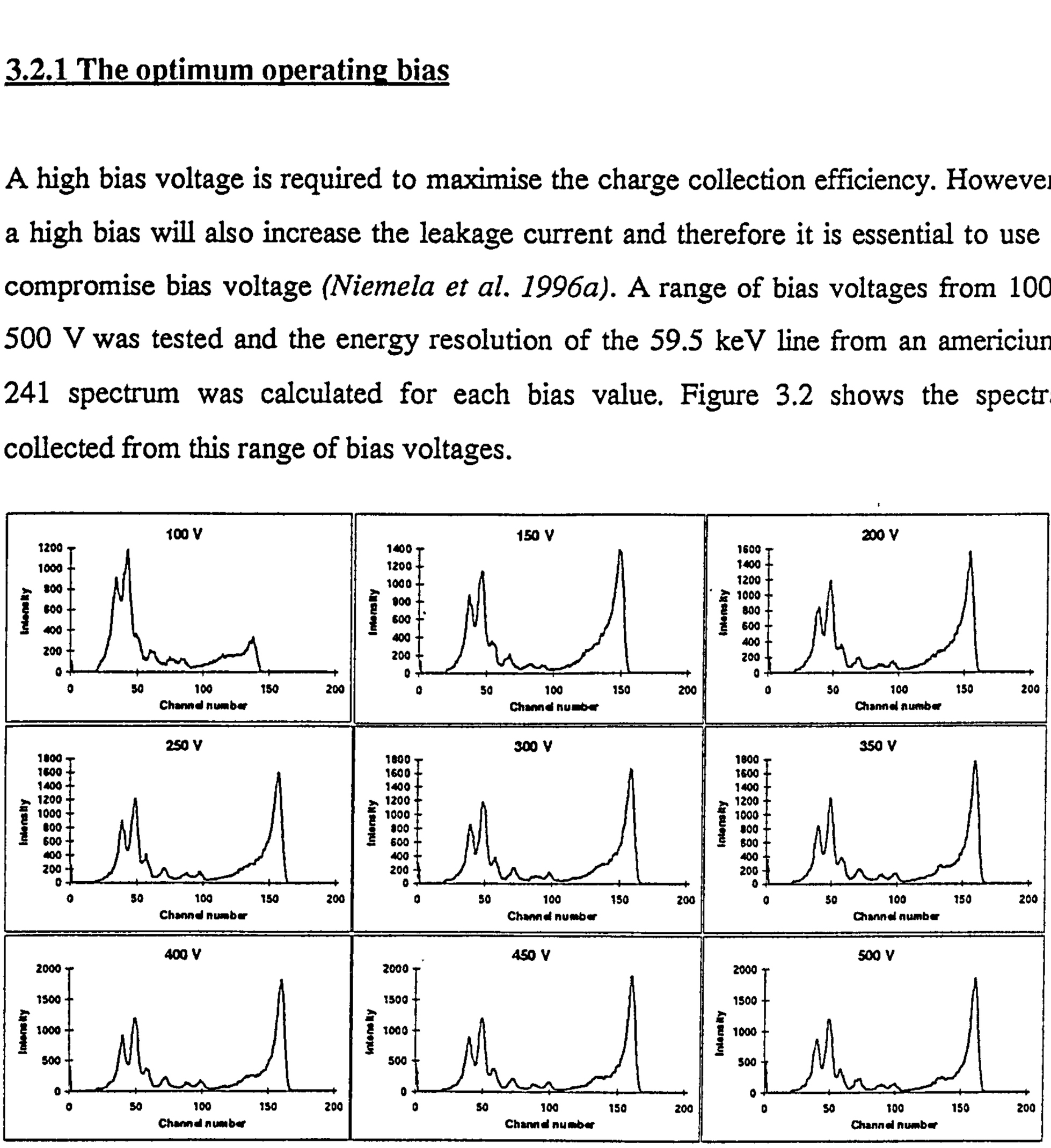

Figure 3.2 Americium 241 spectra measured for a range of bias voltage values

The results from these bias voltage experiments show that the 59.5 keV peak position in figure 3.2 moves to a higher channel when the bias voltage is increased. However, above 100 Vmm^{-1} (i.e. 200V) the change is only 1 channel per 50 V increase. The advantage of the peak position in a higher channel is that the peaks are more spread out over the channels and therefore can be distinguished more easily. However, this is offset by the fact that the more the peaks are spread out the lower the SNR in each channel. It should be noted that this effect can also be controlled by amplifier gain and therefore is not crucial in deciding the optimum settings.

The recommended bias for cadmium zinc telluride is 100 Vmm^{-1} of irradiated thickness *(eV Products)*. This is confirmed by the measurements taken above, as at bias voltage above + 200 V the energy resolution does not significantly improve (see figure 3.3). The energy resolution was calculated as the full width at half maximum (FWHM) of the peak of interest divided by the energy of the peak (i.e. $\Delta E/E$).

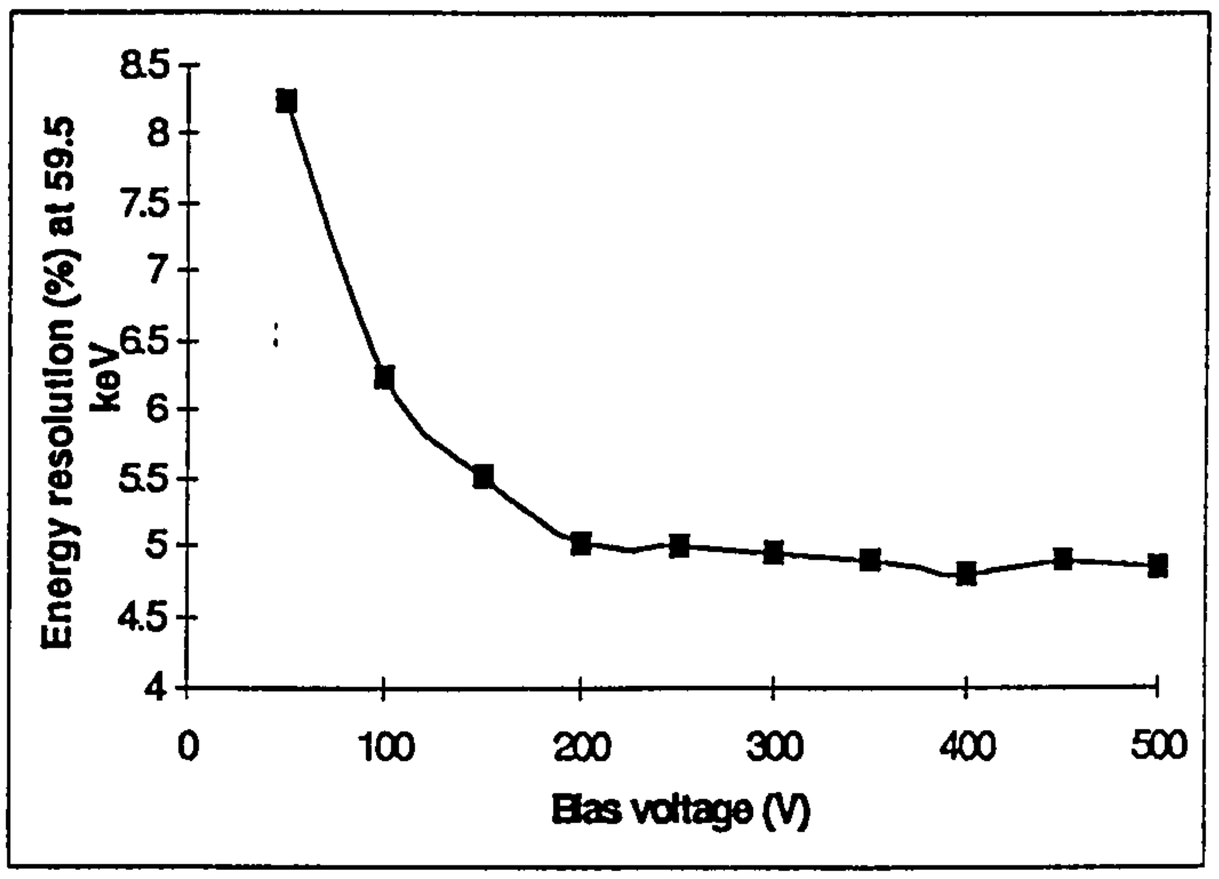

Figure 3.3 Energy resolution at 59.5 keV as a function of bias voltage.

Initially energy resolution improves with increase in detector bias voltage due to improvement in charge collection efficiency, however above 100 Vmm^{-1} the improvement is minimal (see figure 3.3), hence the optimum bias voltage was chosen to be 200 V in order to minimise the leakage current.

3.2.2 Amplifier shaping time

With an operating bias of + 200 V an americium spectrum was measured over a range of shaping times with both gaussian and triangular shaping (which shape the amplified signal to approximately these shapes). Determination of the optimum time constant is best accomplished by trial and error, as calculation of all the factors involved is very complicated *(Nicholson 1974)*. Figure 3.4 shows the effect on the energy resolution at 59.5 keV of the range of shaping times and the triangular and gaussian shapes.

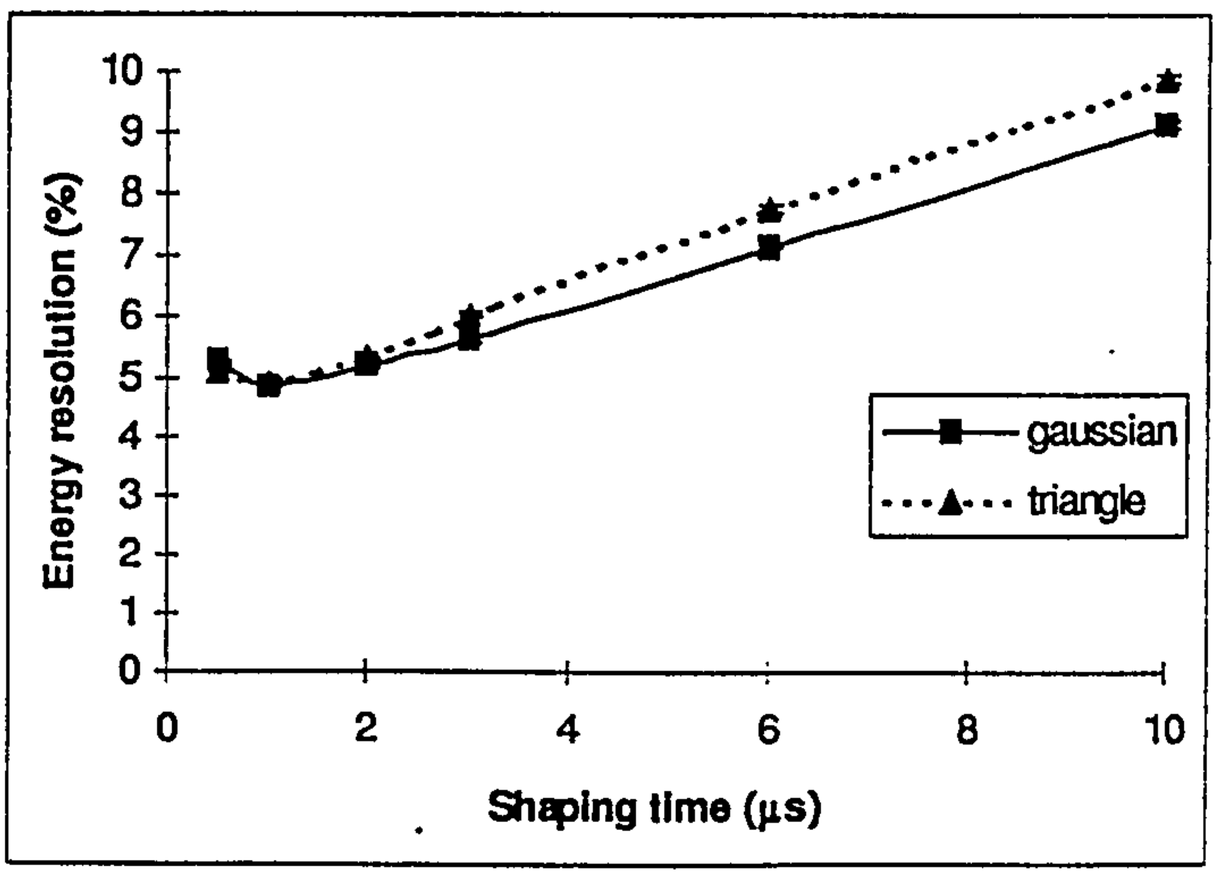

Figure 3.4 Energy resolution at 59.5 keV as a function of shaping time for both gaussian and triangular shaping.

It can be seen that the optimum energy resolution is given by using 1 µs shaping time for both gaussian and triangular shaping pulses. The energy resolution is consistently worse for the triangular shaping. Theoretically, triangular is advantageous over gaussian, as regards signal to noise ratio, but it is very difficult to produce a symmetrical triangular shape with passive circuit elements only *(Knoll 1989)*.

Dead time also increases with pulse shaping time (see figure 3.5) as the likelihood of pulse pile-up is greater. Therefore, 0.5 µs is the optimum for dead time reduction. However, for this work energy resolution is required to be optimised and the increase in the dead time for 1 µs is only 0.3%.

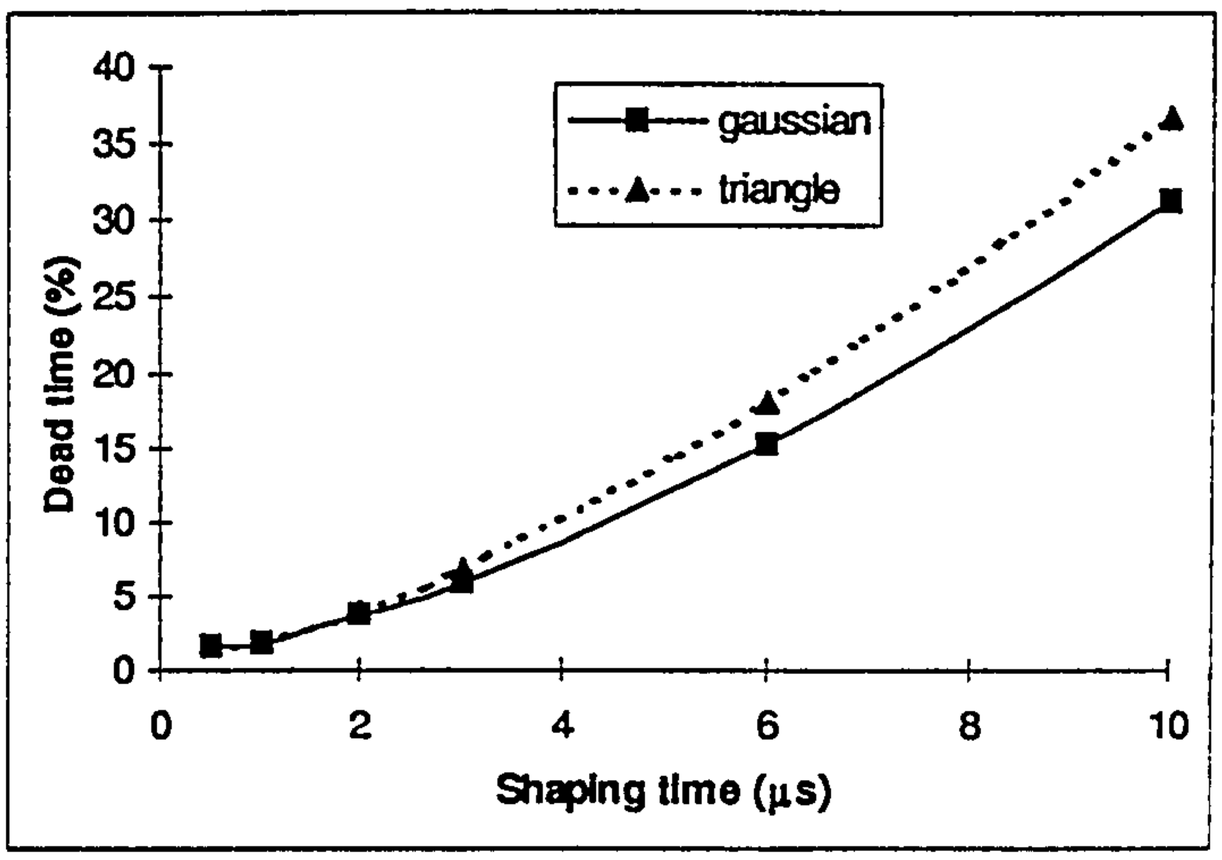

Figure 3.5 Dead time as a function of shaping time for gaussian and triangular shaping

The optimum parameters for this detector, at 59.5 keV ,were thus determined to be +200 V operating bias and 1µs gaussian shaping time. However, at higher count rates the shaping time can cause pulse pile-up effects. Therefore a 0.5 µs gaussian shaping time has been used with this detector for the measurements made in the remainder of this work which are at a higher count rate (approximately 100 times that for the americium source used).

3.2.3 Measurement of the energy resolution

Although the energy resolution quoted in the literature was 4% at 59.5 keV, it is likely that there will be some variation in energy resolution between individual detectors. Therefore it was necessary to measure the energy resolution of this detector so that the collimation for the system could be optimised for it. Using the detector with the bias and shaping time optimised (as described in sections 3.2.1 and 3.2.2), the spectrum was measured and the energy resolution calculated for two radio-isotopes of different energies. These radio-isotopes were americium 241 and cobalt 57, with the main characteristic peaks at 59.5 keV and 122 keV respectively. The detector was irradiated by placing a source 10 cm in front of the window face of the detector. Figures 3.6 and 3.7 show the spectra measured from these isotopes for the eV-180 detector.

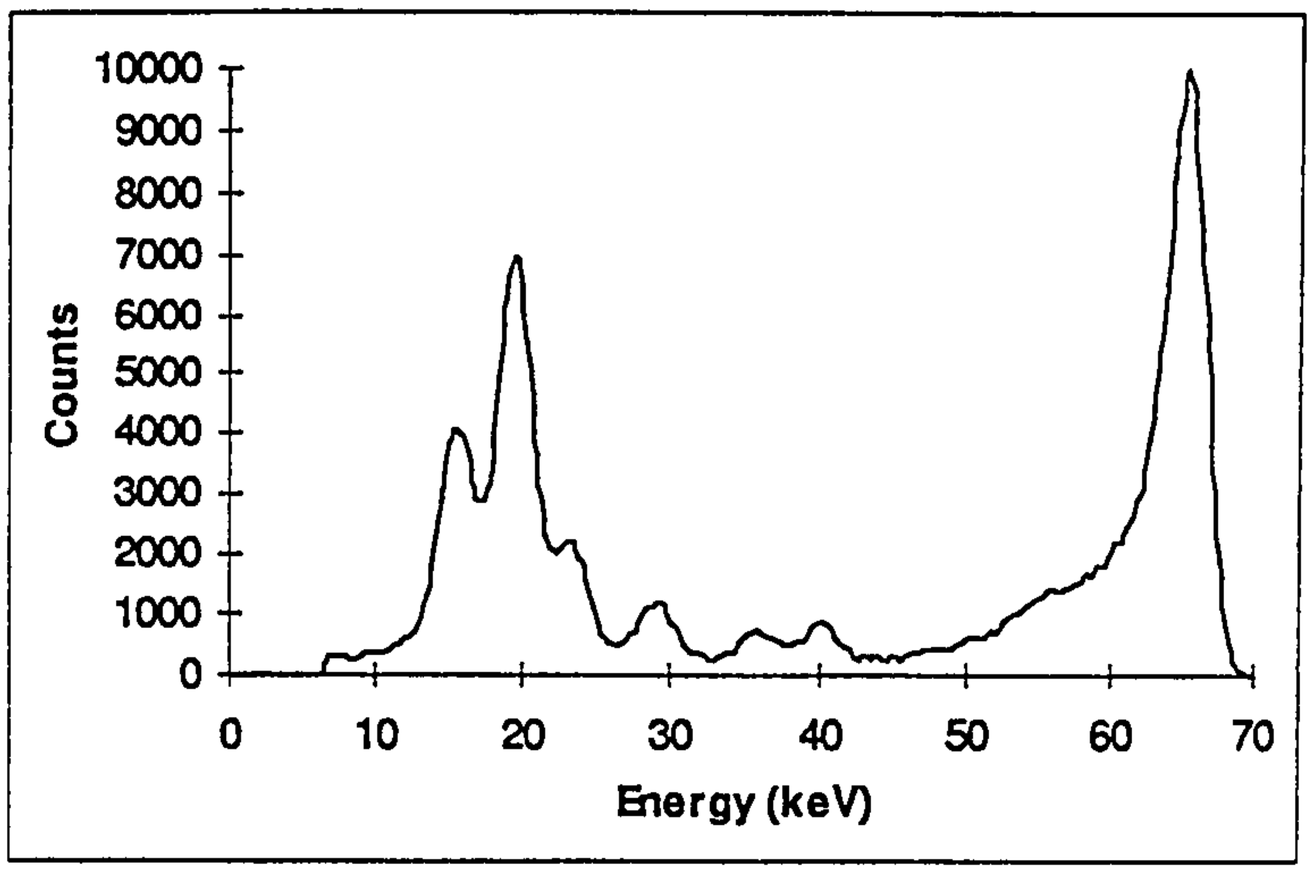

Figure 3.6 Americium 241 spectrum measured with the eV-180 cadmium zinc telluride detector

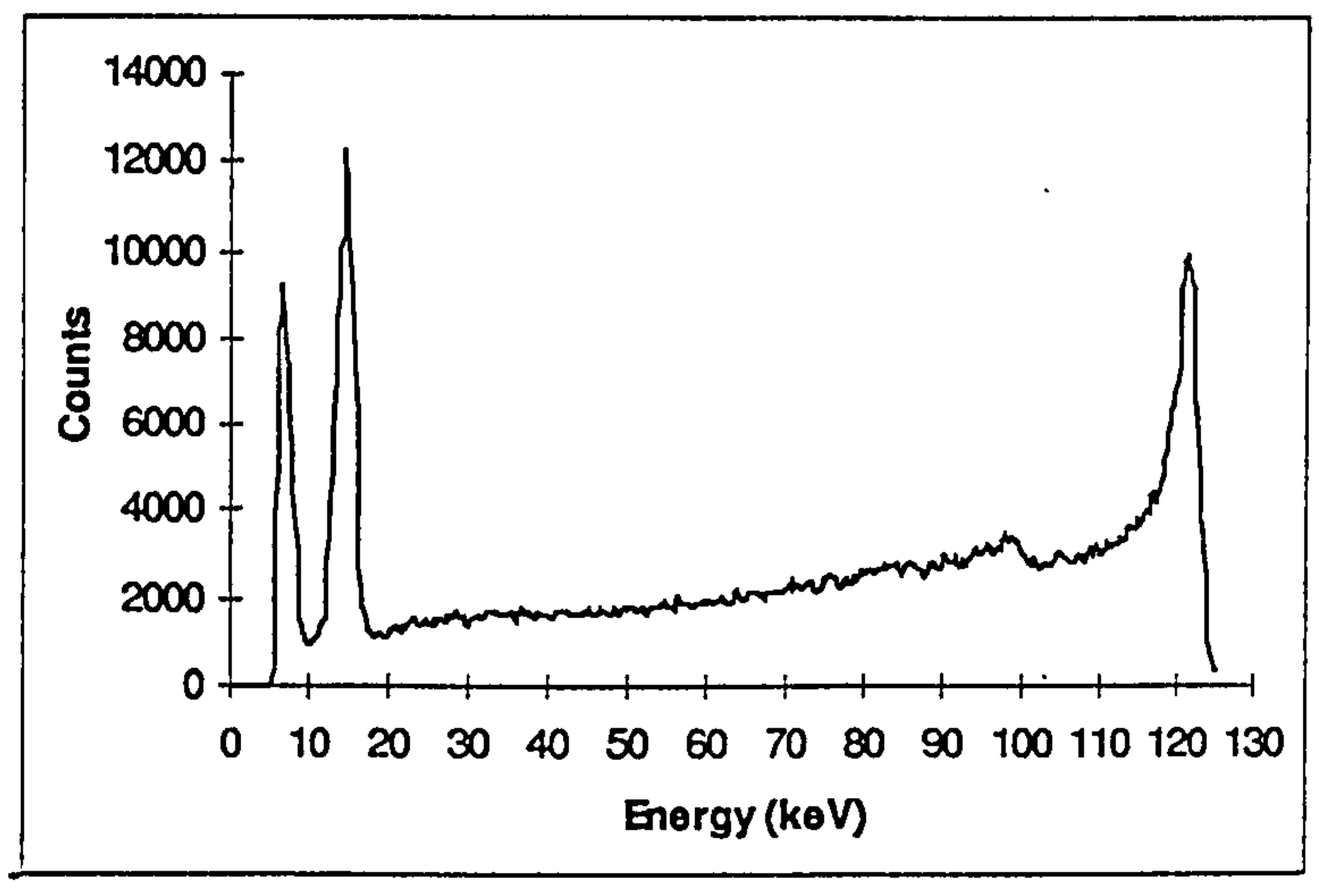

Figure 3.7 Cobalt 57 spectrum measured with the eV-180 cadmium zinc telluride detector

Each spectrum was measured for sufficient time to achieve 10,000 counts in the peak of interest, thus ensuring statistics of 1% error ($\sqrt{N}/N$). The energy resolution was calculated by interpolating the position of the channel which contained half the counts at the maximum. These positions were then used to calculate full width at half maximum. The energy resolution is calculated as this width (converted into energy) divided by the energy of the main peak (i.e. $\Delta E/E$). The error on this calculation is the

width of the energy channel at the main peak. Table 3.1 shows the resolutions for each isotope given as percentages of the energy of the peak.

Isotope name	Energy of peak of interest	Measured energy resolution
Americium^{241}	59.5 keV	4.9% +/- 0.5%
Cobalt^{57}	122 keV	3.6% +/- 0.5%

Table 3.1 Energy resolution for americium 241 and cobalt 57

The energy resolution for this individual detector was measured to be 4.9% and was less than the specified value of 5.8% given by eV products for this detector.

3.3 Considerations for collimation design

In order to design collimation suitable for a cadmium zinc telluride detector, to be used for the detection of explosives in baggage, various preliminary investigations were undertaken to identify what the optimum system should be. These included collimation shape and size. A coherent scatter system was set up for the cadmium zinc telluride detector. A full description of the coherent scatter system can be found in section 1.6.1.

3.3.1 Collimation acceptance angles

The width of the collimator slits together with the spacing between the two sets of slits defines the acceptance angle of the collimator. Table 3.2 shows the angular acceptance of the collimators as a percentage of the scatter angle, for the range of acceptance angles suggested by the modelled work in section 2.4.1.

	Collimation acceptance angle		
Scatter angle	**0.19°**	**0.38°**	**0.76°**
3°	6.37 %	12.73 %	25.33 %
4°	4.77 %	9.54 %	19.00 %
5°	3.82 %	7.64 %	15.20 %
6°	3.18 %	6.37 %	12.67 %
7°	2.72 %	5.46 %	10.86 %

Table 3.2 The angular blurring caused by different collimation acceptance angles for a range of scatter angles (shown as a percentage of the scatter angle)

The shaded cells show the angles and collimation acceptance angles when the angular blurring is greater than the energy resolution of the detector i.e. angular blurring is the dominant blurring function. This is true for the majority of the range of scatter angles and acceptance angles considered, thus the acceptance angle of the collimators should be carefully considered.

3.3.2 Design of the collimation

The collimation used in an energy dispersive coherent scatter system is of paramount importance. As has been previously discussed, too wide a collimator will cause so much angular blurring that the unique scatter signatures will not be able to be identified. However, it is also the collimation that is responsible for the reduction in intensity of the primary and scattered flux and therefore also affects the time for which the measurements must be taken. Thus any collimation for a new system must be carefully designed to take these factors into consideration.

Two types of collimation were investigated. The first was pin-hole collimation that consists of two small circular holes to define the beam before scatter (primary beam) with a further two holes to define the beam after scatter (secondary beam). The advantage of this type of collimation is that the spectral blurring, caused by the range

of scatter angles allowed by the collimators, is minimised. However, the disadvantage is that the flux is severely reduced and only interrogates a small volume of the scattering material and may therefore enhance localised orientational effects. The second type of collimation was slit collimation which overcomes, to some extent, the problem of reduced flux by providing a greater cross-sectional area for the beam. However the disadvantage is that more spectral blurring is caused by a greater range of angles being allowed by the increased length of the slit.

Measurements were taken with both types of collimation for the purpose of a direct comparison. The collimator separation of 150 mm and source to collimator distance were consistent for both collimation types. The slit widths used were 0.5 mm, 1 mm and 2 mm (which are equivalent to the 0.19°, 0.38° and 0.76° acceptance angles determined in section 2.4.1). All measurements are of SX2 at 5° scattering angle (chosen as an average scatter angle where the peaks are clearly visible) for 100 s. Figures 3.8 and 3.9 show the effect of the two types of collimation.

The variation in peak intensity for the broad peak at 40-45 keV is due to the localised orientational effects which are enhanced in the pinhole measurements. This effect can also be seen in the 0.5 mm slit collimation as this has the smallest scatter volume of the slit collimator examples.

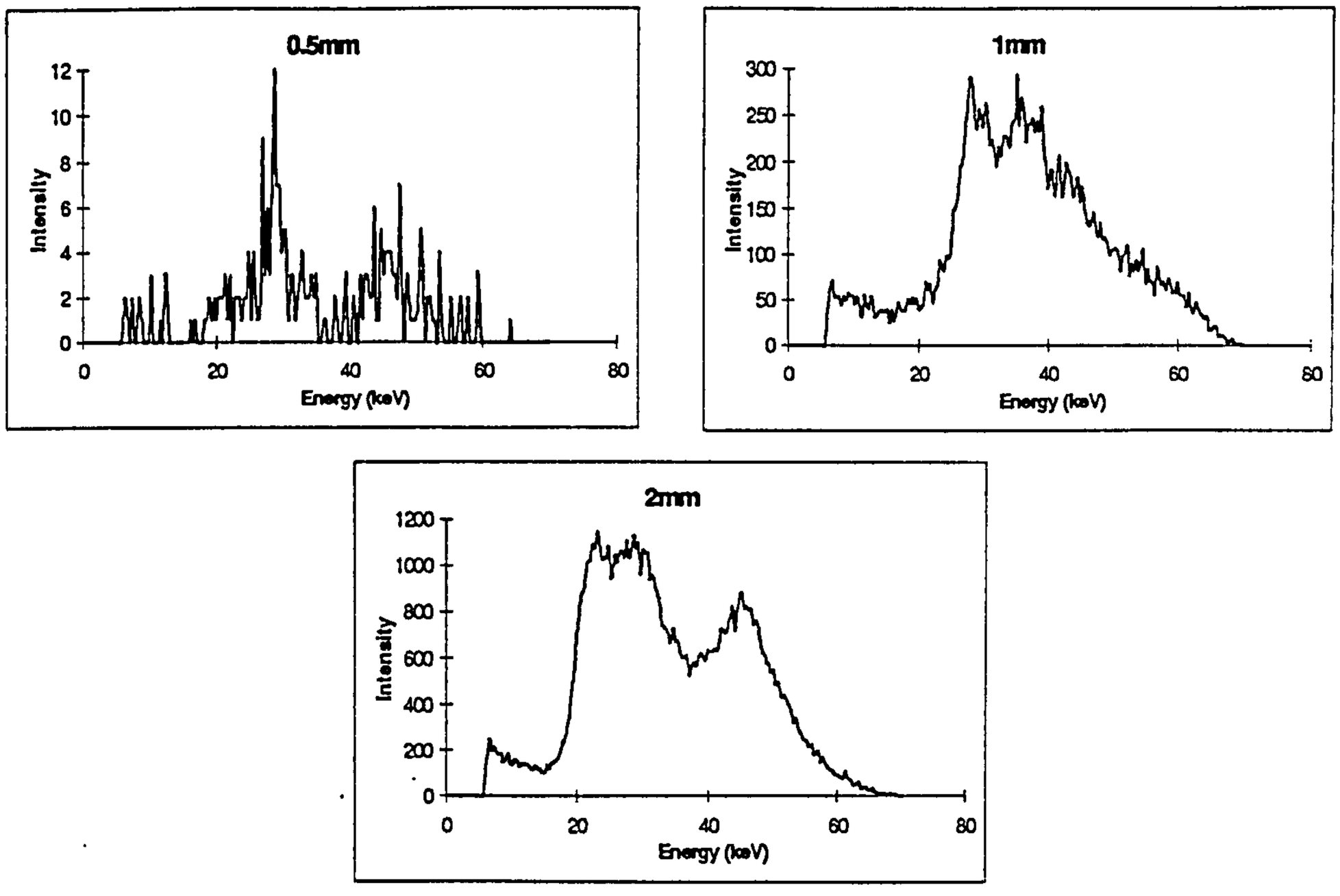

Figure 3.8 The effect of pin hole collimation

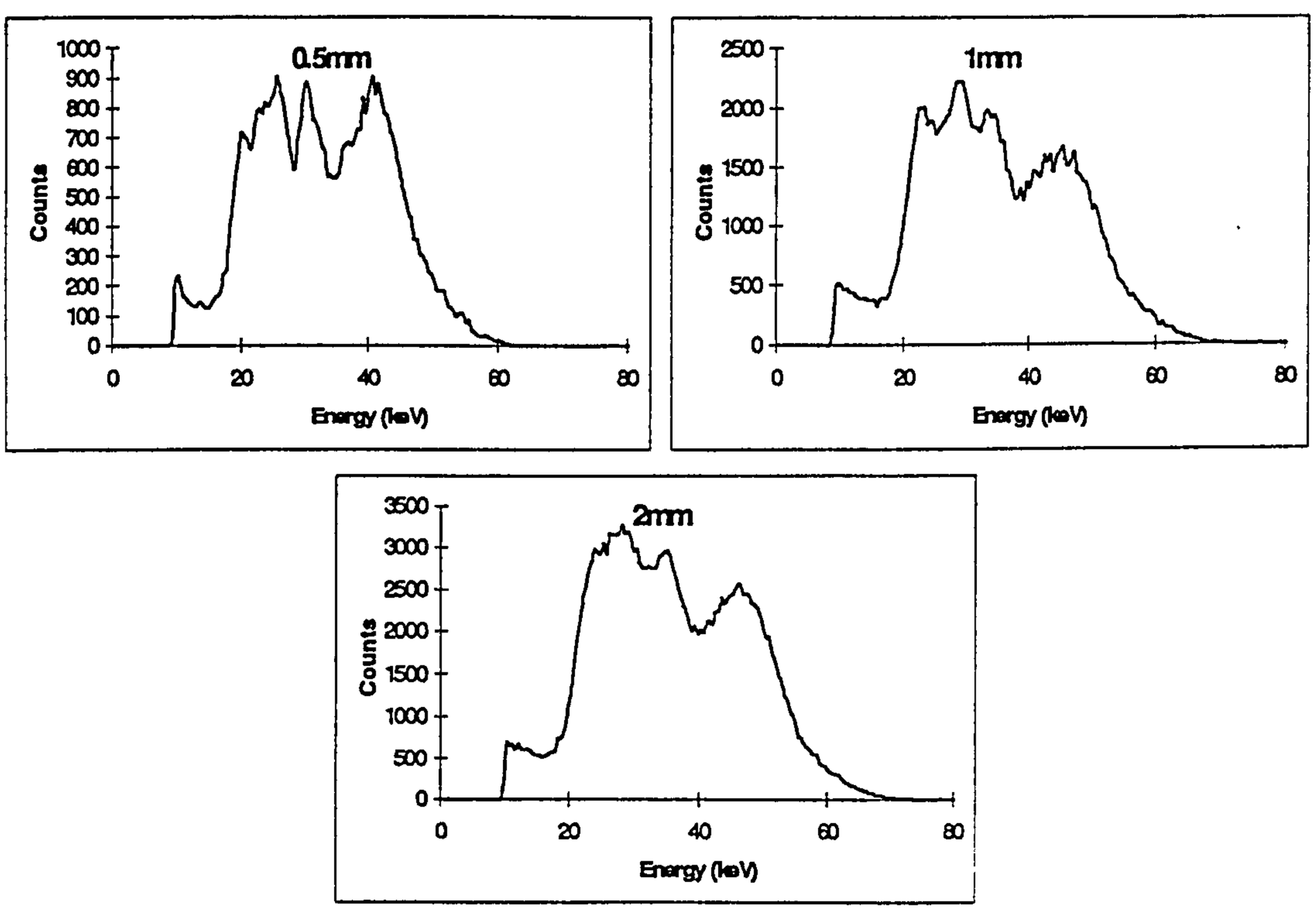

Figure 3.9 The effect of slit collimation.

Table 3.3 shows the cross-sectional areas for each of the collimators and the integrated counts in the spectrum for each. The value of the ratio I/C (where I is the integrated counts in the spectrum and C is the cross-sectional area of the collimator) shows that the counts are proportional to the cross-sectional area (except for 0.5 mm pinhole which was difficult to align). Therefore it should be expected that the slit collimators should allow greater intensity as they have greater cross-sectional area. The height of the slit collimators was defined by the size of the detector crystal (5 mm).

Type and width of collimator	Cross-sectional area (C)	Integrated counts (I)	I/C
Pinhole, 0.5 mm	0.2 mm^2	281	1405
Pinhole, 1.0 mm	0.8 mm^2	20158	25198
Pinhole, 2.0 mm	3.1 mm^2	87031	28074
Slit, 0.5 mm	2.5 mm^2	50963	20385
Slit, 1.0 mm	5 mm^2	133437	26687
Slit, 2.0 mm	10 mm^2	203992	20399

Table 3.3 The cross-sectional areas and integrated counts from the two types of collimation considered

The improvement in angular blurring by the pinhole collimators, due to being restricted in the vertical direction, is minimal. Whereas, the slit collimation gives greatly increased integrated intensity. Also the scatter volume is greater for the slit collimation and so reduces the localised orientational effects. Therefore slit collimation was chosen for the increased intensity and hence the possibility of shorter measurement times.

3.4 Measurement of coherent scatter signatures of various typical materials

To optimise the geometrical characteristics of the system, various samples of 20 typical materials that are often found as baggage contents, were measured. Although there is a huge range of substances that could constitute luggage contents, there are certain materials that are quite common. Several studies have been carried to test other methods of baggage scanning *(Yedida and Shea 1992, Lacey 1995, Campbell 1997)* and the materials chosen for this work (as listed in table 3.4) are based on those studies. They include five foodstuffs, six toiletries, five clothing materials and four miscellaneous items. Measurements were also made of the two samples of explosives SX2 and Semtex.

chocolate	deodorant	toothpaste	aluminium
coffee	shampoo	acrylic	ceramic
marzipan	soap	cotton	glass
sugar	sun-cream	leather	paper
tea	talc	wool	rubber

Table 3.4 Typical contents of baggage

The measurements were made with slit collimation of acceptance angles 0.19°, 0.38° and 0.76° as suggested by the model. The primary collimation was maintained at 0.38° acceptance angles for all variations of secondary collimators. The measurement time was 100s to ensure good statistics and the scatter signatures were taken at angles between 3° and 8° in intervals of 1°. The incident X-ray spectrum was 70 kVp and the X-ray tube current was 20 mA. Figures 3.10, 3.11 and 3.12 show the scatter signatures measured for six of these samples at 5° scatter angle, for these three acceptance angles respectively. The peaks corresponding to the two explosive samples are the most important to identify, since these are the materials which must be differentiated from

the others. These peaks are at 21 keV, 28 keV and 43 keV (corresponding to 3.3Å, 5Å and 6.7Å respectively).

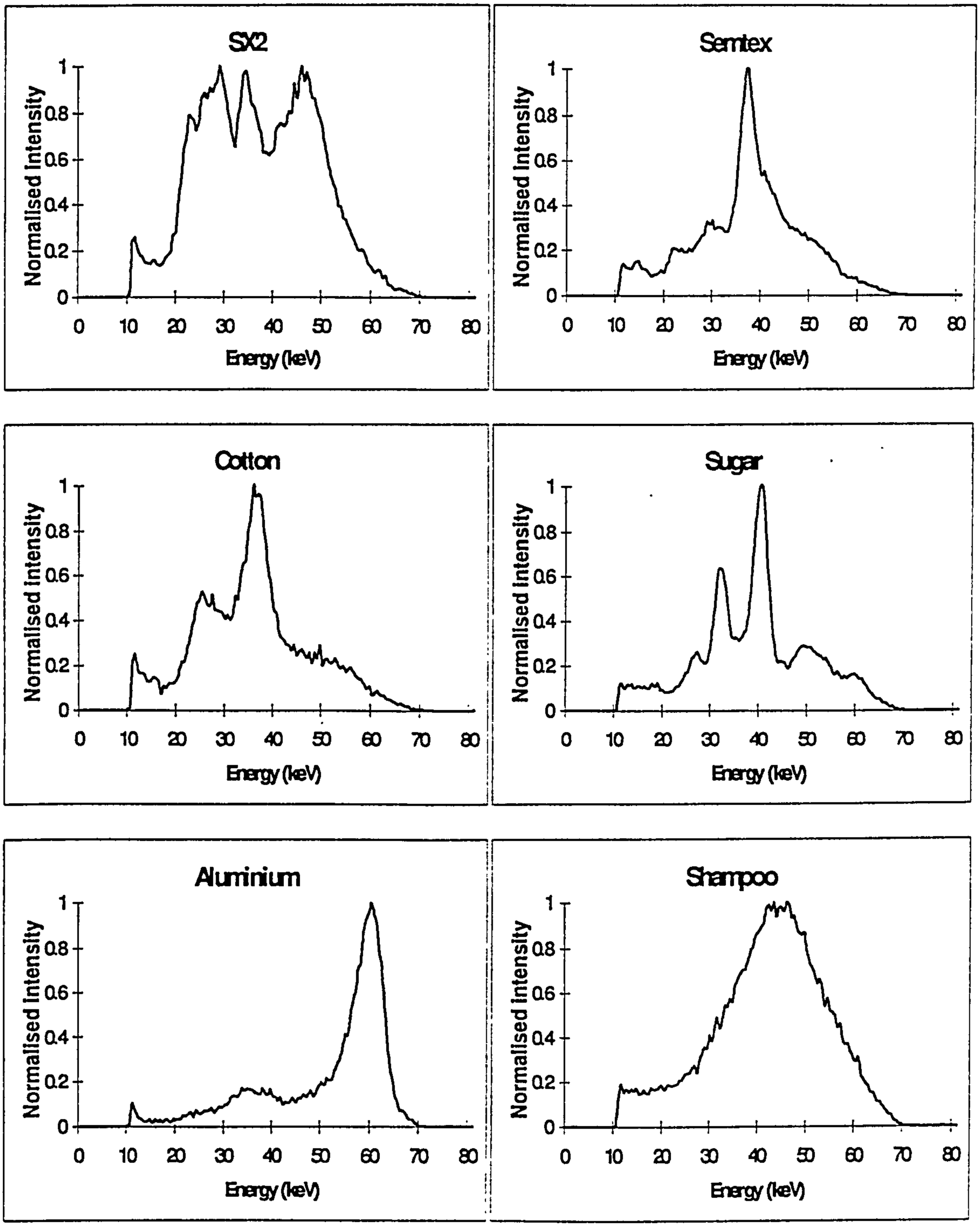

Figure 3.10 Examples of the scatter signatures of six of the materials listed in table 3.4. All measurements were taken at 5 degree scatter angle with 0.19° collimation acceptance angle and for 100s measurement time.

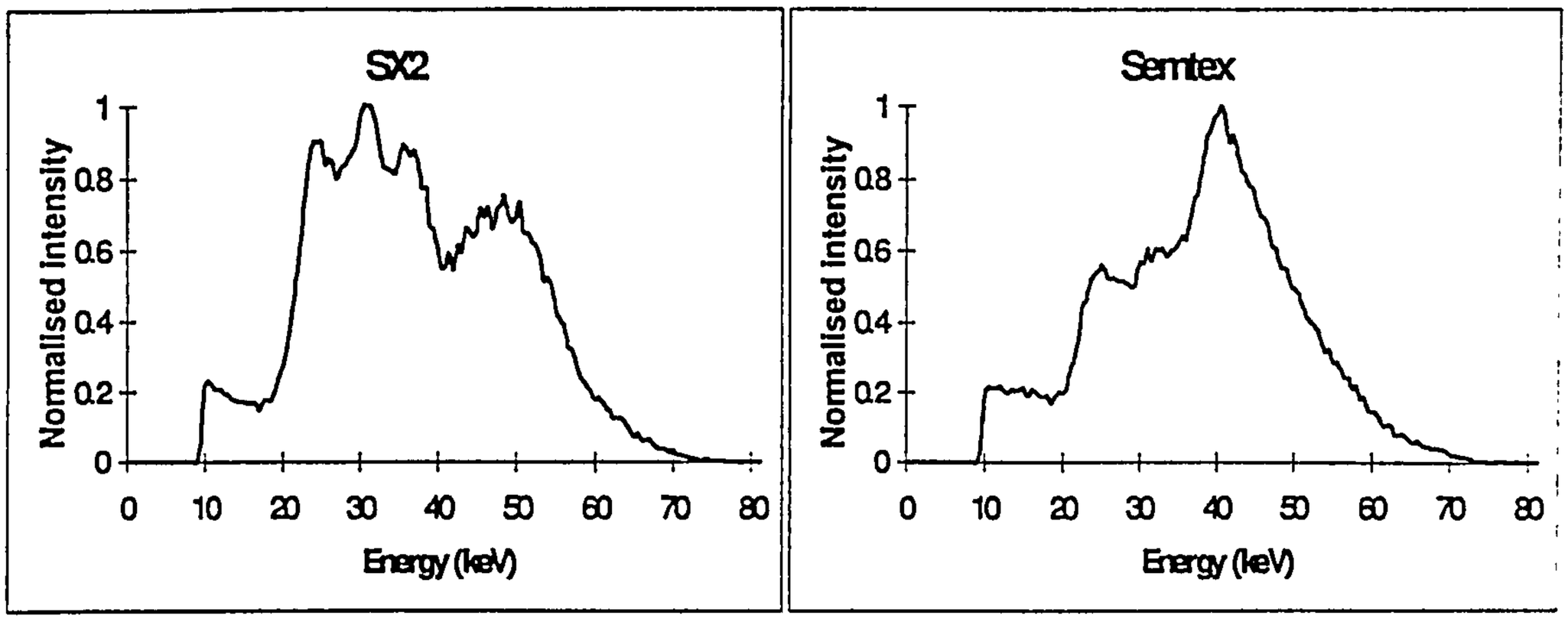

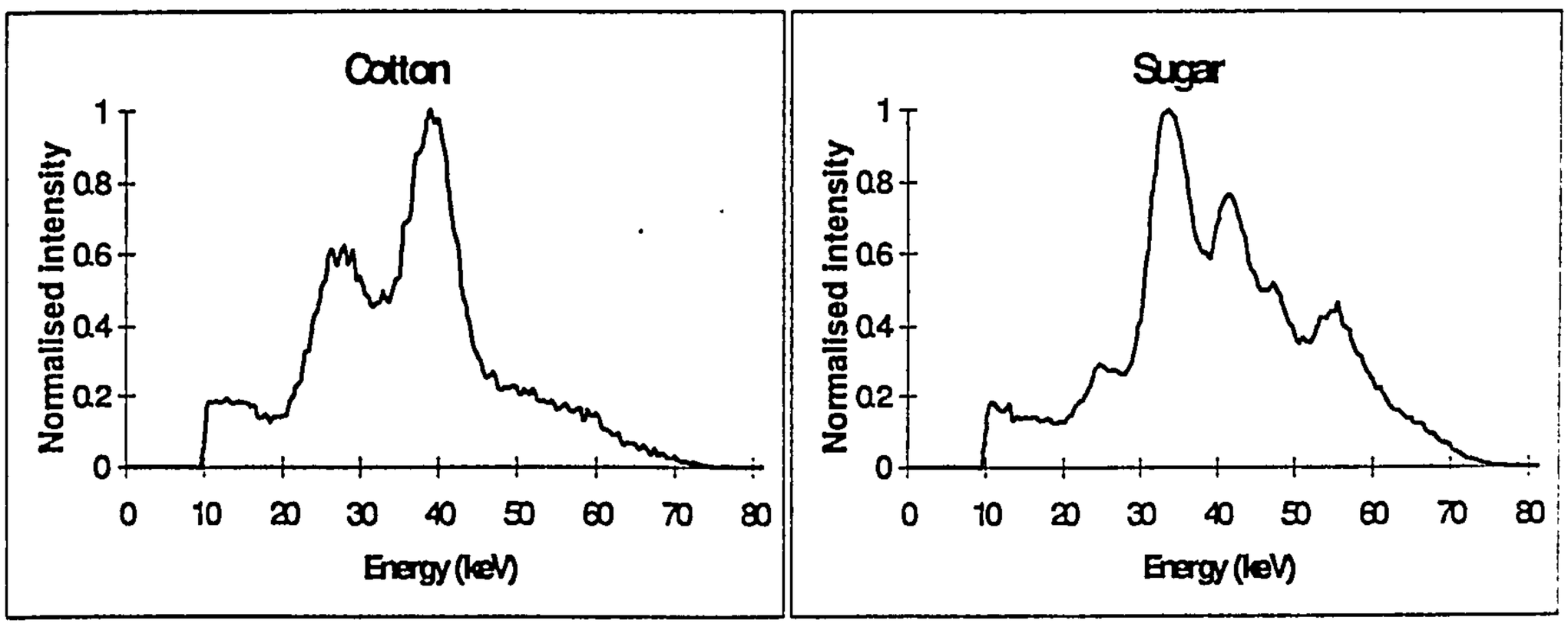

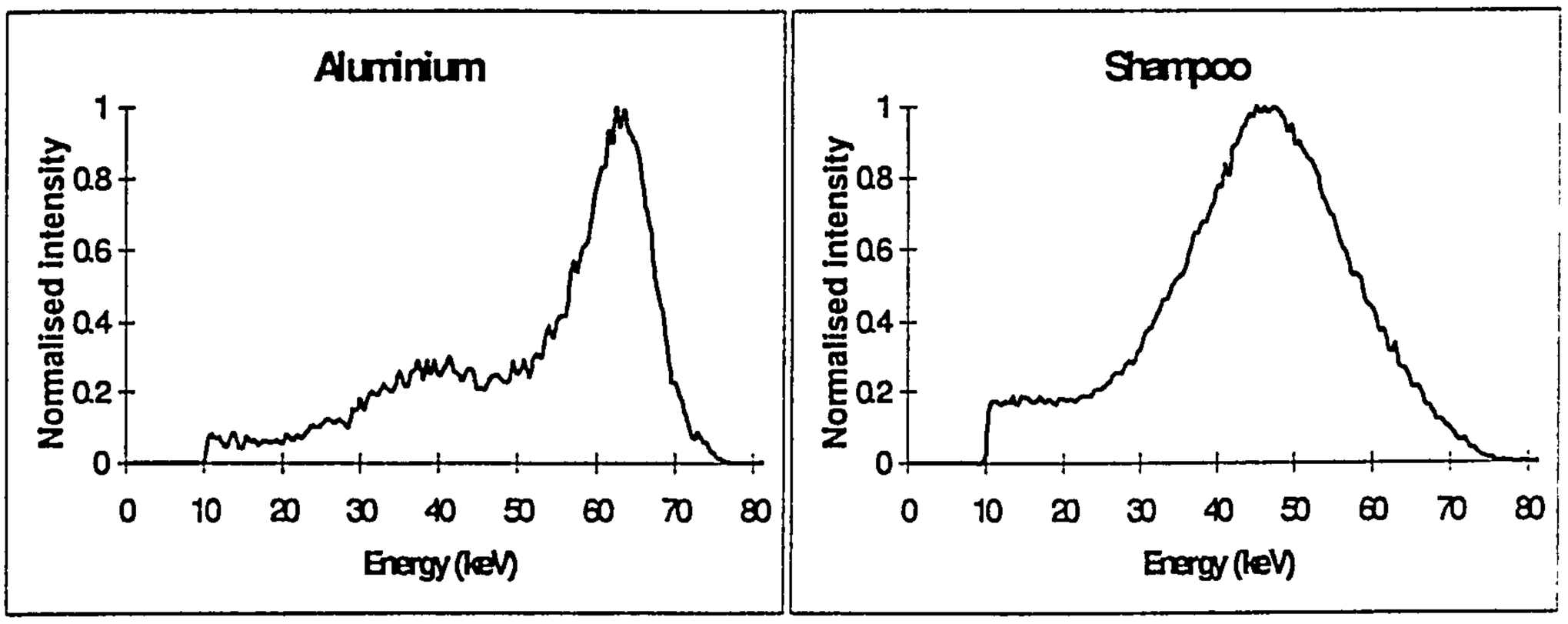

Figure 3.11 Examples of the scatter signatures of six of the materials listed in table 3.4. All measurements were taken at 5 degree scatter angle with 0.38° collimation acceptance angle and for 100s measurement time.

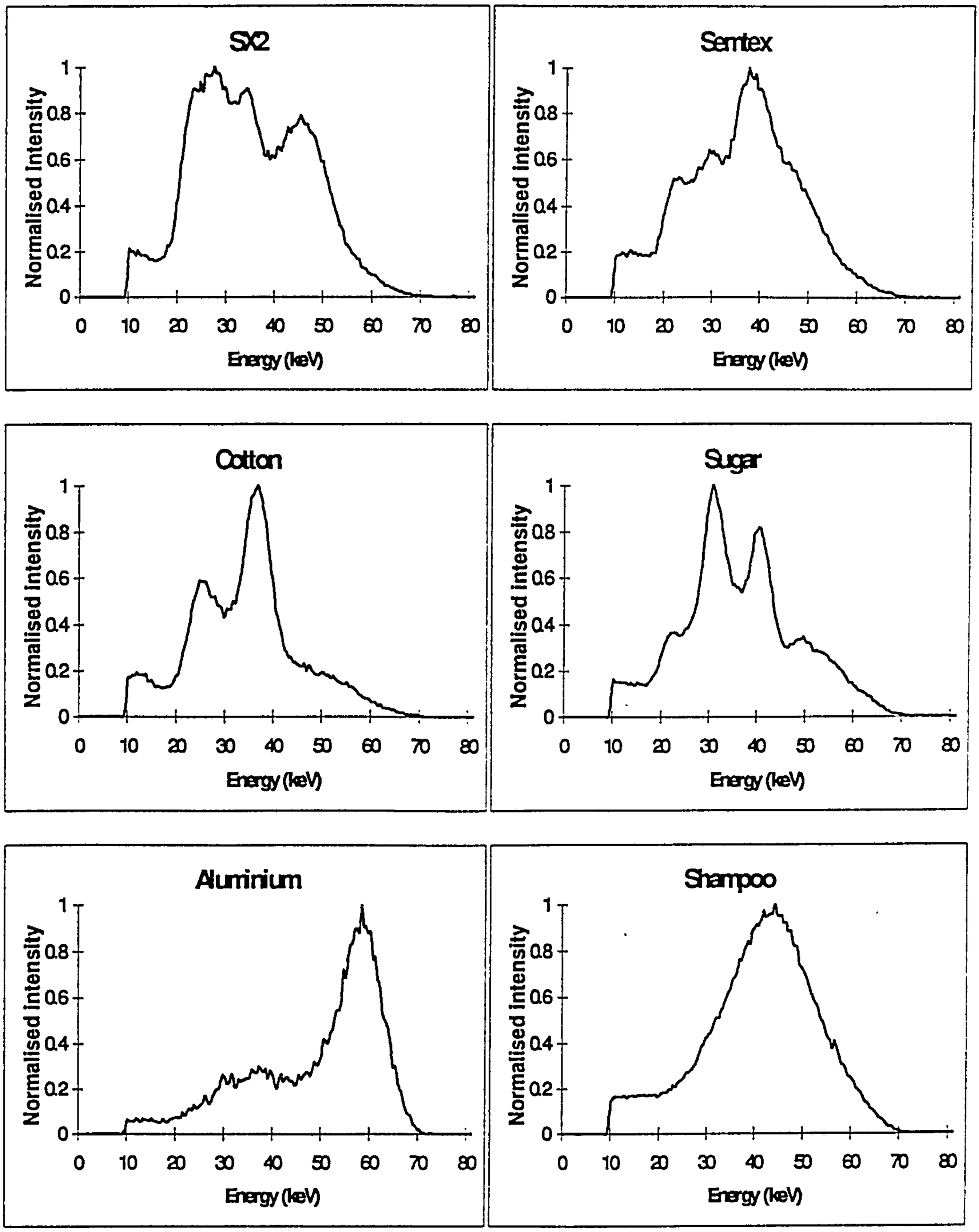

Figure 3.12 Examples of the scatter signatures of six of the materials listed in table 3.4. All measurements were taken at 5 degree scatter angle with 0.76° collimation acceptance angle and for 100s measurement time.

From these results it was decided that the 0.76° collimation caused too much blurring for easy identification of the explosive samples. This is particularly noticeable for the SX2 as the two peaks at 21 and 28 keV (5 Å and 6.7 Å planar spacings) can no longer be individually recognised. At 3°, 4°, 6° and 7° there were also significantly fewer peaks clearly recognisable for the 0.76° collimation acceptance angle than for the 0.38° and 0.19°. Therefore 0.19° and 0.38° acceptance angles of collimation were chosen as suitable to use with the cadmium zinc telluride detector.

It should also be noted that the collimation has very little effect on the patterns for the amorphous material (shampoo). As many case contents are amorphous, this is an important effect, as the difference between amorphous and crystalline materials is enhanced for tighter collimation. This could therefore help to distinguish between the explosives and the benign contents.

3.5 Simulation of a multiple angle system with single detector and single angle collimator

A simple version of a multiple angle experimental system was designed to simulate a full multiple angle system. A single detector, single angle collimator system was built on a 1 m long optical bench, pivoted at the scatter point, with a collimator and detector attached directly to the optical bench. Figure 3.13 shows a diagram of the set-up. This system was used to measure the scatter signatures from the required range of angles, in order to simulate results which may be obtained from a multiple angle system. This allowed an investigation into whether a multiple angle system with a cadmium zinc telluride detector might give reasonable results for the detection of explosives.

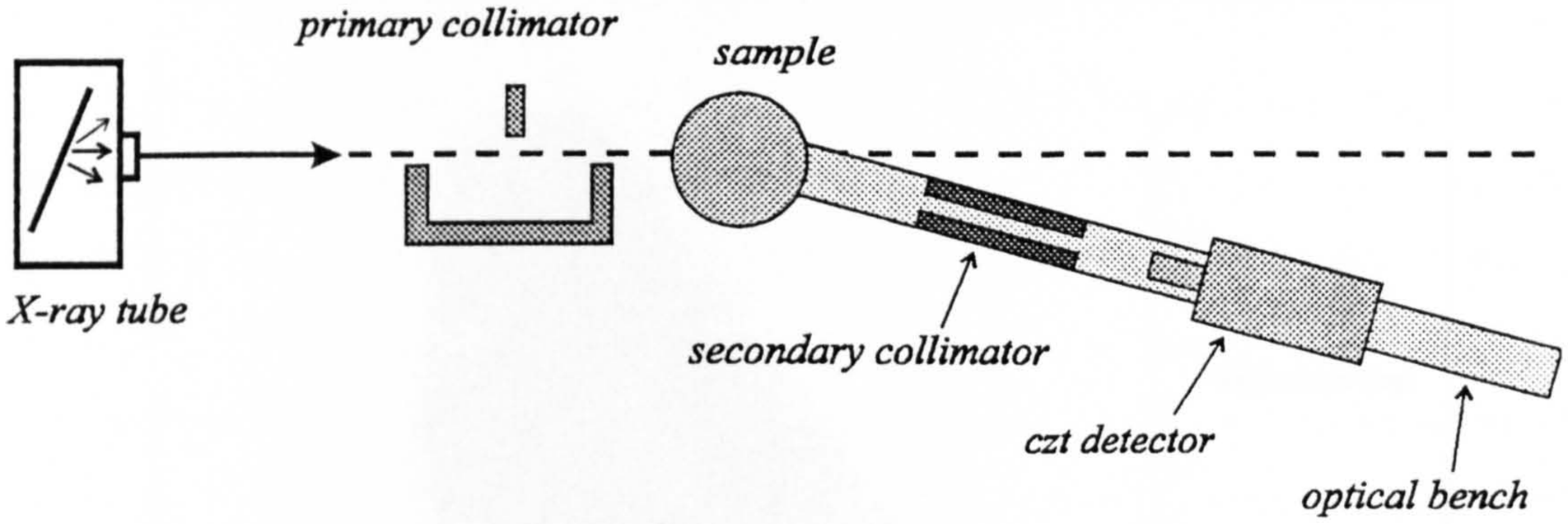

Figure 3.13 A diagram of the single cadmium zinc telluride (czt) detector and collimator simulation of a multiple angle system

The bench was pivoted underneath a platform onto which a sample can be placed. Positions for angles of 3° to 7.5° were marked at intervals of 0.5°. The bench could then be rotated to be set at any angle required. These intervals were chosen as they were shown by the modelled results to be the minimum needed to give sufficient angular resolution in the energy angle diagrams. The collimation used had an acceptance angle of 0.38° as was shown to be suitable in the previous section.

Measurements of the scatter signatures of SX2 and Semtex were taken at each angle for 100s each. This measurement time was chosen to achieve high statistical accuracy within the energy-angle plot. The X-ray tube current and peak voltage were used, as previously described in section 3.4. Figures 3.14 and 3.15 show the energy-angle plots for samples of SX2 and Semtex, taken with this single detector / single angle collimator system. These plots also show how that the planar spacings for both materials are satisfied by a range of angles and incident intensities.

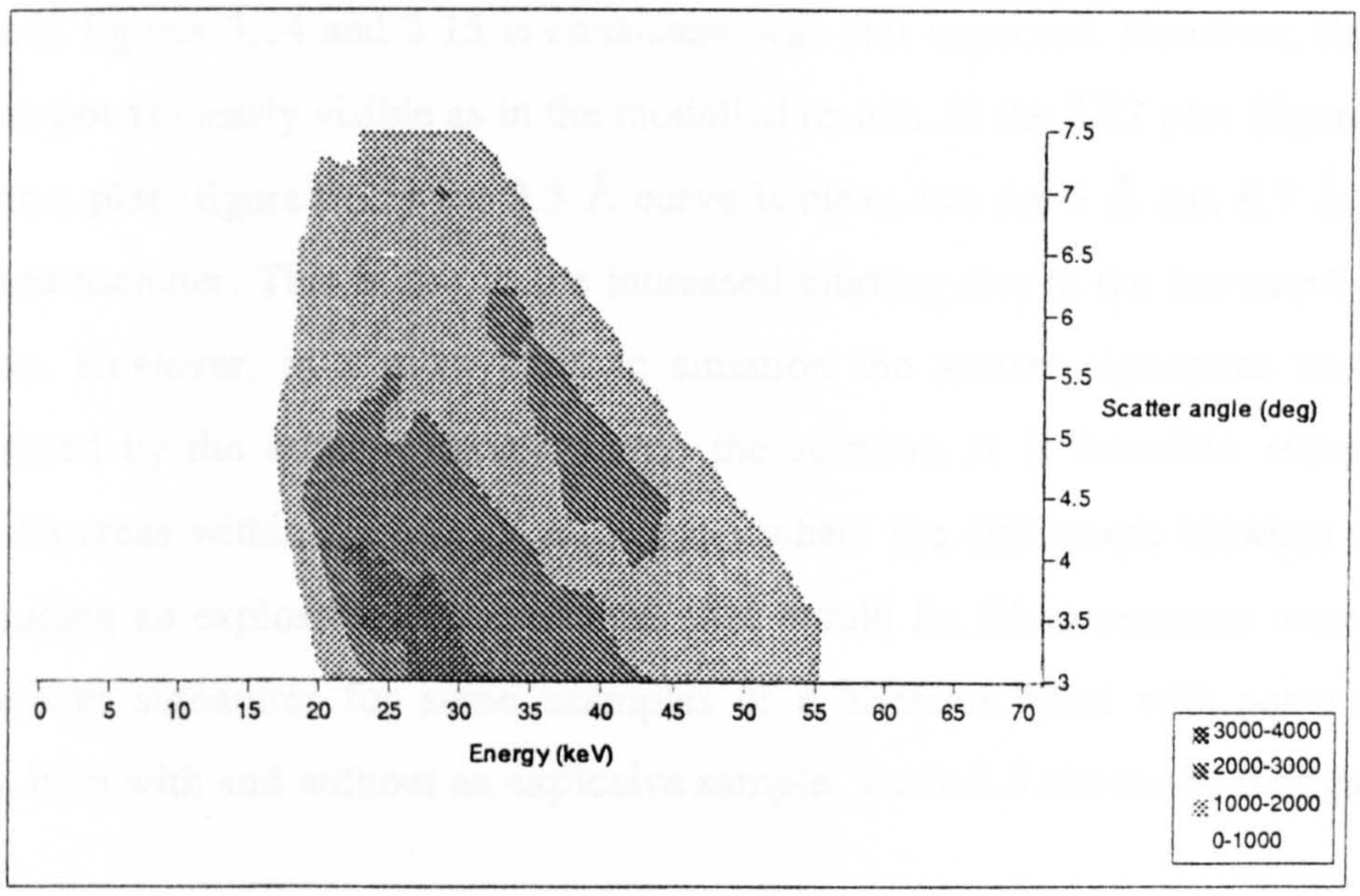

Figure 3.14 The energy-angle plot for a 6 mm sample of SX2 taken with the single detector / single angle collimator simulation at 0.5° intervals for 100 s (with 0.38° collimation)

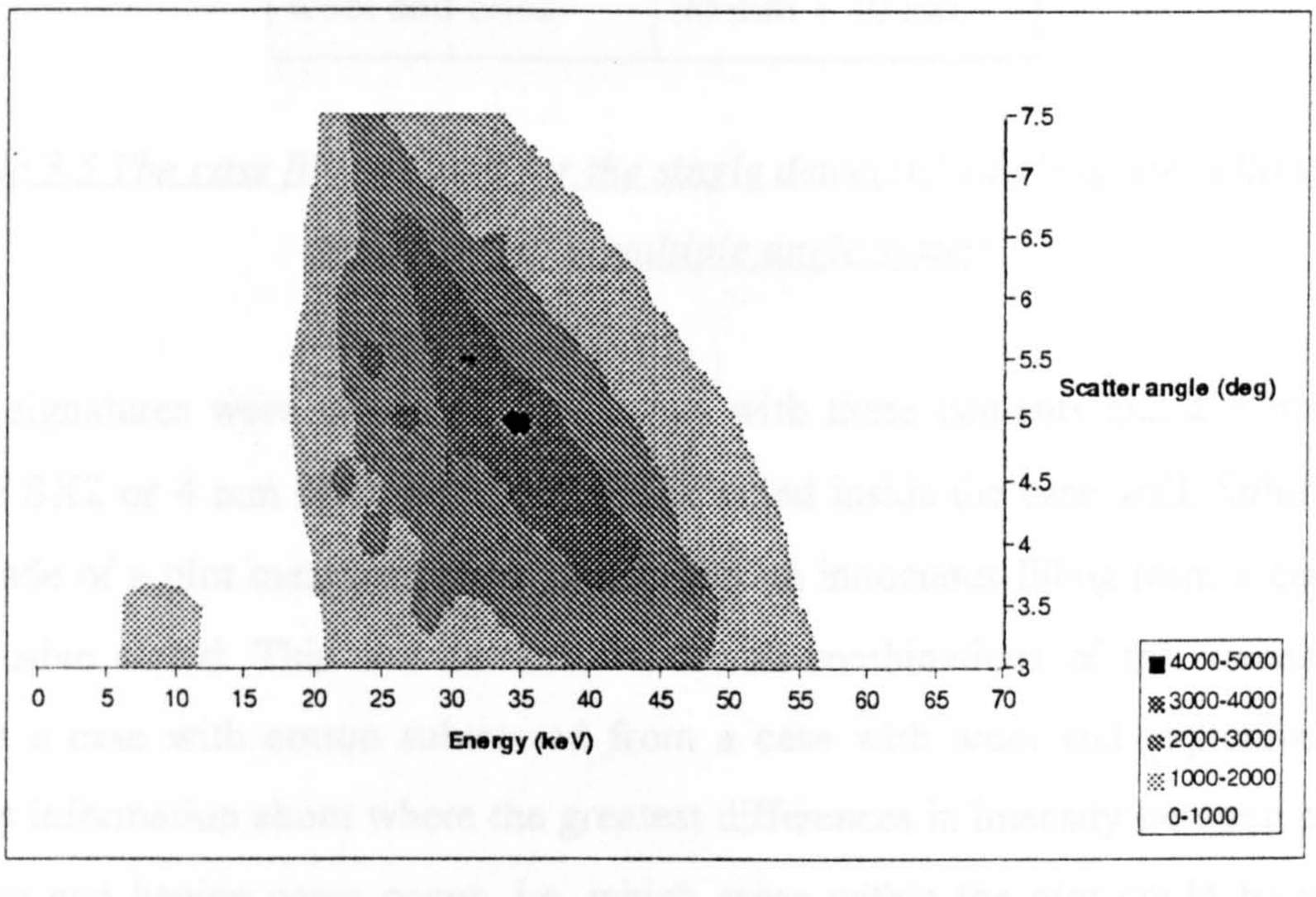

Figure 3.15 The energy-angle plot for a 4 mm sample of Semtex taken with the single detector / single angle collimator simulation at 0.5° intervals for 100 s (with 0.38° collimation)

The data in figures 3.14 and 3.15 is consistent was that expected. However, the three curves are not as clearly visible as in the modelled results. In the SX2 plot (figure 3.14) and Semtex plot (figure 3.15) the 3.3 Å curve is clear, but the 5 Å and 6.7 Å curves are blurred together. This is due to the increased blurring due to the increased energy resolution. However, in a more realistic situation the scatter signatures would be contaminated by the other materials within the suitcase. It is therefore essential to identify the areas within the energy angle plots where the differences between a filled case including an explosive and a harmless case would lie. Measurements were taken of the scatter signatures for some examples of a briefcase filled with some simple contents, both with and without an explosive sample. Table 3.5 shows the fillings used.

materials	**thicknesses**
cotton	100 mm
cotton and book	90 mm + 10 mm
wool	100 mm
wool and book	90 mm + 10 mm

Table 3.5 The case fillings used for the single detector / single angle collimator simulation of a multiple angle system

Scatter signatures were measured from cases with these contents and a 3 mm thick piece of SX2 or 4 mm thick piece of Semtex taped inside the case wall. Subtractions were made of a plot measured from a case with an innocuous filling from a case with an explosive added. This was carried out for all combinations of the contents (for example a case with cotton subtracted from a case with wool and explosive). This provides information about where the greatest differences in intensity between plots of explosive and benign cases occur, i.e. which areas within the plot could be used to identify the presence of an explosive. Figures 3.16, 3.17 and 3.18 show the plots for a case with a cotton filling, a case with a cotton filling with a 3 mm piece of SX2 added and the subtraction of these two plots. All signatures were collected with a measurement time of 100s.

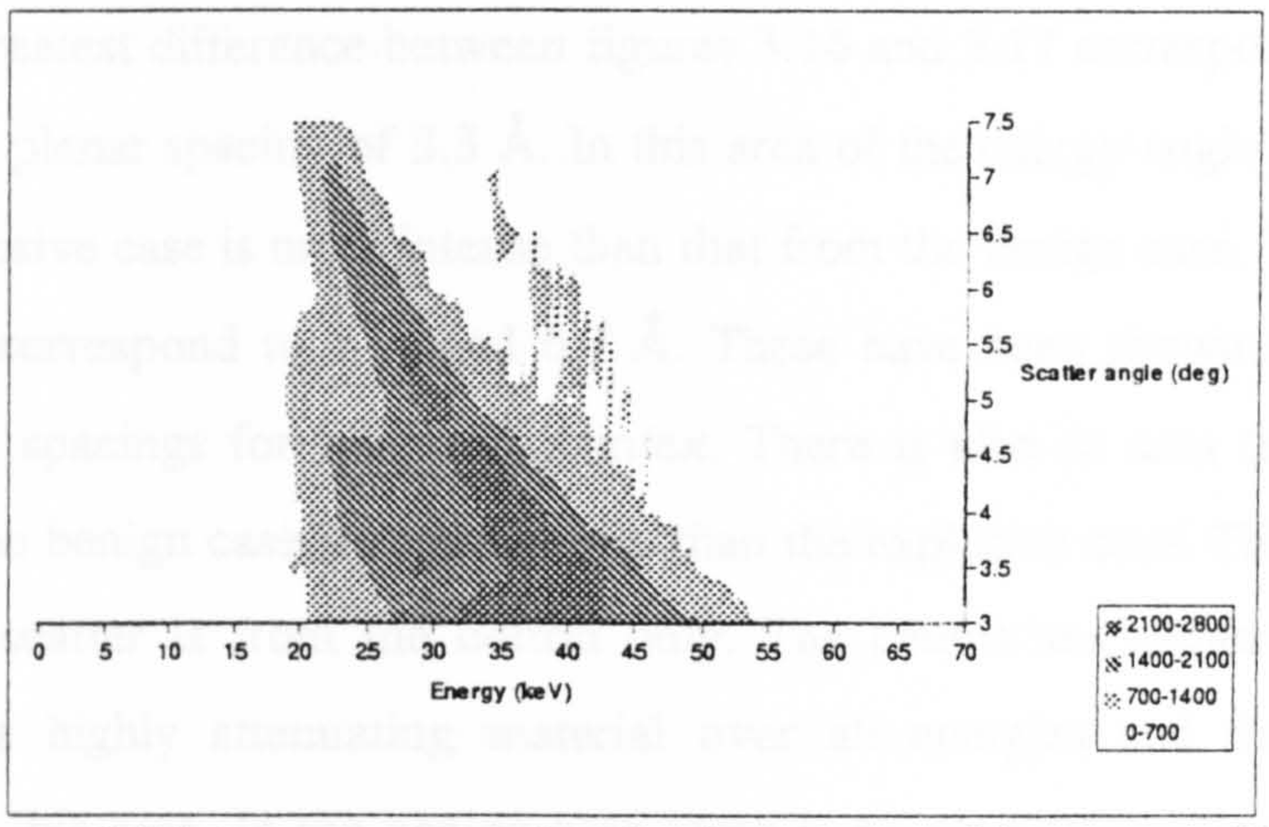

Figure 3.16 An energy-angle plot for a case with a cotton filling

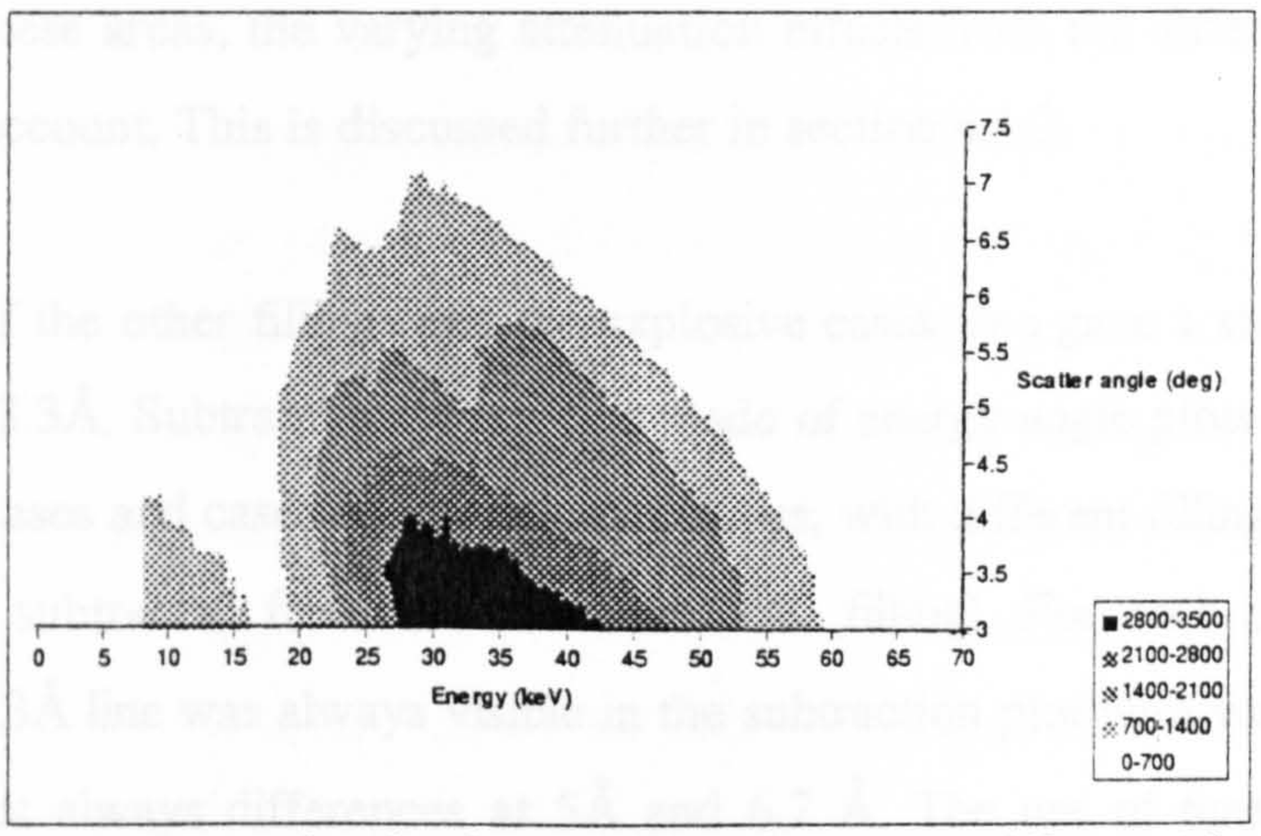

Figure 3.17 An energy-angle plot for a case with a cotton filling with a piece of SX2 added

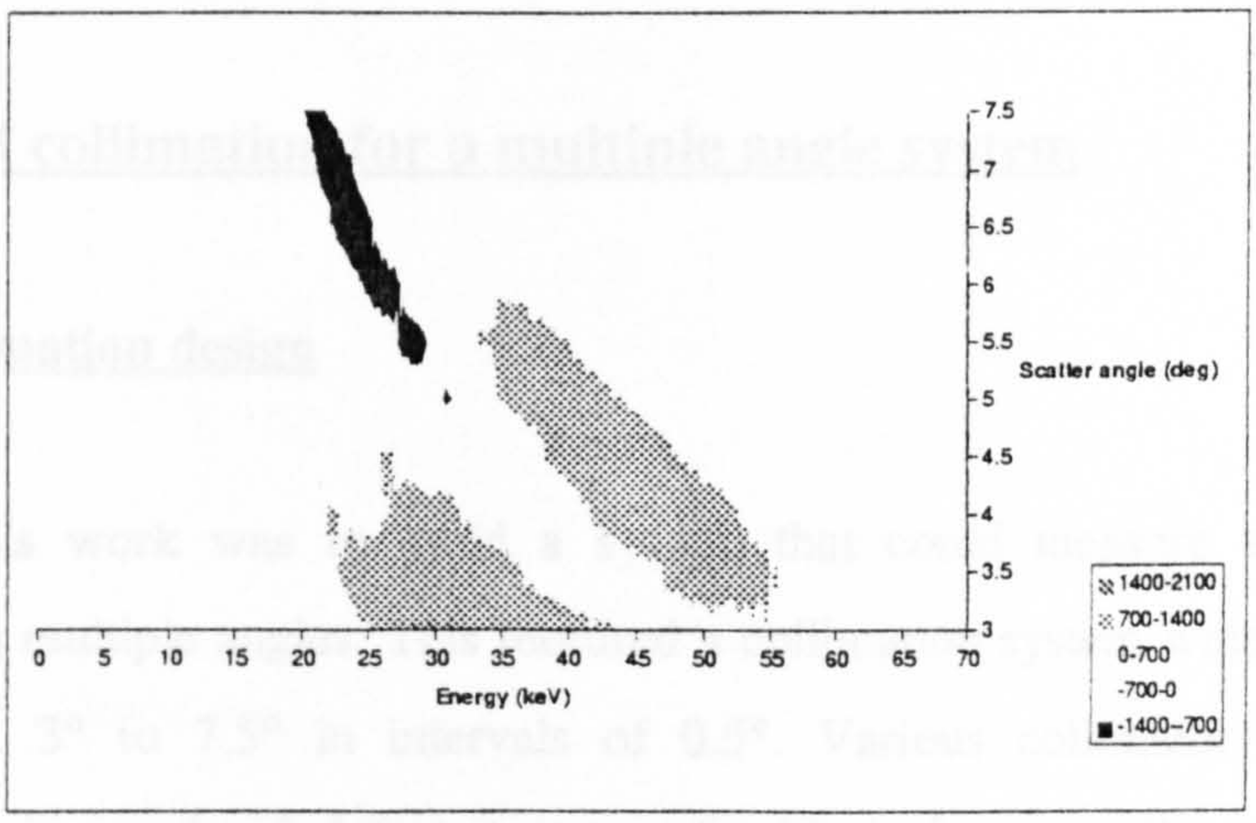

Figure 3.18 An energy-angle plot of the subtraction of figures 3.16 and 3.17

The area of greatest difference between figures 3.16 and 3.17 corresponds to coherent scatter from a planar spacing of 3.3 Å. In this area of the energy-angle plot the scatter from the explosive case is more intense than that from the benign case. The other areas of difference correspond to 5 Å and 6.7 Å. These have been shown to be the most intense planar spacings for SX2 and Semtex. There is also an area (negative in this plot) where the benign case is more intense than the explosive case. This is because in this area the scatter is from the cotton only. The counts are negative because the explosive is a highly attenuating material over all energies and therefore causes attenuation in this area. In the benign case there is no such attenuation and therefore the scatter from this area is stronger for the benign case. In direct comparisons of intensities in these areas, the varying attenuation effects from the different cases must be taken into account. This is discussed further in section 4.1.2.

Subtractions of the other fillings and the explosive cases also gave a strong difference in the area of 3.3Å. Subtractions were also made of energy-angle plots corresponding to innocuous cases and cases containing explosives, with different fillings (for example a wool filling subtracted from a cotton and SX2 filling). For each combination of contents the 3.3Å line was always visible in the subtraction plot with varying intensity. There were not always differences at 5Å and 6.7 Å. The use of these three planar spacings for an analysis procedure is discussed further in section 4.3.1.

3.6 Design of collimation for a multiple angle system

3.6.1 The collimation design

The aim of this work was to build a system that could measure all the scatter signatures from multiple angles. This required a collimation system which included all ten angles, i.e. 3° to 7.5° in intervals of 0.5°. Various collimator designs were considered, but it was decided that it was preferable to have a collimator made of a single block of material so that no relative movement can take place within the structure of the collimator. In designing a collimator the cost, weight, attenuation

properties and ease with which the material can be worked must all be taken into consideration. Hence, it is important make the collimator from a suitable material.

From the scatter signatures measured in section 3.4 it was decided to build two collimators for the single detector system, one with a slit width of 0.5 mm and the other with a slit width of 1.0 mm. Both were 150 mm in length which gave acceptance angles of 0.19° and 0.38° respectively. The slit height was 10 mm so as to ensure that the 5 mm height of the detector crystal was fully irradiated.

Figure 3.19 shows a diagram of the design of the collimator. Scatter angles 3°, 4°, 5°, 6° and 7° are positioned to scatter to one side of the incident beam and angles 3.5°, 4.5°, 5.5°, 6.5° and 7.5° are positioned on the other side. This is because the spacing between these angles is very small unless the detectors are a long way from the scatter point. The reduction in flux as the detectors are moved further away from the source of radiation is governed by an inverse square relationship. Therefore it was convenient to keep the detectors and collimator as close to the scatter point as possible. By positioning the scatter angles alternately on either side of the collimator there is more space available between the individual slits. This is an important factor to ensure that each detector only receives scatter from one scatter angle. A compromise between spacing of the detector positions and maximising the flux was found with a scatter to detector distance of 286 mm. This allowed 5 mm between each collimation slit.

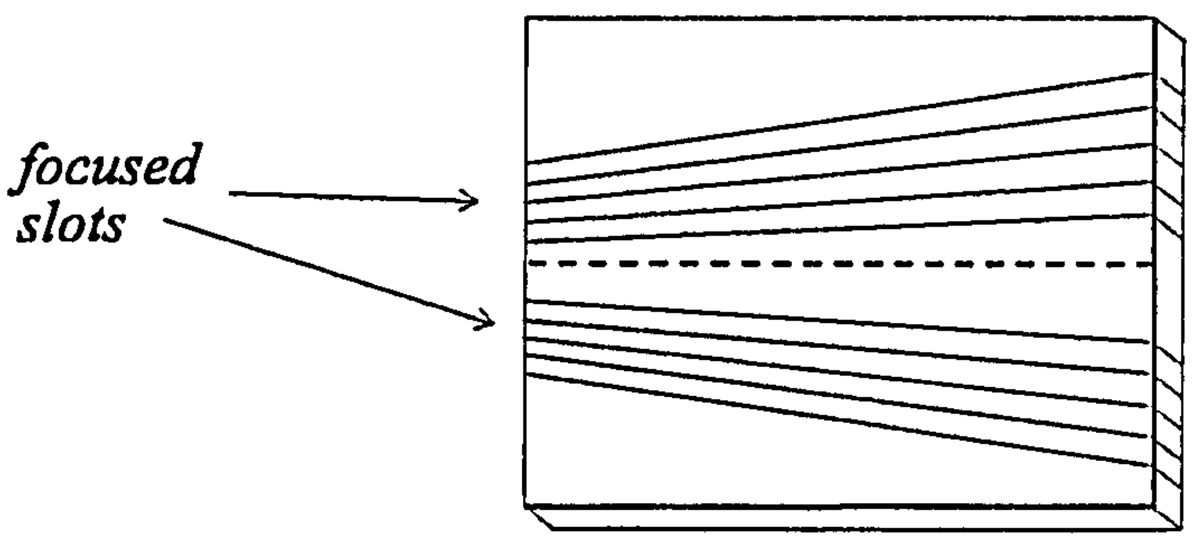

Figure 3.19 A diagram of the design of the multiple angle collimator

The material chosen was dural (aluminium alloy), as it is light weight (density = 2.71 gcm^{-3}), cheap and easy to work with. In designing a collimator it is important to consider whether a photon could reach the detector by passing through the collimator material. Linear attenuation calculations *(Berger and Hubbell 1987)* were carried out for photons travelling along paths other than those required (i.e. passing between the slits). The collimator was designed to be 150 mm in length as a beam of 70 keV photons would be attenuated by more than 99% in entering in to one slit and travelling through the collimator body to pass out of an adjacent slit. This is considered as acceptable transmission properties for a collimator *(Sorenson and Phelps 1987)*.

A system with an array of multiple detectors is described in Chapter 5, but first the single eV-180 detector was used to simulate an array of detectors by moving it to each collimator slit in turn. This allowed the design and testing of the multiple angle collimator to be carried out without having to take the energy resolution and efficiency effects of different detectors into account.

3.6.2 Testing the multiple angle collimation

The most important factor in the multiple angle system was whether the ten slits in the collimator all focused at the same point. If the collimators do not focus on the same point then scatter signatures would be measured from different positions in the case. The collimators were tested by measuring the positions of the slits at both ends of the collimator and plotting out the focal point. Figures 3.20 and 3.21 show the results from these measurements.

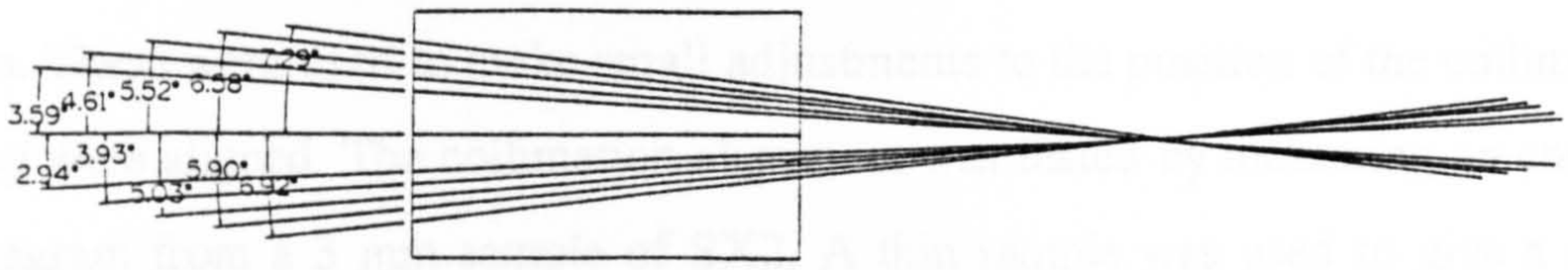

Figure 3.20 Testing the focal point of the 0.19° collimator

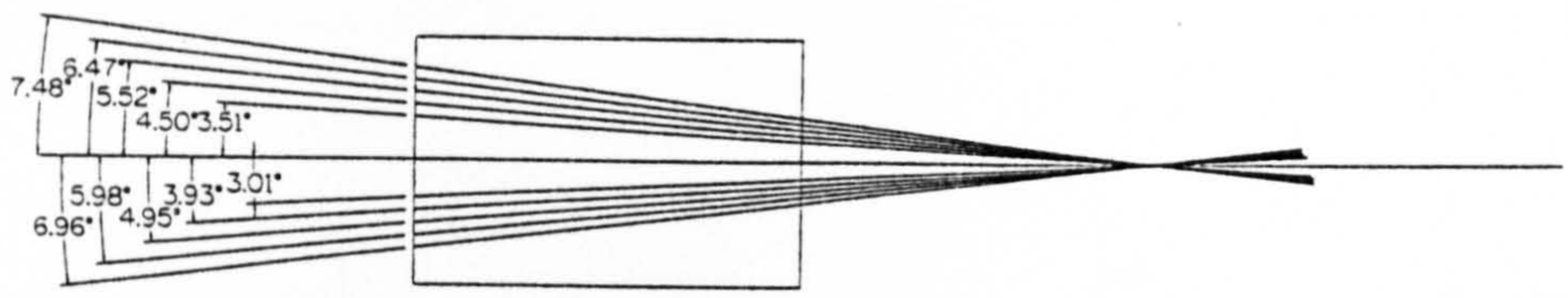

Figure 3.21 Testing the focal point of the 0.38° collimator

It can be seen in the plots of the focal points of the two detectors that the 0.38° collimator focuses well and all the angles are within ±0.05°. The 0.19° collimator does not focus quite so well and the angles are within ±0.1°, however this is less than the acceptance angle of the slits and therefore the error is not detrimental. For the 0.19° collimator the 7.5° slot crosses the incident beam at a point much further from the collimator than the others. However, since this is an extreme angle in the energy angle plot and it has the lowest coherent scatter cross-section, it was therefore decided to accept this collimator.

The collimators were then set up in the coherent scatter system using a laser beam, pivoted at the scatter point, to align each angle. The collimators were mounted on rotation and translation units, which could adjust the position of the collimator in the plane parallel to the laboratory table, and could also be adjusted in the vertical direction. These were used to make small adjustments to the position of the collimators until they were aligned. The collimation alignment was tested by measuring an energy-angle diagram from a 3 mm sample of SX2. A thin sample was used to give a more stringent test of the focal point. Figures 3.22 and 3.23 show the energy angle diagrams of the sample of SX2 measured using the 0.19° and 0.38° multiple angle collimators.

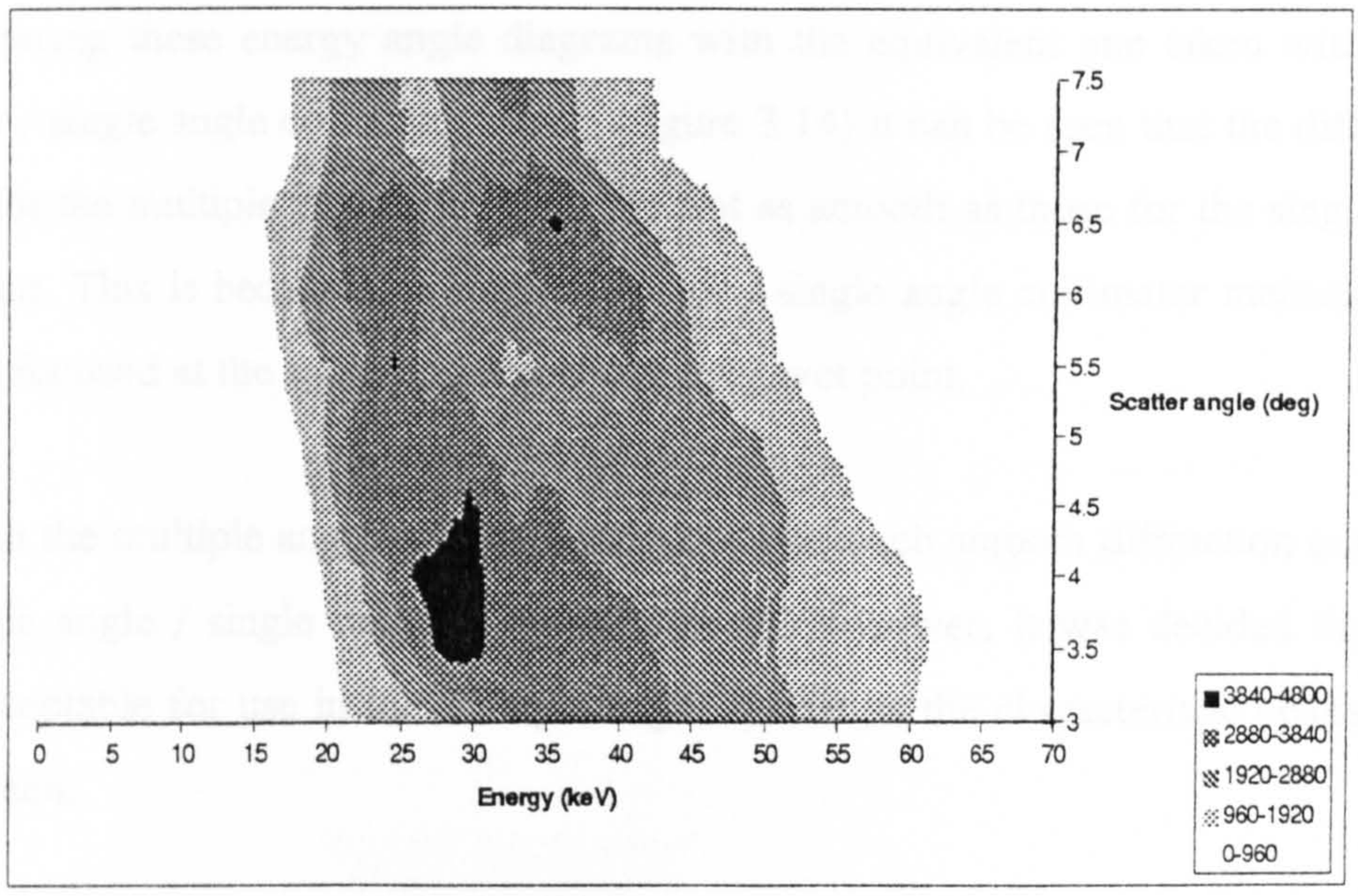

Figure 3.22 An energy-angle diagram of a 3 mm sheet of SX2 using the 0.19° multiple angle collimator

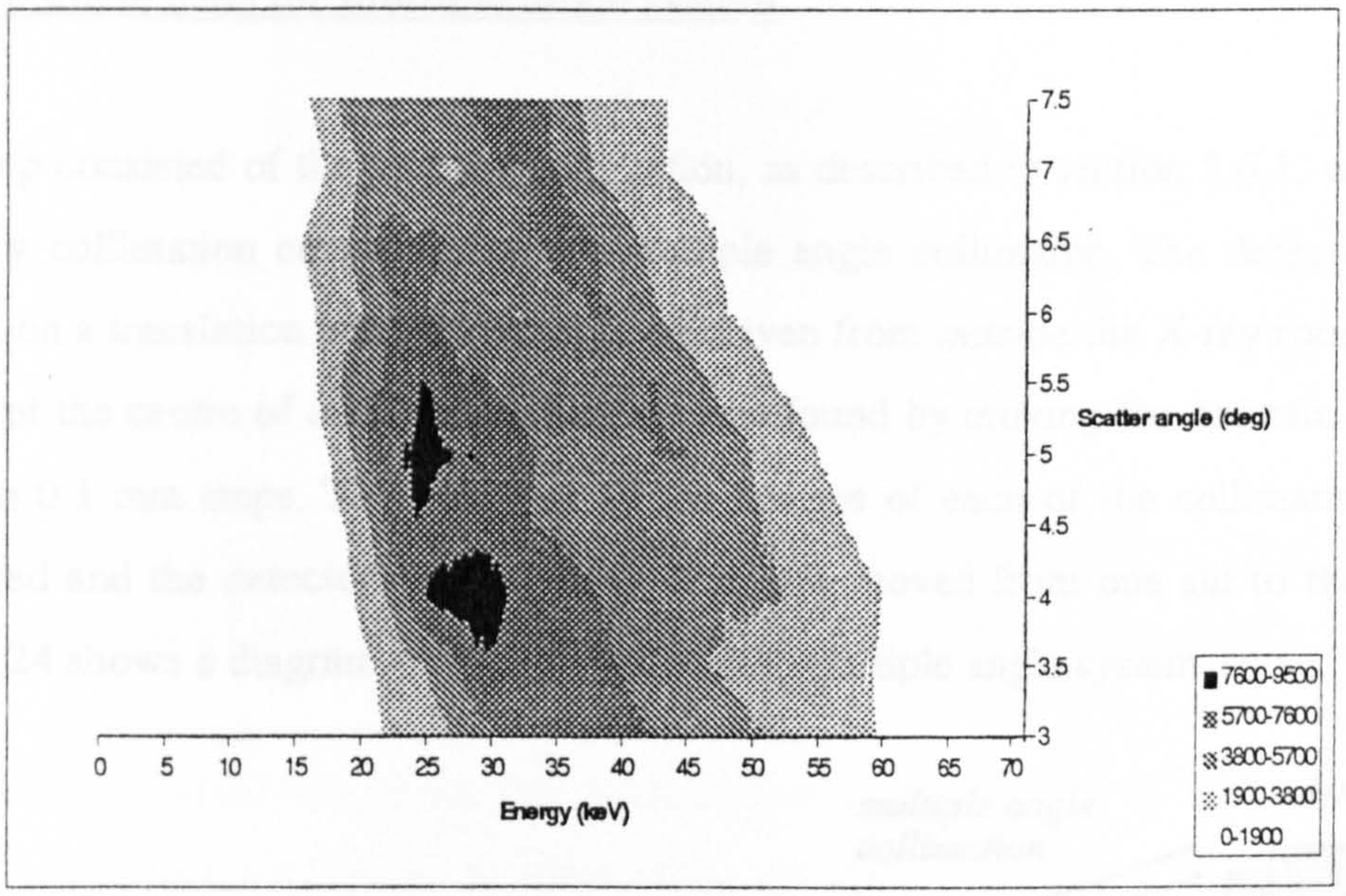

Figure 3.23 An energy-angle diagram of a 3 mm sheet of SX2 using the 0.38° multiple angle collimator

In comparing these energy angle diagrams with the equivalent one taken with single detector / single angle collimator set-up (figure 3.14) it can be seen that the diffraction curves for the multiple angle collimator are not as smooth as those for the single angle collimator. This is because the single detector / single angle collimator measurements were all focused at the same position above the pivot point.

Although the multiple angle collimators do not give such smooth diffraction curves as the single angle / single detector measurements. However, it was decided that they were acceptable for use in the multiple angle system as the characteristic peaks could still be seen.

3.7 Description of the multiple angle system

3.7.1 The single detector multiple angle system

The set-up consisted of the primary collimation, as described in section 1.6.1, with the secondary collimation consisting of the multiple angle collimator. The detector was mounted on a translation unit which could be driven from outside the X-ray room. The position of the centre of each collimation slit was found by moving the detector across the slit in 0.1 mm steps. The positions of the centres of each of the collimation slits were noted and the detector could then be remotely moved from one slit to the next. Figure 3.24 shows a diagram of the single detector multiple angle system

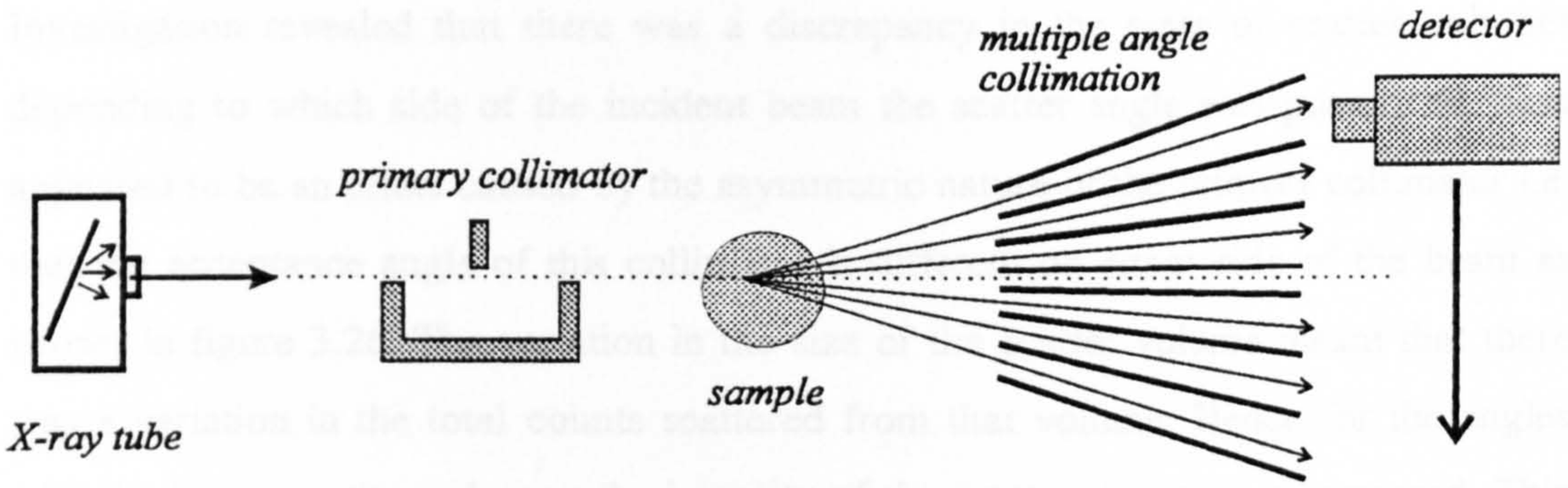

Figure 3.24 A diagram of the single detector multiple angle coherent scatter system

3.8 Effects of the multiple angle collimation

There was a variation in intensity between the angles scattered to either side of the incident beam (i.e. on either side of the multiple angle collimator). This caused a periodic variation in intensity which varied every 0.5° angle (figure 3.25 shows an example of this). The effect can be seen as a wobble in the edges of the scatter signatures. This effect was not so obvious for the thin samples as the scatter volume was not filled .

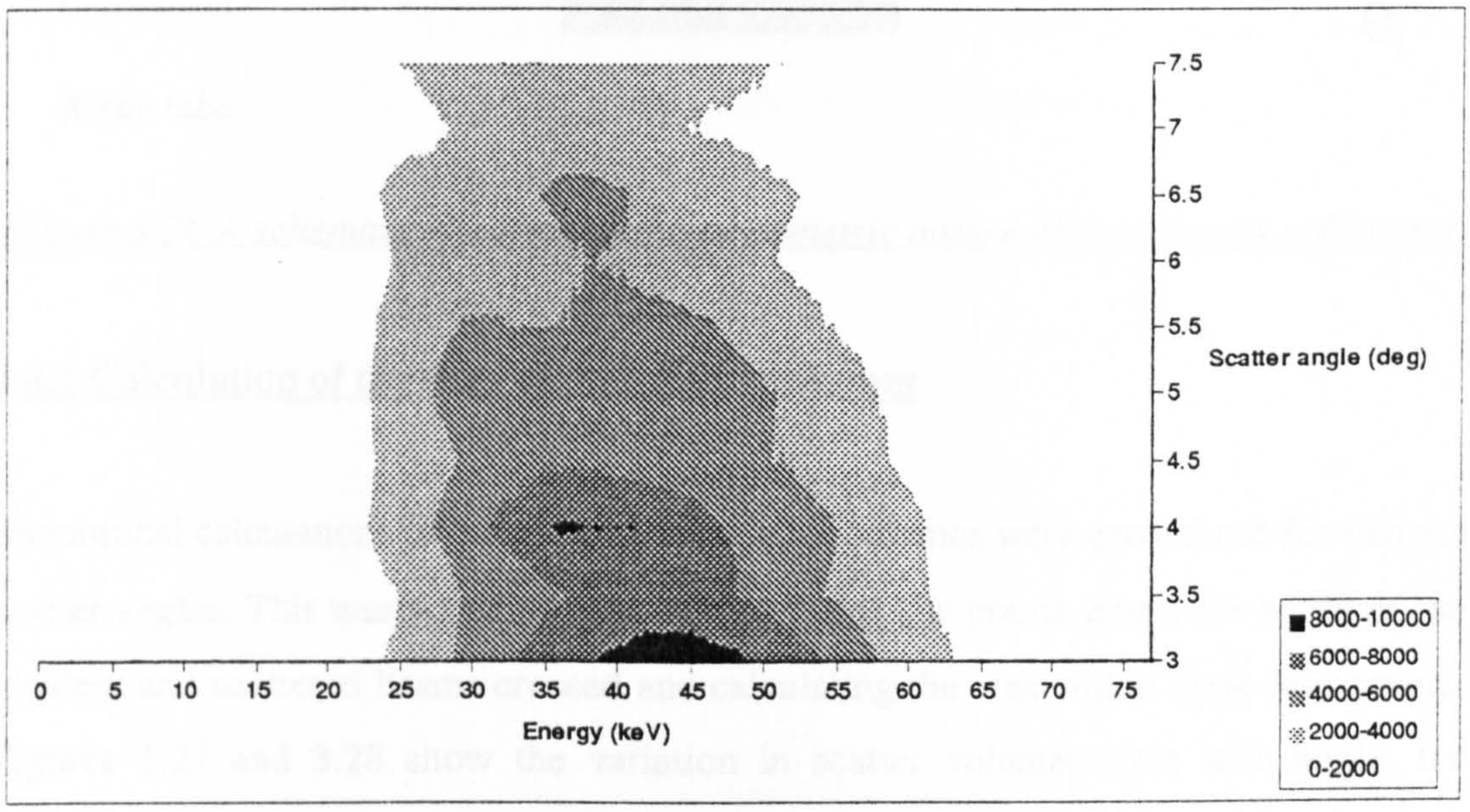

Figure 3.25 The variation in intensity between the angles scattered on either side of the primary collimator for a case with a cotton filling and explosive

Investigation revealed that there was a discrepancy in the sizes of scatter volumes depending to which side of the incident beam the scatter angle was positioned. This appeared to be an effect caused by the asymmetric nature of the primary collimator i.e. that the acceptance angle of this collimator is different on either side of the beam as shown in figure 3.26. The variation in the size of the scatter volume meant that there was a variation in the total counts scattered from that volume. Hence for the angles with the larger scatter volumes, the intensity of the scatter signature is increased. This

causes the variation in appearance between adjacent angles in the energy-angle diagram. The following section describes this is more detail.

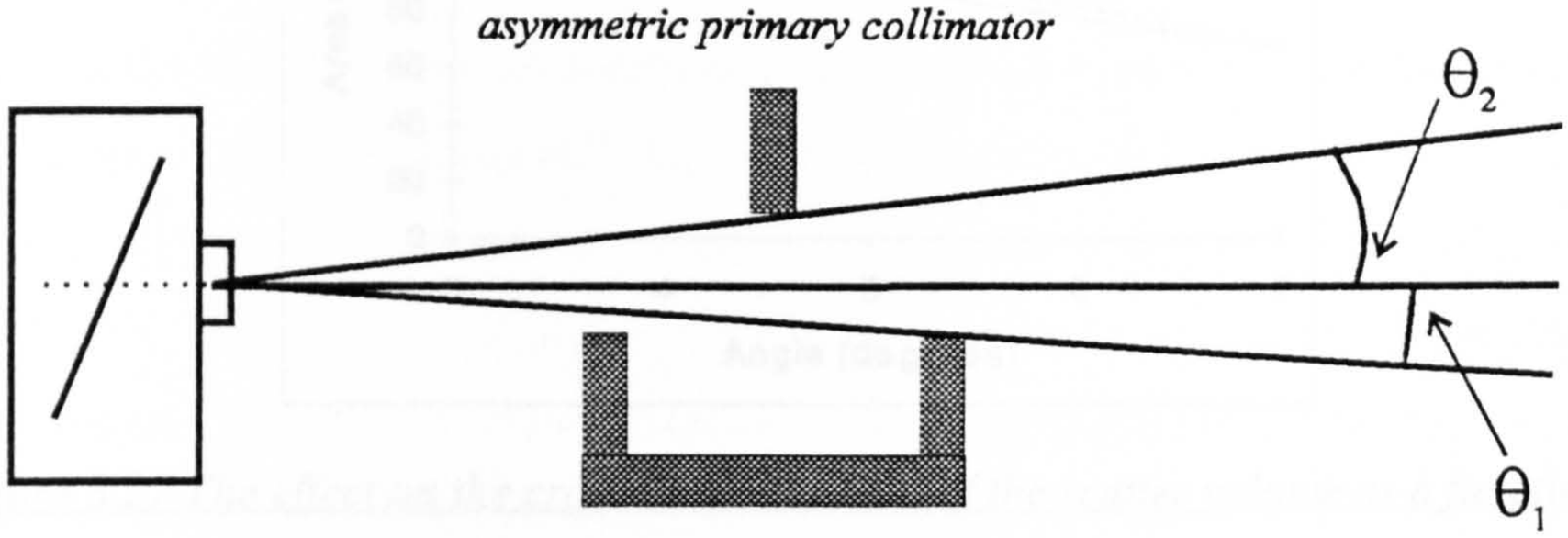

Figure 3.26 A schematic diagram of the asymmetric nature of the primary collimator

3.8.1 Calculation of the sizes of the scatter volumes

Theoretical calculations of the sizes of the scatter volumes were carried out for various scatter angles. This was accomplished by calculating the points where the edges of the incident and scattered beams crossed and calculating the area within these four points. Figures 3.27 and 3.28 show the variation in scatter volumes sizes with angle, for scatter angles on either side of the incident beam. Totally asymmetric collimation (i.e. both primary and secondary collimation are asymmetric) is shown in figure 3.27. Partially asymmetric collimation (i.e. primary collimation is asymmetric and secondary collimation is symmetric) is shown in figure 3.28. θ_1 and θ_2 are for scatter angles to the side as shown in figure 3.26.

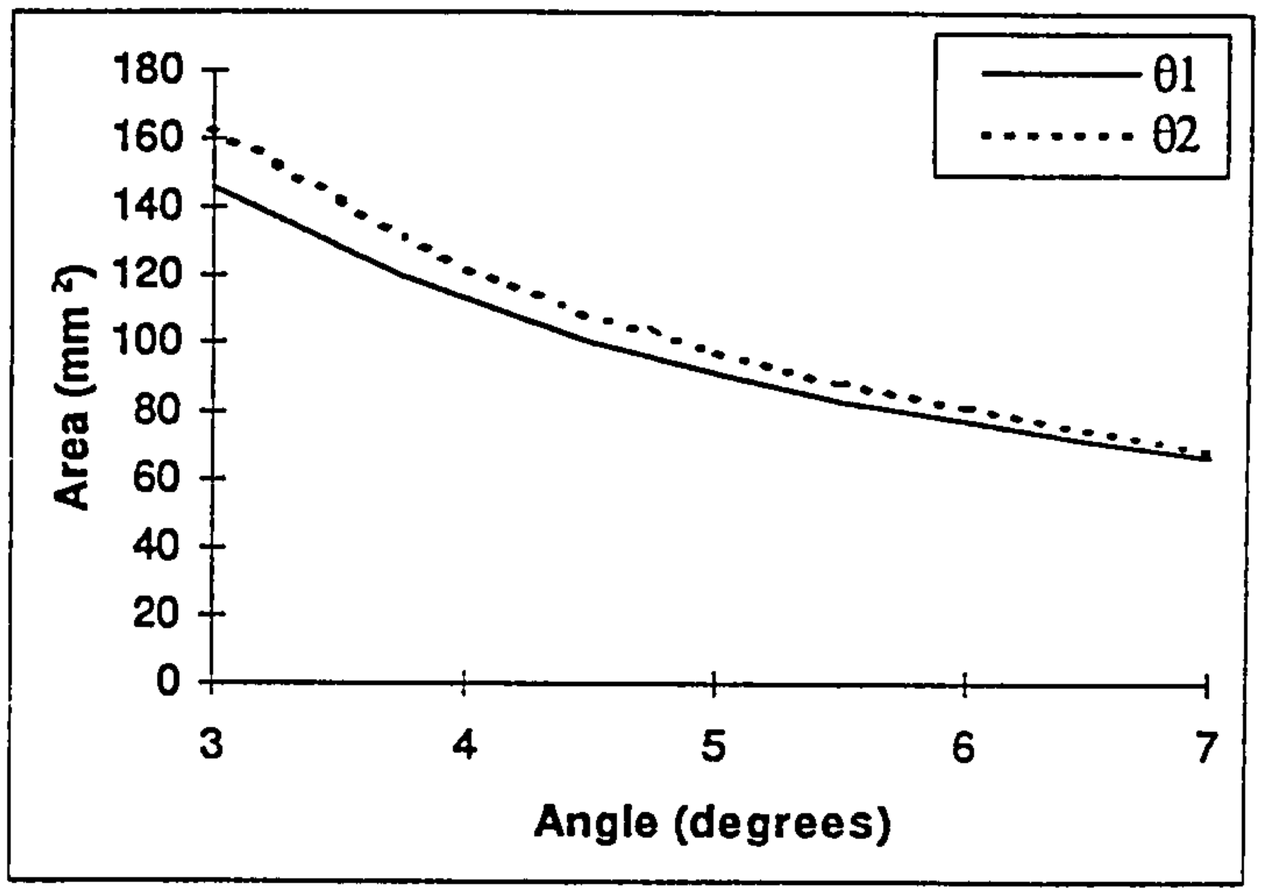

Figure 3.27 The effect on the cross-sectional area of the scatter volume as a function of angle for totally asymmetric collimation

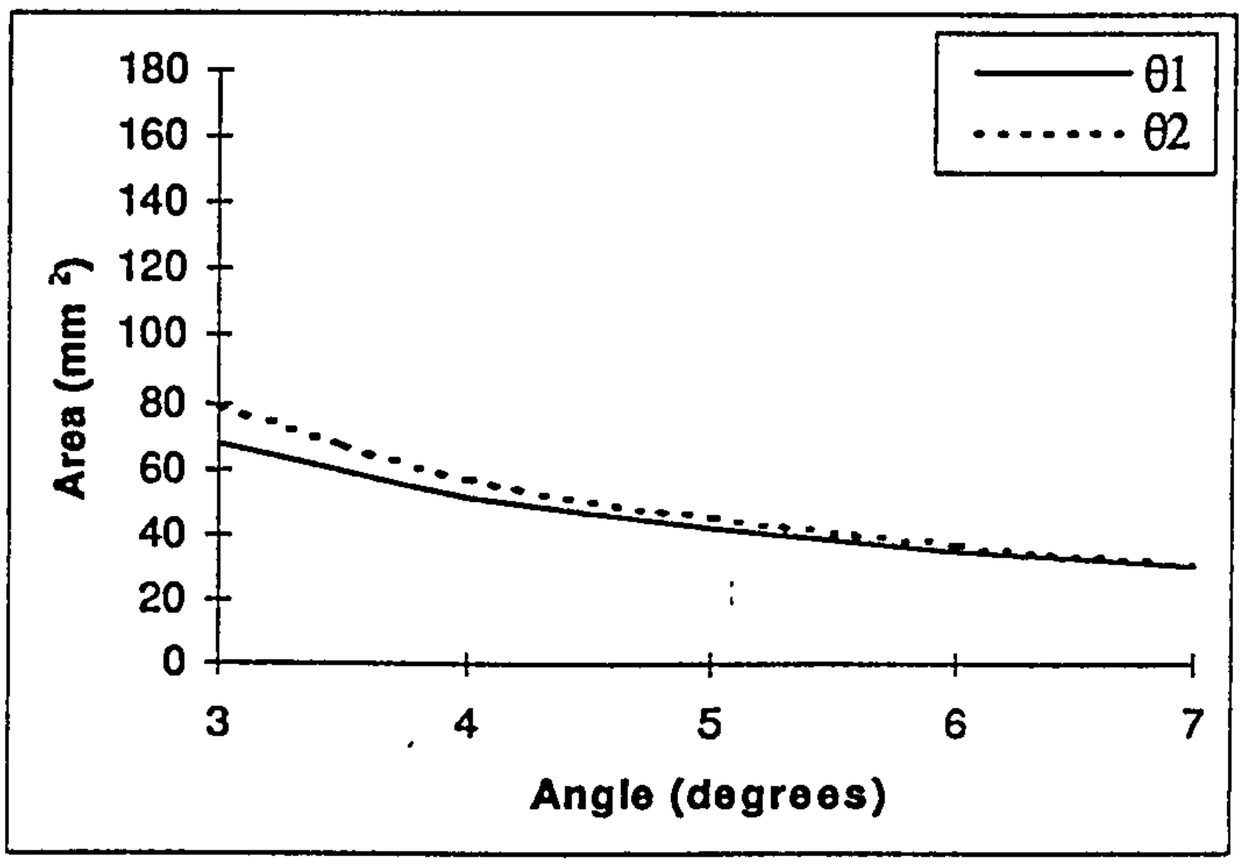

Figure 3.28 The effect on the cross-sectional area of the scatter volume as a function of angle for partially asymmetric collimation

The collimation on the original single scatter angle system had been designed as totally asymmetric so as to make alignment of the collimators easier. This is because the open design of this asymmetric collimation allows the user to see the laser beam, which was used for alignment of the collimators, passing through the collimator. (It should be noted that this system has also been used for other coherent scatter measurements for which the asymmetry did not cause variations in scatter volume size as all measurements were taken to one side of the incident beam.)

The greatest variation between the cross-sectional areas on either side is for the totally asymmetric collimation. This is as expected as there is a difference between θ_1 and θ_2 (see figure 3.26) for both the incident and secondary collimation. There is also an overall increase in cross-sectional area for the totally asymmetric collimation with respect to the partially asymmetric collimation. This is due to the design of the multiple angle scatter collimators being different from the original single angle collimator. The opening angle of the symmetrical secondary collimation is smaller (0.38° compared with 0.57°). Also the dimensions of the system are slightly smaller for the multiple angle system (286 mm sample to detector distance compared with 570 mm for the totally asymmetric system), hence the scatter volumes are smaller.

3.8.2 Measurement of scatter volumes

The scatter volumes were also mapped out experimentally to investigate the variation of intensity of scatter to either side of the incident beam. Mapping out of the scatter volumes also determined the variation in sensitivity across the horizontal cross-sectional area of the volume. Both the partially and totally asymmetric collimation were investigated.

The collimation width was set at 1 mm (the 0.38° collimator) and an aluminium wire of 0.5 mm diameter was used to measure the scatter. This meant that the wire was thinner than the collimation width yet thick enough to produce a scatter intensity with good statistics. The wire was then mounted vertically on two translation stages perpendicular to each other (see figure 3.29).

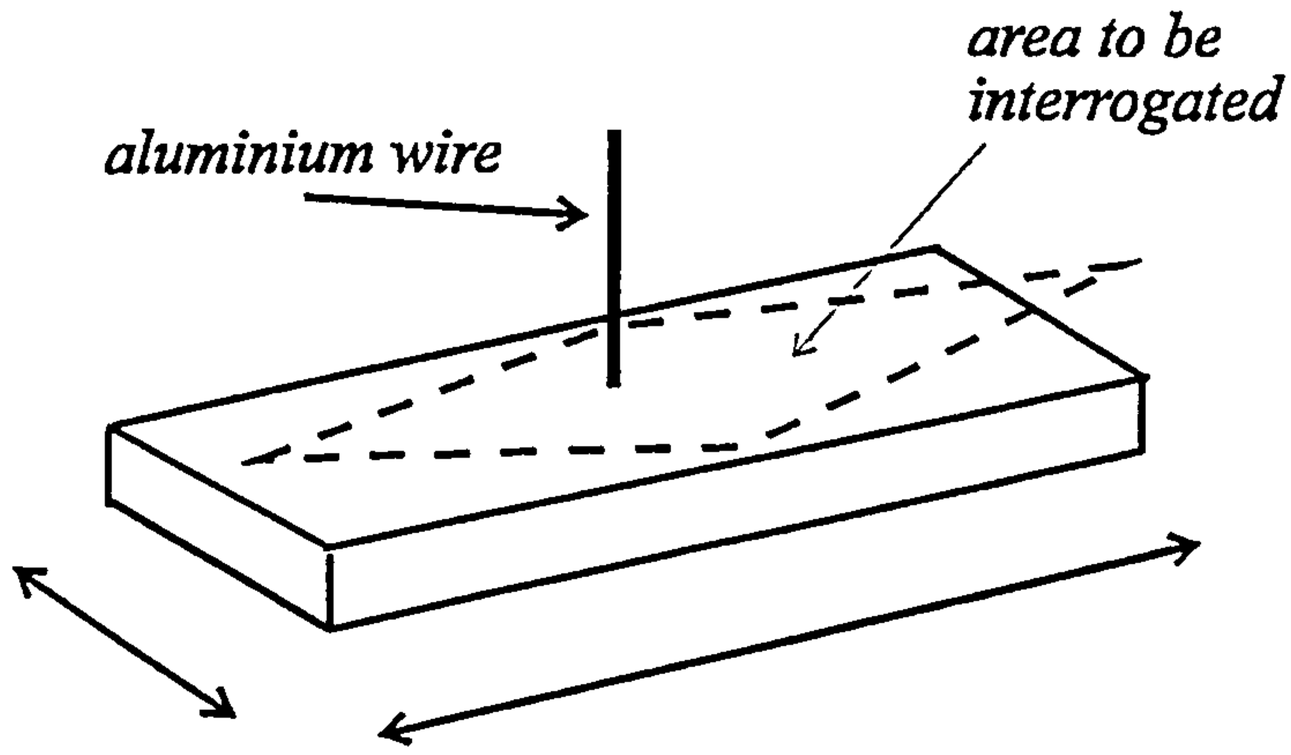

Figure 3.29 A diagram of the equipment used to map out the scatter volume

Translation stages were used to move the wire to ten positions perpendicular to the incident beam and ten positions parallel to the incident beam (i.e. 100 points), within the scatter volume. At each position the scatter from the wire was measured. The integrated scatter was then calculated and plotted at each point. Figure 3.30 shows the variation of intensity and shape of the scatter volume for totally asymmetric collimation at scatter angles of 3°, 5° and 7°. It should be noted that, due to the scatter volumes being ~5 mm wide and up to 150 mm long, the scales representing distances parallel to the beam have been reduced.

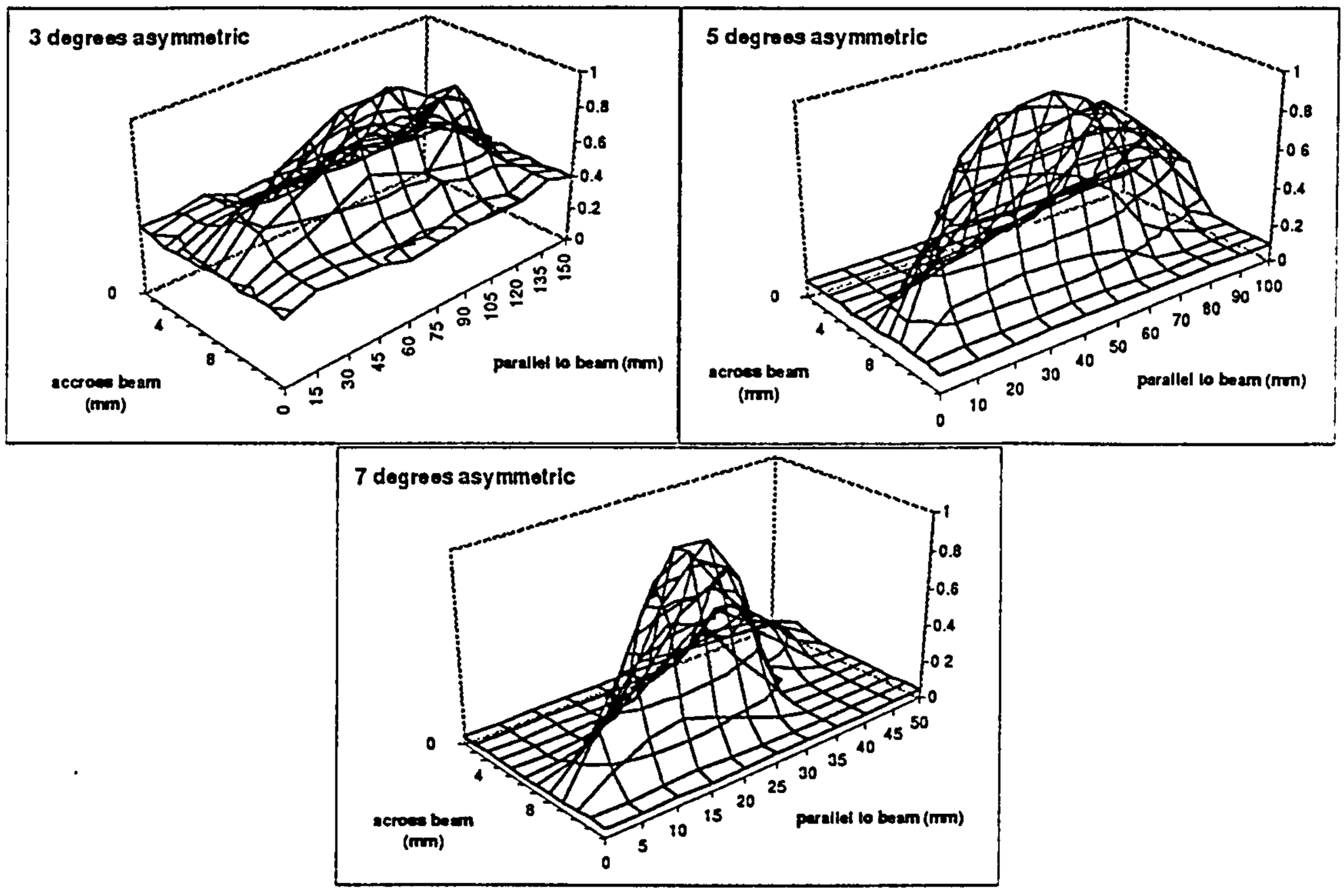

Figure 3.30 The variation of intensity within the scatter volume for 3°, 5° and 7° scatter angles for totally asymmetric collimation

It can be seen from the plots in figure 3.30 that the scatter volume increases in length, in the direction parallel to the beam, with reduction in scatter angle. Also, the background counts for the 3° plot are greater than those for the other angles. This is thought to be for two reasons. The first is that the cross-sectional area of the scatter volume for 3° is greater than for 5° and 7°, and therefore more scatter was measured from the base supporting the wire. Use of a longer piece of wire, to increase the distance from the scatter volume to the base, would have reduced the scatter from the base. However, the length required to do this, of such thin wire, was difficult to keep vertical and vibrated with each movement of the translation stage. The second reason for the increased background is that the integrated scatter intensity is less at 3° than for 5° and 7°. This is because the most intense planar spacing for aluminium occurs at 3° at a high energy within the 70 kVp spectrum and hence with reduced intensity. Therefore in the normalised plot for 3°, the effect is that the background counts are increased relative to the background for 5° and 7°.

However, for all the angles measured, the maximum intensity is in the central part of the volume, this is in approximately the same position for all of the scatter angles. It is at this position that the greatest range of scatter angles occurs. That is, at the edges of the volume the range of acceptance angles detected is very limited, whereas in the centre it is large. This result agrees with previous computer simulations *(Luggar et al. 1996b)*. The variation in intensity is further enhanced by the difference in intensity across the focal spot in the X-ray tube.

The method of experimentally mapping out the scatter volume was also used to investigate the variation in size and shape when adjacent angles were scattered to either side of the incident beam. Figure 3.31 shows the difference between 5° scattered to one side and 5.5° scattered to the other side for the partially asymmetric collimation.

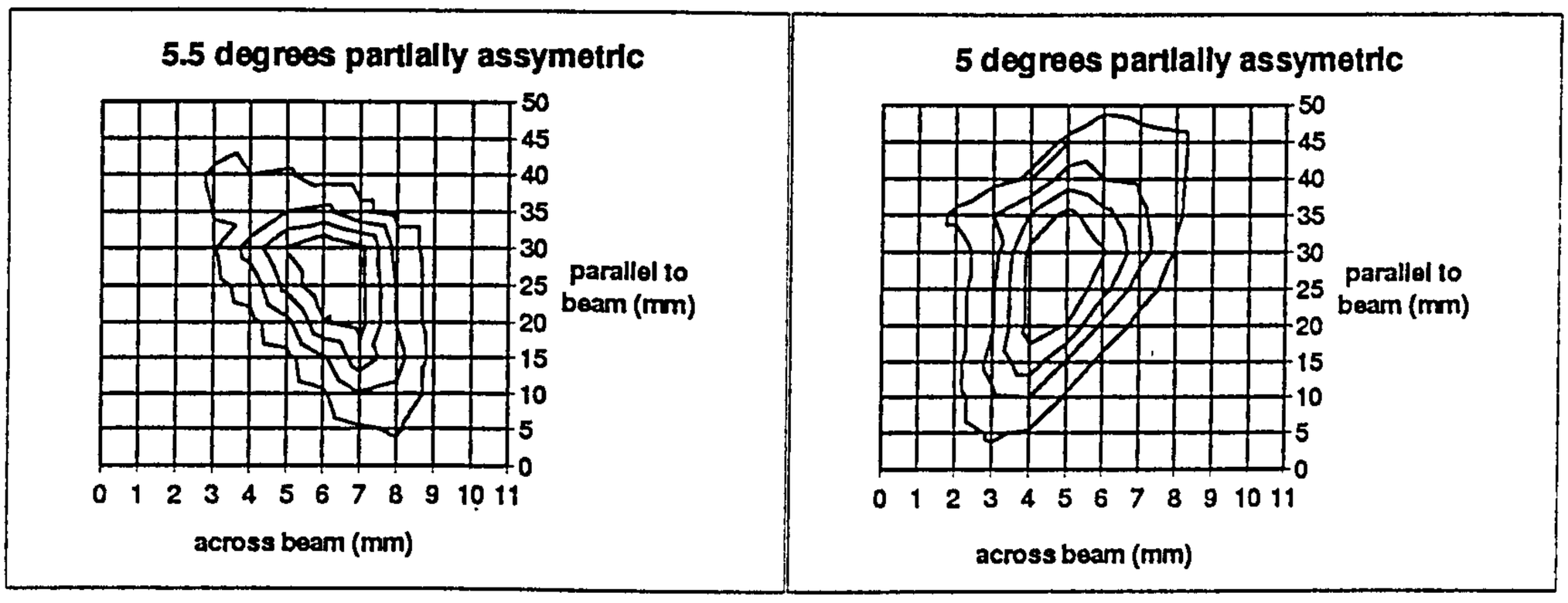

Figure 3.31 The variation in scatter volume shape for scattering to either side of the incident beam for partially symmetric collimation

The volume measured for 5° is longer than for 5.5°. This is because the 5° angle is scattered to the side of the primary collimator with the single leaf i.e. the side with the greatest acceptance angle. Figure 3.32 shows a schematic diagram of the difference in the shape of the cross-sectional area for the scatter angle on either side of the incident beam. Also, 5° is expected to be a slightly longer scatter volume than 5.5° because it is a smaller angle.

A comparison of 5° scatter volume for the totally asymmetric collimation (figure 3.30) and for the partially asymmetric (figure 3.31) shows that the size of the totally symmetric volume is longer. This is confirmed by the calculated cross-sectional areas (see figures 3.27 and 3.28).

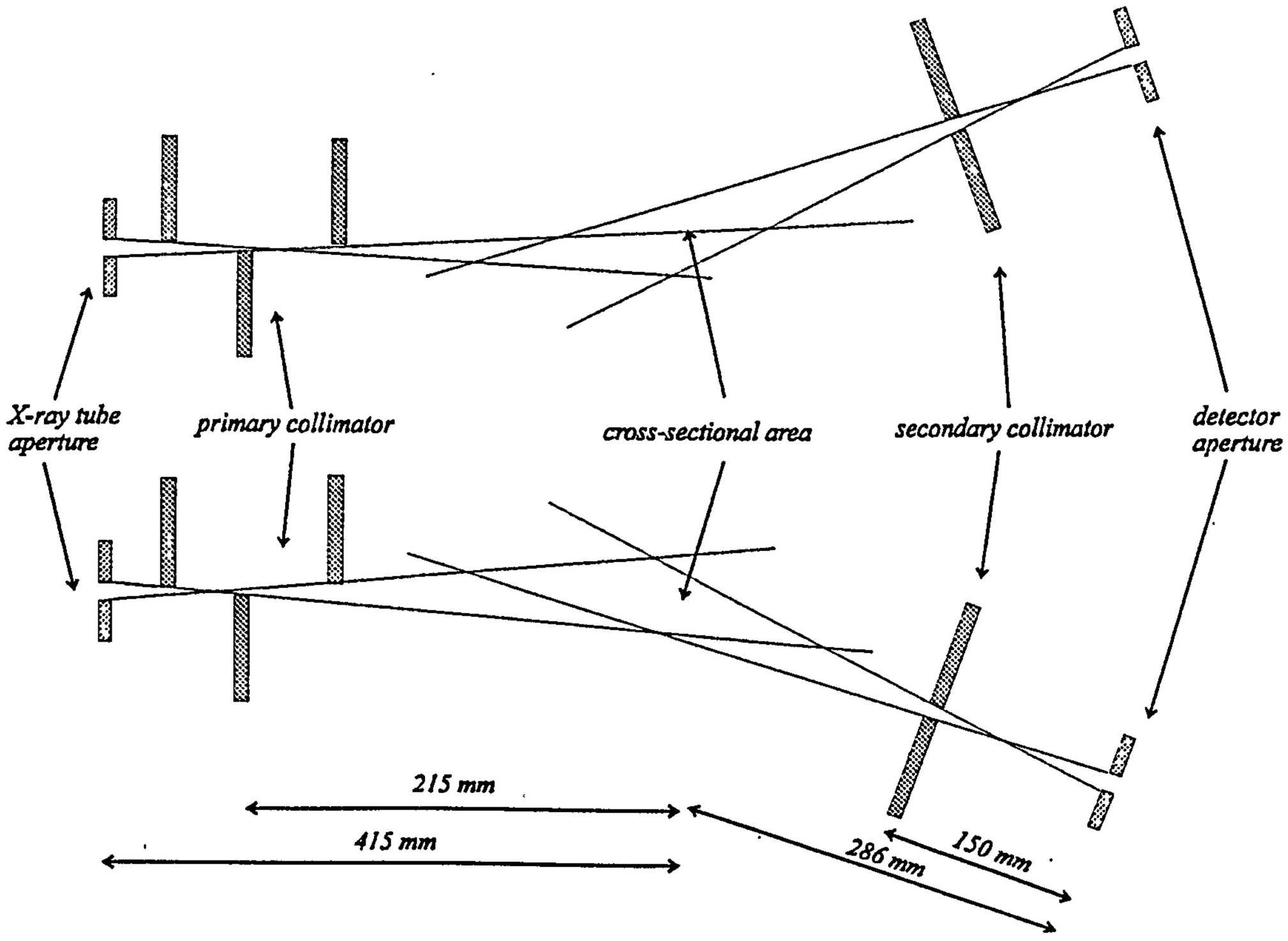

Figure 3.32 A schematic diagram of the cross-sectional shape for the scatter volumes for partially asymmetric collimation with scatter angles on either side of the incident beam (not to scale)

3.8.3 Comparison of the calculated and measured scatter volumes

These experimental results also show that the angles scattered towards the side of the incident beam with the smaller acceptance angle have relatively smaller scatter volumes than the angles scattered to the side with the larger acceptance angle. This confirms the effect seen in the energy-angle diagram in figure 3.25 and also the calculated results shown in figure 3.31.

The increase in the intensity seen in the experimental energy-angle plot in figure 3.25 is 23% between 4.5° and 5°. However, it is expected that there is also a reduction in intensity in changing from 4.5° to 5° due to the change in differential coherent cross-section between these two angles. The variation in the calculated scatter volume is a 28% increase from 4.5° to 5°. Therefore it is concluded that the effect of the varying intensity in the energy-angle is due to the collimation.

3.9 Conclusions

This chapter has described the evaluation of the performance of the cadmium zinc telluride detector and the energy resolution has been optimised to be 4.9% at 59.5 keV. Two types of collimation were investigated and slit collimation chosen, over a pinhole design, as the angular blurring was not significantly increased, however the flux and scatter volume were increased.

Two coherent scatter systems have been designed and built to match this detector. The first had a single angle collimator and was used to confirm that the peaks corresponding to planar spacings of 3.3 Å, 5 Å and 6.7 Å could be used for detection of RDX based explosives. This system also provided an energy angle diagram with which measurements from the multiple angle collimator could be compared. It was found (section 3.5) that even with various fillings used, the characteristic diffraction curves from the explosives were still visible. This was true for all fillings for the 3.3 Å peak and for some of the fillings for the 5 Å and 6.7 Å peaks. Thus, the fillings do not mask the presence of the explosive.

The second system was designed with a multiple angle collimator and has been used to provide the results for the analysis procedure in chapter 4. This chapter has also investigated the effects of asymmetry in the collimation and it was found that scatter volumes on either side of an asymmetric beam vary in size. It was also found that the most intense scatter was from the centre of the scatter volume, due to the range of scatter angles which can occur at this position.

CHAPTER 4

AN ANALYSIS TECHNIQUE FOR THE DETECTION OF EXPLOSIVES IN THE PRESENCE OF TYPICAL BAGGAGE CONTENTS

The results of the scatter signatures taken from typical baggage contents with the single detector multiple angle scatter system and the analysis procedures that have been developed are described in this chapter. Various methods based on the used of energy windows are discussed and the optimum is chosen. This analysis procedure is also compared with methods previously used by other workers.

4.1 The experimental procedure

This section will describe how the experimental measurements were made on the system, described in section 3.7.1, details of the suitcase contents and how they were chosen.

The single detector multiple angle coherent scatter system with a cadmium zinc telluride detector was used, as shown previously in figure 3.20. The detector was moved to each scatter angle in turn by a motor driven translation unit, controlled from outside the X-ray room. A measurement of the scatter signature was taken at each scatter angle and spectra for the ten scatter angles were plotted together to form an energy-angle diagram. These diagrams were constructed for a range of measurement times (see section 4.1.1), with the X-ray tube set at 70 kVp and 20 mA, and with the

two multiple angle collimators of 0.19° and 0.38° acceptance angle (for the remainder of this thesis these shall be referred to as θ_c). Various contents were used in the case, these are described in more detail in section 4.1.3.

4.1.1 Measurement times

The data acquisition time affects the statistical noise in the spectrum. Figure 4.1 shows examples of scatter signatures taken at 1 s, 10 s, 100 s and 1000 s. The 1000 s measurement has very good statistics, for instance, the counts (N) on the main peak at 25 keV are 18000 and therefore $\sqrt{N}/N$ (the error on Poissonian measurements) gives an accuracy of 0.75%. However, this is an excessively long measurement time for a baggage scanning system and therefore measurements were taken at 100 s (with peak accuracy of 2.3%), 10 s (with peak accuracy of 7.3%) and 1 s (with peak accuracy of 22.4%). (for the remainder of this thesis these shall be referred to as t_m). Although the 1 s measurement time gives poor statistics it was used with the suggestion that the combination of several spectra together, corresponding to the different angular positions of the detector, would improve those statistics.

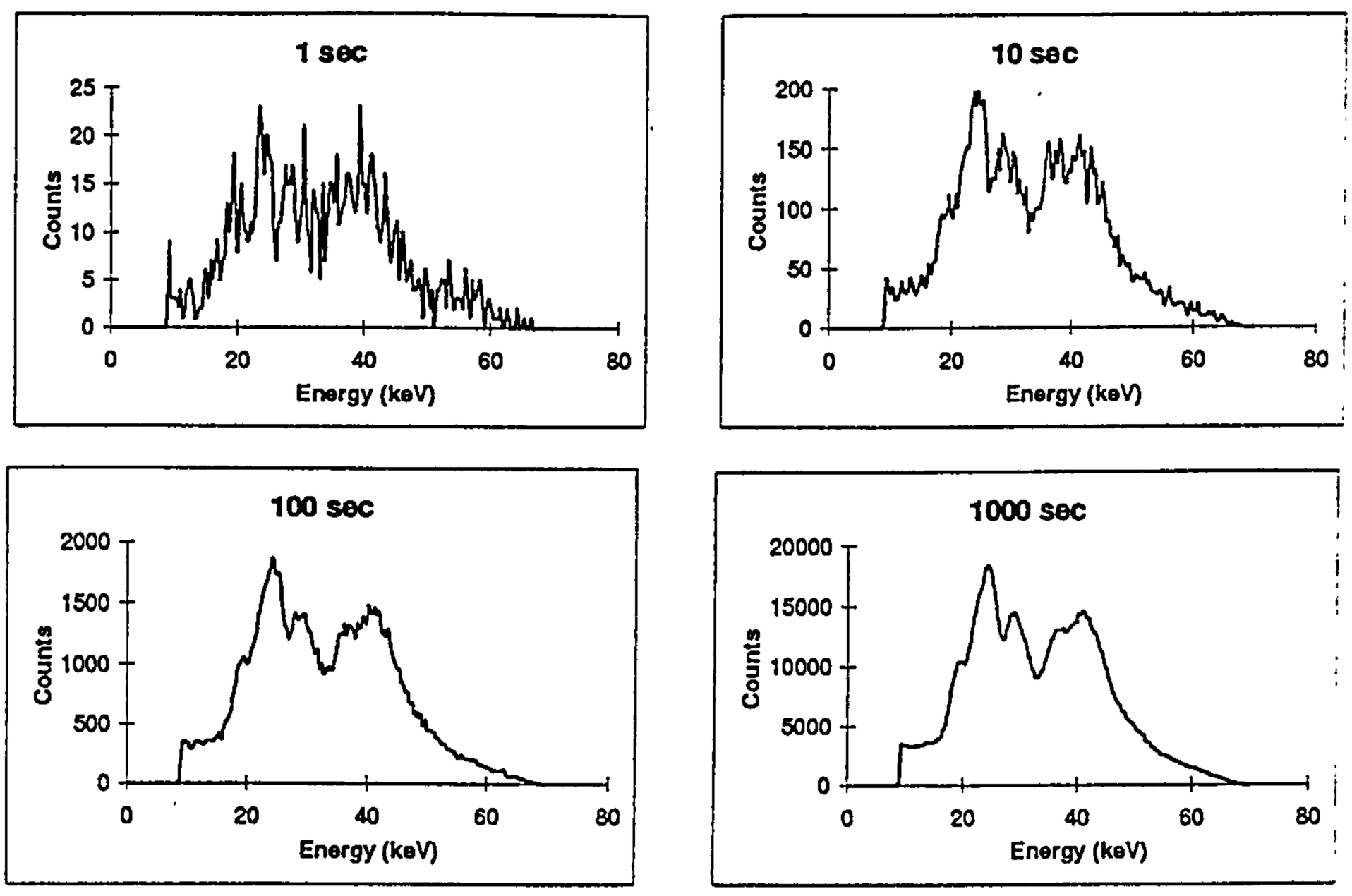

Figure 4.1 The effect on the noise in the scatter signature of different measurement times

At short measurement times the diffraction peaks become very difficult to identify since the probability of random noise having an intensity similar to that of a peak becomes greater. Ideally the scatter signatures would be measured for a period long enough to ensure that the statistical noise becomes inconsequential. However, for any practical system, and especially those designed for applications where radiation dose or throughput are limited, the measurement time must be as short as can be tolerated. The overall detection time will also be dictated by the method of analysis used and will be discussed in section 4.3, which investigates a suitable analysis procedure for the multiple angle coherent scatter signatures.

4.1.2 Scatter signature measurement method

Each case was positioned at the scatter point between the primary and secondary collimators, in the multiple angle coherent scatter system. The reference point for the repositioning of the suitcase was the outside edge of the case closest to the detector. This position was marked on the laboratory table. As discussed in section 1.1.1, sheet explosive is often hidden in a false bottom or side of a case. For this study, the sheets of explosive have been attached to the inside of the side of the case. The case was positioned so that the centre of the scatter volume was located on the inside of the suitcase wall (see figure 4.2). This maximised the counts from the explosive by placing it at the widest part of the scatter volume. Thus, also minimising the spectra resulting from the materials, other than the explosive, filling the remaining part of the volume. Furthermore, in placing the scatter volume in this position, some of the scatter volume is outside the case. This was a useful effect as it meant that the explosive filled a relatively greater part of the active scatter volume.

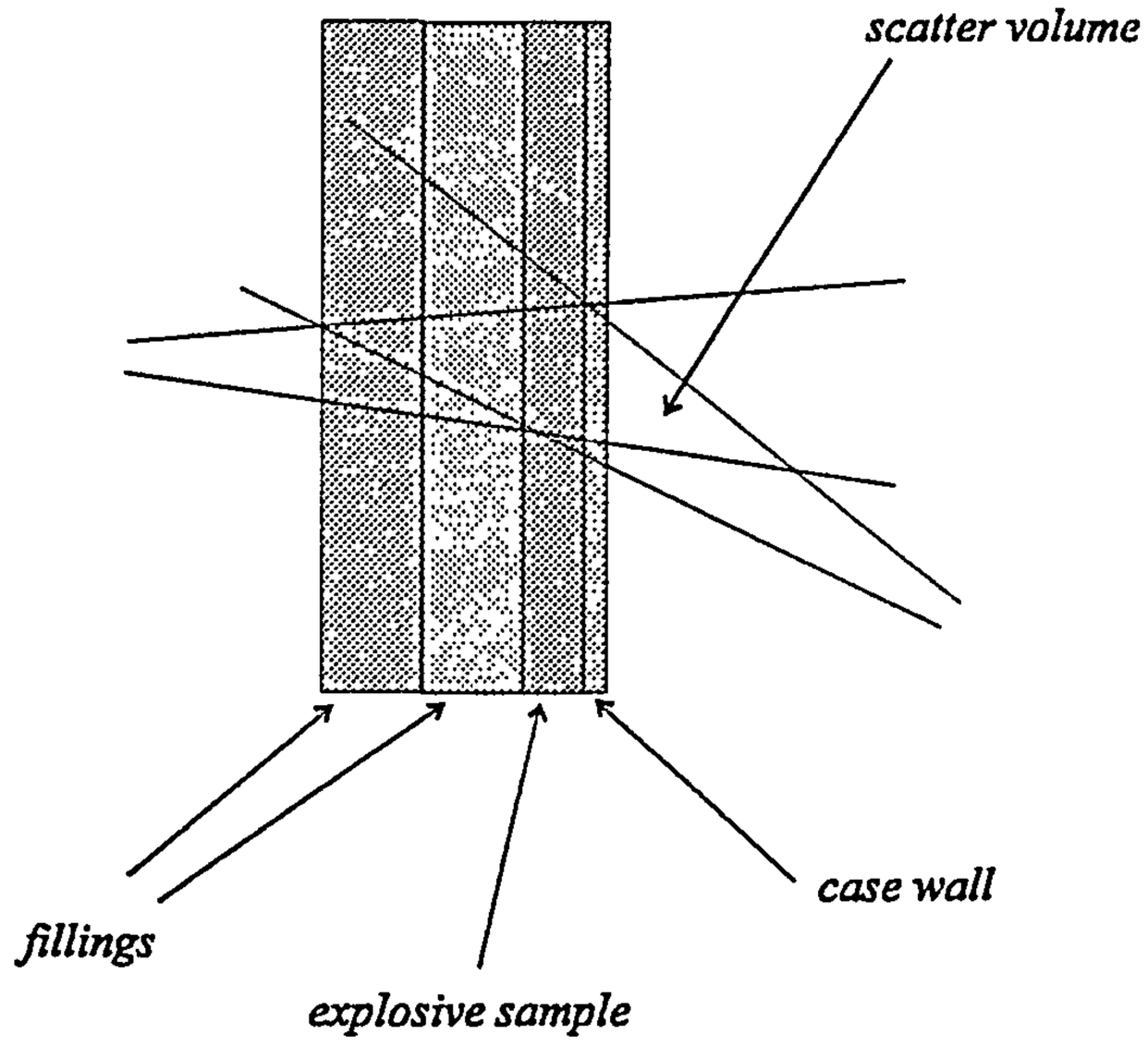

Figure 4.2 The position of the scatter volume within the case

Each case was filled as follows. The positions of the fillings were marked inside the case and the individual fillings were fixed securely. All of the materials used as fillings were at least 100 times larger than the width of the collimation beam. Also, with the exception of a small portable radio, all the materials were homogeneous, which facilitated easy repositioning. Scatter measurements were taken at each of the ten angles with the detector moved to each of the slits in the collimator in turn.

Transmission measurements were also taken of each of the case contents and case. These were made to correct for the variation in attenuation effects caused by the different fillings *(Strecker 1995)*. By dividing each scatter spectrum by the transmission spectrum, taken from the same case, the attenuation was corrected relative to the other cases, i.e. these were normalised. All cases have been corrected in this manner prior to any analysis procedure.

To make this measurement required for the attenuation correction the detector was aligned with the centre of the incident beam (i.e. 0°) with the case between the X-ray tube and the detector. The detector was shielded by lead housing with a 1.5 mm slot over the entrance window which served as a collimator for the transmitted beam. The

tube current was reduced to 2 mA to avoid flooding the detector response and the transmitted photons were measured for 10 s. This measurement time gave an error of < 1% on the integrated counts and this normalisation procedure did not significantly affect the statistical errors associated with the scattered spectra. A deeper discussion of errors is given in section 4.3.3.

4.1.3 Case fillings

In order to assess the ability of a system to detect explosives in practical situations, it is important to recognise that the number and range of materials in baggage is extremely large. Although it would be prohibitively time consuming to reproduce this range of materials in the laboratory, an assessment of the system may be made by investigating typical commonly occurring materials. For this study the case used was a hard briefcase made of ABS (a rigid plastic) and the number of variations of case contents was eight. These contents were chosen in several ways. Four sets of contents were based on typical fillings used by other workers *(Grodzins 1991, Yedida and Shea 1992, Vartsky et al. 1993, Lacey 1995)*.

Two of the fillings were chosen based on information received on a visit to the security section of Terminal 1 at London's Heathrow airport. The detection system currently used at Heathrow is dual energy transmission imaging, which supplies information on approximate atomic number of materials investigated. The two situations which cause the greatest difficulties for such a system are large areas of metal, e.g. aluminium, and high density organics. The cause of these problems is that the metals effectively shield contents behind them due to being highly attenuating materials and that the high density organics are difficult to distinguish from plastic explosives as they have a similar effective atomic number *(Campbell 1997)* and thus mimic explosives. The final two fillings were based on *a priori* knowledge (from the preliminary experiments in section 3.4) of materials which are good scatterers and therefore might be difficult to characterise from other good scatterers, by a coherent scatter system. Table 4.1 shows a list of the fillings and the information on which they are based. Overall, the fillings

have been chosen to provide known situations in which the explosive is difficult to detect.

FILLING (and approximate thickness)	REASON FOR CHOICE
1. Cotton* (80 mm) and chocolate*** (20 mm)	Chocolate known from previous measurements as a good scatterer Cotton is a common filling
2. Cotton* (44 mm), shoe* (6 mm) and shampoo* (50 mm)	All common fillings (shoe is made of rubber (3 mm), leather (1 mm) and plastic (2 mm))
3. Polyester* (10 mm), cotton* (20 mm), wool* (50 mm) and book* (20 mm)	All common fillings
4. Shoe* (6 mm), cotton* (44 mm) and wool* (50 mm)	All common fillings
5. Plastic portable radio* (50 mm), wool* (30 mm) and book* (20 mm)	All common fillings Radio chosen as has many constituent parts and devices occasionally hidden inside
6. Talcum powder*** (50 mm), cotton* (20 mm) and wool* (30 mm)	Talcum powder known from previous measurements as a good scatterer Others common fillings
7. Marzipan** (5 mm), cotton* (20 mm), shoe* (6 mm) and wool* (69 mm)	Marzipan difficult to distinguish from explosive in current baggage scanners as high density organic Others common fillings
8. Aluminium** (3 mm), cotton* (20 mm), shoe* (6 mm) and wool* (71 mm)	Aluminium can shield other materials in current method of transmission imaging Others common fillings

Table 4.1 The eight case fillings and reasons for the choices

(Grodzins 1991, Yedida and Shea 1992, Vartsky et al. 1993, Lacey 1995*

*** Campbell 1997*

**** From Chapter 4 preliminary measurements)*

The scatter signatures for each case were measured as is described in section 4.1.2. Different sheets of explosive were taped to the inside of the case wall. This wall was always positioned so as to be on the side nearest the detector. Each of the eight cases was measured with the filling only and then with each of the explosive samples added in turn. These were the samples, provided by the PSDB, as shown in table 4.2. The minimum thickness determined to be a threat on board an aircraft is 3 mm *(Lacey 1995)*.

Explosive name	Thickness
SX2	3 mm
SX2	6 mm
Semtex	4 mm

Table 4.2 The explosive samples used in the eight cases

4.2 Other methods for analysing coherent scatter for baggage scanning

The analysis procedure for the multiple angle system has been designed to be as simple as possible and to distinguish safe from explosive cases. In order to ascertain whether it could be a feasible method for use in baggage scanning, the results from other techniques are first considered. This, unfortunately is rather difficult, as information such as false alarm rate is kept confidential in the commercial world and therefore is not available. However, several workers have published some interesting results and these are reviewed.

A statistical method of data analysis known as principal component analysis (PCA) has been applied to coherent scatter signatures from individual scatter angles measured with a high purity germanium detector *(Luggar et al. 1997)*. A software program called Unscrambler 6.1 *(Camo AS)* was used to perform this task. The software was trained on one set of data and then tested on a different set. The samples used

consisted of a suitcase, made of ABS, with various fillings of cotton, wool and books. The test asked the qualitative questions 'is there Semtex present?' or 'is there SX2 present?'. The results showed that the Semtex could be identified at a minimum measurement time of 0.2 s and the SX2 at 0.1s. Work has also been carried out to test this method of analysis on data measured with a cadmium zinc telluride detector *(Luggar et al. 1996a)*. This showed that the cadmium zinc telluride data was significantly poorer than that taken with a germanium detector. The minimum times required to identify Semtex and SX2 with the cadmium zinc telluride detector were 10 s and 5s respectively. However, it should be taken into account that the cadmium zinc telluride detector used for these measurements had approximately one third the irradiated area of crystal than that of the germanium detector used for the comparison. The main disadvantage of the PCA is the amount of computational expense required, but also that the presence of Semtex and SX2 have to be ascertained individually. Another point of interest is that the PCA method requires longer measurement times for Semtex than for SX2.

Other methods that have been investigated for the analysis of coherent scatter X-ray signatures for detection of explosives include peak based classification *(Strecker 1995, Hnatnicky 1996)*, which uses a library of spectra with information on peak position intensity and width, and neural net based techniques *(Strecker 1995, Wilder 1995)*, which identify nodes within the spectra. Most of the papers published on this subject do not give a great deal of information on the detection rates of prototype scanners, because of strict commercial confidentiality laws. However, Strecker (1995) has published results for the peak based classification for three levels of signal to noise ratios which are approximately equivalent to the three levels studied in this work (i.e. measurement times of 1s, 10s and 100s). These were that the low noise (~100 s) gave 100% detection rate for 2.4 % false alarms, the medium noise (~10 s) gave 100% detection rate for 30 % false alarms and the high noise (~1 s) gave 100% detection rate for 80 % false alarms. However, it should be noted that these were results of distinguishing one individual material from another.

The results for the neural net based technique was 90% detection rate for 6% false alarms. Strecker concluded that for pure samples the neural net technique was better, but that for mixtures of materials the peak based method was superior. The results from the analysis of the work in this thesis will be compared with the work described in this section at the end of this chapter.

4.3 Methods for determining the presence of an explosive from multiple angle scatter signatures

This section will discuss the methods of analysis that have been developed for the multiple angle coherent scatter system. This analysis procedure aims to provide a simple method of detecting the presence of an explosive within an energy-angle plot from a suitcase. The analysis does not attempt to achieve any kind of identification of the type of explosive, merely a binary decision, explosive or no explosive. The possible effect of using this analysis method for a wider range of suitcase contents and explosives will also be discussed, at the end of this chapter.

A method of setting windows over certain areas of the energy-angle diagrams is suggested as suitable for use with the multiple angle coherent scatter system. This is because it can be designed and optimised, based on knowledge of coherently scattered signatures and then it is suggested that threshold values could provide a positive or negative answer.

Windows have been set on each scatter spectra, from an individual angle, to correspond to a particular atomic planar spacing. The counts from this diffraction peak have then been integrated between the limits defined by the window. This has been carried out for all ten scatter angles and the integrated counts from each angle have been added together to give the total integrated counts. This gives an approximately $\sqrt{10}$ improvement in the SNR over the total integrated counts from an individual planar spacing in comparison with the counts from a single angle. However, it is expected that this improvement is less than $\sqrt{10}$, since the diffraction peaks are only satisfied by

the most intense part of the incident spectrum at a single angle. Other angles are satisfied by a less than maximum intensity.

The data for each experimental energy-angle diagram was put into a spreadsheet (Microsoft Excel 5.0). Windows could then be set by summing together the counts from certain cells within the spread sheet. These calculations could be carried out quickly and simply by setting up different equations within the spreadsheets.

4.3.1 Choice of window positions

The planar spacings of interest required to identify a RDX based explosive have been determined in section 2.1.1 and 2.4.3 as being 3.3 Å, 5 Å and 6.7 Å. The decision as to where to position the windows within the energy-angle plot was confirmed by two sets of experimental results.

The first criterion on which the positions of the windows was decided was from the data taken using the single detector / single angle collimator simulation (see section 3.5, figures 3.14 and 3.15). In these data 3.3 Å is the strongest line for Semtex and the 2nd strongest for SX2, 5Å is the 2nd strongest for Semtex and the 3rd strongest for SX2 and 6.7 Å is the strongest for SX2 and the 3rd strongest for Semtex.

The second reason was also based on the data taken with the single detector / single angle collimator system. Simple fillings of cotton, wool and books were used, both with and without samples of SX2 and Semtex. The energy-angle plot for each of these was subtracted from each of the others in turn to determine where the areas of greatest difference occurred (figure 3.18). It was observed that even if cotton, wool and books were added to the case, the positions of the identifying peaks for the explosives were still visible. All the plots showed an intensity that was greater (to a varying extent) for the explosive cases at energies corresponding to a planar spacing of approximately 3.3 Å.

In assessing these two sets of data it was possible to determine a level of importance for each of the three planar spacings. This was based not only on the information given above, but also from the scatter and linear attenuation effects of other materials in the cases. The photons satisfying the 3.3 Å spacing occur at energies higher than those for the 5 Å and 6.7 Å spacings and therefore suffer less attenuation. Thus, it follows that the photons satisfying the 5 Å spacing also suffer less attenuation than those for the 6.7 Å spacing.

The cases (see table 4.1) containing sugar based products (chocolate and marzipan) were very efficient scatterers. This is because sugar can take on forms that are highly crystalline in nature. The most intense diffraction lines for these materials correspond to a range of planar spacings between 7 Å and 4 Å *(JCPDS database)*. Hence, scatter measured in the 5 Å and 6.7 Å windows can be intensified by coherent scatter from the sugar components. As sweets and confectionery items are often carried in luggage the effects of this particular material should be taken into consideration.

The window at 3.3 Å was therefore assigned the greatest importance due to suffering less attenuation and not being intensified by scatter from a common filling (sugar). The importance of the windows for 5 Å and 6.7 Å planar spacings are much the same, except that the photons at 6.7 Å will suffer more attenuation due to satisfying the Bragg condition at a lower energy. Also the 6.7 Å planar spacing has slightly less overall intensity in the standard diffraction and single detector / single angle collimator measurements.

Therefore in summary, the windows were placed at energies satisfied by planar spacings of 3.3 Å, 5 Å and 6.7 Å, with the 3.3 Å window being the most important. The remainder of this section will discuss how the widths of these windows were optimised and which combinations of windows gave the best results.

4.3.2 Error analysis and statistics

Before the windows are optimised and statements made about the suitability of these analysis methods, it is important to be aware of the effects of the statistical errors associated with these measurements. Radiation measurements are independent events and are therefore governed by Poissonian statistics. For any given measured value, N, there is a 68.3% chance that the true value of N is within $N \pm \sqrt{N}$ where the standard deviation, $\sigma = \sqrt{N}$ *(Sorenson and Phelps 1987)*. If several values of N are added together then the propagated error is $\sqrt{M}$ where $M = \Sigma N$.

In setting a threshold for distinguishing between an explosive and a safe case, the difference in the values for the two integrated counts must be statistically significant. Errors of 2σ give a 95% confidence that the difference between two values of N is significant and error bars of 3σ give 99% confidence *(Sorenson and Phelps 1987)*. Ideally 3σ error bars would be used for the higher confidence value, however the effects of using both 2σ and 3σ error bars have been investigated.

4.3.3 Summed windows

A simple method with which to use windows is to sum together the total integrated counts (across the ten angles) in those windows corresponding to different planar spacings and to set a threshold which differentiates between cases with and without explosives. The following section investigates the potential of summing various combinations of windows. All the data used has been previously corrected for attenuation effects of the case fillings.

4.3.3 1 Three windows

By analysing the three windows together the number of other materials on the JCPDS database which also have strong diffraction peaks in these three windows is ten. That is, the number of materials which could mimic an explosive is smaller than that which would arise from a single window. This search of the database at 3.2 Å-3.4 Å, 4.9 Å-

5.1 Å and 6.6 Å-6.8 Å showed that 6 of these are organics and the other 4 are inorganics. The database was searched for lines that were within 0.1 Å on either side of the required line, as the blurring effects of the collimation and detector would mean that they could affect the number of counts in the window. Although many of these materials are crystalline substances that have been measured for research purposes, it cannot be ruled out that some of them could be carried in baggage. The majority are of higher atomic number than the organic materials investigated here and hence could be identified as being in a different atomic number window from an explosive, by dual energy transmission baggage scanning methods. It should be noted that the search of this database will reveal only those materials which have one of the three most intense lines within the specified range. Therefore there may be other materials which have a fourth or fifth most intense line within the range, but which would not be shown.

The errors for the counts in summed windows can be calculated by the following equation (4.1) *(Sorenson and Phelps 1987),* where N is the summed counts in a single window:

$$\sigma(N_1 \pm N_2 \pm N_3 \pm \ldots) = \sqrt{N_1 + N_2 + N_3 + \ldots} \qquad [4.1]$$

Therefore the error for multiple windows is the square root of the counts in the summed windows. Error bars of 3σ and 2σ have been used to assure that the probability of random fluctuations is less than 1% and 5% respectively.

The counts in each window were summed together and the total plotted for each case filling. The aim is to be able to set a threshold above which the summed counts for the cases with explosive occur and below which are the summed counts from the safe cases. The summed counts were plotted as shown in figure 4.3. The summed total integrated counts from each case have been plotted with four points, one for the benign case and three for the different types and thicknesses of explosives. The errors have been marked as three standard deviations above and below the sum. As can be seen in figure 4.3, a threshold was marked at the lowest error bar for the explosive

case with the least counts. Any benign case which fell above this line could therefore be considered as a false alarm i.e. a result falsely appearing to be an explosive.

It can be seen from figure 4.3 that cases 1 and 7 (the two with sugar products) have higher summed counts than the other cases. Also, that case 5 has low counts due to the radio containing a lot of air. A summary of the effects of each of the case contents for all the analysis variations is given in section 4.5.

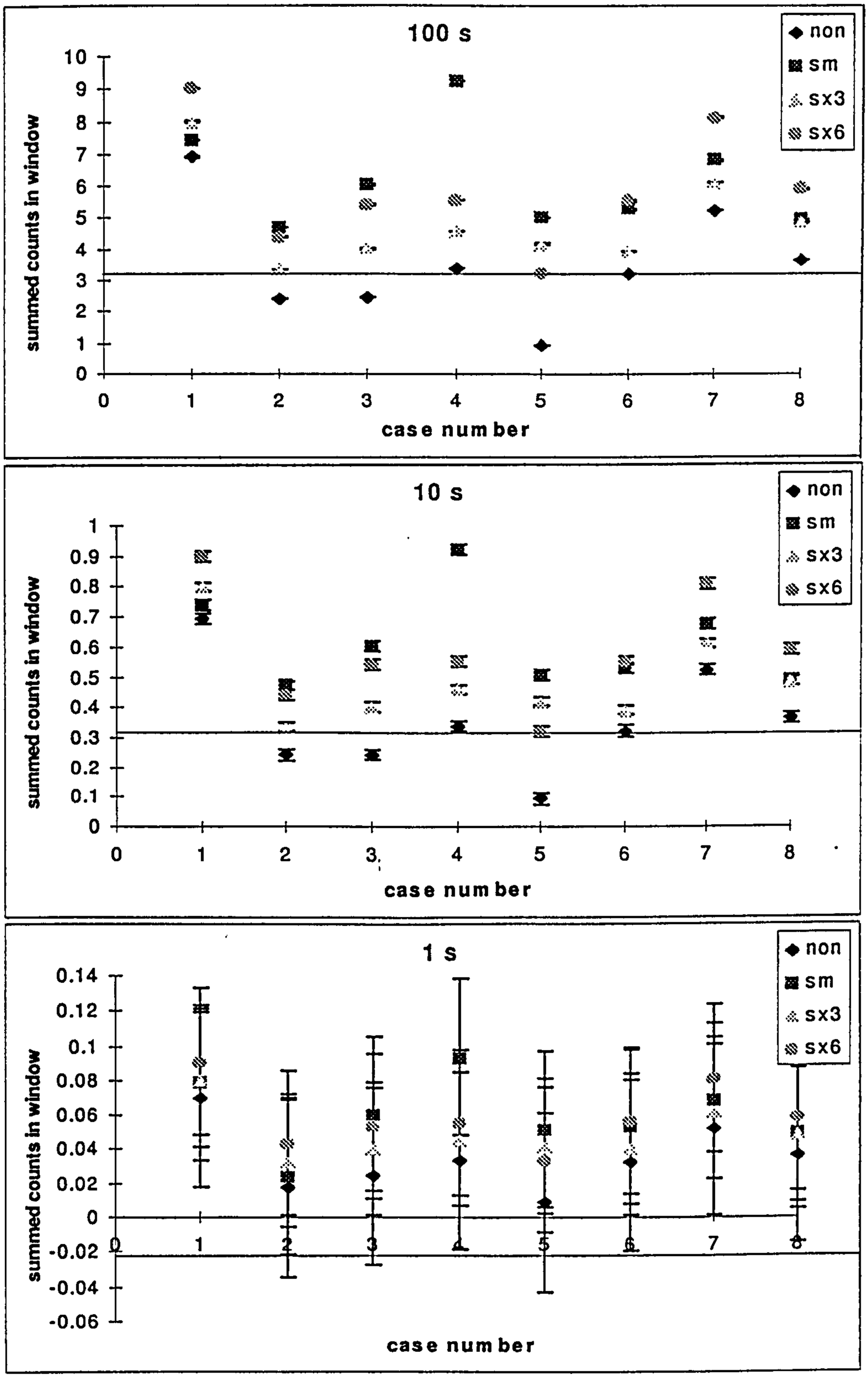

Figure 4.3 A plot for three summed windows for θ_c=0.38° at t_m=1 s, 10 s and 100 s with 3σ error bars. A threshold has been marked for 100% detection rate. (non=benign, sm=4 mm Semtex, sx3=3 mm SX2, sx6=6 mm SX2)

It can be seen in figure 4.3 that the error bars for 1 second are sufficiently large compared with the summed counts that it is not possible to set a threshold. Therefore the measurement time of 1 second will not be considered further.

The width of the windows were optimised by investigating the effect on the errors for various window widths. In setting a range of window widths there are two effects to be taken into account. The first is that narrow windows are more specific to the required planar spacings. The second is that wider windows give improved statistics and therefore have smaller error bars. Error bars of 3σ were used for this procedure. Table 4.3 shows the percentage of false alarms for a 100% detection rate for five window widths set for the 3.3 Å planar spacing. The percentage of false alarms was used, rather than the number of false negatives (explosive cases mistaken as benign), because in testing a baggage scanning system the ideal threshold should be set such that no explosives are missed. The utility of the system is then assessed by the number of false alarms it will cause *(Yedidia and Shea 1992, Wilder et al. 1995, Hnatnicky 1996)*.

θ_c and t_m	0.75 keV	2.25 keV	3.75 keV	5.25 keV	6.75 keV
0.38° 100s	37.5%	37.5%	37.5%	37.5%	37.5%
0.38° 10s	100%	87.5%	62.5%	62:5%	62.5%
0.19° 100s	62.5%	50%	50%	50%	50%
0.19° 10s	100%	100%	100%	100%	100%

Table 4.3 The percentage of false alarms for 100% detection rate for a range of window widths centred at 3.3 Å (for two collimation acceptance angles and two measurement times)

It can be seen in table 4.3 that for window widths above 3.75 keV there is no reduction in the number of false alarms for θ_c=0.38° and t_m=10 s (100 s measurements have no variation) and above 2.75 keV there is no reduction for θ_c=0.19° and t_m=100 s (at 10 s there is no variation). Therefore there is no gain in increasing the window beyond 3.75 keV width. Narrower widths cause increased statistical noise which cause the error

bars to increase and therefore make distinguishing between two points more difficult. At wider widths there is a greater probability of including counts from other planar spacings. Hence 3.75 keV was determined to be the optimum window width for the 3.3 Å window for both collimators. The optimisation of the windows for 5 Å and 6.7 Å was carried out in the same way. The optimum width for the 5 Å window was 3.5 keV and for the 6.7 Å window was 3 keV.

With the window widths optimised for all three windows the false alarm rate was investigated for all three windows summed together. Table 4.4 shows the number of false alarms occurring for the three windows summed together for two collimation acceptance angles and two measurement times (the maximum number of false alarms is 100%).

Collimation acceptance angle, θ_c	**Measurement time (s) t_m**	**False alarms with windows at 3.3 Å, 5 Å and 6.7 Å**	
0.38°	100	62.5%	(62.5%)
0.38°	10	62.5%	(62.5%)
0.19°	100	50%	(50%)
0.19°	10	75%	(62.5%)

Table 4.4 The percentage of false alarms for 100% detection rate for a sum of three windows and for two collimation acceptance angles and two measurement times (2σ error results are shown in brackets)

In comparing the results of the false alarm rates for θ_c=0.38° and 0.19°, the 0.38° acceptance angle has a slightly lower rate of false alarms for t_m=10 s. This is thought to be due to the 0.38° acceptance angle having improved statistics. The integrated counts are approximately twice those for θ_c=0.19° and therefore the value of $\sqrt{N}$, for the calculation of the error bars, is only 40% larger. However, θ_c= 0.19° has a lower false alarm rate for t_m=100 s. The variation in results using 2σ errors rather than 3σ errors is

only apparent for the measurements at θ_c=0.19° and at t_m=10 s. This is due to the SNR being lower and therefore the errors having a greater effect.

The false alarm rates for the three windows added together are not higher than for other methods (30% false alarm for integrated counts equivalent to t_m=10 s, *Strecker 1995*). This is thought to be because the other materials in the cases particularly the sugar based materials cause an increase in the total integrated counts in the 5 Å and 6.7 Å windows. This has the effect of increasing both the counts in the benign and explosive cases and hence, within the plot of the summed counts, the points are relatively nearer to each other.

4.3.3.2 Two windows

In order to reduce the effect of the sugar substances on the results, windows were used over two planar spacings only. As 3.3 Å has been suggested as being the most important this was carried out for two combinations of windows at 3.3 Å and 5 Å, and also for windows at 3.3 Å and 6.7 Å. This increases the number of other materials matching the intense diffraction lines on the JCPDS database to 434 for 3.2-3.4 Å and 4.9-5.1 Å and to 267 for 3.2-3.4 Å and 6.6-6.8 Å. However, most of these materials are crystalline inorganic materials that are considered unlikely to be carried in large quantities.

As with the triple windows, a threshold was set at the lowest level of the case with the least summed counts. This was to establish the false alarm rate, whilst maintaining 100% detection rate, for the two sets of windows. The results are shown in table 4.5 (2σ results are inside the brackets).

Collimation acceptance angle, θ_c	Measurement time (s) t_m	False alarms for windows at 3.3 Å and 5 Å	False alarms for windows at 3.3 Å and 6.7 Å
0.38°	100	62.5% (62.5%)	37.5% (37.5%)
0.38°	10	62.5% (62.5%)	62.5% (62.5%)
0.19°	100	50% (50%)	37.5% (37.5%)
0.19°	10	75% (62.5%)	100% (75%)

Table 4.5 The number of false alarms for 100% detection rate for two sets of two windows and for two collimation acceptance angles and two measurement times(2σ error results are shown in brackets)

The windows at 3.3 Å and 6.7 Å have better false alarm rates than for 3.3 Å and 5 Å, except for θ_c=0.19°collimation and t_m=10 s. This is thought to be because the counts from the sugar based products are stronger at 5 Å than at 6.7 Å. This is likely to be the case for a larger range of contents too as there are fewer materials with strong counts at 6.7 Å than at 5 Å *(JCPDS database 1961)*.

4.3.3.3 A single window

In order to try to eliminate the effect of sugar products, a single window was investigated at 3.3 Å only. The planar spacing of 3.3 Å has been suggested to be the most representative in distinguishing an explosive from benign materials (see section 4.3.1). Therefore the analysis was carried out by using a single window for this spacing only. Single windows for 5 Å and 6.7 Å were also investigated for comparison purposes.

A search was carried out on the JCPDS database for the purposes of comparison of the number of other materials found to also have peaks at this planar spacing. Of the 77,000 entries on the database, 13,622 (i.e. 17.7%) also have one of their three most intense peaks between 3.2 and 3.4 Å. The number of materials on the JCPDS database

with strong peaks between 4.9 Å and 5.1 Å is 3,521 (4.5%) and between 6.6 Å and 6.8 Å is 1,718 (2.2%). For the 22 materials measured in section 3.4, only the amorphous materials showed any broad peaks at 3.3 Å. These amorphous substances are not strong scatterers and therefore are not considered to compete with the strength of scattering for this spacing from the explosives.

Table 4.6 shows the false alarm rates for the individual windows at 3.3 Å, 5 Å and 6.7 Å.

Collimation acceptance angle, θ_c	Measurement time (s) t_m	False alarms for a window at 3.3 Å	False alarms for a window at 5 Å	False alarms for a window at 6.7 Å
0.38°	100	37.5% (37.5%)	62.5% (62.5%)	62.5% (62.5%)
0.38°	10	62.5% (62.5%)	75% (62.5%)	100% (100%)
0.19°	100	50% (50%)	62.5% (62.5%)	50% (50%)
0.19°	10	100% (100%)	100% (100%)	100% (100%)

Table 4.6 The number of false alarms for 100% detection rate for three individual windows and for two collimation acceptance angles and two measurement times (2σ error results are shown in brackets)

The investigation of the individual and summed windows revealed that the single window at 3.3 Å gave the lowest false alarm rate for 100% detection rate. The poor false alarm rate observed with 5 Å and 6.7 Å is because the other main peaks for the explosives also share similar planar spacings with strong peaks in sugar based products. Therefore both individual windows, at 5 Å and 6.7 Å, and summed windows are affected.

4.3.3.4 Conclusions from summed windows

The conclusions which can be drawn from this study of single and summed windows are as follows.

There is no variation in results between using error bars of 3σ or 2σ t_m=100 s. This is because the statistics are sufficient to provide error bars which are small in comparison with the summed counts. However, the false alarm rate is affected by the choice of error bars of 3σ or 2σ for measurements at t_m=10 s.

The lowest false alarm rates are from 3.3 Å (θ_c=0.38°) and 3.3 Å + 6.7 Å (θ_c=0.38°and 0.19°) for t_m=100 s where a 37.5% false alarm rate was achieved. The lowest false alarm rates for t_m=10 s were with θ_c=0.38°, but there was no difference between the 3.3 Å and the combinations of two and three summed windows.

These results produce a false alarm rate which is higher than those achieved by Strecker for the peak based look-up method (30% false alarm at t_m=10 s). However, the results given by Strecker are for simpler combinations of materials than given here and the thickness of explosive used has not been quoted. The method developed in this work has been tested for detecting 3 mm of explosive within a fully packed suitcase.

4.3.4 Ratios of windows

Identification of materials by diffraction methods not only depends on the intensities of peaks at certain planar spacings, but also on the ratios of those peaks. In other words, two different materials could have peaks at the same planar spacings, but with varying intensities. Hence, the ratios of those peaks may be a potential method to distinguish them. Therefore, ratios of the counts in the windows were also investigated. This was carried out with the same three planar spacings as described previously and three pairs of peaks were used, 3.3 Å / 5 Å, 3.3 Å / 6.7 Å and 6.7 Å / 5 Å. The ratios were used in this configuration so that the counts from the explosive samples were always greater than the counts from the benign samples. The results from these are given in the following section.

The error on ratios is given by equation 4.2 *(Sorenson and Phelps 1987)*

$$V\left(N_1 \times / \div N_2 / \div N_3 \ldots\right) = \sqrt{1/N_1 + 1/N_2 + 1/N_3 + \ldots} \qquad [4.2]$$

4.3.4.1 Three different ratios

The results from the analysis, based on ratios of the total integrated counts in the windows, are shown in table 4.7.

Collimation acceptance angle, θ_c	Measurement time (s) t_m	False alarms for the ratio windows at 3.3 Å and 5 Å	False alarms for the ratio windows at 3.3 Å and 6.7 Å	False alarms for the ratio windows at 6.7 Å and 5 Å
0.38°	100	75 % (75%)	75% (75%)	87.5% (87.5%)
0.38°	10	87.5% (87.5%)	100% (100%)	100% (87.5%)
0.19°	100	87.5% (87.5%)	100% (100%)	87.5% (87.5%)
0.19°	10	87.5% (87.5%)	100% (100%)	100% (100%)

Table 4.7 The percentage of false alarms for 100% detection rate for three combinations of ratios of two windows at 3.3 Å, 5 Å and 6.7 Å , for two collimation acceptance angles and two measurement times (2σ error results are shown in brackets)

There is no difference between the false alarm rate for 2σ and 3σ, except for t_m=10 s and θ_c=0.38° with ratio of 6.7 Å and 5 Å. This is because the errors are greater for the ratio method than for the summed method.

4.3.4.2 Conclusions from ratios of windows

The false alarm rates for the ratios of windows are higher than for the summed windows because the variation in the counts in the 5 Å and 6.7 Å windows is great. Thus, the effect is that the ratios also vary. In setting a threshold for the explosive case with least counts, this large variation means that most of the other benign cases fall above the threshold as false alarms.

4.4 Results from analysis of individual samples of explosive

This investigation has, so far, concentrated entirely on distinguishing any explosive from any benign case, as type of explosive is not required to be known. However, each individual explosive sample (i.e. 3 mm SX2, 6 mm SX2 and 4 mm Semtex) was also investigated to determine whether the false alarm rate would be better if, for instance, the minimum thickness to be identified were 6 mm. This was to determine the limits at which this multiple angle system would provide acceptable false alarm rates (e.g. the minimum thickness it could detect). It should be noted that, in the work of Strecker there is no indication of the thickness of explosive samples used. Table 4.8 shows the number of false alarms for 100% detection rate for the three explosive samples, for the nine different combinations of windows (single, summed and ratios) and the two collimation acceptance angles. Only 10 s measurement times are shown as this is a more stringent test, as shown in section 4.3, due to an increase in statistical noise.

Window (Å)	Collimation acceptance angle	SX2 (3 mm)		SEMTEX (4 mm)		SX2 (6 mm)	
		3 σ	2 σ	3 σ	2 σ	3 σ	2 σ
3.3	0.38°	62.5	62.5	25	0	25	0
	0.19°	100	100	100	87.5	62.5	62.5
5	0.38°	75	62.5	62.5	37.5	62.5	25
	0.19°	100	100	100	75	75	62.5
6.7	0.38°	100	100	100	100	87.5	87.5
	0.19°	100	100	100	100	100	100
3.3+5	0.38°	62.5	62.5	25	25	25	25
	0.19°	75	62.5	50	50	50	25
3.3+6.7	0.38°	62.5	62.5	25	25	25	25
	0.19°	100	75	50	37.5	50	37.5
3.3+5+ 6.7	0.38°	62.5	62.5	25	25	25	25
	0.19°	75	62.5	50	37.5	37.5	25
3.3 / 5	0.38°	87.5	87.5	62.5	50	37.5	37.5
	0.19°	87.5	87.5	37.5	12.5	37.5	25
3.3 / 6.7	0.38°	100	100	37.5	37.5	37.5	37.5
	0.19°	100	100	25	25	75	75
6.7 / 5	0.38°	100	87.5	100	100	100	87.5
	0.19°	100	100	100	100	87.5	87.5

Table 4.8 The percentage of false alarms (for 100% detection rate) for the individual explosive samples at two collimation acceptance angles for t_m=10 s (both 3σ and 2σ error bar results are shown). The light shading shows results which have a lower false alarm rate than those obtained by Strecker and the darker shading shows the lowest false alarm rates.

4.4.1 Discussion of results from individual samples

Several conclusions can be drawn from table 4.8.

In general the thicker the explosive the easier the sample is to detect. This is as expected as a thicker piece of explosive will produce more counts per unit time because it takes up a greater proportion of the scatter volume.

The 6 mm sample of SX2 had a 0% false alarm for the 3.3 Å window for θ_c=0.38°, if 2σ error bars were used, and 25%, if 3σ error bars were used. 3.3 Å + 5 Å, 3.3 Å + 6.7 Å and 3.3 Å + 5 Å + 6.7 Å also gave 25% false alarm rates for θ_c=0.38°.

For the 4 mm sample of Semtex there was a 0% false alarm rate from the 3.3 Å window with θ_c=0.38°, if 2σ error bars were used. Again, 3.3 Å + 5 Å, 3.3 Å + 6.7 Å and 3.3 Å + 5 Å + 6.7 Å, for θ_c=0.38°, gave 25% false alarm, regardless of the error bars used.

For the 3 mm sample of SX2 the lowest false alarm rates (62.5%) were for the three variations of summed windows and 3.3 Å alone with θ_c=0.38°.

The variation between the results obtained using 2σ and 3σ error bar results is particularly important for the Semtex and 6 mm sample of SX2 with a single window at 3.3 Å where θ_c=0.38° gives 0% false alarms.

Overall the 3.3 Å window gave the best results, as this was the only window were 0% false alarms were achieved. This is also consistent with the earlier results for all the explosive samples being detected together.

The minimum thickness of explosive which achieved 0% false alarms with this system and analysis procedure was 4 mm.

The 0.38° collimation acceptance angle allowed more counts per unit time and therefore the error bars were smaller. However, this result is offset by the increased blurring of the diffraction lines caused by the wider collimation. That is, it is more likely that materials with diffraction lines to either side of the window being measured will contribute to the integrated counts. Overall, investigating t_m=10 s as the most practical measurement time, θ_c=0.38° gave lower false alarm rates. Therefore, it is concluded that use of this larger collimation acceptance angle is preferable.

4.4.2 Other possible variations for this analysis technique

Whilst developing this analysis technique several other variations of window combinations were considered. These included the possibility of weighting the windows with a certain factor according to their relative importance. This was decided to be a useful consideration for future work, but has not been carried out on this set of data as the weighting would rely very much on the results of this limited data set. Therefore, the benefit of weighting the windows could be falsely enhanced or reduced. Another variation considered was to reduce the number of angles used for each window. This would mean that only the angles with the strongest scatter for a particular window would be used and therefore the differences between benign and explosives could be enhanced. However, it was rejected on the grounds that the statistical noise would be increased.

4.4.3 The effectiveness of this analysis technique on other explosives

The JCPDS database was searched for several other explosives, which have not been used in this work to determine whether the analysis procedure described here could be of benefit in detecting these other materials. Table 4.9 shows the other types of explosives with their relative diffraction peak intensities between 3.2 and 3.4 Å and the rating of this peak (i.e. strongest, second strongest....).

Name of explosive	Relative intensity of peak between 3.2-3.4 Å	Rating of peak between 3.2-3.4 Å
3,4-Dinitrotoluene	39	5th
2,6-Dinitrotoluene	80	3rd
2,4-Dinitrotoluene	100	1st
HMX	56	2nd
2,4,6-Trinitrotoluene	70	3rd
Picric acid	12	22nd

Table 4.9 Other explosives with peaks and their relative intensities between 3.2 and 3.4 Å and the rating of the peak

It can be seen from this table that some of the other explosives found on the database have intense peaks between 3.2 Å and 3.4 Å which could also be identified by placing a window centred at 3.3 Å. It is suggested that 2,6-Dinitrotoluene, 2,4-Dinitrotoluene, HMX and 2,4,6-Trinitrotoluene might be also be identified by this technique, but that 3,4-Dinitrotoluene and Picric acid may not.

4.5 The effects of each case filling

This section discusses the individual effects of the components of the eight combinations of case contents which have been used in this work. The effects that each of the variations of contents have on the positions of the summed scatter points in the scatter plots and the likelihood of causing a false alarm will be discussed.

- Case 1 Cotton and chocolate

This produces one of the most intense scattered spectra because the predominant ingredient in the chocolate is sugar, which is a crystalline substance and therefore produces strong scatter peaks. A further reason for the high scatter is that cotton is not

a highly attenuating material. As the chocolate causes the integrated counts for 5 Å and 6.7 Å to be intense, this case most often causes a false alarm.

- Case 2 Cotton, shoe and shampoo

The fillings in this case are not good scatterers, however the shampoo is quite attenuating and therefore the detected counts are quite low. This can be corrected by the transmission counts, but overall the counts tend to be low or medium compared with the other case contents and hence does not often cause a false alarm.

- Case 3 Polyester, cotton, wool and book

These materials are neither good scatterers nor heavily attenuating. Therefore, although the counts are low, this is not changed very much by the attenuation correction based on the transmitted counts. The contents of this case do not cause any false alarms except when the counts from case number five are extremely low when a single window is placed at 6.7 Å.

- Case 4 Shoe, cotton and wool

These materials are neither good scatterers nor heavily attenuating. Therefore, although the counts are low, this is not changed very much by the attenuation correction with the transmitted counts. The counts for case four are higher than those obtained for case number three as the rubber in the shoe contributes to increasing the counts, and hence this case is often classified as a false alarm.

- Case 5 Plastic radio, wool and book

The radio has many different small components in it, which meant exact repositioning was difficult. Some of the components are possibly very attenuating, such as capacitors, and other parts cause very little attenuation, such as air gaps. For this case it is suggested that the part of the radio used for the transmission measurement

consisted of different components from the part used for the scatter measurement. Therefore, the transmission correction for this case was not accurate. The air gaps meant that the counts from this case were generally the lowest of all. The effect was that this case usually dictated the position of the threshold and therefore if the threshold was low then several other cases produced several false alarms. This is a problem that could easily occur in future measurements and therefore care should always be taken to measure the attenuation from the same position as the scatter.

- Case 6 Talcum powder, cotton and wool

Talcum powder is a good scatterer (although the most intense planar spacing is at 2.3 Å) and therefore the total integrated counts from this material are high. This has the effect of increasing the threshold which would be required to distinguish benign cases from explosive cases. Talc is a highly attenuating material and therefore the counts are also increased by the transmission correction procedure. Overall this case generally had average to high intensity, and hence was often marked as a false alarm.

- Case 7 Marzipan, cotton; shoe and wool

This is very similar to the case containing chocolate. Both marzipan and chocolate are mainly made of sugar and therefore scatter very strongly. Marzipan is also a relatively dense material and therefore the counts are increased by the transmission correction procedure.

- Case 8 Aluminium, cotton, shoe and wool

Aluminium has an intense planar spacing at approximately 2.2 Å and has a high coherent scatter differential cross-section at angles of 5° and greater. However, this is a thin sheet and therefore the proportion of the scatter volume that it takes up is small. Hence the integrated intensities for this case are average and only occasionally cause a false alarm.

In conclusion the case fillings used in this study have shown that there is a wide range of total integrated scatter counts from different case contents. The attenuation correction procedure goes some way towards making the background counts from the benign case contents more uniform. However, there is still a large variation in the level of scatter from each case. There are also problems associated with fillings that may contain air gaps and therefore have almost no scatter from these volumes. These have the effect of lowering the threshold. The fillings, used for this study, were chosen in order to test some of the more difficult combinations of fillings as determined both by dual energy transmission techniques and previous coherent scatter measurements (see section 4.1.3). Therefore, it is suggested that the majority of other fillings in a wider study would fall within the range shown here. However, there may also be materials, not considered here, which may increase the range.

Within a more realistic baggage scanning system there may be methods available to reduce these effects. These include transmission images of the cases that could help identify gaps. Also, dual energy transmission images have the capability of assigning atomic number windows to materials, so mineral substances such as talcum powder would be shown as a different colour to the organic sugar based products and hence could be disregarded.

A further suggestion for how to improve this method is that, instead of taking a single measurement from a single point, a scanned measurement is taken from various positions across the case. The advantage would be that the other contents of the case would be averaged out and hence any materials with extreme effects such as the chocolate / marzipan or the air gaps would have a smaller effect. The disadvantage of this method would be that if a measurement was taken in a position with no explosive, and this was added to a measurement from a position that did have explosive, then the counts from the explosive would in effect be reduced. Therefore, in order for this method to work, an imaging system would first have to provide knowledge as to where the sheet of explosive might be.

4.6 Comparison with the other analysis methods

As has been previously discussed in section 4.2 there is very little other data with which this work can be directly compared. The work of Strecker et al. (1995) has achieved a 30% false alarm rate for 100% detection rate for medium noise levels which are equivalent to the 10 s measurements in this work. However it is not known what the thicknesses of explosive were in this work (although in a prior publication, samples of "greater than 1 cm^3" were used, *Strecker et al. 1993*) and also the measurements were made on individual samples. Therefore the results from this thesis appear to be of a similar false alarm rate as those of Strecker and for the 6 mm sample of SX2 and 4 mm ample of Semtex, perhaps lower.

In comparison with the carried out by Luggar et al. (1996a), the time required to identify Semtex with the cadmium zinc telluride detector system, described in this chapter, was the same and for the SX2 was a factor of 2 longer.

The false alarm rates for some other techniques such as nuclear techniques (15% false alarm rate for 95% detection rate for a thermal neutron activation method *(Gozani 1996)*) are lower than for coherent scattering measurements however these systems are less practical to be used in an airport due to their size, cost and time required to make the measurement (e.g. 10 minutes).

4.7 Conclusions from this analysis procedure

This chapter has investigated the use of windows set at the three most intense planar spacings for SX2 and Semtex. Nine variations of sums, ratios and single windows have been used. The conclusions that can be drawn from this analysis procedure are as follows:

For t_m=10 s, the detection rate for the two thickest samples is best when a single window is placed at 3.3 Å with θ_c=0.38°. This is due to few of the other case contents having strong diffraction lines at this planar spacing and also this combination of collimation acceptance angle and measurement time improve statistical noise.

If the confidence limits are reduced to 95%, then the results for the single window at 3.3 Å, with θ_c=0.38° are that there were 0% false alarms for a threshold set for 100% detection rate for a 4 mm sample of Semtex and a 6 mm sample of SX2.

The variation of the position of the points in the scatter plots is greater when windows at 5 Å and 6.7 Å are included. This is because some of the other case contents used, such as sugar based products, are strong scatterers for planar spacings of 5 Å and 6.7 Å, and therefore the counts in these windows are detrimentally enhanced.

Although the single window at 3.3 Å gave the lowest false alarm rate, the use of multiple windows mean that there are fewer other materials which could mimic the explosive.

Overall θ_c= 0.38° gave lower false alarm rates than θ_c=0.19°. This is due to improved statistical noise.

The thicker the piece of explosive the easier it is to identify as a threat. This has been shown to be the case over the majority of the combinations of windows.

It is therefore concluded that, in comparison with other methods that have been used to analyse coherently scattered signatures, the window method developed in this work is of a similar accuracy. It also requires similar measurement times as for the PCA method with a cadmium zinc telluride detector, however the time required to process the data and detect the explosive is quicker. Therefore, the method of a multiple angle detection and the analysis procedure developed with it, appear promising.

The final part of this work is to build a full array of detectors and investigate the design factors needed to be taken into consideration if this system were to be attached to a baggage scanner. The following chapter will describe a coherent scatter system with an array of ten detectors.

CHAPTER 5

AN INVESTIGATION INTO AN ARRAY SYSTEM

The final chapter of this thesis investigates the requirements which would need to be taken into consideration in building a multiple angle system with an array of detectors. The aim was to propose how a multiple detector array system should be designed which could be attached to an existing baggage scanner.

Having built and tested a simulated detector array with a single cadmium zinc telluride detector, a full array of ten detectors was constructed. The dimensions of an existing baggage scanner *(Robinson 1996)* were used to provide a realistic geometry. The tunnel for the baggage to pass through was 440 mm in height. The space available, above the tunnel, for the detectors, secondary collimator and electronics was 485.7 mm. The system was therefore set up with these geometrical limits taken into account. The X-ray tube used was the tungsten target industrial X-ray tube, as has been used previously in this work.

5.1 The array system

Using the dimensions as described above, an array system was constructed. Various changes were made from the previous single detector / multiple angle system. These included the detectors, the electronics and the collimators and these are discussed in the remainder of this section.

5.1.1 The detectors

Discussions with eV Products *(Parnham 1996a)* lead to the design of individual small cubic detectors which could be combined to form an array. The cadmium zinc telluride crystals were 5 x 5 x 2 mm, as before. The overall size of each of these detectors was 10 x 10 x 10 mm^3 and the preamplifiers were designed to fit, with the detector crystal, inside the detector housing. The crystal and electronics were potted in silicon rubber. The housing was made of 100 μm of brass with a window for irradiation. Figure 5.1 shows a cross-sectional diagram of one of these detectors.

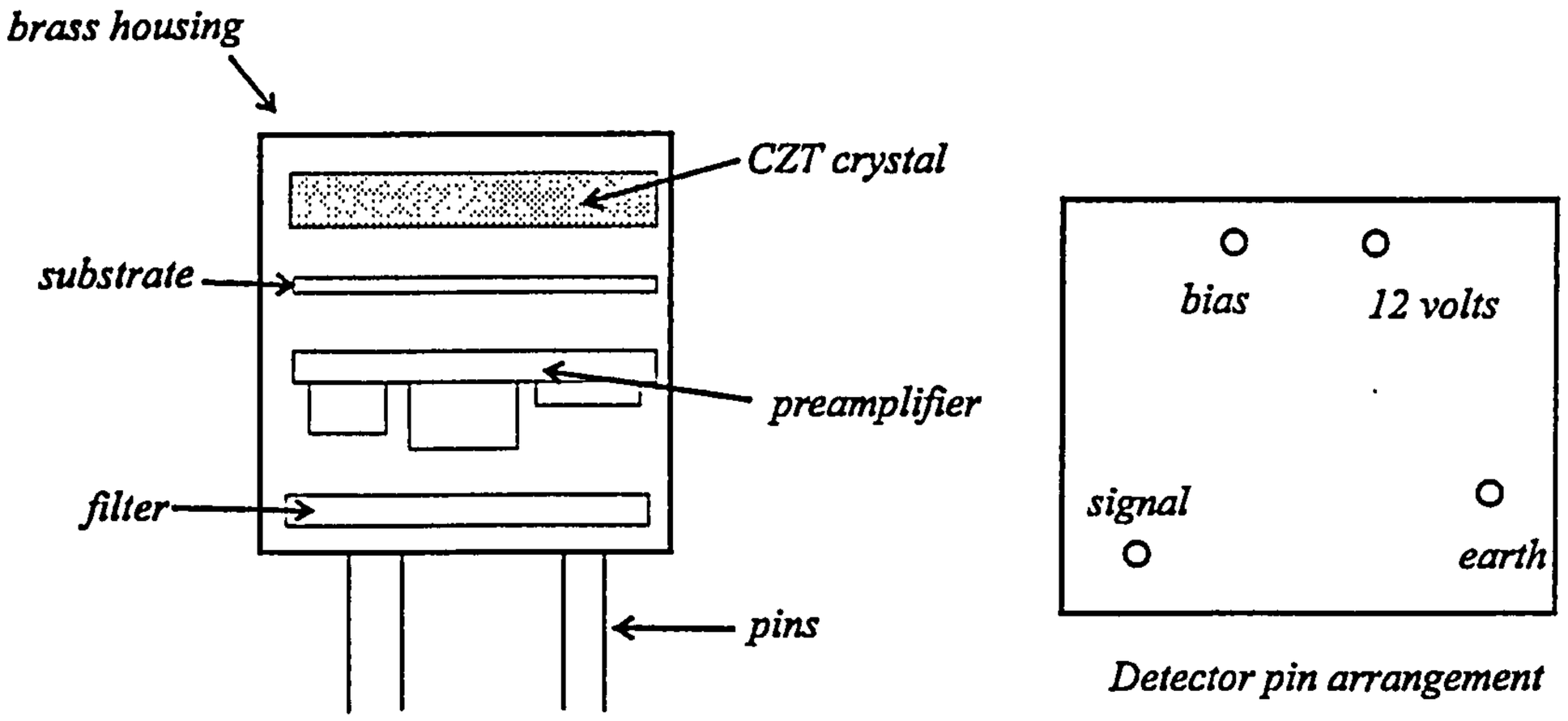

Figure 5.1 A cross-sectional diagram of one of the array cadmium zinc telluride detectors (the layout of the pins is also shown)

5.1.2 The construction of the detector array

The detectors were positioned in two groups of five and mounted on two boards in a linear array. The location of the detectors was such that the scatter angles were measured on either side of the primary beam, as with the previous single detector system. Each detector had a 12 V supply for the preamplifier, a 200 V bias supply, an earth connection and a signal output. The 12 V supply to the preamplifiers needed to be filtered and this was built in a separate box. Each detector had a discrete 12 V preamplifier and 200 V bias supply. Figure 5.2 shows a photograph of the configuration of the array.

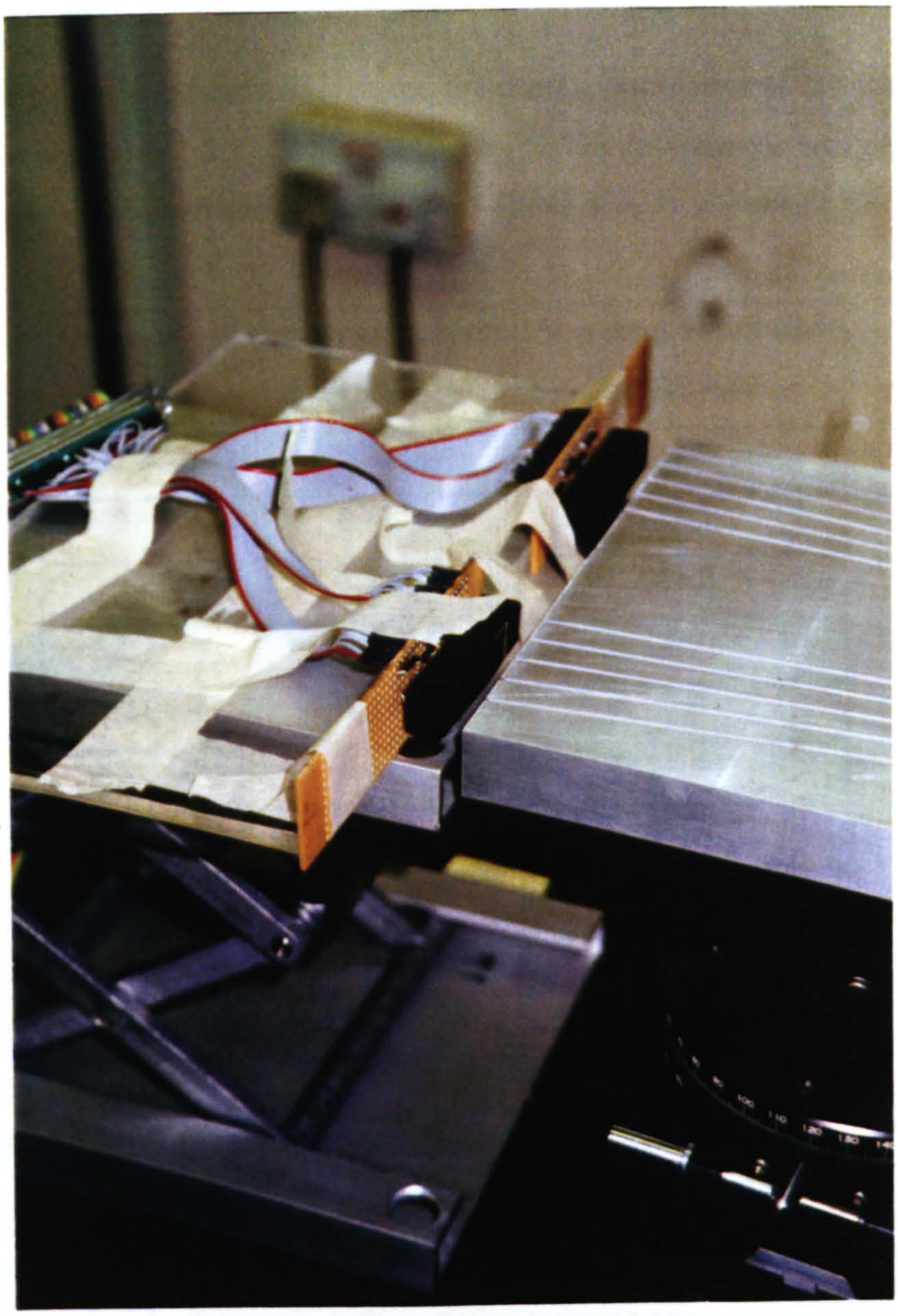

Figure 5.2 A photograph of the detector array

5.1.3 Energy resolution of the detectors

Two radio-isotopes were used to measure the energy resolutions of the ten detectors (as described in section 3.2.3). Table 5.1 shows the results from the energy resolution measurements for two isotopes of americium 241 (59.5 keV) and cobalt 57 (122 keV).

Detector number	% energy resolution at 59.5 keV	% energy resolution at 122 keV
1	11.7	11.6
2	6.7	17.3
3	6.5	13.6
4	6.8	8.9
5	6.9	7.6
6	6.6	17.64
7	6.6	6.8
8	5.5	6.0
9	6.1	13.8
10	6.6	9.9

Table 5.1 The energy resolutions of the ten detectors at 59.5 keV and 122 keV.

It can be seen form table 5.1 that the energy resolutions of the new small detectors were inferior to that for the single cadmium zinc telluride detector (eV-180). The range of energy resolutions at 59.5 keV was from 5.5% (detector 8) to 11.7% (detector 1). The mean energy resolution of the ten detectors is 7.0% which is 2.1% more than the original single detector. The detectors were positioned in the array such that the detector 1 (worst energy resolution) was measuring scatter from 7.5° which was at the extreme of the energy angle diagram. The other detectors were used for the remaining scatter angles.

5.1.4 Collimators for the array

The secondary collimator had the same design as before (see section 3.6.1), but was increased to 200 mm in length (see figure 5.3). This was the maximum collimation length that would fit inside the baggage scanner. The slit width was increased to 1.3 mm to maintain the acceptance angle of the collimator at θ_c=0.38°, as used previously. Again, dural (aluminium alloy) was used as a suitable material. The primary collimator was changed to a symmetrical design and the acceptance angle of the primary collimator was reduced from 0.57° to 0.38°. The changes in collimation meant that the average momentum resolution (equation 2.5) for the array (16.73%) was approximately maintained from the previous single detector system (16.57%). The effect of using symmetrical primary collimation was to remove the effect of different size scatter volumes on either side of the primary beam.

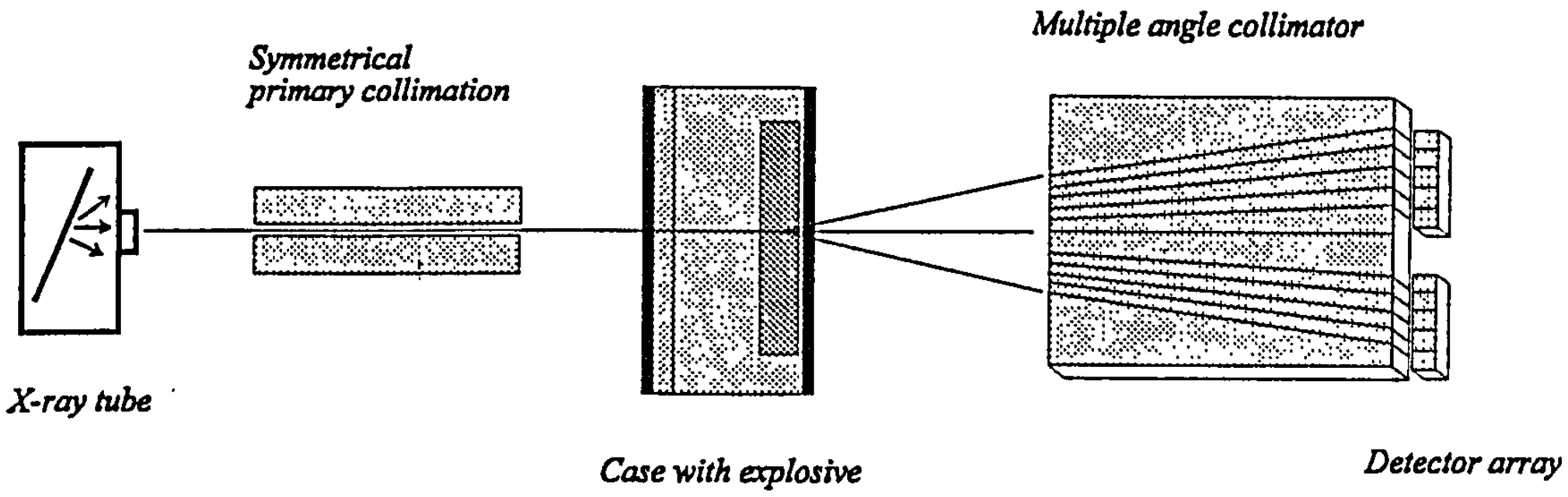

Figure 5.3 The collimation and detector array

5.1.5 Electronics for the array

In order to measure ten signals simultaneously, a multiple channel analyser with ten inputs was used. A multiple channel version of the Spectrum Master (920-16) and Maestro software were used with five EG&G Ortec (855) dual spectroscopy amplifiers. Figure 5.4 shows a schematic diagram of the electronics system.

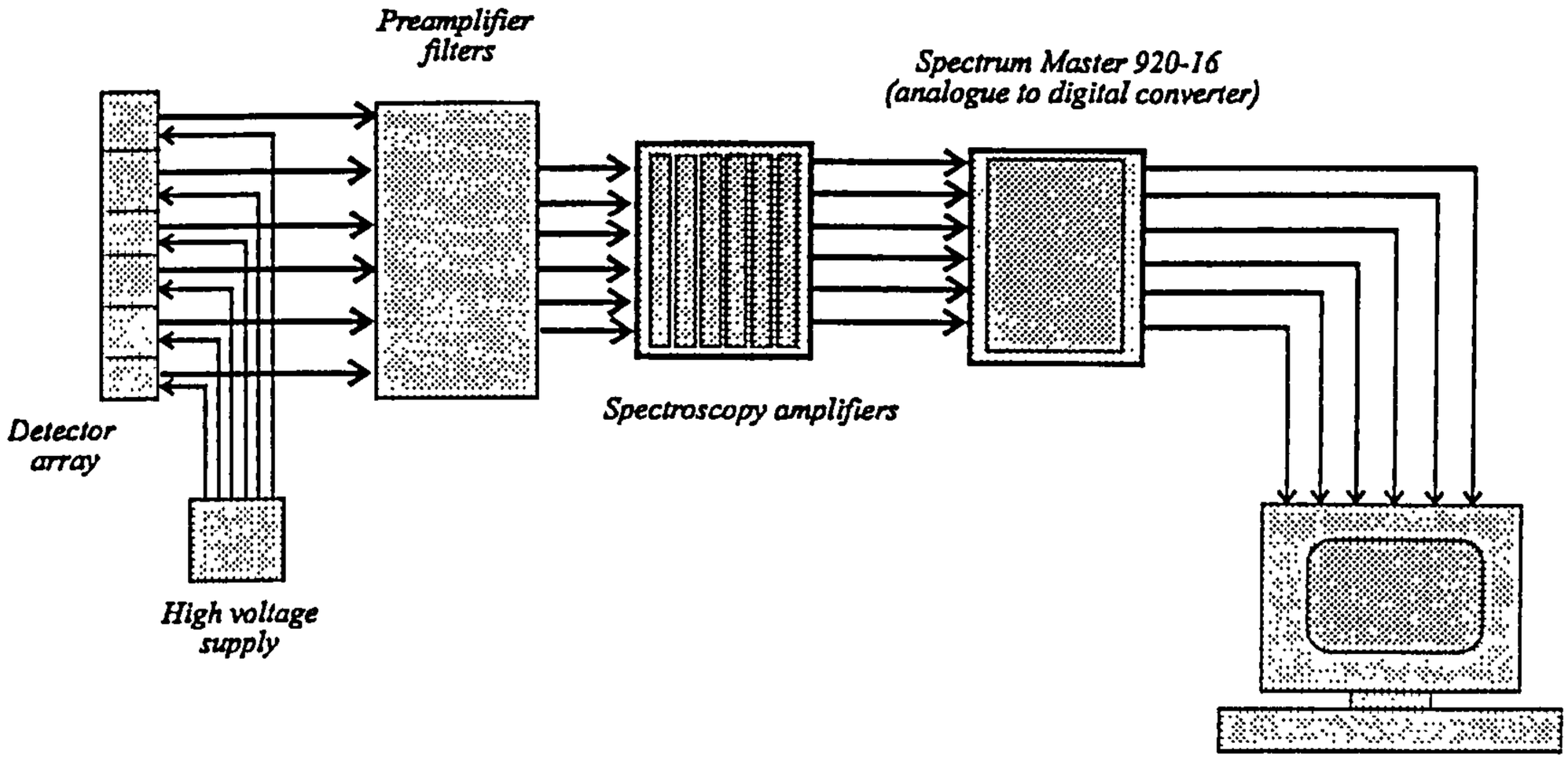

Figure 5.4 A schematic diagram of the electronics associated with the prototype (only 6 detectors are shown)

The effect of measuring ten signals simultaneously was that the current at which the X-ray tube was run had to be reduced to 10 mA. This was because the dead time required by the Spectrum Master to process the ten signals increased to more than 30% if the X-ray tube was run at 20 mA, as used previously. At 10 mA the dead time was less than 10%.

5.1.6 Changes in the geometry

The new geometrical dimensions meant that the space between the scatter point and the collimator had to be increased (from 136 mm to 440 mm) in order to allow for the dimensions of the tunnel. The widths of the collimation slits were also increased from 1 mm to 1.3 mm. These reduced the solid angle subtended by the detector by a factor of 3.95. The change in primary collimation also reduced the incident flux by a factor of 1.5. The change in tube current reduced the flux by a factor of 2. Changing the geometry and electronics of the system had the effect of reducing the integrated counts per unit time in comparison with the single detector / multiple angle system used previously and the increase in geometrical dimensions meant an increase in scatter in

the air. Also it should be noted that reproduction of the alignment of a system with different geometrical dimensions is difficult. Overall the measurement time was found, by empirical methods, to require to be increased by a factor of 19 to maintain the integrated counts in the scatter signatures from the single detector system.

5.1.7 Measurement times

From the results taken from the single detector system it was proposed that a shorter measurement time could still give the same false alarm rates. It can be seen in figure 5.5 that an interpolation can be carried out of the percentage errors between the measured points. From this graph it is possible to determine to what extent the errors could be tolerated whilst maintaining the false alarm rate. That is, what is the shortest time in which the measurement could be taken whilst not causing the overlap of error bars between benign and explosive cases. That is, it provides the shortest time achievable without increasing the false alarm rate. This time was then used for measurements on the array system. This interpolation was carried for all eight cases and the maximum percentage error acceptable for 3 mm of SX2, is 8% which could be obtained in t_m=5 s. The maximum percentage errors acceptable for 6 mm of SX2 and 4 mm of Semtex are 12% and 10% respectively which can again be obtained in t_m=5 s.

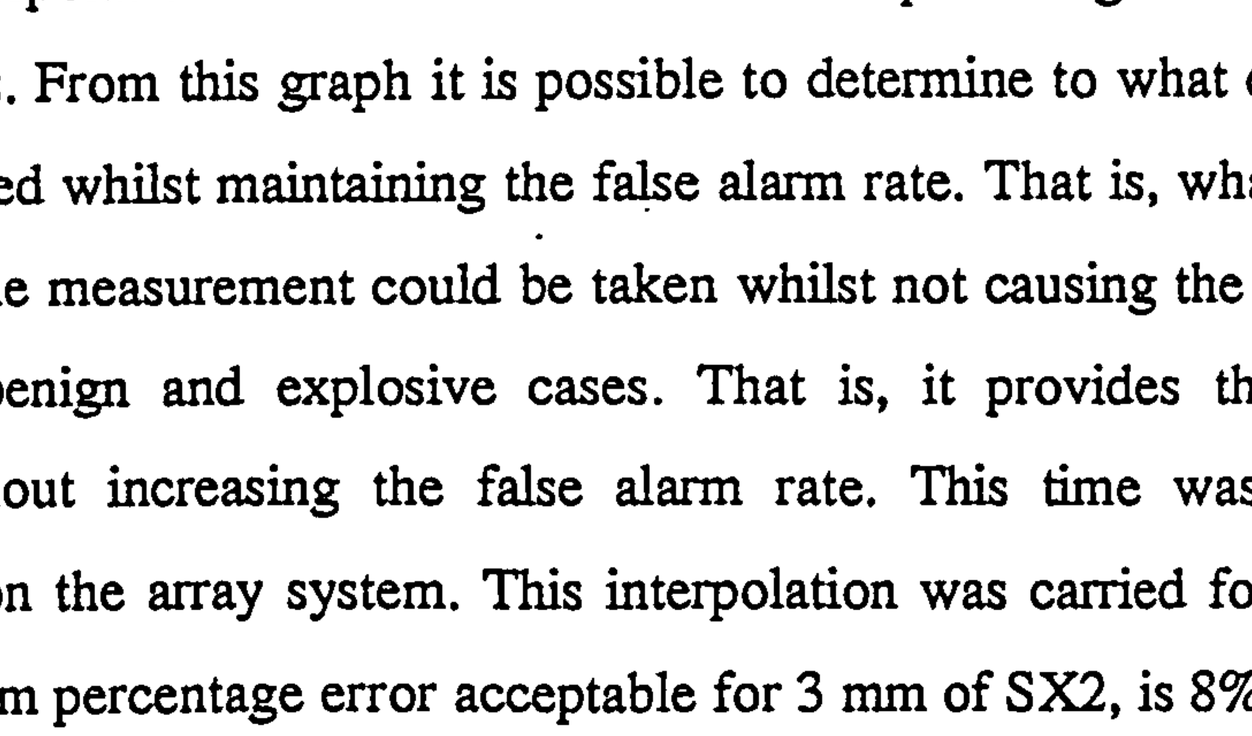

Figure 5.5 The percentage error as a function of time for the 3.3 Å window with 0.38° collimation for the benign case contents of case 1, as measured with the single detector / multiple angle system

Hence, t_m=5 s was determined to be the minimum time required. Measurement times of 7 s and 14 s were also taken in order to assess the improvement which increased measurement time would make. These times must be multiplied by a factor of 19 to maintain the integrated counts for the array system and therefore were taken at t_m=95s, 135 s and 270 s.

5.2 Evaluating the array system

The full array system was set-up as shown in figure 5.6. The dimensions were designed to fit within the new geometry, and included the width of the tunnel.

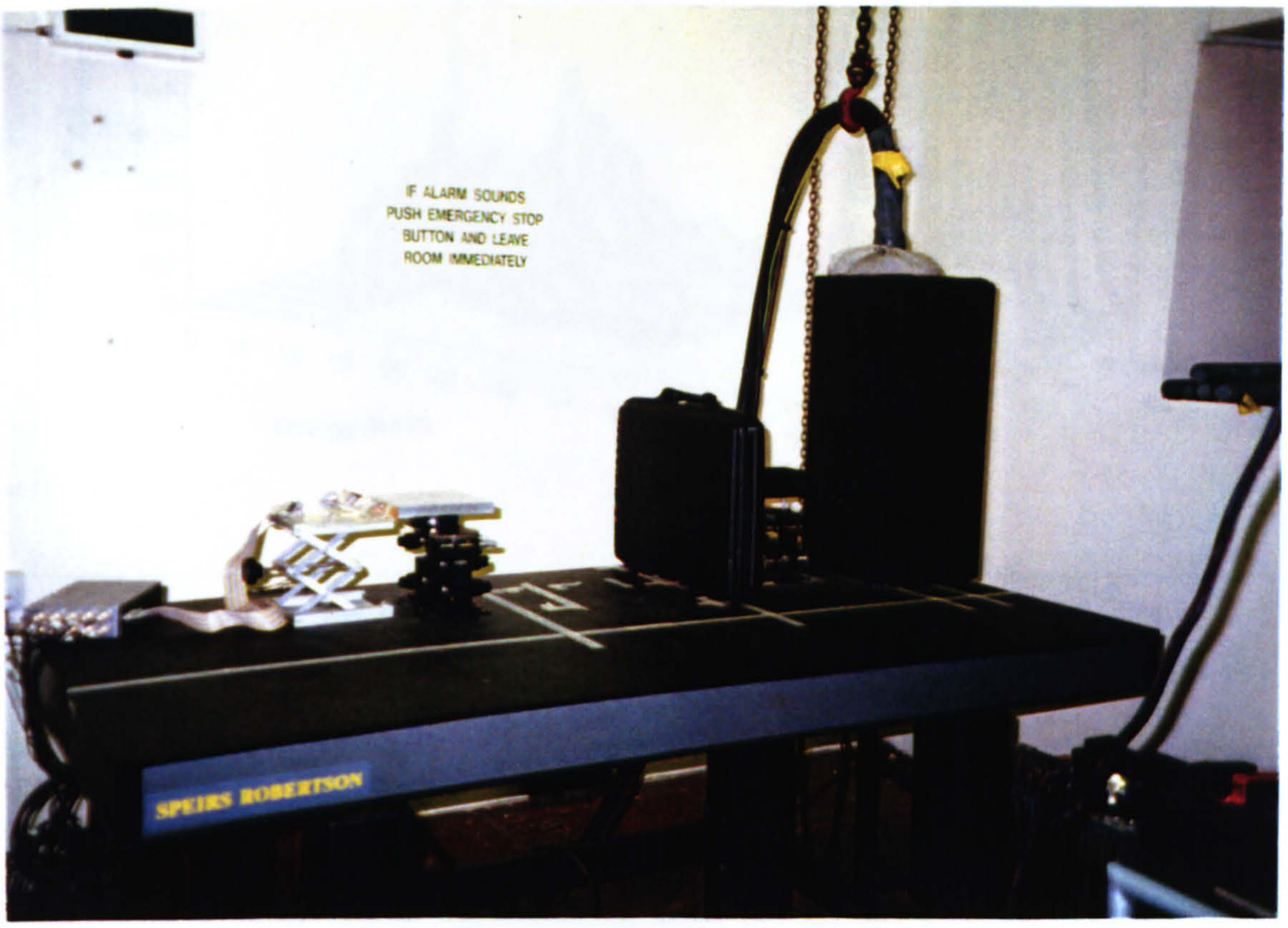

Figure 5.6 A photograph of the complete array system

Before using the array system it was necessary to test the alignment and total efficiency (i.e. the geometric and intrinsic efficiency together) of each detector and respective collimation slit. This was carried out in two ways. The first was to place an americium 241 source at the scatter point and irradiate the ten detectors uniformly and simultaneously. This provided information on the relative efficiencies of the individual detector units. Figure 5.7 shows the americium spectra for the ten collimated detectors. It can be seen that for the same measurement time the detectors have different efficiencies. The varying energy resolutions can be also be seen. This is also shown in table 5.2.

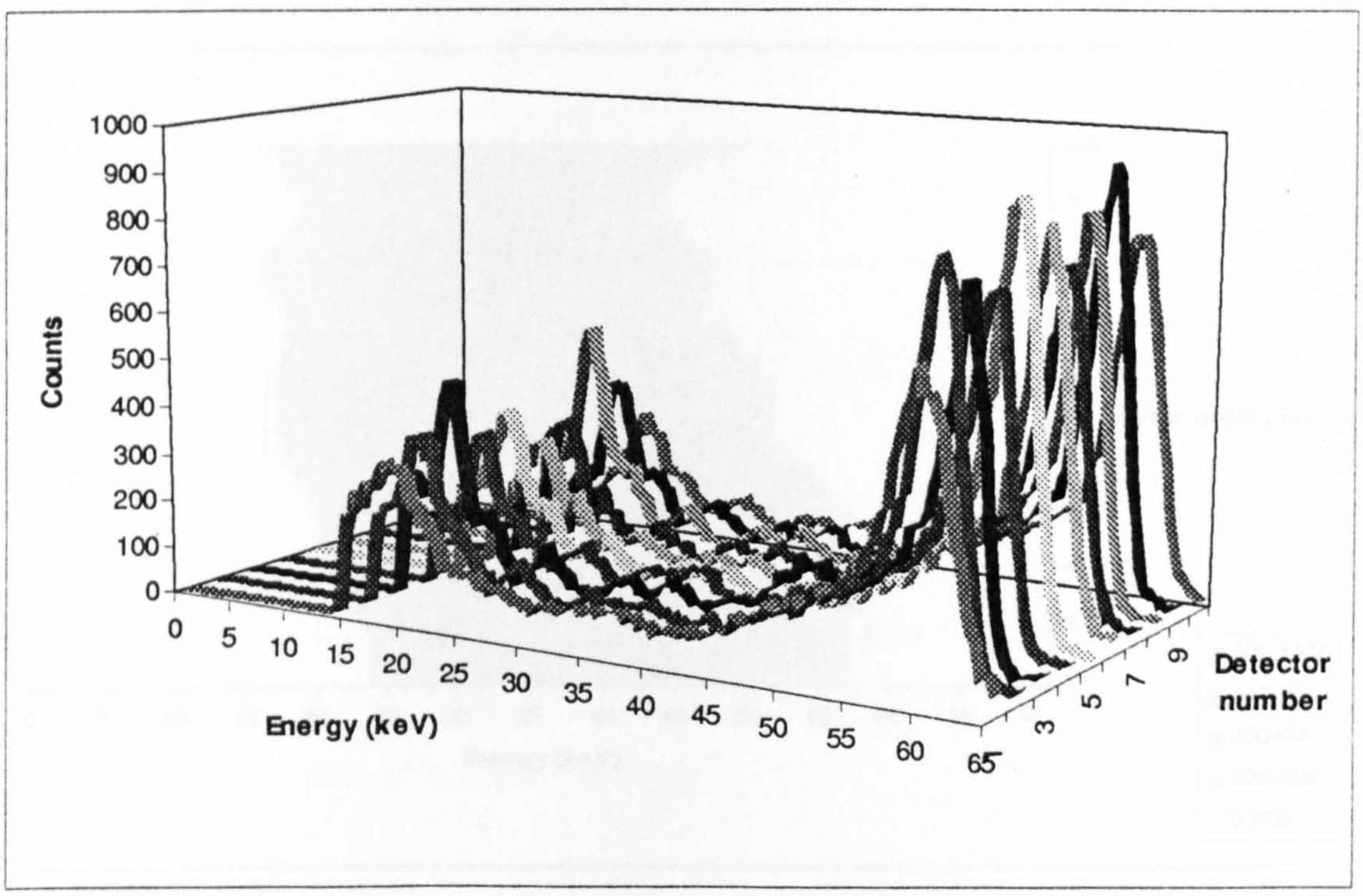

Figure 5.7 The americium 241 spectra for the ten detectors measured with collimation

To determine the effect that the variations in the detector response and the effects of the collimation had on the energy angle diagrams and also to assess the alignment of the whole system, scatter signatures of SX2 for an energy-angle diagram were obtained. Figure 5.8 shows the energy angle diagram for a 3 mm sheet of SX2.

The integrated counts for the ten detectors show the variation in efficiency. Table 5.2 shows the relative efficiencies for the ten detectors normalised to the most efficient. This ranges from 1 for detector number 1 to 0.87 for detector number 7.

The summary of the characteristics of the array shown in table 5.2 can be matched with the variations in intensity and peak width seen in the energy angle diagram in figure 5.8. For instance the detector at 7° has low efficiency and medium energy resolution and hence has a low intensity, whereas the detector at 7.5° has high efficiency and poor energy resolution and therefore has a wide peak with strong intensity.

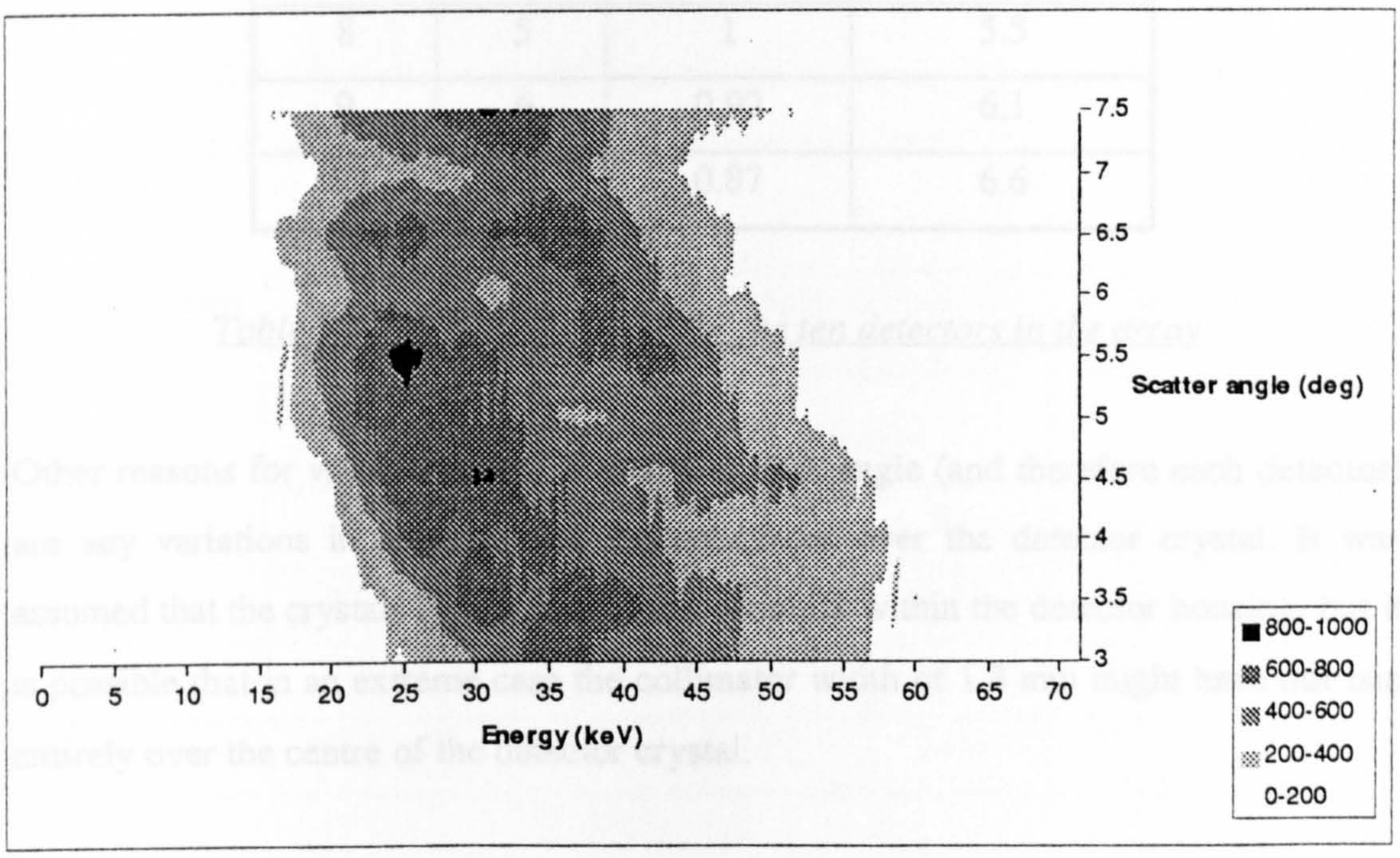

Figure 5.8 An energy angle diagram for 3 mm SX2 measured with the array

The variation in efficiency can be corrected for by dividing each scatter signature by the relevant relative efficiency factor. However, to correct for energy resolution variations would be much more difficult as a deconvolution procedure would be required.

Detector number	Scatter angle (°)	Relative total efficiency	Energy resolution at 59.5 keV (%)
1	7.5	1	11.7
2	6.5	0.96	6.7
3	5.5	0.97	6.5
4	4.5	0.90	6.9
5	3.5	0.94	6.9
6	3	0.91	6.6
7	4	0.87	6.6
8	5	1	5.5
9	6	0.92	6.1
10	7	0.87	6.6

Table 5.2 The characteristics of the ten detectors in the array

Other reasons for variation in the intensity at each angle (and therefore each detector) are any variations in alignment of the collimator over the detector crystal. It was assumed that the crystals lay approximately centrally within the detector housing, but it is possible that in an extreme case the collimator width of 1.3 mm might have not lain entirely over the centre of the detector crystal.

However, for purposes of comparing different case contents and determining the presence of an explosive it is not necessary to correct for the variation in efficiency across the array since the analysis procedure is a relative method.

5.3 Results from the array

The array was used to measure the scatter signatures from the same eight case contents as were used to test the single detector system. This was so that a direct comparison between the two systems could be made. The analysis procedure was carried out as before with a single window placed at 3.3Å, as shown to be the optimum window for this application in Chapter 4. The measurements were taken for the same integrated counts as for t_m=10s with the single angle system. The measurement times had to be increased 19 fold (as explained in section 5.1.6) and were t_m=95 s, 135 s and 270 s (equivalent to t_m=5 s, 7 s and 14 s in the single angle system as explained in section 5.1.7). The analysis procedure was carried out as in Chapter 4 i.e. with a single window at 3.3 Å. The percentage of false alarms producing by setting a threshold for a 100% detection rate was calculated and is shown in table 5.3.

Measurement time (s) t_m	**% false alarms for all explosive samples (i.e. 3 mm SX2)**		**% false alarms for 4 mm sample of Semtex**		**% false alarms for 6 mm sample of SX2**	
	3σ	**2σ**	**3σ**	**2σ**	**3σ**	**2σ**
95	100	100	100	100	100	100
135	100	100	75	37.5	75	37.5
270	87.5	75	50	37.5	37.5	37.5

Table 5.3 The percentage of false alarms for 100% detection rate for three measurement times and a single window at 3.3 Å (results are shown for 2σ and 3σ error bars)

It can be seen from table 5.3 that the false alarm rates are higher than those shown in Chapter 4. Previously t_m=10 s gave results of 0 % false alarms for 100% detection rate for 4 mm of Semtex and 6 mm of SX2 using 2σ error bars. The false alarm rates for the same parameters with the array are 100% for both explosive samples. However, the false alarm rates for the longer measurement times of 135 s and 270 s are lower

and the best false alarm rates are achieved for 4 mm of Semtex and 6 mm of SX2 at 270 s with 2σ error bars which gave a 37.5% false alarm rate. The increase in measurement time meant the error bars were smaller, hence the lower false alarm rates. However at very long measurement times the improvement in SNR with increase in measurement time becomes negligible. Hence, there is insignificant improvement in the false alarm rate.

The reason for this change in results is that in changing the primary collimation to symmetrical and moving the secondary collimation further away, the shape of the scatter volume became longer along the incident beam axis and narrower perpendicular to this axis (see figure 5.9) The overall cross-sectional area increased by a factor of 2.02 and the fraction taken up by 3 mm of explosive at a 5° scatter angle was 2.21% in the array system compared with 6.57% in the single detector system (see table 5.4). The effect of the fraction of the volume taken up by the explosive becoming smaller was that the relative number of scatter counts from the explosive were less. This meant that the difference in counts between the explosive case and the safe case was smaller, thus making the explosive threshold more difficult to set.

Explosive type and thickness	Percentage of volume in single detector system at 5° scatter angle	Percentage of volume in array system at 5° scatter angle
3 mm SX2	6.57	2.21
4 mm Semtex	8.76	2.95
6 mm SX2	13.14	4.42

Table 5.4 The percentage of the scatter volume (shown at 5°) taken up by the three explosive samples

The change in shape and length of scatter volume also meant that the composition of other materials was slightly different even though the cases were packed in the same way as before. This had an effect on the positions of the scatter points in the plot used to set the threshold.

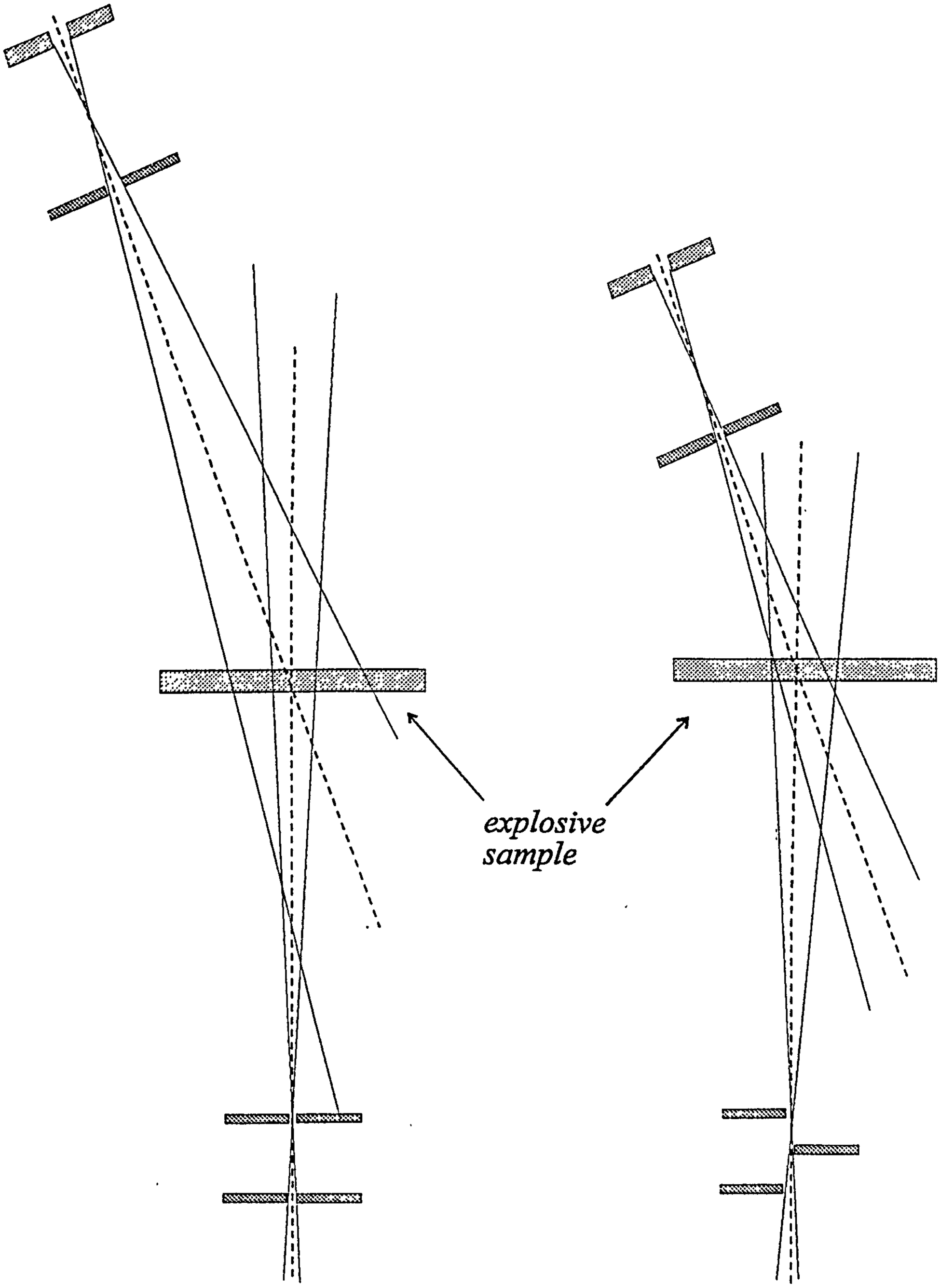

Figure 5.9 A schematic diagram of the change in scatter volume shape from single detector system to the array system.

In comparison with the false alarm rate achieved by Strecker (1995), a 37.5% false alarm rate is lower than 30% by 7.5%. The continuation of Strecker's work was presented by Hnatnicky (1996). They have built a working baggage scanning system and require 90s at 10 kW power to scan a medium size bag. The tube power used in this work is 0.7 kW and therefore if the same flux were used as for at 10 kW, t_m=270 s would be reduced to t_m=18.9 s. However, an increase in power for this array system would require changes to be made to the Spectrum Master to overcome the dead time problems which this would cause.

5.4 Conclusions

The results from this array system have shown that the shape and size of the scatter volume is important, and thus the proportion of the volume taken up by the explosive should be maximised. It is recommended that the collimation be designed to maximise the width and minimise the length of the scatter volume along the incident beam axis. This would increase the fraction of volume which the sheet of explosive, positioned perpendicular to the incident beam, took up. It is suggested that this could be achieved by placing the secondary collimators and detectors directly underneath the tunnel in which the baggage was travelling. The X-ray tube and primary collimation should be above the tunnel and thus a greater distance from the scatter volume. The configuration for the baggage scanner, used to provide the geometrical dimensions for this study, is that the X-ray tube is below the tunnel and the detectors are above. Therefore, for a scanner which included a coherent scatter system, the scanner used here is not ideal. The measurement time is an important factor for a system to be used as a baggage scanner. A compromise must be found between long measurement times to reduce statistical noise in the measured spectra and shorter times which allow a realistic throughput in an airport situation. However, this will also be determined by the maximum power at which the X-ray tube can be run and the limit of the rate at which the ADC can process all the detectors simultaneously.

CHAPTER 6

CONCLUSIONS AND FUTURE WORK

6.1 Discussion and conclusions

The aim of this work was to investigate whether using multiple angles in a coherent scatter system was a feasible way of measuring scatter signatures. Multiple angles were suggested to be an effective way of measuring scatter signatures from more than one material simultaneously for two reasons. The first reason was that each of the planar spacings of interest would be satisfied by the most intense part of the incident spectrum. The second was that the optimum angle for each of the required materials is available. In this work this has been Semtex and SX2, amongst the various case fillings which have been used. A further part to this investigation was to determine whether multiple angles could be used with detectors which did not require the cryostatic cooling of the previously used germanium detectors. It was also to suggest a method of analysis for the energy angle plots formed by the scatter signatures across a range of angles. Finally to make suggestions as to what design considerations would be required if this system were to be attached to a baggage scanner. This section will summarise each part of this project and discuss whether the aims were achieved and what the outcome was.

6.1.1 The detector chosen for the system

Cadmium zinc telluride was chosen as the detector acceptable to use with a multiple angle scatter system because of its suitable energy resolution, size and efficiency. It is also an easy detector to use as there are no cryogenic cooling requirements and it only

needs power for the preamplifier and a bias supply. These are important considerations for building an array of detectors.

6.1.2 Modelling of the energy-angle diagrams

A model was used to determine what the angular blurring requirement of collimation for the detectors would be and how many of these detectors would be needed. It was tested against measured signatures of the explosive SX2. The primary requirement of the model was the diffraction data of the material. Therefore, the diffraction data for the SX2 was measured with a standard diffractometer. From this diffraction data three main planar spacings were identified which occurred in both SX2 and Semtex. These were proposed to be used for the basis of the analysis procedure.

The orientation of the explosive in the incident X-ray beam was found to have a strong effect on the intensities of the diffraction peaks. This also affects the standard diffractometer measurements. Empirical corrections were made to the intensities used for the model and this corrected diffraction data was found to be similar to that measured from a randomly orientated powder sample of pure RDX. The model was also used to investigate energy-angle diagrams. It was concluded that the acceptance angle of the collimators should be less than 0.76° and that the number of detectors required was ten.

6.1.3 Design of the collimation

Multiple angle collimators have been designed to collect scattered photons at angles from 3° to 7.5° in 0.5° intervals. Acceptance angles of 0.19° and 0.38° were found to be suitable to use with the cadmium zinc telluride detector. Aluminium was found to be a suitable material as it not only attenuates the photons sufficiently, but is also a light and easy material to machine.

Various designs of collimation were considered and slit collimation was chosen for the increased intensity it provides. The multiple angle collimator for the system was

designed symmetrically and this was found to reduce the effect of variation in scatter volume size on either side of the primary beam.

6.1.4 Development of the analysis procedure

The aim of the analysis procedure was that it would be easy to carry out and would not require much computational analysis. This has been achieved with the use of windows on the energy channels. These have been optimised in both position and width for the specific application of baggage scanning for RDX based explosives. Nine variations of windows at the three planar spacings were investigated. It has been found that a single window at 3.3 Å gave the lowest false alarm rate. In comparison with other methods for analysing coherent scatter signatures from explosives, this method has been found to be comparable in both the false positive rates produced and integrated counts required. For thicker samples of Semtex and SX2 the window at 3.3 Å was found to provide a 0% false alarm rate for a 10 s measurement time, if random fluctuations were tolerated to the 5% level.

6.1.5 The detector array

The final aim of this work was to investigate an array system based on the knowledge gained from the single detector system. The array system was set-up and it was then compared directly with the single detector system. The measurement times required for the array were longer than for the single detector system. This was due to the changes in dimensions and reduction in the X-ray tube current.

The false alarm rates for the array were higher than for the single detector system and this was due change in the fraction of the scatter volume taken up by the explosive. The results from the array and single angle system suggest that the explosive must occupy more than 8.76% of the scatter volume in order to be detected with the multiple angle system with a window at 3.3 Å. Suggestions of how to optimise the scatter volume shape for explosive detection have been given.

6.2 Further developments

More long term developments that might improve a multiple angle array are discussed in this section, including cooling of detectors, pulse processing, changes in the detector crystal shape and individual collimation design. Some suggestions for other applications are also given.

6.2.1 Cooling of the detectors

It has been shown that cooling of cadmium zinc telluride detectors to 0°C can significantly improve the energy resolution performance *(Niemela and Sipila 1996, Parnham 1996b)*. This can be achieved using peltier cooling of the detector crystal and preamplifier. It is suggested that the whole detector array could be encased within a thermoelectric cooling system. Although this means a return to permanent cooling of the detectors (one of the disadvantages of a germanium detector), peltier cooling requires much less maintenance, is cheaper than the use of liquid nitrogen and is less bulky. An improvement in energy resolution would also allow an increase in collimation acceptance angle (whilst maintaining momentum resolution) and thus an increase in flux, providing shorter measurement times. If suitable measurement times were achieved then improving the energy resolution could also improve the momentum resolution of the system and thus be more specific to the required planar spacings. This would allow narrower windows without increasing the error bars and thus could help to reduce the false alarm rate.

6.2.2 Pulse processing methods

Recent work has also been done to improve the spectroscopic performance of cadmium zinc telluride detectors by pulse processing methods. These have included rise time discrimination *(Hess et al. 1994, Jordanov et al. 1996, Niemela et al. 1996a and b)* and rise time compensation *(Lund et al. 1996a, Redus et al. 1996)*. Rise time discrimination compensates for the effects of charge trapping by removing the slow rise time pulses caused by trapped holes. However, this has the disadvantage of

removing a significant number of the pulses. As the application of baggage scanning requires short measurement times, the loss of pulses would not be desirable. Rise time discrimination corrects the slow rise time pulses and adds them to the correct energy peak. Although this requires intense processing, it has the advantage of not reducing the count rate.

Other methods that have been used to improve the energy resolution are changes in the electrode configuration and geometry. These have included coplanar electrodes *(Luke 1996)* which work like a Frisch grid in a gas detector and coaxial *(Lund et al. 1996b)* and hemispherical geometries *(Luke 1996)*.

6.2.3 Development of the detector shape

In this work the detector crystal was 5 x 5 x 2 mm. In using collimation of 1 mm or 1.33 mm width this means that much of the crystal is not used. It has been shown that the blurring effect of using slit collimation, as compared to pinhole collimation, is not significantly greater. Therefore detectors of narrower width and greater height, i.e. which match the size and shape of the collimator, would be geometrically more efficient. That is, there would not be unused parts of the crystal. Also a greater irradiated surface area suggests that the integrated counts per unit time would be increased and therefore the measurement time could be reduced.

6.2.4 Improvements for baggage scanning

Primarily an extensive range of types of baggage and contents must be measured. This would allow further refinements of the width and positions of the energy windows. The collimation should be designed so as to maximise the fraction of the scatter volume taken up by the explosive. The power at which the X-ray tube is run should be as high as possible whilst staying within the safety limits for photographic film and also within the limits of the electronic processing systems. An increase in power would allow shorter measurement times. Security systems for hold baggage usually use several methods to scan the baggage *(Campbell 1997)*. Therefore emphasis should be placed

on those materials for which these other systems have high false alarm rates, and less on those which can be easily identified.

6.2.5 Other applications for this method

There are various difficulties associated with the application of scanning baggage that make it a complicated problem to solve. These are that the background material is unknown and can change across the item of luggage. This in turn means that there is a great variation both in the scatter and attenuation properties of the materials being measured. There are also various types of explosive to be detected and the thickness and quantity will also vary. The following section suggests some applications that may not suffer so many complications and therefore for which it is suggested the multiple angle scatter signature method could be successfully applied.

Other applications with which coherent scatter systems have been used include the detection of contaminants in food products, for example plastic in jam or chocolate *(Luggar and Gilboy 1994)*, and the diagnosis of osteoporosis in bone *(Royle and Speller 1991, Farquharson 1996)*. It is suggested that the technique of multiple angle coherent scatter could be used in both of these applications.

For the detection of contaminants on the production line of food, the type of contaminant is often known and therefore the windows in the energy angle plots could be designed to identify these materials. As in baggage scanning, this is a qualitative technique and the quantity of contaminant is not required. This could perhaps be a simpler application than the detection of explosives in baggage as the background material (i.e. the product) would be uniform and known. However, the measurement times required might be restrictive.

The application of diagnosis of osteoporosis in bone is rather different since the ratio of bone to marrow in the centre of the bone is the required measurement. It is suggested that two windows could be used, one for each of the two substances. The ratio of the integrated counts in these two windows could then be calculated and then

be calibrated against known amounts of bone and marrow. If a bone to marrow ratio were determined at which the loss of bone became a medical problem then an automatic threshold could be set. Dose considerations would also have to be taken into account.

A further application could be to detect explosives in postal items. Again this is a qualitative application. However, it should be simpler than baggage scanning as the background material would be mainly paper based materials. The difficulty would be that the measurement time would have to be very fast (perhaps less than 1 second per item) since the quantity of mail passing through the sorting offices is very large.

6.3 Closing remarks

This work has shown that the use of multiple angles for the detection of coherent scatter signatures is a promising method for applications where more than one material is required to be detected. It is also a technique for which a simple method of analysing the data could be provided and measurement times could be shorter than existing systems. However, it has been shown that the geometry of the system must be designed so as to maximise the fraction of the scatter volume occupied by the material which is required to be detected. Further development of detectors and collimation design may help to facilitate the use of coherent scatter as a method of identifying materials in realistic situations.

REFERENCES

Akutagawa W., Zanio K. and Mayer J.W. (1967) *CdTe as a gamma detector.* Nuclear Instrumentation and Methods Vol. 55 p383-385

Arlt R., Czoch K-H. and Rundquist D.E. (1992) *Overview of the use of CdTe detectors for the verification of nuclear material in nuclear safeguards.* Nuclear Instrumentation and Methods A Vol. 322 p575-582

Armantrout G.A., Swierkowski S.P., Sherohman J.W. and Yee J.H. (1977) *What can be expected from high Z semiconductor detectors?* IEEE Transactions on Nuclear Science Vol. 24 No. 1 p121-125

Armstrong R., McDaid S.M., Cooper M.J. and Harding G. (1993) *Potential applications of a novel X-ray source in material characterisation.* SPIE Vol. 2092 Substance Detection Systems, Innsbruck p411-416

Bao X.J., Schlesinger T.E. and James R.B. (1995) *Electrical properties of mercuric iodide, Chapter 4 Semiconductors for room temperature nuclear detector applications* Ed. Schlesinger T.E. and James R.B. Pub. Academic Press p111-165

Barber H.B. (1996) *Application of II-VI materials to nuclear medicine.* Journal of Electronic Materials Vol. 25 No. 8 p1232-1240

Berger M.J. and Hubbell J.H. (1987) *XCOM: Photon cross-sections on a personal computer.* NSBIR 87-3597.

Bertuccio G., Pullia A., Canali C., Nava F. and Lanzieri C. (1997a) *Schottky junction on semi-insulating LEC gallium arsenide for X and γ-ray spectrometers operated at and below room temperature.* IEEE Transactions on Nuclear Science Vol. 44 No. 2 p117-124

Bertuccio G., Pullia A., Lauter J., Forster A. and Luth H. (1997b) *Pixel X-ray detectors in epitaxial gallium arsenide with high energy resolution capabilities (fano factor experimental determination).* IEEE Transactions on Nuclear Science Vol. 44 No. 1 p1-5

Birch R., Marshall M. and Ardram G.M. (1979) *Catalogue of spectral data for diagnostic X-rays.*

Blaffert T. (1995) *Theory of stochastic signal processing for the optimisation of CXRS explosives detection.* SPIE Vol. 2511 Law enforcement technologies, Munich p108-119

Blum L. (1971) *X-ray scattering from liquids with nearly spherical molecules.* Journal of Computational Physics Vol. 7 p592-602

Booth A.D. and Llewellyn F.J. (1947) *The crystal structure of pentaerythritol tetranitrate.* Journal of the Chemical Society Vol. 23 p 837-846

Bradley D.A. and Ghose A.M. (1984) *Photon scattering in biomedically important elements.* Physics in Medicine and Biology Vol. 29 No. 11 p1385-1397

Bradley D.A. and Ghose A.M. (1987) *Differential coherent scattering cross-section measurements* Nuclear Instrumentation and Methods A Vol. 255 p57-65

Bradley D.A., Dance D.R., Evans S.H. and Jones C.H. (1989) *Quantitative measurement of small-angle gamma ray scattering from water, nylon and Lucite.* Medical Physics Vol. 16 No. 6 p851-857

Brett C.J., Foran S.G.A. and Harris J.E.C. (1986) *Particle characterisation of nitramines.* Directorate of Quality Assurance/Technical Support Materials Centre (Commercial in Confidence) Report

Burger A., Nason D., van den Berg L. and Schieber M. (1995) *Growth of mercuric iodide, Chapter 3 Semiconductors for room temperature nuclear detector applications* Ed. Schlesinger T.E. and James R.B. Pub. Academic Press p86-108

Butler J.F., Lingren C.L. and Doty F.P. (1992) *$Cd_{1-x}Zn_xTe$ gamma ray detectors.* IEEE Transactions on Nuclear Science Vol. 39 No. 4 p605-608

Cambridge thesaurus of Physics (1984) Ed. Denney R.C. and Foster S. Pub. Cambridge University Press

Campbell T. (1997) *Personal communication.* British Aerospace Association

Cartwright N. (1994) *Reaching consensus on technical standards through ICAO: The work of an ad hoc group of specialists on the detection of explosives.* Journal of Testing and Evaluation Vol. 22 No. 3 p277-279.

Chirco P., Zanarini M., Caroli E., Donati A., Dusi W., Stephen J.B. and DiCocco G. (1996) *Comparative evaluation of the temperature dependence of the different noise sources in CdTe detectors* Nuclear Instrumentation and Methods A Vol. 380 p127-131

Cohen N.S. (1997) *Personal Communication*

Cowley J.M. (1981) *Diffraction Physics.* 2nd Ed. Pub. North-Holland, Amsterdam, Holland. p73-75

Dawson C., Horrocks J.A. Kwong R., Speller R.D. and Whitfield H.N. (1996) *Low angle X-ray scattering signatures of urinary calculi.* World journal of Urology Vol. 14 p43-47

De Nobel D. and Kroeger F.A. (1962) *US patent no. 3,033,791*

Dearnaley G. and Nearthrop D.C. (1964) *Semiconductor counters for nuclear radiation*. Pub E&FN Spon., London

Deich V. and Roth M. (1996) *Improved performance of lead iodide nuclear radiation detectors*. Nuclear Instrumentation and Methods A Vol. 380 p169-172

Doty F.P., Butler J.F., Schetzin J.F. and Bomers K.A. (1992) *Properties of CdZnTe crystals grown by high pressure Bridgman method*. Journal of Vacuum Science Technology Vol. B10 p1418

Dusi W., Caroli E., DiCocco G., Donati A., Landini G., Chirco P. and Scannavini M.G. (1995) *A study of temperature dependence of some relevant parameters performed on a set of CdTe detectors*. IEEE Transactions on Nuclear Science Vol. 42 No. 4 p263-266

Eberhardt J.E., Ryan R.D. and Tavendale A.J. (1970) *High resolution nuclear radiation detectors for epitaxial n-GaAs*. Applied Physics Letters Vol. 17 p427-429

Eberhardt J.E., Ryan R.D. and Tavendale A.J. (1971) *Evaluation of epitaxial n-GaAs for nuclear radiation detection*. Nuclear Instrumentation and Methods Vol. 94 p463-476

Eddy P. (1997) *Head on crash*. Sunday Times Magazine 28th September p58-60

EEV Ltd (1996), Chelmsford, Essex

EG&G Ortec (1996), Wokingham, Berkshire

Eisen Y. (1996) *Current state of the art industrial and research applications using room temperature CdTe and CdZnTe solid state detectors*. Nuclear Instrumentation and Methods A Vol. 380 p431-439

Entine G., Waer P., Tiernan T. and Squillante M.R. (1989) *A survey of nuclear detector applications*. Nuclear Instrumentation and Methods A Vol. 283 p282-290

Eurorad (1996), Strasbourg, France

eV Products (1996), Saxonburg, Pennsylvania, USA

Evans R.D. (1982) *The Atomic Nucleus*. Pub. Krieger, New York p674-676

Evans S.H., Bradley D.A., Dance D.R., Bateman J.E., Jones C.H. (1991) *Measurement of small-angle photon scattering for some breast tissues and tissue substitute materials*. Physics in Medicine and Biology Vol. 36 No. 1 p7-18

Excel 5.0c (1994) Microsoft Corporation

Fainberg A. (1992) *Explosives detection for aviation security*. Science Vol. 255 No. 5051 p1531-1537

Farquharson M.J. (1996) *Characterisation of bone tissue using coherently scattered X-ray photons*. PhD Thesis, University of London

Fultz K.O. (1994) *Aviation security: development of new security technology has not met expectations*. General Accounting Office Report, American Association of Airport Executives. (http://www.airportnet.org/DEPTS/federal/gao/avsec.htm)

Giessen W.C. and Gordon G.E. (1968) *X-ray diffraction: A new high speed technique based on X-ray spectrography*. Science Vol. 159 p973-975

Gozani T. (1992) *Nuclear based techniques for cargo inspection - a review*. Contraband and Cargo Inspection Technology International Symposium, Washington p9-19

Gozani T. (1996) *Inspection techniques based on neutron interrogation.* SPIE Vol. 2936 Physics based technologies for the detection of contraband, Boston p9-20

Grodzins L. (1991) *Nuclear techniques for finding chemical explosives in airport luggage.* Nuclear Instrumentation and Methods B Vol. 56/57 p829-833

Grodzins L. (1993) *Detecting contraband in luggage* Nuclear Instrumentation and Methods B Vol. 79 p597-600

Hage-Ali M. and Siffert P. (1992) *Status of semi-insulating cadmium telluride for nuclear detectors.* Nuclear Instrumentation and Methods A Vol. 322 p313-323

Hage-Ali M., Koebel J.M., Regal R., Siffert P., Prat V and Simon H. (1996) *Cadmium telluride small probes for gamma ray spectrometry* Nuclear Instrumentation and Methods A Vol. 380 p427-430

Hall J. and Jacoby B. (1993) *Analysis of a proposed Compton backscatter imaging technique.* SPIE Vol. 2092 Substance detection systems, Innsbruck p448-459

Hamilton W.J., Rhoger D.R., Sen S., Kalisher M.H., James K., Reid C.P., Gerrish V. and Baccash C.O. (1994) *Very high resolution detection of gamma radiation at room temperature using P-I-N detectors of CdZnTe and* HgI_2. IEEE Transactions on Nuclear Science Vol. 41 No. 4 p989-992

Hardie-Brown D., Lillicrap S.C. and Scott J (1987) *Phantom materials for photon scattering measurements.* Physics in Medicine and Biology Vol. 32 No. 9 p1175-1178

Harding G. (1995) *Optimisation criteria for CXRS baggage inspection.* SPIE Vol. 2511 Law enforcement technologies, Munich p64-70

Harding G. and Kosanetsky J. (1985) *Elastic scatter computed tomography*. Physics in Medicine and Biology Vol. 30 No. 2 p183-186

Harding G. and Kosanetzky J. (1987) *Status and outlook of coherent X-ray scatter imaging*. Journal of Optical Science of America Vol. 4 No. 5 p933-944

Harding G., Armstrong R., McDaid S. and Cooper M.J. (1995) *A k-edge filter technique for optimisation of the coherent-to-Compton scatter ratio method.* Medical Physics Vol. 22 No. 12 p2007-2014

Harding G., Kosanetzky J. and Neitzel U (1987) *X-ray diffraction computed tomography*. Medical Physics Vol. 14 No. 4 p515-525

Harding G., Newton M. and Kosanetzky J. (1990) *Energy dispersive X-ray diffraction tomography*. Physics in Medicine and Biology Vol. 35 No. 1 p33-41

Harding W.R., Hilsum C., Moncaster M.E., Narthrop D.C. and Simpson O. (1960) *Gallium arsenide for γ-ray spectrometry*. Nature Vol. 187 (4735) p405

Heiskanen K.A. and Roder F.L. (1996) *Explosive detection systems: The real world experience* SPIE Vol. 2936 Physics based technologies for the detection of contraband, Boston p142-155

Hess R., De Antonis P., Morton E.J. and Gilboy W.B. (1994) *Analysis of the pulse shapes obtained from single crystal $Cd_{0.9}Zn_{0.1}Te$ radiation detectors*. Nuclear Instrumentation and Methods A Vol. 353 p76-79

Hnatnicky S. (1996) *CRXS explosives detection airport prototype*. SPIE Vol. 2936 Physics Based Technologies for the Detection of Contraband, Boston p180-187

Hubell J.H., Viegele W.J., Briggs E.A., Brown R.T., Cromer D.T. and Howerton R.J. (1975) *Atomic form factors, incoherent scattering functions and photon scattering cross-sections*. Journal of Physical Chemistry Reference Data Vol. 4 p471-538

Hussein E.M.A., Gokhale P., Arendtsz N.V. and Laurence A. (1996) *Inspection of cargo containers using gamma radiation*. SPIE Vol. 2936 Physics based technologies for the detection of contraband, Boston p210-218

Iwanczyk J.S., Patt B.E., Wang Y.J., Croft M., Kalman Z. and Mayo W. (1995) *Mercuric iodide detectors systems for identifying substances by X-ray energy dispersive diffraction*. IEEE Transactions on Nuclear Science Vol. 42 No. 4 p606-610

James R.B., Schlesinger T.E. Lund J.C. and Schieber M. (1995) *$Cd_{1-x}Zn_xTe$ spectrometers for gamma and X-ray applications, Chapter 9 Semiconductors for room temperature nuclear detector applications* Ed. Schlesinger T.E. and James R.B. Pub. Academic Press p336-378

Johns H.E. and Cunningham J.R. (1983) *The physics of radiology*. 4th Ed. Pub. Charles C. Thomas Appendix A p722-736

Johns P.C. and Yaffe M.J. (1983) *Coherent scatter in diagnostic radiology*. Medical Physics Vol. 10 No. 1 p40-50

Joint Committee for Powder Diffraction Studies (1961) Ed. W.F. McClune, Pennsylvania, USA.

Jones L.T. and Woollam P.B. (1975) *Resolution improvement in CdTe γ detectors using pulse discrimination*. Nuclear Instrumentation and Methods Vol. 124 p591-595

Jordanov V.T., Pantazis J.A. and Huber A.C. (1996) *Compact circuit for pulse rise time discrimination*. Nuclear Instrumentation and Methods A Vol. 380 p484-486

Kerr S.A., Kouris K., Webber C.E. and Kennett T.J. (1980) *Coherent scattering and the assessment of mineral concentration in trabecular bone*. Physics in Medicine and Biology Vol. 25 No. 6 p1037-1047

Khusainov A.Kh. (1992) *Cadmium telluride detectors with thermoelectric cooling* Nuclear Instrumentation and Methods A Vol. 322 p335-340

Knoll G.F. (1989) *Radiation detection and measurement*. 2nd Ed. Pub John Wiley and sons. p572-573

Kosanetsky J., Knoerr B., Harding G. and Neitzel U. (1987) *X-ray diffraction measurements of some plastic materials and body tissues*. Medical Physics Vol. 14 No. 4 p526-532

Lacey R.J (1995, 1996 and 1997) *Personal communication* Police Scientific Development Branch

Lavietes A.D., McQuaid J.H. and Paulus T.J. (1996) *Preliminary uranium enrichment analysis results using cadmium zinc telluride detectors* Nuclear Instrumentation and Methods A Vol. 380 p406-409

Leginus J. (1993) *Portable sensors for drug and explosive detection*. SPIE Vol. 2092 Substance detection systems, Innsbruck p360-363

Leichter I., Karellas A., Craven J.D. and Greenfield M.A. (1984) *The effect of the momentum transfer on the sensitivity of a photon scattering method for he characterisation of tissues*. Medical Physics Vol. 11 No. 1 p31-36

Lorenz M., Van Ryn J., Mark H., Market M. and Eisert W.G. (1994) *Portable γ ray spectrometry for simultaneous monitoring of radiotracers in vivo using CdTe and CZT radiation detection probes*. Nuclear Instrumentation and Methods A Vol. 353 p448-452

Luggar R.D. and Gilboy W.B. (1994) *Applications of Rayleigh scattered photons to substance identification*. Nuclear Instrumentation and Methods A Vol. 353 p650-653

Luggar R.D. and Gilboy W.B. (1995) *Contrast enhancement for Rayleigh scatter radiography*. SPIE Vol. 2511 Law Enforcement Technologies, Munich p56-63

Luggar R.D., Farquharson M.J., Horrocks J.A. and Lacey R.J. (1997) *Multivariate analysis of statistically poor EDXRD spectra for the detection of concealed explosives*. Accepted for publication in X-ray Spectrometry

Luggar R.D., Gilboy W.B and MacCuaig N. (1993) *Industrial potential of Rayleigh scattered X-rays for identification of low Z materials*. SPIE Vol. 2092 Substance Detection Systems, Innsbruck p411-416

Luggar R.D., Horrocks J.A., Farquharson M.J. Speller R.D. and Lacey R.J. (1996a) *Real time analysis of scattered X-ray spectra for sheet explosives detection*. SPIE Vol. 2936 Physics based technologies for the detection of contraband, Boston p291-228

Luggar R.D., Horrocks J.A., Speller R.D. and Lacey R.J. (1996b) *Determination of the geometric blurring of an energy dispersive X-ray diffraction (EDXRD) system and its use in the simulation of experimentally derived diffraction profiles*. Nuclear Instrumentation and Methods A Vol. 383 p610-618

Luggar R.D., Horrocks J.A., Speller R.D., Royle G.J. and Lacey R.J. (1995) *Optimisation of a low angle X-ray scatter system for explosive detection*. SPIE Vol. 2511 Law Enforcement Technologies, Munich p46-55

Luke P.N. (1996) *Electrode configuration and energy resolution in γ ray detectors.* Nuclear Instrumentation and Methods A Vol. 380 p232-237

Lund J.C., Olschner F. and Burger A. (1995) *Lead iodide crystals and detectors. Chapter 11 Semiconductors for room temperature nuclear detector applications* Ed. Schlesinger T.E. and James R.B. Pub. Academic Press p444-463

Lund J.C., Olsen R., Van Scyoc J.M. and James R.B. (1996a) *The use of pulse processing techniques to improve the performance of $Cd_{1-x}Zn_xTe$ gamma ray spectrometers.* IEEE Transactions on Nuclear Science Vol. 44 No. 3 p1411-1416

Lund J.C., Olsen R.W., James R.B., Van Scyoc J.M., Eissler E.E., Blakely M.M., Glick J.B. and Johnson C.J. (1996b) *Performance of a coaxial geometry $Cd_{1-x}Zn_xTe$ detector.* Nuclear Instrumentation and Methods A Vol. 377 p479-483

Manfredotti C., Murrir., Quirini A., and Vasanelli L. (1977) *PbI_2 as nuclear particle detector.* IEEE Transactions on Nuclear Science Vol. 24 p126-128

Martens G., Bomsdorf H., Harding G., Kazenbach J. and Linde R. (1993) *Coherent X-ray scatter imaging for foodstuff contamination detection.* SPIE Vol. 2092 Substance Detection Systems, Innsbruck p411-416

Mayer J.W. (1962) *Gallium arsenide as a radiation detector.* Nucleonics Vol. 20 p60

Mayer M., Boykin D.V., Cherry M.L., Courville J.F., Doty F.P., Drake A., Guzik T.G., Hamel L.A., Larson K., Macri J.R., McConnell M.L., Ryan J.M. and Tousignant O. (1997) *Performance and simulation of CdZnTe strip detectors as sub-millimetre resolution imaging gamma radiation spectrometers.* IEEE Transactions on Nuclear Science Vol. 44 No. 3 p922-928

McCrone W.C. (1950) *Crystallographic data for RDX (Cyclotrimethylenetrinitramine)* Analytical Chemistry Vol. 22 No. 7 p954-955

McDaid S.M., Hunt J.A., Cooper M.J. and Harding G. (1995) *A fast X-ray scatter ratio method for security screening applications*. SPIE Vol. 2511 Law Enforcement Technologies, Munich p79-85

McGregor D.S. and Kammerand J.E. (1995) *Gallium arsenide radiation detectors and spectrometers, Chapter 10 Semiconductors for room temperature nuclear detector applications* Ed. Schlesinger T.E. and James R.B. Pub. Academic Press p384-437

Morin L.R.M. and Berroir A. (1983) *Calculation of X-ray single scattering in diagnostic radiology*. Physics in Medicine and Biology Vol. 28 No. 7 p789-797

Mossop J.R., Kerr S.A., Bradley D.A., Chong C.S. and Ghose A.M. (1987) *The use of coherent gamma ray scattering for the characterisation of materials*. Nuclear Instrumentation and Methods A Vol. 255 p419-422

Muntz E.P. Fewell T., Jennings R. and Bernstein H. (1983) *On the significance of very small angle scattered radiation to radiographic imaging at low energies*. Medical Physics Vol. 10 No. 6 p819-823

Narten A.H and Levy H.A. (1971) *Liquid water: Molecular correlation functions from X-ray diffraction*. Journal of Chemical Physics Vol. 55 No. 5 p2263-2269

Nava F., Bertuccio G., Vanni P., Canali C. Cavallini A., Castaldini A. and Polenta L. (1997) *Improved performance of GaAs radiation detectors with low temperature ohmic contacts*. IEEE Transactions on Nuclear Science Vol. 44 No. 3 p943-948

Ndlovu A.M., Farrell T.J. and Webber C.E. (1991) *Coherent scattering and bone mineral measurements. The dependence of sensitivity on energy and angle.* Medical Physics Vol. 18 No. 5 p985-989

Neitzel U., Kosanetzky J. and Harding G (1985) *Coherent scatter in radiographic imaging: a Monte Carlo simulation study.* Physics in Medicine and Biology Vol. 30 No. 12 p1289-1296

Nelson W.R., Hirayama H. and Rogers D.W. (1985) *The EGS4 code system.* Stanford Linear Accelerator Centre. SLAC report 265.

Newton M., Hukins D. and Harding G. (1992) *Bone composition measured by X-ray scattering.* Physics in Medicine and Biology Vol. 37 No. 6 p1339-1347

Nicholson P. (1974) *Nuclear Electronics* Pub. John Wiley and Sons Ltd p88-121

Niemela A., Sipila H and Ivanov V.I. (1996a) *Improving CdZnTe X-ray detector performance by cooling and rise time discrimination.* Nuclear Instrumentation and Methods A Vol. 377 p484-486

Niemela A., Sipila H. and Ivanov V.I. (1996b) *High resolution p-i-n CdTe and CdZnTe X-ray detectors with cooling and rise time discrimination.* IEEE Transactions on Nuclear Science Vol. 44 No. 3 p1476-1480

Parnham K.B. (1996a) *Personal communication*

Parnham K.B. (1996b) *Recent progress in $Cd_{1-x}Zn_xTe$ radiation detectors.* Nuclear Instrumentation and Methods A Vol. 377 p487-491

Patt B.E., Iwanczyk J.S., Wang Y.L., Tornai M.P., Levin C.S. and Hoffman E.J. (1996) *Mercuric iodide photodetector arrays for gamma ray imaging.* Nuclear Instrumentation and Methods A Vol. 380 p 295-300

Patt B.E., Tornai M.P., Iwanczyk J.S., Levin C.S. and Hoffman E.J. (1997) *Development of an intraoperative gamma camera based on a 256-pixel mercuric iodide detector array*. IEEE Transactions on Nuclear Science Vol. 44 No. 3 p1242-1248

Persliden J. and Carlsson G.A. (1986) *Calculation of the small angle distribution of scattered photons in diagnostic radiology using a Monte Carlo collision density estimator*. Medical Physics Vol. 13 No. 1 p19-24

Polski P.A. (1994) *International aviation security research and development: Technical note*. Journal of Testing and Evaluation Vol. 22 No. 3 p267-274.

Ponpon J.F. and Siffert P. (1996) *Detecteurs de rayons X a semi-conducteurs. Evolutions recentes*. Journal de Physique IV Vol. 6 p703-719

Ponpon J.P. and Sieskind M. (1996) *Recent advances in γ and X-ray spectrometry by means of mercuric iodide detectors*. Nuclear Instrumentation and Methods A Vol. 380 p174-178

Redus R, Squillante M and Lund J (1996) *Electronics for high resolution spectroscopy with compound semiconductors*. Nuclear Instrumentation and Methods A Vol. 380 p312-317

Richter M. and Siffert P. (1992) *High resolution gamma ray spectroscopy with CdTe detector systems* Nuclear Instrumentation and Methods A Vol. 322 p529-537

Robinson M. (1997), i2i vision, Nottingham *Personal communication*

Rossi M., Baldazzi G., Querzola E., Guidi G., Scannavini M.G., Chirco P., Zanavini M., Casali F. and Azevedo S. (1996) *High energy tomography using cadmium zinc telluride detectors*. Nuclear Instrumentation and Methods A Vol. 380 p419-422

Roth S. and Willig W.R. (1971) *Lead iodide nuclear particle detectors*. Applied Physics Letters Vol. 18 p328-331

Roy R.C., Pratt R.H. and Kissell L. (1993) *Rayleigh scattering by energetic photons: development of theory and current status*. Radiation Physics and Chemistry Vol. 41 No 4/5 p725-738

Royal Ordnance (1997), ICI, Bridgwater, Somerset *Personal Communication*

Royle G.J. (1992) *Elastic photon scatter for tissue analysis*. PhD Thesis, University of London

Royle G.J. and Speller R.D. (1991) *Low angle X-ray scattering for bone analysis*. Physics in Medicine and Biology Vol. 36 No. 3 p383-389

Royle G.J. and Speller R.D. (1995) *Quantitative X-ray diffraction analysis of bone and marrow volumes in excised femoral head samples*. Physics in Medicine and Biology Vol. 40 p1487-1498

Ruhter W.D. and Gunnick R. (1994) *Application of CZT detectors in ^{235}U enrichment measurements*. Nuclear Instrumentation and Methods A Vol.353 p 716-718

Scannavini M.G. (1996) *Personal communication*

Scheiber C. and Chambron J. (1992) *CdTe detectors in medicine : a review of current applications and future perspectives*. Nuclear Instrumentation and Methods A Vol. 322 p604-614

Schieber M., James R.B., Lund J.C., McGregor D.S., Gilbert T.S., Van Scyoc J.M., Olsen R.W. Pontau A.E., Schlesinger T.S. and Toney J. (1996a) *State of the art wide-bandgap semiconductor nuclear radiation detectors.* Il nuovo cimento Vol. 109 No. 9 p1253-1260

Schieber M., Lund J.C., Olsen R.W., McGregor D.S., Van Scyoc J.M., James R.B., Soria E. and Bauser E. (1996b) *Material properties and room temperature nuclear detector response of wide bandgap semiconductors.* Nuclear Instrumentation and Methods A Vol. 377 p492-495

Schlesinger T.E. and James R.B. (1995) *Semiconductors for room temperature room temperature applications* p 292 Pub. Academic Press

Shah K.S., Bennett P., Klugerman M., Moy L., Grignano L., Dmitriyev Y., Squillante M.R., Olschner F. and Moses W.W. (1997) *Lead iodide optical detectors for gamma ray spectroscopy.* IEEE Transactions on Nuclear Science Vol. 44 No. 3 p448-450

Shah K.S., Olschner F., Moy L.P., Bennett P., Misra M., Zhang J., Squillante M.R. and Lund J.C. (1996) *Lead iodide X-ray detection systems* Nuclear Instrumentation and Methods A Vol. 380 p266-270

Sorenson J.A. and Phelps M.E. (1987) *Physics in Nuclear Medicine.* 2nd Ed. Pub. W.B. Saunders Company p117-123, 189 and 332

Speller R.D. and Royle G.J. (1992) *Tissue characterisation using low angle X-ray scattering.* Journal of X-ray Science and Technology Vol. 3 p77-84

Speller R.D., Horrocks J.A. and Lacey R.J. (1993) *X-ray scattering signatures for material identification.* SPIE Vol. 2092 Substance Detection Systems, Innsbruck p 411-416

Speller R.D., Malden C.H., Ng E., Horrocks J.A., Luggar R.D. and Lacey R.J. (1996) *System tuning for X-ray scatter measurements in explosive detection.* SPIE Vol. 2936 Physics based technologies for the detection of contraband, Boston p191-200

Squillante M.R. and Entine G. (1992) *New applications of CdTe nuclear detectors.* Nuclear Instrumentation and Methods A Vol. 322 p569-574

Stix G. (1992) *Explosive Images.* Scientific American January p116

Strecker H. (1995) *Simulation based training and testing of classification schemes for CXRS explosives detection.* SPIE Vol. 2511 Law Enforcement Technologies, Munich p88-98

Strecker H., Harding G., Bomsdorf H., Kazenbach J., Linde R. and Martens G. (1993) *Detection of explosives in airport baggage using coherent X-ray scatter.* SPIE Vol. 2092 Substance Detection Systems, Innsbruck p399-410

Tornai M.P., Patt B.E., Iwanczyk J.S., Levin C.S. and Hoffman E.J. (1997) *Discrete scintillator coupled mercuric iodide photodetector arrays for breast imaging.* IEEE Transactions on Nuclear Science Vol. 44 No. 3 p1127-1133

Unscrambler 6.1 (1996), Camo AS

Urbanski T. (1984) *Chemistry and technology of explosives* Vol. 4 Pergamom Press p372-382

Vartsky D., Engler G., Goldberg M.B. and Kvauss R.A. (1993) *A method for detection of explosives based on nuclear resonance absorption of gamma rays in* ^{14}N. SPIE Vol. 2092 Substance detection systems, Innsbruck p307-315

Westmore M.S., Fenster A. and Cunningham I.A. (1996) *Angular dependent coherent scatter measured with a diagnostic X-ray image intensifier-based imaging system*. Medical Physics Vol. 23 No. 5 p723-733

Whited R.C. and Schieber M.M. (1979) *Cadmium telluride and mercuric iodide γ radiation detectors*. Nuclear Instrumentation and Methods Vol. 162 p113-123

Wilder J., Garcia A. and Wiener S. (1995) *Neural net based explosives recognition with coherent X-ray scatter*. SPIE Vol. 2511 Law enforcement technologies, Munich p99-107

Williamson J.F. and Morin R.L. (1983) *An efficient method of randomly sampling the coherent angular scatter distribution*. Physics in Medicine and Biology Vol. 28 No. 1 p57-62

Willig W.R. (1971) *Mercury iodide as a gamma spectrometer*. Nuclear Instrumentation and Methods Vol. 96 p615-616

Yedida B. and Shea P. (1992) *Relating contraband detection effectiveness to cargo content signatures*. Contraband and Cargo Inspection Technology International Symposium, Washington p417-424